To the Graduate Council:

I am submitting herewith a dissertation written by Nurhan Vatansever entitled "Effect of Molecular Weight and Pressure on Crystallization of Cis-Polyisoprene". I have examined the final copy of this dissertation for form and content and reccomend that it be accepted in partial fulfillment of the requirements for the degree of Doctor of Philosopphy, with a major in Polymer Engineering.

Paul J. Phillips, Major Professor

We have read this dissertation
and recommend its acceptance:

Accepted for the Council:

Vice Provost
and Dean of The Graduate School

EFFECT OF MOLECULAR WEIGHT AND PRESSURE ON CRYSTALLIZATION OF CIS-POLYISOPRENE

A Dissertation

Presented for the

Doctor of Philosophy

Degree

The University of Tennessee, Knoxville

Nurhan Vatansever

December 1986

To My Parents

ACKNOWLEDGEMENTS

The author would like to express her appreciation to her advisor, Professor Paul J. Phillips for his important contributions, suggestions and guidance during the course of this work.

The author thanks The National Science Foundation for the financial support provided throughout this work.

The author appreciates the discussions with fellow students Eddy N. Dalal, Hsui Tseng and Deepak R. Parikh, and the technical help provided by the departmental electronic and machine shops.

The author also expresses appreciation to her husband Ali Vatansever, who has been a co-worker, for his input and encouragement throughout this work.

Finally, the author wishes to thank her committee, Professors P.J. Phillips, J.E. Spruiell, E.S. Clark and J.D. Kovac.

ABSTRACT

Cis-polyisoprene from hevea rubber has been fractionated by non-solvent precipitation. Crystallization in fractions has been studied at atmospheric pressure and at 0.5 kilobar using transmission electron microscopy of osmium tetroxide stained thin films. Analyses of kinetics data at atmospheric pressure using Secondary Nucleation Theory showed that fractions of molecular weight greater than or equal to 897,000 show only regime III kinetics, a fraction of molecular weight 543,000 showed both regime II and regime III kinetics and the lower molecular weight fractions showed all three regimes together. Studies at 0.5 kilobar demonstrated the possibility that the regime III-II transition is kinetic in nature. Morphological studies provided additional evidence for the regime I-II transition. An increase in branching was observed below that transition temperature. In the regime I region, spherulites, axialites and single crystals grow concurrently in the film showing molecular weight fractionation during crystallization.

TABLE OF CONTENTS

SECTION PAGE

1. INTRODUCTION.....1

2. REVIEW OF THEORETICAL BACKGROUND AND LITERATURE.....4

2.1. Polymer Molecular Weights.....4
2.1.1. Molecular Weight and Molecular Weight Distribution.....4
2.1.2. Fractionation.....7

2.2. Polymer Crystallization.....11
2.2.1. Crystallization Concepts.....11
2.2.2. Single Crystals.....11
2.2.3. Spherulites.....14
2.2.4. Axialites.....17

2.3. Fold Surface.....17
2.3.1. Nature of the Fold Surface.....17
2.3.2. Arguments About the Fold Surface Structure.20

2.4. Secondary Nucleation Theory.....22
2.4.1. Model.....22
2.4.2. Total Flux.....26
2.4.3. Inital Lamellar Thickness.....27
2.4.4. Retardation Factor.....30
2.4.5. Free Energy Of Fusion.....31
2.4.6. Growth Rates.....32
2.4.6.1. Regime I Growth.....32
2.4.6.2. Regime II Growth.....33
2.4.6.3. Regime III Growth.....35
2.4.7. Regime Test.....37
2.4.8. Limitations and Criticisms.....40

2.5. Melting of Polymer Crystals.....42
2.5.1. Thermodynamic Considerations.....42
2.5.2. Kinetic Considerations.....43

2.6. The Glass Transition.....44

2.7. Effect of Molecular Weight.....46

2.8. Effects of Pressure.....49
2.8.1. Morphology.....49
2.8.2. Crystallization Kinetics.....51
2.8.3. Melting Temperature.....52
2.8.4. Glass Transition Temperature.....53

3. EXPERIMENTATION.....57

3.1. Material Preparation and Characterization.....57
3.1.1. Preparation of Dilute Solutions.....57
3.1.2. Molecular Weight Fractionation Studies.....58
3.1.3. Intrinsic Viscosity Studies.....61
3.1.4. Gel Permeation Chromatography.....63

3.2. Atmospheric Pressure Crystallization Studies.....66
3.2.1. Specimen Preparation.....66
3.2.2. Osmium Tetroxide Staining.....67
3.2.3. Transmission Electron Microscopy.....69

3.3. High Pressure Crystallization Studies.....71
3.3.1. Equipment.....71
3.3.2. High Pressure Cell.....74
3.3.3. Temperature Control.....76
3.3.4. Experimental Procedure.....78

4. RESULTS.....80

4.1. Crystallization of Guayule Rubber.....80
4.1.1. Lamellar Growth Studies.....81
4.1.2. Morphology.....89

4.2. Studies of Hevea Rubber at Atmospheric Pressure...94
4.2.1. Fractionation Studies.....94
4.2.2. Molecular Weight Studies.....94
4.2.3. Lamellar Growth Studies.....97
4.2.4. Morphology.....107
4.2.5. Branching Studies.....137

4.3. Crystallization of Hevea Rubber Fractions at 0.5 kilobar.....146
4.3.1. Linear Growth Rate Studies.....146
4.3.2. Morphology.....149

5. DISCUSSION.....166

5.1. Kinetics.....167

5.1.1. Analyses of Guayule Rubber at Atmospheric Pressure.....167
5.1.2. Analyses of Hevea Rubber Fractions at Atmospheric Pressure.....174
5.1.3. Analyses of Hevea Rubber Fractions at 0.5 Kilobar.....192

5.2. Morphology.....203

5.2.1. General Morphology.....204
5.2.2. Lamellar Width.....211

5.2.2. Lamellar Width.....211
5.2.3. Lamellar Thickness.....217
5.2.4. Branching.....239

6. CONCLUSIONS.....252

6.1. Crystallization Regimes.....252

6.2. Lamellar Thickening.....253

6.3. Fold Surface Free Energies.....253

6.4. General Morphology.....254

6.5. Branching.....254

6.6. Lamellar Width.....254

7. SUGGESTIONS FOR FURTHER WORK.....255

7.1. Effect of Molecular Weight Distribution.....255

7.2. Regime Reversion.....255

7.3. High Temperature Crystallization.....256

7.4. The Influence of Regime Transition on Mechanical Properties.....256

7.5. Effect of Trans Units on Regime Transition.....257

7.6. Pressure Effects.....257

LIST OF REFERENCES.....258

APPENDIX 264

VITA.....269

LIST OF TABLES

TABLE		PAGE
1	Fractionation data	95
2	Molecular weight data for fractions	96
3	Analyses of atmospheric pressure kinetics data of unfractionated guayule rubber	173
4	Results of Lauritzen-Hoffman regime test for the fraction of molecular weight 313,000 in the regime I and regime II regions	187
5	Analyses of atmospheric pressure kinetic data of lower molecular weight fractions with indicated molecular weights	190
6	Analyses of atmospheric pressure kinetic data of higher molecular weight fractions with indicated molecular weights	191
7	The change of σ_e with pressure	197
8	The change of the regime III-II transition temperature with pressure	200
9	The change of σ_e with molecular weight	236
10	Analyses of lamellar thickness data	238

LIST OF FIGURES

FIGURE		PAGE
1	The distribution of molecular weights in a high polymer	6
2	A typical lamellar single crystal in polymers	13
3	A polymer spherulite with chain folded lamellae (schematic, from Hoffman et al. 1976)	15
4	A common progression of habits leading to the spherical form of a mature spherulite (from Bassett 1981)	16
5	Schematic representations of (a) the adjacent re-entry model and (b) the "switchboard model"	19
6	Idealized schematic model for polymer lamella crystal growth (from Hoffman et al. 1976)	23
7	Free energy of formation of a chain folded surface nucleus (from Hoffman et al. 1976)	25
8	Regime I, Regime II and Regime III crystallization (schematic)	34
9	Schematic representation of $\log G + U^*/2.3\ RT$ against $1/T(\Delta T)$ for regimes I,II and III	38
10	Fractionation apparatus	59
11	Schematic diagram of a transmission electron microscope	70
12	Lamellar growth of guayule rubber at -26 ^{o}C	72
13	High pressure generating system (schematic)	73
14	High pressure cell (schematic)	75
15	Sample holder used in the high pressure cell	77
16	Lamellar growth of guayule rubber at -21 ^{o}C and at -5 ^{o}C	82
17	Lamellar growth rate versus crystallization temperature for guayule rubber	83

18 Lamellar growth rate versus crystallization temperature for O-hevea rubber (Andrews 1964), ●-guayule rubber from pilot plant, ●-fresh rubber extracted from plant (Rensch et al. 1986).....84

19 Schematic representation of the "side-on" and "edge-on" orientation of the lamellar crystals with respect to the electron beam.....86

20 A histogram of lamellar thickness of guayule rubber at -15 °C.....87

21 Lamellar thickness as a function of crystallization temperature for α and β lamellae of ●-natsyn (Edwards et al. 1980), O-aged pilot plant guayule rubber (Rensch et al. 1986) and ▲-α lamellae of fresh pilot plant guayule rubber.....88

22 α-spherulite of guayule rubber crystallized at -26 °C.....90

23 A highly branched β-spherulite in guayule rubber crystallized at -26 °C.....91

24 α-spherulite of guayule rubber showing microgel particle at center.....92

25 α-spherulite of guayule rubber grown at -26 °C.....93

26 Molecular weight distribution of the hevea rubber fraction of molecular weight 351,000.....98

27 Molecular weight distribution of the hevea rubber fraction of molecular weight 313,000.....99

28 Molecular weight distribution of the hevea rubber fraction of molecular weight 102,000.....100

29 Lamellar growth of hevea rubber fractions with molecular weights O-313,000 and ●-1,421,000 at -20 °C.....101

30 Lamellar growth rate versus crystallization temperature for hevea rubber fractions with the indicated molecular weights.....102

31 Lamellar growth curve of hevea rubber fraction of molecular weight 313,000.....104

32 Lamellar growth curve of hevea rubber fraction of molecular weight 543,000.....105

33 Lamellar thicknesses as a function of crystallization temperature for the hevea rubber fractions of indicated molecular weights.....106

34 Histograms of lamellar thicknesses of the hevea rubber fractions of (a) molecular weight 543,000 at -2.2 °C (b) 1,421,000 at -30 °C.....108

35 α-spherulites of a hevea rubber fraction of molecular weight 313,000.....110

36 β-spherulite of a hevea rubber fraction of molecular weight 313,000.....111

37 α-β bimodal spherulite of a hevea rubber fraction of molecular weight 313,000 grown at -30 °C.....112

38 Spherulites of hevea rubber fraction of molecular weight 313,000 growing at -20 °C.....113

39 α and β spherulites growing in hevea rubber fraction of molecular weight 313,000.....114

40 β spherulite growing in a hevea rubber fraction of molecular weight 313,000 at -15 °C....115

41 A sheaf showing both the "edge-on" and platelet-like growth of a hevea rubber fraction of molecular weight 313,000 at -5 °C.....116

42 Platelet-like growth observed in a hevea rubber fraction of molecular weight 313,000 at -7.3 °C...117

43 Lamellae observed in a hevea rubber fraction of molecular weight 313,000 at -7.3 °C.....118

44 Single crystals observed from hevea rubber fraction of molecular weight 313,000 at +3 °C.....120

45 Discontinuities observed in lamellae of a hevea rubber fraction of molecular weight 313,000 at -3.5 °C.....121

46 Platelet-like growth observed in a fraction of molecular weight 313,000 at +1.8 °C.....122

47 Co-nucleated single crystal and axialite grown at +1.8 °C.....123

48 A sheaf-like spherulite in which the equatorial growth process is suppressed in the fraction of molecular weight 543,000 at -40 °C.....124

49 Growing sheaves in a fraction of molecular weight 543,000 at -20 °C.....125

50 Spherulites in a fraction of molecular weight 543,000 at -20 °C.....126

51 Row-nucleated lamellae in a fraction of molecular weight 543,000 at -10 °C.....127

52 Row-nucleated lamellae in a fraction of molecular weight 543,000 at -5 °C.....128

53 An axialite and lamellae growing in the "edge-on" orientation in a fraction of molecular weight 543,000 at -0.6 °C.....130

54 A single crystal growing in a fraction of molecular weight 543,000 at -.0.6 °C.....131

55 "S" shaped lamella in a fraction of molecular weight 543,000 at +2.2 °C.....132

56 Platelet-like growth along with lamellae growing in the "edge-on" orientation in a fraction of molecular weight 543,000 at +2.2 °C.....133

57 Lozenge shaped crystals in a fraction of molecular weight 1,421,000 at -26 °C.....134

58 An α-β bimodal spherulite in a fraction of molecular weight 897,000 at -34 °C.....135

59 A growing sheaf in which the equatorial growth process is suppressed in a fraction of molecular weight 897,000 at -34 °C.....136

60 Branching frequency versus temperature of the hevea rubber fraction of molecular weight 313,000.....138

61 Branching frequency versus temperature of the hevea rubber fraction of molecular weight 543,000.....139

62 Two growing sheaves in a fraction of molecular weight 543,000 at +1.4 °C.....140

63 Heterogeneous nucleation in a fraction of molecular weight 543,000 at -2.2 °C.....141

64 A growing sheaf in a fraction of molecular weight 543,000 showing clear branch points.....142

65 Row nucleation in a fraction of molecular weight 543,000 at -2.2 °C.....143

66 A growing sheaf in a fraction of molecular weight 543,000 at -5 °C.....144

67 A sheaf nucleated from a microgel in a fraction of molecular weight 897,000 at -5 °C.....145

68 Lamellar growth rates as a function of crystallization temperature at O-atmospheric pressure,□-0.5 kbar for the fraction of molecular weight 351,000.....147

69 Lamellar growth rates as a function of crystallization temperature at O-atmospheric pressure,□-0.5 kbar for the fraction of molecular weight 543,000.....148

70 Lamellar thicknesses as a function of crystallization temperature at 0.5 kbar for the fractions of molecular weights O-351,000 and □ -543,000.....150

71 A histogram of lamellar thickness of the fraction of molecular weight 543,000 at -17 °C and at 0.5 kbar.....151

72 A histogram of lamellar thickness of the fraction of molecular weight 543,000 at +4.2 °C and at 0.5 kbar.....152

73 Growing sheaves in a fraction of molecular weight 351,000 at 0 °C and at 0.5 kbar.....153

74 Platelet-like growth in a fraction of molecular weight 351,000 at 0 °C and at 0.5 kbar.....155

75 Platelet-like growth observed in a fraction of molecular weight 543,000 at 0 °C and at 0.5 kbar..156

76 Platelet-like growth in a fraction of molecular weight 543,000 at 0 °C and at 0.5 kbar.....157

77 A single crystal in a fraction of molecular weight 351,000 at 0 °C and at 0.5 kbar.....158

78 A hexagonally oriented specie in a fraction of molecular weight 543,000 at 0°C and at 0.5 kbar...159

79 High pressure phase in a fraction of molecular weight 351,000 at 0 °C and at 0.5 kbar.....160

80 Nucleation density as a function of pressure at 0 °C for the fraction of molecular weight 543,000.....161

81 Nucleation density as a function of pressure at 0 °C for the fraction of molecular weight 351,000.....162

82 Average crystal thickness as a function of crystallization temperature at 0.5 kbar for the fractions of molecular weights ●-351,000 and O-543,000.....163

83 Plot of nucleation density versus the reciprocal average length at 0.5 kbar for the fractions of molecular weights ●-351,000 and 543,000.....164

84 Plots of kinetics data of guayule rubber at atmospheric pressure (a)experimental values U^* = 17.2kJ/mol, T_∞ = 150.7 K;(b)U^* = 6.28 kJ/mol and T_∞ = 171 K.....169

85 Plots of kinetics data of (a)α-lamellae of aged pilot plant,(b)β-lamellae of aged pilot plant,(c)α-lamellae of fresh guayule rubber and (d)α-lamellae of fresh pilot plant.....172

86 Plots of kinetics data of hevea rubber fraction of molecular weight 1,421,000 at atmospheric pressure (a)experimental values U^* = 17.2kJ/mol, T_∞ = 150.7 K;(b)U^* = 6.28 kJ/mol and T_∞ = 171 K...176

87 Plots of kinetics data of hevea rubber fraction of molecular weight 897,000 at atmospheric pressure (a)experimental values U^* = 17.2kJ/mol, T_∞ = 150.7 K;(b)U^* = 6.28 kJ/mol and T_∞ = 171 K...177

88 Plots of kinetics data of hevea rubber fraction of molecular weight 543,000 at atmospheric pressure (a)experimental values U^* = 17.2kJ/mol, T_∞ = 150.7 K;(b)U^* = 6.28 kJ/mol and T_∞ = 171 K...178

89 Plots of kinetics data of hevea rubber fraction of molecular weight 313,000 at atmospheric pressure (a)experimental values U^* = 17.2kJ/mol, T_∞ = 150.7 K;(b)U^* = 6.28 kJ/mol and T_∞ = 171 K...179

90 Plots of kinetics data of hevea rubber fraction of molecular weight 351,000 at atmospheric pressure (a)experimental values U^* = 17.2kJ/mol, T_∞ = 150.7 K;(b)U^* = 6.28 kJ/mol and T_∞ = 171 K...180

91 A diagram illustrating the omega defect schematically (from Hoffman 1985).....184

92 Plot of kinetics data of hevea rubber fraction of molecular weight 351,000 at 0.5 kbar.....194

93 Plot of kinetics data of hevea rubber fraction of molecular weight 543,000 at 0.5 kbar.....195

94 Plot of kinetics data of unfractionated hevea rubber (Phillips and Edwards 1975) at 0.5 kbar □-interpolated points.....196

95 Growth rate contours for cis-polyisoprene (from Phillips and Edwards 1975) and the change of equilibrium melting temperature (T_m^o) with pressure (Dalal 1982).....202

96 Fractionated growth in regime I region at -5 ^oC...206

97 A single crystal growing in a fraction of molecular weight 313,000 at +1.8 ^oC.....207

98 A single crystal in a fraction of molecular weight 313,000 at +1.8 ^oC.....208

99 Plot of average lamellar width as a function of undercooling in a fraction of molecular weight 313,000 (parallel lines represent the highest and lowest values measured).....212

100 Plot of average lamellar width as a function of undercooling in a fraction of molecular weight 543,000 (parallel lines represent the highest and lowest values measured).....213

101 Histograms of lamellar width in a fraction of molecular weight 543,000 at (a) -20^oC (b)-0.6^oC...214

102 Plots of lamellar thickness versus $1/f\Delta T x 10^3$ for the hevea rubber fractions of molecular weights O-313,000, ◐-351,000,□-543,000 and ▲-897,000.....219

103 Plots of lamellar thickness versus $1/f\Delta T x 10^3$ at 0.5 kbar for the hevea rubber fractions of molecular weights O-351,000 and□-543,000.....221

104 A histogram of lamellar thickness of hevea rubber fraction of molecular weight 313,000 at -26 °C and at atmospheric pressure.....222

105 A histogram of lamellar thickness of hevea rubber fraction of molecular weight 543,000 at -0.6 °C and at atmospheric pressure.....223

106 A histogram of lamellar thickness of hevea rubber fraction of molecular weight 313,000 at +1.8 °C and at atmospheric pressure.....224

107 A histogram of lamellar thickness of hevea rubber fraction of molecular weight 543,000 at +1.4 °C and at atmospheric pressure.....225

108 A histogram of lamellar thickness of hevea rubber fraction of molecular weight 351,000 at +4.2 °C and at 0.5 kbar.....228

109 A histogram of lamellar thickness of hevea rubber fraction of molecular weight 351,000 at -11 °C and at 0.5 kbar.....229

110 A histogram of lamellar thickness of hevea rubber fraction of molecular weight 351,000 at -4.8 °C and at 0.5 kbar.....230

111 A histogram of lamellar thickness of hevea rubber fraction of molecular weight 351,000 at 0 °C and at 0.5 kbar.....231

112 A histogram of lamellar thickness of hevea rubber fraction of molecular weight 351,000 at -17 °C and at 0.5 kbar.....232

113 A histogram of lamellar thickness of hevea rubber fraction of molecular weight 543,000 at -11 °C and 0.5 at kbar.....233

114 A histogram of lamellar thickness of hevea rubber fraction of molecular weight 543,000 at -4.8 °C and at 0.5 kbar.....234

115 A histogram of lamellar thickness of hevea rubber fraction of molecular weight 543,000 at 0 °C and at 0.5 kbar.....235

FIGURE PAGE

116 (a) A high magnification picture showing a branch point in a fraction of molecular weight 543,000 at -15 ^{o}C (b) shows the same area as in (a) but tilted 12^{o} with respect to the electron beam 243

117 Schematic representation of figure 116.....245

118 (a) A Picture showing a branch point in a fraction of molecular weight 543,000 at -10 ^{o}C (b) shows the same area as in (a) but tilted 12^{o} with respect to the electron beam (c)tilted 18^{o}...246

119 A high magnification picture showing the point "C" in figure 118 in more detail.....249

120 Impurities causing crystal branching.....251

1. INTRODUCTION

Temperature, molecular weight, molecular weight distribution and pressure are important variables in polymer crystallization. Depending on the temperature range used, polymers may crystallize in three different regimes, denoted as I,II and III. Within each regime a different relationship exists between the surface nucleation rate and substrate completion rate (Lauritzen and Hoffman 1973). In regime I, a single nucleation event causes the completion of the substrate length. In regime II, multiple nucleation occurs and the rate of formation of surface nuclei is comparable to the rate of strip completion. Experimentally the regime I-II transition has been observed in polyethylene fractions and found to be molecular weight dependent (Hoffman 1975). For larger undercoolings, a third regime was proposed by Phillips in 1979 and developed in mathematical form by Hoffman 1983 in which surface nucleation becomes so rapid that substrate completion is dominated by nucleation events. Nuclei may also form on other growing strips prior to substrate completion. The regime II-III transition has been observed in polyoxymethylene (Pelzbauer and Galeski 1972 Hoffman 1983), cis-polyisoprene (Dalal and Phillips 1984), polypropylene (Clark and Hoffman 1984) and polyphenylene

sulphide (Lovinger et al.1985). Among these, only the work with polyphenylene sulphide involves two different molecular weights with polydispersities in the range 1.3-1.7. The other studies considered only single samples of unfractionated polymers. But it is known that a broad molecular weight distribution can obscure regime transitions (Tseng and Phillips 1984). Therefore the use of relatively narrow molecular weight fractions is desirable.

The effect of pressure on the regime transition temperature is important to the understanding of the nature of the transition. If the change of transition temperature with pressure follows the changes of glass transition temperature with pressure, a diffusion controlled mechanism can be concluded. If the transition temperature changes with the pressure as melting temperature, then the transition is thermodynamic and controlled by the nucleation process. The latter effect has been observed for bulk linear polyethylene, the pressure dependence of the transition following that of the equilibrium melting point (Phillips and Tseng 1985).

The objective of this dissertation is to obtain and analyze the growth rate data for natural cis-polyisoprene (hevea rubber) as a function of molecular weight. Different molecular weight fractions of cis-polyisoprene have been prepared using non-solvent fractionation. Following the characterization of molecular

weight, growth rate and lamellar thickness data were obtained using transmission electron microscopy of osmium tetroxide stained thin films. The growth rates at 0.5 kilobar of two different molecular weight fractions have also been studied. Studies at higher pressures could not be carried out because of the complete absence of lamellar morphology at pressures above 0.5 kilobar. The Lauritzen-Hoffman approach was chosen for the analyses of growth rate data because of its simplicity and good agreement with earlier experimental observations.

Analyses of growth rate data showed molecular weight dependent regime I-II and regime II-III transitions. For the highest molecular weight fractions (897,000 and above) only regime III growth was observed whereas a regime II-III transition was detectable in lower molecular weight fractions. Kinetic analyses of the growth rate data of the fraction of molecular weight 313,000 revealed the existence of all three regimes for the first time in any polymer. This provides the first definitive evidence for regime theory.

2.REVIEW OF THEORETICAL BACKGROUND AND LITERATURE

2.1. Polymer Molecular Weights

2.1.1. Molecular Weight and Molecular Weight Distribution

In polymers, the molecules do not all have the same molecular weight and there is a distribution of molecular weights which is quite broad. The conventional definition of molecular weight (the weight in grams of molecules x Avagadro's number) is inadequate for polymers. An average number is defined to describe the molecular size. The simplest way of doing this is dividing sample weight by the number of molecules. The molecular weight defined this way is known as the number average molecular weight ($\bar{M}_n$), which is given by the following equation;

$$\bar{M}_n = \frac{\Sigma M_i N_i}{\Sigma N_1} \qquad (2.1.1)$$

where N_i is the number of molecules with the molecular weight M_i. The second common average molecular weight used is the weight average molecular weight ($\bar{M}w$) and is defined as;

$$\bar{M}_w = \frac{\Sigma N_i M_i^2}{\Sigma N_i M_i} \qquad (2.1.2)$$

The weight average molecular weight is always greater than or equal to the number average molecular weight for a polydisperse polymer as will be obvious from a comparison of equations (2.1.1) and (2.1.2). Equality of $\bar{M}_w$ and $\bar{M}_n$ would correspond to a perfectly uniform (monodisperse) system (Figure 1). The ratio of these average molecular weights is often used as a guide to the dispersity of the chain lengths in a polymer sample. The greater the $(\bar{M}_w/\bar{M}_n)$ value, the greater is the dispersity.

Another frequently used molecular weight average in polymers is the viscosity average molecular weight $(\bar{M}_v)$. The viscosity of a dilute solution of a polymer is significantly greater than the viscosity of the solvent employed. The frictional properties of polymer molecules in solution are the basis of the theoretical dependence of the solution viscosity on the molecular weight and hydrodynamic volume. The calculation of the molecular weight from viscosity measurements is described in detail in section 3.1.3. Viscosity average molecular weight is given as;

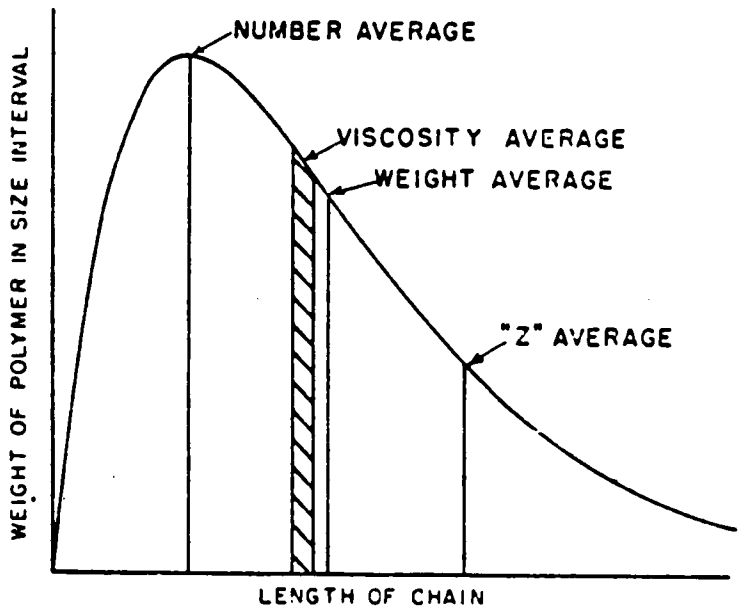


Figure 1 The distribution of molecular weights in a high polymer.

$$\bar{M}_v = \frac{\Sigma(N_i M_i)^{1+a}}{\Sigma(N_i M_i)^{1/a}} \qquad (2.1.3)$$

where "a" is the Mark-Houwink constant which varies from 0.5 to 1.0 and is a function of polymer and solvent.

2.1.2. Fractionation

Since most polymers are heterogeneous with respect to molecular weight, their physical and mechanical properties are influenced by this molecular weight distribution. Fractionation is the orderly separation of a polymer into a number of fractions of different molecular weights, each of which is more homogeneous than the original polymer.

There are two types of fractionation procedures; analytical, by which the molecular weight distribution curves are produced without isolating the fractions, and preparative, in which each individual fraction is isolated and characterized. Some preparative fractionation techniques are fractional precipitation, turbidimetric titration and column elution. Of these, only the fractional precipitation method will be described here.

Fractional precipitation can be achieved in different ways. The most frequently used ones being addition of non-solvent and lowering of temperature. In fractionation of polymers from a solvent/non-solvent system, the precipitation of the fractions is achieved through a stepwise decrease in the solvent power of the system by gradual addition of non-solvent. Since solubility decreases with increasing molecular weight, the first precipitated phase is expected to be the highest molecular weight fraction. In the temperature lowering method successive precipitation of polymer species from a solution occurs by controlled cooling.

In fractionation which is based on decreasing solubility of a polydisperse sample with increasing molecular weight, the fractionation theory may be summarized as follows: the Flory-Huggins treatment of polymer solutions arrives at an expression for the partial molal free energy of mixing of a solvent with a polymer, ΔG , by neglecting the higher terms in volume fraction (Johnson et al. 1967)

$$\frac{\Delta G}{R\,T} = \ln (1-v_2) + (1 - \overline{DP}_n^{-1})\, v_2 + X_1 v_2^{\,2} \qquad (2.1.4)$$

where R is the gas constant, T is absolute temperature, v_2 is the volume fraction of polymer, $\overline{DP}_n$ is number average degree of polymerization and X_1 is the polymer-solvent

interaction parameter. The interaction parameter can be obtained using equation (2.1.5) where the activity of the solvent is determined experimentally.

$$(\ln a_1 - \ln v_1)\, v_2 - 1 = \overline{DP}_n^{-1} + X_1 v_2 \qquad (2.1.5)$$

where a_1 is the activity of the solvent and v_1 is the volume fraction of solvent. It is found that the interaction parameter is a measure of solvent power, with the poorer solvents having larger values of X_1. This parameter is also a function of temperature, being given approximately by

$$X_1 = A + B/T \qquad (2.1.6)$$

where T is temperature and A,B are constants. The variation of X_1 with solvent power and temperature forms a basis for several methods of polymer fractionation employing solvent and/or temperature gradients.

Differentiating equation (2.1.4) and putting it equal to zero gives the critical point for phase separation as

$$v_{2(\text{critical})} = 1 \,/\, [1 + (\overline{DP})^{1/2}] \qquad (2.1.7)$$

$$X_{1(\text{critical})} = 0.5\, (\, 1 + 1 \,/\, \overline{DP}^{1/2})^2 \qquad (2.1.8)$$

The critical temperature is related to $X_{1(critical)}$ by the equation

$$T_{critical} = B / (X_{1\ critical} - A) \qquad (2.1.9)$$

Equations (2.1.7) - (2.1.9) show the expected molecular weight dependence of the critical variables. Upon phase separation, a solvent-rich phase(1), and a polymer rich phase(2) are formed. The distribution of a polymer of degree of polymerization ,DP_n, between these two phases is calculated by equating the chemical potentials and results in the equation

$$v_p(1) / v_p(2) = \exp(-\delta\ \overline{DP}_n) \qquad (2.1.10)$$

δ is a function of total polymer concentration in both phases and its value increases with decreasing solvent power. Equation (2.1.10) is one of the bases of fractionation theory, because δ is positive and not a function of $\overline{DP}_n$. The conclusions which may be drawn by inspecting equation (2.1.10) are (a) any polymer of a given molecular weight is always present in phases 1 and 2, (b) the difference in concentration of the two phases for any species increases with increasing molecular weight; i.e. the higher molecular weight fraction is enriched in phase 2.

2.2. Polymer Crystallization

2.2.1. Crystallization Concepts

It is known that many polymers despite their long chains can crystallize to some extent. X-ray diffraction patterns from these polymers indicate the existence of long range order resulting from crystalline regions of at least several hundred angstroms in size. There are several factors which affect the tendency of polymers to form crystalline phases such as structural regularity of the chains, absence of bulky, irregularly spaced substituents which inhibit the chain segments from fitting into a crystal lattice, and the presence of vibrational and rotational motions in the chains so that different conformations can be assumed. Some polymers satisfying these conditions do crystallize from melt or solution in the form of thin lamellae of the order of 100 angstroms thick, in which the molecules are folded back and forth on themselves.

2.2.2. Single Crystals

On cooling a dilute solution of a semi-crystalline polymer, lamellar single crystals are formed. Polyethylene molecules were shown to form single crystals from dilute solution by Keller (1957). Based on electron diffraction experiments which indicated that molecules are normal to the

lamellae, Keller concluded that polymer molecules in the crystals are folded back and forth on themselves. This fact was supported by similar observations of Fischer (1957) and Till (1957).

Single crystals are in the form of thin platelets about 100 Angstroms thick whose large upper and lower surfaces consist of molecular folds (Figure 2). The size, shape and regularity of the crystals depend on the growth conditions. Such factors as solvent, temperature, concentration and the rate of growth are important. The thickness of lamellae, for example, depends on the crystallization temperature as well as on any further annealing treatments.

Growth of the lamellae occurs predominantly along the lateral faces of the single crystal. The growth is normally visualized as a folding up of molecules along these faces forming folded ribbons parallel to the prism faces. This leads to a subdivision of the crystal into distinct sectors, there being as many sectors as there are prism faces, distinguished by the plane of folding. In many cases observations of the distinctness of the sectors become possible because of a hollow pyramidal morphology. Actually most crystals are like tents, the different sectors forming the panels. Generally, however, these pyramids flatten during the normal course of sample collection and the crystals have wrinkles as a natural result of the flattening

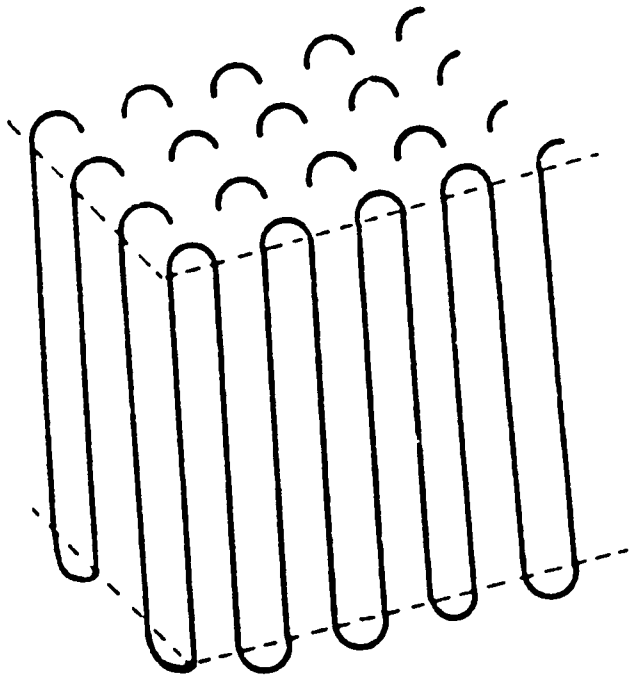


Figure 2 A typical lamellar single crystal in polymers.

process. In well formed diamond shaped polyethylene single crystals, studies (Lindenmeyer 1963) showed that cleavage occurs readily along the planes which are parallel to the prism faces in each sector.

2.2.3. Spherulites

When polymers are crystallized from the melt spherulitic morphologies are commonly observed. Spherulites consist of chain folded lamellae radiating out from a central nucleus (Figure 3) which grow linearly with time until impingement occurs with other spherulites. Precisely how a spherulite develops depends on how it is nucleated. A common path of growth is shown in Figure 4. First, primary crystallization is started with a fibril or an inhomogeneous entity and evolves through sheaf-like embryos before attaining the final spherical shape. This is maintained until neighboring spherulites impinge, then they become polyhedra. Secondary crystallization proceeds within each spherulite, transforming a portion of the remaining amorphous material between lamellae. The fine structure of the spherulite will depend on the nature of the branching and on the form of crystals between branches. In practice, most spherulites appear to be a radiating array of fibrous crystals branching at small angles. Polymer chain axes in the spherulite are approximately perpendicular to the radius of the spherulite as deduced from X-ray studies. Twisting of

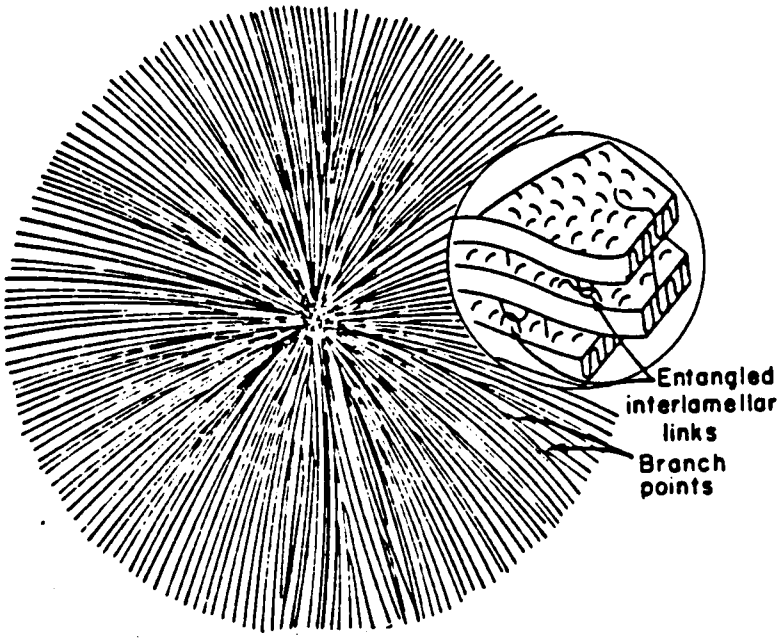


Figure 3 A polymer spherulite with chain folded lamellae (schematic, from Hoffman et al. 1976).

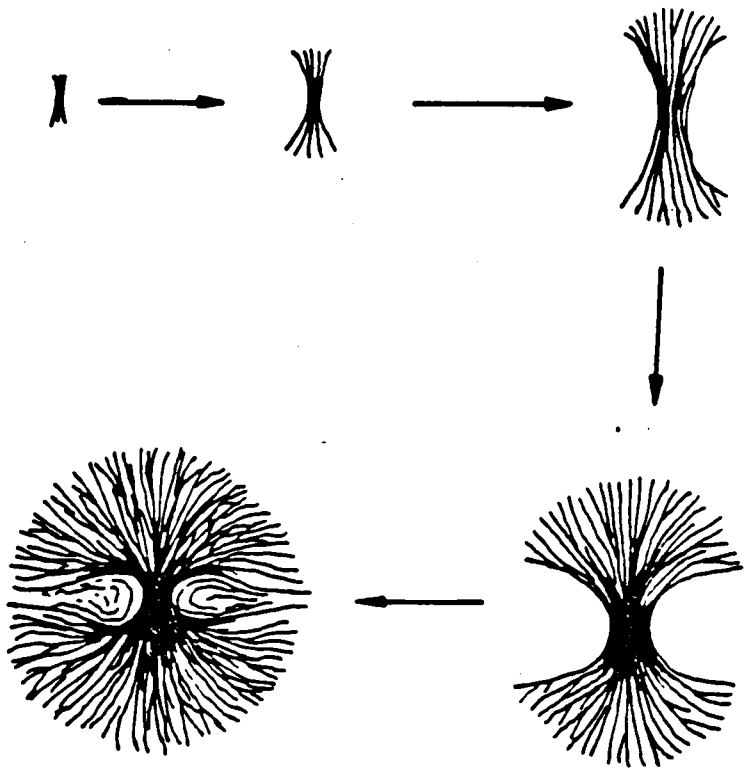


Figure 4 A common progression of habits leading to the spherical form of a mature spherulite (from Bassett 1981).

the lamellae can cause concentric rings in optical extinction patterns if occurring in a regular manner and at the same radial distance for all lamellae.

2.2.4. Axialites

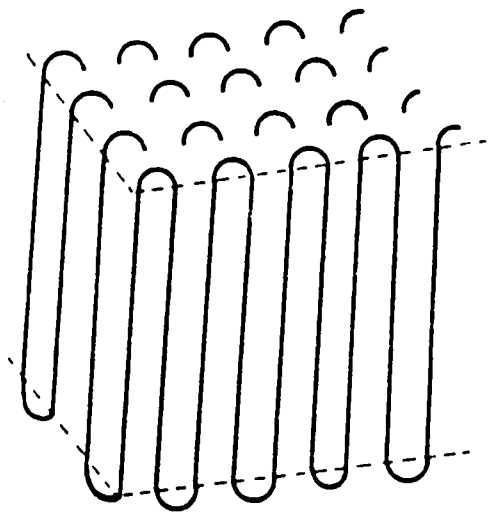
Axialites are aggregates of crystal lamellae and they exhibit the different characteristics of polymer single crystals and spherulites depending on the angle of view. Axialites are like two slightly open books placed back to back. It has been suggested that there are tie molecules (Hearle 1982) or crystalline portions between the lamellae so that the extent of splaying is limited. Axialites can crystallize in a variety of supermolecular structures such as hedrites which have hexagonally oriented fibrous lamellae which may incorporate a screw dislocation, ovoids which have radially oriented fibrous lamellae and spiral ovoids which have spirally oriented fibrous lamellae (Rabek 1980).

2.3.Fold Surface

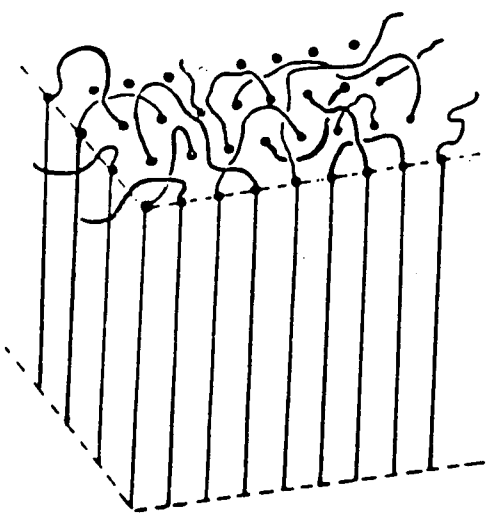
2.3.1. Nature of the Fold Surface

There has been considerable controversy about the nature of the fold surface structure. One extreme model explaining the fold surface structure is the adjacent re-entry (AR) model, which involves regular folding and was

proposed by Keller (1957). The other extreme model with irregular re-entry was proposed by Flory (1962), and is known as the "switchboard model" (Figure 5). This model was postulated primarily on the basis of space limitations at the crystal-liquid interface and the density defect nature of single crystals. In this model it was believed that folding exists, but that the molecule reenters the crystal somewhat randomly but predominantly in a non-adjacent manner. The fold surface would be very rough with loops of various lengths due to this random reentry, entanglements, etc.. Mandelkern's (1975) interzonal model is similar to the switchboard model. The outermost amorphous region sandwiches an interzonal one before passing into the ordered crystalline state of the crystal. In the AR model there are short, uniform and tight folds resulting in a regularly folded surface. The only possible defects are the ends of molecules which could either form as short length flexible rods (or cilia) above the folded surface or else fold back into the crystal. In the case of single crystals formed from mixtures of deuterated and normal hydrogen bearing polyethylene chains, Bank and Krimm (1969) were able to show conclusively through a detailed analysis of infrared spectra that the predominant type of folding involves re-entry of the emergent stem into an adjacent position on the crystal face. However, the existence of intercrystalline and lamellar links show that non-adjacent re-entry (NAR) must



a



b

Figure 5 Schematic representations of (a) the adjacent re-entry model and (b) the "switchboard model".

certainly occur to some extent in melt crystallized polymers. National Bureau of Standards (NBS) researchers have been the major contributors and supporters of the AR model. The researchers accept the mode of folding as "predominantly AR" with a probability of AR (p_{ar}) less than unity. Typically p_{ar} = 0.6 - 0.8 is claimed. Hoffman (1979) suggested p_{ar} = 0.3 - 0.5 could be possible under extreme conditions such as very high molecular weight and large undercoolings.

The assumption of AR is used in kinetic theories of polymer crystal growth in order to obtain a reasonably simple treatment. It is adequate for the prediction of growth rate and lamellar thickness for the case of crystallization from both the melt at low supercoolings and from dilute solution.

2.3.2. Arguments About the Fold Surface Structure

A summary of the issues which are the most controversial on the nature of fold surface are given below

Density: It is well established that polymer single crystals have densities below the X-ray value, determined from the unit cell dimensions. According to the switchboard model, the defect is attributed to the amorphous zone arising mostly from NAR on a large scale. In the AR model the density defect is attributed to surface roughness in the form of long loose folds ("loops").

Neutron Scattering: Neutron Scattering is an experimental tool which is based on elastic scattering of isotopically distinct guest molecules introduced in a host matrix. Since neutrons are scattered by nuclei, a proton scatters very differently from a deuteron. Therefore it is possible to study "solid solutions" of an isotopically labelled molecule in a chemically very similar matrix. Depending on the angular range of investigation, information on size, shape and trajectory of a single polymer molecule can be obtained. Small angle neutron scattering at very low angles gives the radius of gyration of the tagged molecules. Results on melt grown crystals showed that the radius of gyration is slightly smaller (ca 10%) after crystallization than in the melt. It has been suggested that the conformation of the molecule undergoes only minor adjustments as it goes from the molten to the crystalline state. Based on this observation, the supporters of the switchboard model (Flory and Yoon 1978) claimed that AR is mostly or entirely absent for the stems that are in the crystal. On the other hand Hoffman (1979) explained the liquid-like radius of gyration in semi-crystalline polymers as a result of the tie molecules and multiple nucleation of a molecule at distant points on the same lamella, even though a considerable fraction of stems in the crystal exhibit AR.

Mobility in the crystallizing melt: Yoon and Flory (1979) contended that the rates of molecular disentanglement were

not high enough to allow AR folding. Klein (1979) and DiMarzio (1979) pointed out that reptation increases the expected rates of rearrangements so that at least short sequences of AR folds should be possible. Reptation is a process first proposed by de Gennes (1971, 1976) and involves the motion of a polymer molecule along its length. Hoffman (1982) formally included the effect of reptation in the crystallization process, resulting in a reciprocal dependence of molecular weight on growth rate.

2.4. Secondary Nucleation Theory

In this dissertation, Lauritzen-Hoffman theory (Lauritzen and Hoffman 1973) is used to analyze the kinetic data because it is simple to apply, has a wide range of applicability and gives good correlation with experimental data. This section is essentially a summary of the review of Hoffman et al (1976) together with recent advances in some aspects of the theory.

2.4.1. Model

The model used is shown in Figure 6 where a, b ,l are the width, thickness and the height of the surface nucleus respectively. The height "l" is fixed at a specified undercooling, L is the crystal width, σ and σ_e are the lateral and fold surface free energies. The surface nucleus

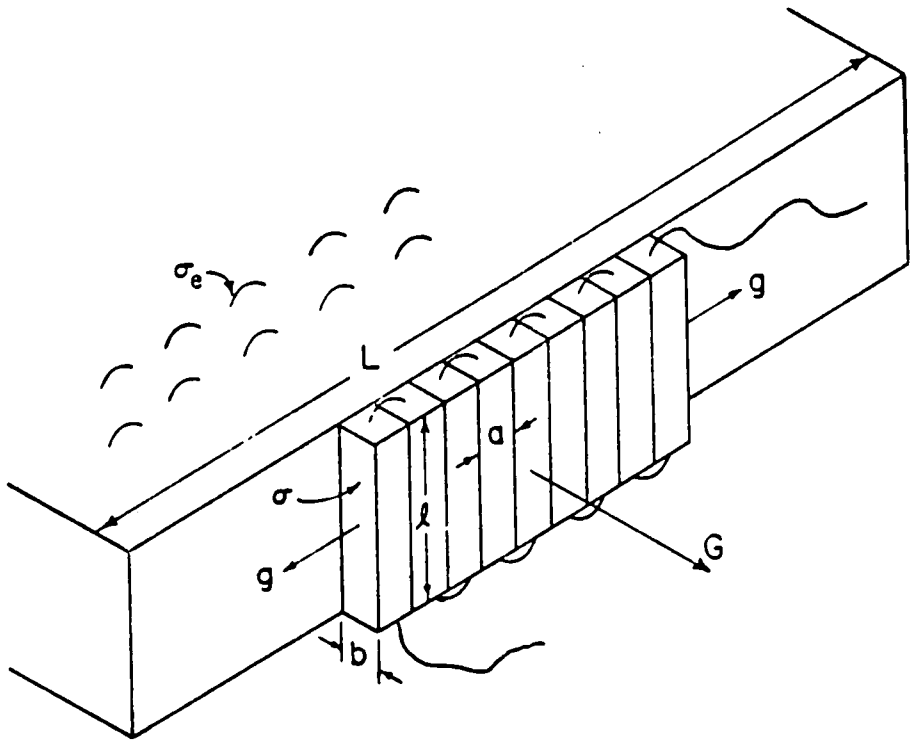


Figure 6 Idealized schematic model for polymer lamella crystal growth (from Hoffman et al. 1976).

grows along the "g" direction, however the measured growth is in the "G" direction. When v stems and $v_f = v - 1$ folds have been formed the free energy of formation is (ignoring the chain end effects)

$$\varphi_v = 2bl\sigma + 2v_f ab\sigma_e - vabl\Delta f \qquad (2.4.1)$$

for large the equation becomes

$$\varphi_v = 2bl\sigma + vab(2\sigma_e - l\Delta f) \qquad (2.4.2)$$

The surface nucleus is believed to start from a polymer segment or a set of segments, from the solution or undercooled melt, attaching itself to the crystal surface, and then coming into crystallographic register with the substrate forming the first stem at a cost $2bl\sigma$. The molecule then folds back on itself and starts to crystallize adjacent to the first stem. The adjacent position is the most probable site for re-entry after folding since attachment on a non-adjacent position will add a large extra term $2bl\sigma$. By repeating this act, a surface nucleus begins to approach the region of stability as it spreads in the direction "g". The surface nucleus goes through a maximum in its free energy of formation at or near the first stem ($v=1$) and then gradually approaches the region of stability as it increases in size (Figure 7). Thus here we have a set of

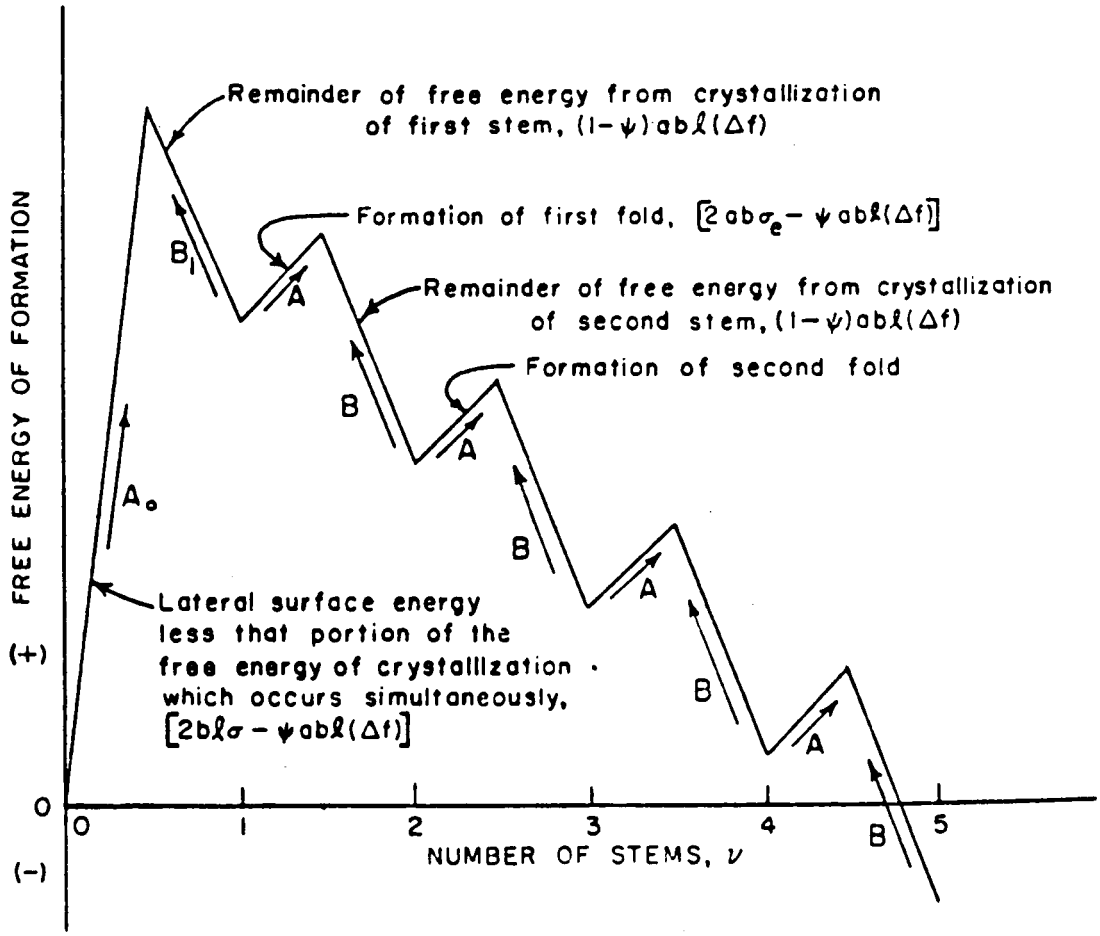


Figure 7 Free energy of formation of a chain folded surface nucleus (from Hoffman et al. 1976).

connected rate processes such that the rates of forward and backward reactions between the states $v=0$ and $v=1$ are A_0 and B_1 respectively. This corresponds in general to a nucleation controlled process where a large barrier resulting from creation of new surfaces must first be overcome to initiate the nucleus, with subsequent steps leading to the stable region.

2.4.2. Total Flux

The net flow of polymer from sites in the liquid ($v=0$) to the first stem of polymer in the nucleus ($v=1$) of a new layer of polymer crystals is designated as "S".

$$S = N_0 A_0 - N_1 A_1 \qquad (2.4.3)$$

N_0 and N_1 are the occupation numbers for $v=0$ and 1 respectively. The net rate of formation of nuclei of length "l" is;

$$S(l) = \beta N_0 \exp \{[-2bl\sigma + \psi abl\,(\Delta f)] / kT\}$$
$$x\ [1-\exp\{[-abl(\Delta f)-2ab\sigma_e]/kT\}] \qquad (2.4.4)$$

β is the retardation factor which accounts for retardations to molecular motion resulting from the fact that polymer molecules must be transferred to the site of crystallization. ψ is a fraction of the free energy of

fusion apportioned to the activation free energy of the forward reaction. The value of ψ may then be related to whether or not the polymer molecule is physically adsorbed on the surface prior to crystallographic attachment onto the substrate. Total flux ,S_T, is found by summing equation (2.4.4) over all possible values of 1. Assuming that possible values of 1 are increments of the monomer repeat length l_n, the summation can be replaced by the integral,

$$S_T = (1/l_n) \int_{2\sigma_e/(\Delta f)}^{\infty} S(1)dl$$

$$= N (\beta/l_n) p \exp(2ab\sigma_e \psi/kT) x \exp[-4b\sigma\sigma_e/(\Delta f)kT) \qquad (2.4.5)$$

where;

$$p = \frac{kT}{2b\sigma - ab(\Delta f)\psi} - \frac{kT}{2b\sigma + (1-\psi)ab(\Delta f)} \qquad (2.4.6)$$

2.4.3. Initial Lamellar Thickness

The average value of 1 is defined as the initial lamellar thickness l_g^* and is calculated from the flux according to

$$l_g^* = (1/l_n) \int_{2\sigma_e/(\Delta f)}^{\infty} 1\, S(1)dl \Big/ (1/l_n) \int_{2\sigma_e/(\Delta f)}^{\infty} S(1)dl \qquad (2.4.7)$$

and is found to be

$$l_g^* = \frac{2\sigma_e}{\Delta f} + \frac{kT}{2b\sigma} + \frac{[2 + (1-2\psi)a\,\Delta f] \,/\, 2\sigma}{[1-a(\Delta f)\psi/2\sigma][1+a(\Delta f)(1-\psi)/2\sigma]} \qquad (2.4.8)$$

The last term is "δl" which is seen to be a function of ψ. By setting $\psi=1$ it is found that

$$\delta l = \frac{kT}{2b\sigma} \times \frac{(4\sigma/a)-\Delta f}{(2\sigma/a)-\Delta f} \qquad (2.4.9)$$

It is seen from the denominator of equation (2.4.9) and the fact that $\Delta f = (\Delta h_f)(\Delta T) \,/\, T_m^o$ that δl becomes infinite at the critical undercooling, which is;

$$\Delta T_c = 2\sigma\, T_m^o \,/(\Delta h_f) \qquad (2.4.10)$$

which is referred to as the δl catastrophe. However no such catastrophe has actually been observed in experiments. Investigation of other ψ values e.g. $\psi=0$ gives;

$$\delta l = \frac{kT}{2b\sigma} \times \frac{(4\sigma/a) + \Delta f}{(2\sigma/a) + \Delta f} \qquad (2.4.11)$$

In this case there is no δl catastrophe and l_g falls continuously with temperature. It is noted that the temperature of the δl catastrophe is lowered as ψ is lowered. The value of ψ may be related to whether or not the polymer molecule is physically adsorbed on the surface prior to the actual crystallographic attachment. The condition where $\psi=1$ corresponds to the state where the polymer molecule goes directly from the undercooled melt onto the surface without an intermediate state. On the other hand, if the polymer molecule is physically adsorbed onto the surface prior to the crystallographic attachment, the lateral surface free energy will be incurred first. Then crystallographic attachment leading to the free energy of fusion will take place after a localized migration, leading to ψ values below unity. An example where ψ would equal zero corresponds to a weak adsorption from the undercooled melt between point contacts having a total separation that is just half the fold period, followed by surface migration and crystallographic attachment to the substrate, with simultaneous deposition of other units to complete the stem.

Both conditions $\psi=1$ and $\psi=0$ are regarded as extremes, and the case $1> \psi >0$ is expected in real polymers.

2.4.4. Retardation Factor

The retardation factor (β) accounts for retardations to molecular motion resulting from the fact that polymer molecules must be transported to the site of crystallization. The factor β contains effects resulting from viscosity and surface transport and is expressed in events per second. At low temperatures or very high undercoolings, polymer solutions become very viscous and the retardations may control the flux. Thus β is expected to be strongly dependent on temperature, especially at low temperatures. β can be considered to be the jump rate for local motion and is described as;

$$\beta = (kT/h)\ J_1\ \exp[-U^*/R(T-T_\infty)] \qquad (2.4.12)$$

The factor $\exp[-U^*/R(T-T_\infty)]$ is the temperature dependence of the segmental jump rate in polymers. The values of U^* and T_∞ can be obtained from the temperature dependence of bulk fluidity. The quantity U^* (activation energy for transport of the segments to the site of crystallization) is generally 10-15 % of 4100 cal/mole and T_∞ is usually within about 5-10 ^oK of being 50 ^oK below T_g, generating approximately universal values. However it is possible that the values of U^* and T_∞ applicable to the crystallization process need not be the same as those obtained from bulk fluidity. It was

suggested that this was because crystallization occurred from an adsorbed layer of macromolecules rather than directly from the bulk amorphous region (ψ<1 case). Using empirical values of U^* and T_∞ which are lower than the universal values, a better linear fit has been obtained for the kinetics data of some polymers. The procedure involves assuming a set of values of U^* and T_∞ and the fitting of $\ln G + U^*/R(T-T_\infty)$ to a linear relation in $1/T(\Delta T)f$. The values are then varied separately to maximize the correlation coefficient. This method is very similar to the one suggested by Suzuki and Kovacs (1970) in which the transport parameters are analyzed on the basis of the WLF equation (see section 2.6.). In this approach a reasonable value is given to U^* and then T_∞ is given successive values. The technique involves fitting of data to a straight line, the value of U^* at which linearity is found being calculated.

The term J_1 is inserted into equation (2.4.12) to allow for any barriers not explicitly accounted for by the exponential term. Compared to the exponential term the temperature dependence of J_1 is small, so J_1 will generally act as a pre-exponential factor that simply reduces β.

2.4.5. Free Energy of Fusion

In the expression for total flux, Δf, the free energy of fusion, is the driving force for crystallization. Near the melting point;

$$\Delta f = \Delta h_f - T\Delta S_f = \Delta h_f - T(\Delta h_f)/T_m^o$$

$$= \Delta h_f(1-T_m/T_m^o) \qquad (2.4.13)$$

Δh_f, is the heat of fusion per unit volume at the equilibrium melting point T_m^o and it can be assumed independent of temperature. However at low temperatures, the temperature dependence of Δh_f increases and a correction term ,f, is introduced

$$\Delta f = [\Delta h_f(\Delta T)/T_m^o]f \qquad (2.4.14)$$

The correction term given by Hoffman and Weeks (1962) is;

$$f = 2T/(T_m^o+T)$$

The source of f is the reduction in the heat of fusion with decreasing temperature.

2.4.6. Growth Rates

The growth rates associated with the model described in section 2.4.1, will depend on some function of the product of the net surface nucleation rate and the layer thickness.The polymer crystals can grow in three regimes denoted as I,II and III.

2.4.6.1. Regime I Growth

In regime I, the growth rate is considered to be nucleation controlled. In this regime, in the idealized

case, a nucleus is formed on the growing face and then a strip immediately grows and adds a layer on the face (Figure 8). The linear growth rate in this regime is proportional to the length of the face and is given as

$$G_I = biL = bLS_T/aN \qquad (2.4.16)$$

where N is Avogadro's number, b is the layer thickness, L is the substrate length and i is the net surface nucleation rate. Inserting S_T from equation (2.4.5) into the equation (2.4.16) gives;

$$G = G_0 \exp[-U^*/R(T-T_\infty)] \exp[-4\sigma\sigma_e/(\Delta f)kT] \qquad (2.4.17)$$

For bulk polymers, the factors which are not strongly dependent on temperature are gathered into the pre-exponential factor

$$G_{0(I)} = (kT/h)\, n_s\, J_1 \exp(2ab\sigma_e\psi/kT) \qquad (2.4.18)$$

2.4.6.2. Regime II Growth

In regime II multiple nuclei are formed on the face and the linear growth rate is proportional to the geometric mean of the nucleation rate and the strip growth rate

$$G_{II} = b\,(ig)^{1/2} = b(S_T g/aN)^{1/2} \qquad (2.4.19)$$

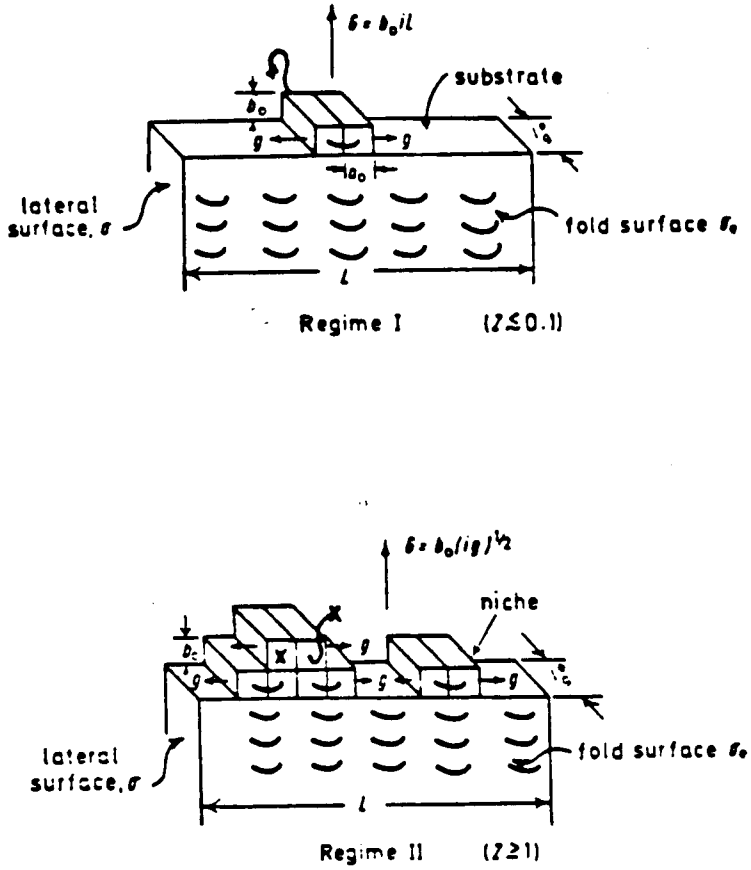


Figure 8 Regime I, Regime II and Regime III crystallization (schematic).

which leads to

$$G = G_0 \exp [-U^*/R(T-T_\infty)] \exp (-2b\sigma\sigma_e/(\Delta f)kT) \quad (2.4\ 20)$$

where G_0 equals

$$G_0 = b\ (kT/h)\ J_1 \exp [\ ab\sigma_e(2\psi\ -1)/kT] \quad (2.4.21)$$

The ratio of G_0 values for regimes I and II is

$$G_{0(I)}\ /G_{0(II)} = n_s \exp(ab\sigma_e/kT) \quad (2.4.22)$$

$$G_{0\ (I)} >> G_{0\ (II)}$$

2.4.6.3. Regime III Growth

In regime III, nucleation becomes so rapid that nuclei are formed even on partially grown strips, and hence the growth rate is again proportional to the nucleation rate. In this case the crystal-liquid interface is rough. In this regime niche separation eventually approaches the molecular width "a". The growth rate for regime III is

$$G_{III} = biL' = bin_s a = bLS_T/aN \quad (2.4.23)$$

where, L'is the effective substrate length, and n_s is the mean number of stems that are laid down in the niche adjacent to the newly nucleated stem.

The linear growth rate in regime III is;

$$G_{(III)} = G_{0\ (III)}\ [-U^*/R(T-T_\infty)]\ \exp[-4b\sigma\sigma_e/(\Delta f)kT] \quad (2.4.24)$$

$$G_{0(III)} = b[(kT/h)n_s'](2ab\sigma_e/kT) \quad (2.4.25)$$

and $$G_{0(I)} / G_{0(III)} = n_s/n_s' = n_s/3 \quad (2.4.26)$$

for polyethylene $n_s = 2.42 \times 10^2$ which yields

$$G_{0(I)} / G_{0(III)} \approx 80$$
$$G_{0(III)} / G_{0(II)} \approx 1.2 \times 10^5 \quad \text{(Hoffman 1983)}$$

The regime II-III transition has been reported for a number of polymers. The growth rate data of Pelzbauer and Galeski (1973) on polyoxymethylene, the work of Dalal and Phillips (1984) on cis-polyisoprene and some studies on polypropylene (Clark and Hoffman 1984), polyphenylene sulphide (Lovinger and Davis 1985) indicated regime II-III transitions in these polymers.

2.4.7. Regime Test

The growth rate equation for the three different regimes has the general form

$$G = G_0 \exp [-U^*/R(T-T_\infty)] \exp [-K_g/T(\Delta T)f] \qquad (2.4.27)$$

where for regimes I and III

$$K_g(I), (III) = 4b\sigma\sigma_e T_m^o/(\Delta h_f)k \qquad (2.4.28)$$

and for regime II

$$K_g(II) = 2b\sigma\sigma_e T_m^o/(\Delta h_f)k \qquad (2.4.29)$$

Therefore a plot of log $G + U^*/R(T-T_\infty)$ against $1/T(\Delta T)$ (Figure 9) will have the same slope for regimes I and III which is twice that of regime II.

To differentiate regime I from regime II Lauritzen (1973) and Lauritzen and Hoffman (1973) suggested a dimensionless parameter ,Z, defined as;

$$Z = iL^2/4g \qquad (2.4.30)$$

In regime I

$$Z = iL^2/4g = (L/2a)^2 \exp(2ab\sigma_e/kT) \exp(-K_g/T\Delta T) \qquad (2.4.31)$$

and $Z \leq 0.01$

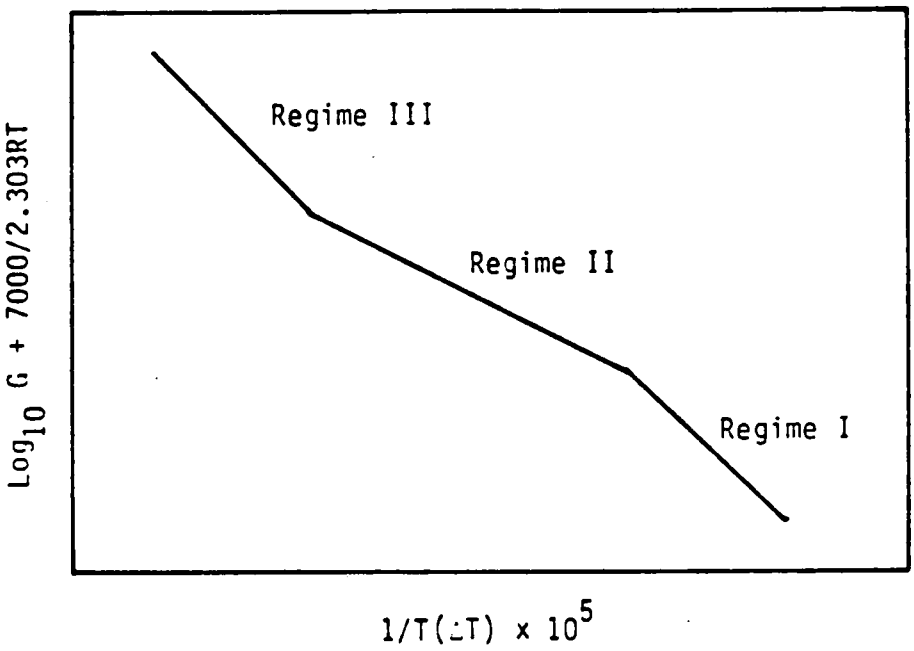


Figure 9 Schematic representation of logG + U^*/2.3 RT against 1/T(ΔT) for regimes I,II and III.

In regime II

$$Z = (L/2a)^2 \exp[2ab\sigma_e(1+\ )/kT] \exp(-2K_g/T\Delta T) \qquad (2.4.32)$$

$$\text{and} \quad Z \geq 1$$

In this procedure first the growth rate data is analyzed to determine K_g. Then using equations (2.4.31) and (2.4.32) with a known value of K_g, it is possible to estimate the range of values of L that are consistent with regime I or regime II behavior. The value of L must be in accord with morphological information. If the above equations give unacceptable values of L for one regime and realistic ones for the other a clear choice can be made between them.

In a recent paper of Hoffman (1985) a model for the physical origin of the substrate length "L" was proposed. L is treated as the persistence length between defects which have a capacity to inhibit surface completion. He concluded that there are three requirements for a regime I-II transition to occur. 1) The chain being flexible enough to form a small amorphous defect at the edge of the substrate 2) Having an equilibrium defect concentration prior to the formation of a new layer and 3) Impinged or stabilized defect of critical size, having a long lifetime. Absence of these requirements was expected to cause a tendency for a gradual reversion to mixed regime I and regime II or even only regime II kinetics above the I-II

transition point. A similar tendency has also been proposed by Goldenfeld (1983,1984). He refers to regime II as a steady state and points out that the kinetics of solution grown crystals are always driven towards regime II.

The subject of regime reversion in relation to our experimental data will be discussed in more detail in the discussion section.

2.4.8. Limitations and Criticisms

LH theory assumes AR (all successive stems belong to the same molecule), but this is desirable simply in order to reduce the calculations to a manageable form. In reality the probability of AR is normally expected to be less than one. The theory does not include the effects of a departure from strict AR. In the case of extended chain crystallization, which involves few or no folds, LH theory is inadequate because of the lack of AR and a large number of folded stems.

Point and Kovacs (1979) extended the LH theory for low molecular weight extended chain crystals of polyethyleneoxide (PEO) and claimed that nucleation theory breaks down for this case because it results in a lateral surface free energy ,σ, which is chain length dependent. However σ values were not too different from the expected ones at high undercoolings where PEO chains undergo several folds. Hoffman (1979) has pointed out that each molecule

folds several times (at least three) and the data of Point and Kovacs are consistent with the theory.

Another limitation of LH theory is the constant fold period. In the theory it is assumed that, a fold plane once nucleated will grow with a constant fold period. This has been found too strict and questioned by Frank and Tosi (1961), Price (1961) and by Lauritzen and Passaglia (1967). The theory postulated by Lauritzen and Passaglia (1967) takes all possible fold periods into account but fails since it predicts that δl increases catastrophically as T reaches a high critical undercooling.

Recently Sadler (1983,1984,1985,1986) has developed a model for polymer crystallization which explains the crystal growth faces as being molecularly rough because of equilibrium effects. The proposed mechanism is described as "continuous growth onto rough growth faces". He claims that the existing theories for polymer crystallization neglect the possibility of a surface entropy term which may lead to rough growth surfaces. According to his model the primary cause in determining the growth rate is pinning on a roughened surface, not nucleation or step creation. The pinning points are places on the crystal boundary where addition and removal of chain units cannot take place. These restrictions are superimposed on the usual addition and removal probabilities which follow the appropriate rate constants. The consequence of pinning and the shorter stems

at the growth face is a high free energy process necessary for the net advance of the crystal. He then concludes that for conditions where σ_e is not large the model could involve pinning rather than nucleation, since the process involving pinning is what primarily controls the growth.

2.5. Melting of Polymer Crystals

The lamellar structure of crystalline polymers influences the properties in a number of ways. The wide melting range of polymers unlike other materials is mainly attributed to variations in the lamellar thickness.

2.5.1. Thermodynamic Considerations

Considering a single lamellar polymer crystal (Figure 2, p.13), the free energy of formation can be written as;

$$\Delta\varphi = 2(a+b)l\sigma + 2ab\sigma_e - abl\Delta f \qquad (2.5.1)$$

where a,b are the lateral dimensions, l is the crystal thickness, and Δf is the bulk free energy of fusion. Since a>>l and b>>l, the first term in equation (2.5.1) may be neglected.

At the melting temperature ,T_m, $\Delta\varphi = 0$. Using this condition and equation (2.4.14) one obtains;

$$T_m = T_m^o \left[1-(2\sigma_e/\Delta h_f l)\right] \qquad (2.5.2)$$

where T_m^o is the equilibrium melting point and Δh_f is the heat of fusion per unit volume of the crystal. According to equation (2.5.2) a plot of T_m versus $1/l$ must be linear with an intercept equal to T_m^o. The value of σ_e can be determined from the slope.

2.5.2. Kinetic Considerations

LH theory predicts that the average lamellar thickness achieves a final value at the end of a crystallization experiment that is γ times larger than the the initial lamellar thickness l_g^*.

$$l = \gamma l_g^* \qquad \gamma>1 \qquad (2.5.3)$$

Combining this equation with equation (2.4.8) and substituting for Δf from equation (2.4.13) yields;

$$l = \frac{2\sigma_e T_m^o}{\Delta h_f \Delta T} + \gamma l \qquad (2.5.4)$$

$(2\sigma_e/\Delta f) >> \delta l$ is a simplifying approximation which seems reasonable for crystals formed at low undercoolings. Then we have

$$T_m = T_m^o - (\Delta T/\gamma) \qquad (2.5.5)$$

The expression suggests that the melting point of a polymer

that has thickened by a factor γ during the crystallization process at T_c(crystallization temperature) is approximately a linear function of its temperature of crystallization.

2.6. The Glass Transition

An amorphous polymer or (the amorphous part of a crystalline polymer) undergoes a glass transition which is manifest in drastic changes in many of its physical properties. On a molecular scale the glass transition is associated with cooperative motion of large chain segments. This motion takes place above the glass transition temperature (T_g) where the material is liquid-like, below T_g large scale cooperative molecular motions are frozen in. The glassy state may be considered as a supercooled liquid. Some theories of the glass transition are based on free volume concepts, others follow either a thermodynamic approach based on entropy calculations, or a kinetic approach, based on relaxational phenomena which accompany the glass transition. Thermodynamic theories consider the glass transition as a second order transition having equilibrium properties whereas kinetic theories consider the glass transition as a rate phenomenon. In this section only WLF theory which is a semi-empirical free volume treatment of relaxation phenomena near T_g will be discussed because of its direct relevance to the analyses of kinetic data.

Williams, Landel and Ferry (1958) have shown that for a variety of amorphous polymers there is a universal relation relating the horizontal shift factor ,a_T, to the temperature. This relation holds at temperatures from T_g to T_g+100 ^oC and is given as;

$$\log a_T = - \frac{c_1(T-T_g)}{c_2 + T-T_g} \qquad (2.6.1)$$

where c_1 and c_2 do not generally vary from one polymer to the other in a major way and have been regarded as universal constants with values of 17.4 and 51.6. In practice, however, each polymer will have its own individual values of c_1 and c_2. In fitting of kinetics data it is important to use individual values wherever available. Although the WLF equation is empirical in nature, its general form can be obtained from free volume considerations. Below T_g the fractional free volume (f) is considered to be constant at a value f_g

$$f = f_g + (T-T_g)\Delta\alpha \qquad (2.6.2)$$

where $\Delta\alpha$ is the difference in expansion coefficients above and below T_g. As the free volume is decreased, say by cooling, molecular motion becomes more difficult. Doolittle (1951) assumed a linear relation between the logarithm of

viscosity and the inverse free volume leading to the equation;

$$\ln a_T \approx \ln \frac{\eta}{\eta_g} = \frac{1}{f} - \frac{1}{f_g} \qquad (2.6.3)$$

Upon substituting equation (2.6.3) into equation (2.6.2) we obtain

$$\log a_T = - \frac{c_1(T-T_g)}{c_2 + T-T_g} \qquad (2.6.4)$$

where $c_1 = 1 / 2.3\, f_g$ (2.6.5)

and $c_2 = f_g / \Delta\alpha$ (2.6.6)

According to the equations (2.6.4) - (2.6.6) the fractional free volume at T_g is approximately 0.025 and the change in expansion coefficients is 0.00048 /^{o}C which are in reasonable agreement with many glass forming polymers.

2.7.Effect of Molecular Weight

Molecular weight and molecular weight distribution are important variables in polymer crystallization. Rate of crystallization, degree of crystallinity and melting temperature are all affected by molecular weight.

The effect of molecular weight on crystallization on a number of polymers has been studied by several groups.

Ergoz et.al. (1972) studied the crystallization of polyethylene fractions. They found that at a fixed crystallization temperature, the crystallization rate goes through a maximum as a function of molecular weight. The location of the maximum depended on the undercooling. They also showed that the maximum degree of crystallinity attainable decreased as molecular weight was increased. In an earlier study, Mandelkern et al. (1967) analyzed data on polyethylene fractions and found a dependence of σ_e(interfacial free energy) on molecular weight. As molecular weight was increased, the interfacial free energy of crystallites increased. They suggested that the change in σ_e with molecular weight indicated a change in interfacial structure with increasing molecular weight. The dependence of molecular weight on melting temperature of polyethylene fractions was also studied by Fatou and Mandelkern (1965). An asymptotic value of 138.5^{o}C for the melting temperature was obtained.

The kinetics of spherulitic growth of poly(phenyl-p-silphenylene) siloxane (TMPS) (Magill 1964) was studied at different crystallization temperatures as a function of molecular weight. Increasing growth rates with decreasing molecular weight were observed. The positions of crystallization maxima were unchanged for different molecular weight fractions. He reported that the pre-exponential term ,G_o, showed a rising trend in the molecular

weight range 8,000 - 430,000. Van Antwerpen and Van Krevelen (1972) have worked on polyethylene terephtalate (PET) fractions and reported a linear relationship between G_o and reciprocal number average molecular weight in the range of 19,000 - 39,000.

Devoy and Mandelkern (1969) analyzed the available kinetic data for polyethylene, TMPS and trans-1,4 polyisoprene and reported that G_o is constant for different molecular weights. They explained this as follows: G_o should depend only on the short range structure of the amorphous polymer and be independent of molecular weight above a critical low value. They described the molecular weight dependence through a molecular weight dependent nucleation term.

Hoffman et al. (1975) examined different molecular weight fractions of polyethylene. Two morphologies were apparent for the intermediate molecular weight fractions over the crystallization range. At large undercoolings, spherulites were found, but at higher crystallization temperatures, growth was axialitic in nature. The transition occurred at around 127^{o}C. The change in morphology has been ascribed to a change in growth mechanism associated with the rate of production of surface nuclei. These two modes of growth, termed regime I and II were described in section 2.4.6 in detail. The regime I-II transition temperature was found to be molecular weight dependent and shifted towards

higher temperatures as the molecular weight was increased in the range from 18,000 to 115,000. For fractions with molecular weights higher than 115,000, only spherulitic regime II growth was observed whereas for low molecular weight fractions (3,600 to 18,000) axialitic regime I growth was feasible.

Recently Hoffman (1982) has formally included the role of reptation in kinetic nucleation theory and tested the approach for linear polyethylene fractions crystallized both in regime I and regime II. Reptation is a process involving the motion of a molecule along its length and was originally suggested by de Gennes (1976). When the theory of polymer crystallization with chain folding is extended to include the effect of reptation, a molecular weight dependence of the overall growth process can be obtained. The general result of the reptation approach is a lowering of the observed growth rate with increasing molecular weight for both regimes.

2.8. Effects of Pressure

2.8.1. Morphology

The effects of pressure on polymer crystallization have been studied by few groups. For sufficiently high pressures, extended chain crystals were reported for polyethylene. These crystals have higher densities, melting

points and lamellar thicknesses than those of normal chain folded crystals. Geil et al. (1962), reported the morphology of polyethylene samples which were melt crystallized under pressure. These samples showed little or no folding. Bassett and Turner (1972), reported a new hexagonal liquid crystalline high pressure phase as existing under those conditions which permitted chain extended polyethylene (CEPE) formation. A phase diagram was constructed from the experimental results of melting peak temperatures of CEPE samples. Bassett (1974) showed that at lower pressures orthorhombic polyethylene is in equilibrium with the melt. At higher pressures and temperatures the fully extended polyethylene crystallizes passing through an intermediate phase which was shown to be hexagonal in nature.

Chain extended lamellae have not been observed in cis-polyisoprene, although a disordered high pressure phase was reported by Edwards and Phillips (1975). At pressures up to three kilobar, three modes of crystals namely, single crystals, spherulites and oblate spheroids were reported.

Tseng and Phillips (1984) investigated the effect of pressure on the morphology of LPE. The pressure crystallized LPE specimens were reported to show banded spherulites below 3.5 kilobars and extended chain crystals above 3.5 kilobars.

2.8.2. Crystallization Kinetics

The work of Phillips and Edwards (1975 a-b, 1976, 1980) was the first and only source of extensive crystallization kinetic data at high pressures. They obtained linear growth rate data for cis-polyisoprene at high pressures ranging from atmospheric pressure to four kilobars. The application of pressure resulted in moving the bell shaped isobaric growth rate curves to higher temperatures and in increasing the maximum growth rate over the first 1.5 kilobar. The analyses of high pressure kinetics data indicated a large and sudden increase in the fold surface free energy (σ_e) with pressure which was attributed to a pressure induced change in fold conformation.

The effect of pressure on crystallization kinetics of trans-polyisoprene was investigated by Davies and Cucarella (1980 a-b). In contrast to the work on cis-polyisoprene, the maximum growth rate of trans-polyisoprene decreased continuously with increasing pressure, which was attributed to a decrease with pressure of the temperature range (T_m^o-T_∞) available for crystallization.

In the work of Tseng (1984) the linear growth rates of LPE and PET at various pressures were determined using the laser light scattering technique. Analyses of growth rate data in terms of the LH nucleation theory

yielded a possible regime II-III transition in PET. Fold surface free energy ,σ_e, of PET was found to increase drastically with pressure which may be due to a significant amount of loose folds and NAR present. On the other hand σ_e of polyethylene was found to be independent of pressure up to two kilobars which implies that the structure of the folded surface does not change i.e. tight folds with AR. Pressure dependence of the regime I-II transition in polyethylene was found to parallel the pressure dependence of the equilibrium melting point, indicating that the transition is thermodynamic in origin.

2.8.3. Melting Temperature

The effect of increasing pressure is to increase the equilibrium melting point. By the Clapeyron equation the melting point at pressure ,p, in atmospheres, is given by

$$(T_m^o)_p = (T_m^o)_{1atm} \exp\{[(V_a-V_c)/\Delta h_f] (p-1)\} \qquad (2.8.1)$$

where: V_a , V_c are the specific volumes of amorphous and crystalline material. Δh_f is the heat of fusion of the polymer. According to equation 2.8.1. T_m^o is a steep function of pressure.

The effect of pressure on the melting points of trans 1-4 polyisoprene (Davies and Cucarella 1980 a-b) and of several polyamides (Gogolewski and Pennings 1977 a-b) have been reported. A linear increase in melting temperature with applied pressure has been noted which is 15°C per kilobar for trans 1-4 polyisoprene and 16°C per kilobar for nylon-6. Baer and Kardos (1965) also studied the influence of pressure on the melting response of various polymers. For the polymers they studied, increases in both the melting temperature and the melting range observed with increasing pressure. Dalal (1983) obtained melting temperature data at pressures up to 2.6 kilobars for cis-polyisoprene by using an optical turbidimetric technique. The plots of crystallization temperature versus melting temperature were linear and shifted to higher temperatures with increasing pressure. Equilibrium melting points at each pressure were obtained from the extrapolation of these plots.

2.8.4. Glass Transition Temperature

The glass transition temperature increases approximately linearly with pressure. According to free volume theories of crystallization in which the glass transition is considered as an isofree volume state (Fox and

Flory 1950) the change of glass transition temperature with pressure is given as:

$$dT_g/dP = \beta_f/\alpha_f = \Delta\beta/\Delta\alpha \qquad (2.8.2)$$

where β_f ,α_f are the free volume compressibility and expansion coefficients. $\Delta\beta$ and $\Delta\alpha$ are the difference between liquid and glass compressibilities and expansion coefficients respectively. The subscript ,f, denotes a constant free volume.

The thermodynamic theories assume the glass transition to be a true second order transition possessing equilibrium properties (Gibbs and DiMarzio 1958). The change of a second order transition temperature with pressure is given by the Ehrenfest relations.

$$dT_2/dP = \Delta\beta/\Delta\alpha = (TV\Delta\alpha)/\Delta C_p \qquad (2.8.3)$$

Goldstein (1963) has pointed out that the above relations will be valid if a single ordering parameter is sufficient to characterize the excess thermodynamic properties of the liquid over those of the glass. If more than one parameter is required then,

$$dT_g/dP = \Delta\beta/\Delta\alpha \qquad (2.8.4)$$

In this case , excess volume determines T_g (as in the free volume theories). In the case of either excess entropy or enthalpy determines T_g, the relation is:

$$dT_g/dP = (T_g V \Delta\alpha)/\Delta C_p \qquad (2.8.5)$$

ΔC_p is the difference in specific heats between the glass and the liquid at the transition.

O'Reilly (1962) has tabulated the empirical values of dT_g/dP for several polymers. For the polymers listed, dT_p/dP ranges between 0.016 ^oC /atm. for polyvinylchloride (PVC) and 0.044 ^oC /atm. for polycarbonates, with most of the values around 0.024 ^oC /atm.

Since it is assumed that the glass transition occurs at a constant value of the fractional free volume, the glass transition parameter c_1 is independent of temperature and pressure as is clear from the equation

$$c_1 = 1/f_g$$

The other constants c_2 and T_∞ by definition are independent of temperature, but vary with pressure. The change of c_2 with pressure can be determined using the following equation:

$$\log v_m(T,P) = \log v_o - [c_1 c_2(P)] / [T - T_\infty(P)] \qquad (2.8.6)$$

where ν_m is the frequency corresponding to a dielectric loss maximum at a temperature T and pressure P.

3. EXPERIMENTATION

3.1. Material Preparation and Characterization

3.1.1 Preparation of Dilute Solutions

The polymer, used in almost all experiments was a form of natural rubber, known as "Hevea Rubber" (cis-polyisoprene). The material was cut from a large block of pale crepe obtained from the Rubber Research Institute of Malaya, Kuala Lumpur, Malaysia.

The second polymer used was also a form of natural cis-polyisoprene known as "Guayule Rubber". The main difference between these two polymers is the presence of long chain branches in the hevea rubber, which also contains natural antioxidants. Guayule rubber contains linear chains and is susceptible to oxidation having no natural antioxidants.

Prior to any use, both of the rubbers were cut into small pieces and purified with acetone on a soxhlet apparatus for 24 hours to remove soluble organic impurities. The extracted material was dried in a vacuum oven at room temperature for 48 hours. Following the drying process the rubber was transferred to a flask and hexane was added so as to produce one to two percent rubber by weight. This dilute polymer solution was allowed to homogenize for three days

with the aid of a magnetic stirrer. Butyl hydroxy toluene (BHT) was added as an antioxidant. This solution was filtered through a very coarse filter paper to remove some of the gel particles. Finer filtration was then carried out using medium and fine filter papers respectively by employing vacuum filtration. In hevea rubber, the gel content is close to 50 percent, whereas in guayule rubber it is only a few percent. During the whole procedure, rubber solution was always kept away from light and oxygen, by wrapping the container with aluminum foil, using glass joints and nitrogen atmosphere whenever feasible.

3.1.2. Molecular Weight Fractionation Studies

Most polymers have a broad molecular weight distribution. Fractionation is an experimental procedure by which the whole polymer is separated into different molecular weight fractions with narrower molecular weight distributions.

In this study fractionation by non-solvent addition was used. The fractionation apparatus used is shown in Figure 10 and consisted of: (1) a mechanical stirrer, with 55 watt power, non-sparking motor, the speed being controlled through a variable transformer, connected to the stirrer; (2) burette, by which non-solvent was added gradually; (3) thermometer; (4) constant temperature water bath; (5) fractionation flask; (6),(7) nitrogen stream inlet

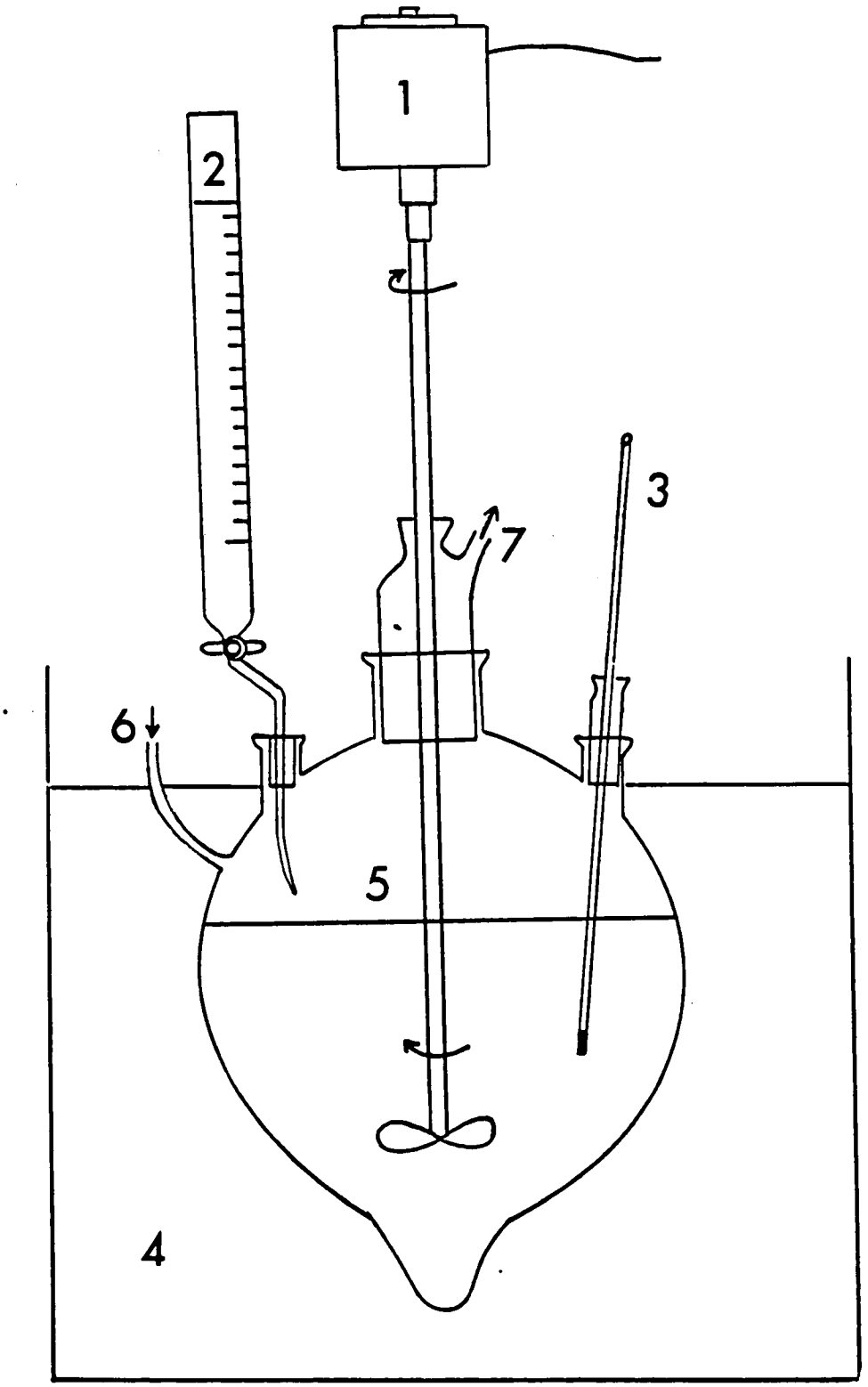


Figure 10 Fractionation apparatus

and outlets respectively. For the fractionation of hevea rubber one liter of dilute polymer solution (about one percent by weight) was prepared as described in section 3.1.1.. This solution was then placed in a three-necked flask of two liter capacity (5). The whole system was kept at a constant temperature of 26^{o} C in a water bath (4) which was covered with black paper to exclude light. The solution was purged with nitrogen gas to produce an inert atmosphere and stirred mechanically (1) during the dropwise addition of 1-propanol which was used as the non-solvent. When the solution attained a milky appearance, the addition of 1-propanol was stopped and the precipitated polymer was allowed to sediment overnight or for several days as necessary. The precipitated phase was separated from the supernatant liquid, by siphoning off the latter. The first precipitated phase is the highest molecular weight fraction and was collected by dissolution in a small amount of hexane. The solution obtained in this way was dropped into a large amount of non-solvent to reprecipitate the fraction as a solid, which was collected and dried to constant weight at room temperature in a vacuum oven. The fractionation process was continued by treating the separated supernatant liquid with a further volume of non-solvent. Subsequent fractions with decreasing molecular weights were obtained by repeating the steps described above.

3.1.3. Intrinsic Viscosity Studies

Viscosity average molecular weights of the fractions were measured by using a Cannon-Ubbelohde four bulb shear dilution type viscometer. First, 0.1 percent solutions of each fraction in tetrahydrofuran (THF) were prepared and filtered through a 0.5 micrometer filter. Filtration was carried out by using a 0.5 micrometer teflon membrane in a holder. The chemically resistant, disposable holder was mounted on the end of a syringe and fast pressure filtration carried out using the aforementioned hand pump system. After filtration, exact concentrations of the solutions were measured by residual weight after drying a measured volume of solution. In a typical viscosity average molecular weight determination, the following steps were followed:

1- A measured volume of solution (about ten mililiters) with a known concentration was loaded into the reservoir of the viscometer.

2-The viscometer was placed into a constant temperature water bath at 25 ^{o}C and the sample allowed 20 minutes to come to the bath temperature.

3- The efflux time for each of the four bulbs was measured to the nearest 0.1 seconds. The viscosity of the sample was calculated by multiplying the efflux time by the viscometer constant.

5- The shear rate at the wall for each bulb was calculated by dividing the shear rate constant by the flow time in seconds.

6- The calculated viscosities were extrapolated to zero shear rate.

7- The sample was then diluted adding a measured quantity of solvent from a pipette and all above steps were repeated for at least four different concentrations and for the pure solvent.

8- The viscosities at zero shear rate, for different concentrations (η) were analyzed to determine the intrinsic viscosity. The intrinsic viscosity [η] was evaluated from the intercept of the plot $(\eta - \eta_o) / c$ vs c at c=0. Where η_o is the viscosity of the pure solvent and c is the concentration of the polymer solution

9- The intrinsic viscosities were converted to molecular weights (M) using the Mark-Houwink equation:

$$[\eta] = K \bar{M}^a \qquad (3.1.1)$$

where "K" and "a" are the constants which were given as 1.09×10^{-4} and 0.79 respectively for cis-polyisoprene in THF at 25 ^{0}C (Subramaniam, 1971). The viscometer constant and shear rate constant for each bulb was given in the Certificate of Calibration sheet supplied with the viscometer.

3.1.4. Gel Permeation Chromatography

Gel Permeation Chromatography (GPC) is a form of solid/liquid chromatography that sorts molecules according to their sizes in solution. The solution of polymer to be analyzed is introduced at the top of the column and then is eluted with solvent. Separation occurs as the polymer molecules in the solvent mobile phase flow through a packed column of porous gel (stationary phase) and diffuse into or out of the pores of the packing. The packing itself has a pore size distribution such that different molecular size species permeate the gel particles to a different extent. The solution emerging from the bottom of the column is detected by a differential refractometer coupled to a recording chart, on which molecular size versus elution volume is plotted.

In this study a Waters Associates Gel Permeation Chromatograph was utilized. The tests were carried out at room temperature with THF as the solvent. Styragel columns with porosities 10^6, 10^5, 10^4 and 10^3 ^oA were used. Toluene was first tried as the carrier solvent since it is a good solvent for rubber and is stable. However the refractive index increment between toluene and natural rubber is small. Thus no satisfactory GPC curves were obtained. THF was subsequently used and better results obtained. In a typical run 0.5 percent rubber solutions were prepared and the

residual microgel was eliminated by forcing each sample through a 0.5 micrometer teflon filter in a holder. Exact concentrations of rubber solutions were determined by residual weight after drying.

Calibration data from which the molecular size of the eluted samples were calculated was constructed by using narrow molecular weight distribution polystyrene (PS) standards. The molecular weights of the PS standards used were 3 100 , 7 600 , 13 000 , 34 500 , 68 000 , 115 000 ,233 300, 600 000 and 1 800 000 grams/mole. It is known that the retention volume depends on the product of intrinsic viscosity and molecular weight in solution irrespective of the chemical nature of the polymer. A given column system at a specified temperature and solvent, may then be calibrated by means of PS standards and this calibration curve can be transformed to give a relationship between the elution volume and molecular weight of other polymers. The relationship for two chemically different polymers identified by subscripts 1 and 2 may be expressed as follows:

$$V_R = f(M_1[\eta]_1) = f(M_2[\eta]_2) \qquad (3.1.2)$$

hence

$$M_1[\eta]_1 = M_2\,[\eta]_2 \qquad (3.1.3)$$

The relationship between intrinsic viscosity and molecular weight is given by the Mark- Hownik equation. [η] is the intrinsic viscosity, M is molecular weight, and V_R is elution volume. Substitution of Eq.(3.1.1) in Eq. (3.1.3) and taking the logarithms yields the following:

$$\log M_2 = \left(\frac{1}{1+a_2}\right) \log \frac{K_1}{K_2} + \frac{1+a_1}{1+a_2} \log M_1 \qquad (3.1.4)$$

By using this equation, the molecular weight of any polymer can be calculated from the calibration curve of another polymer. The following relations were used in this investigation: In THF at 25° C for polystyrene

$$[\eta] = 1.2 \times 10^{-4} \times M^{0.71} \qquad (3.1.5)$$

and for rubber

$$[\eta] = 1.09 \times 10^{-4} \ M^{0.79} \qquad (3.1.6)$$

(Edwards B.C. et al., 1980)

The conversion of the chromatogram data to molecular weight values was done by measuring the chromatographic height, H_i, at selected values of elution volume. Then these elution volumes were related to molecular weight, M_i, by the calibration curve. For each M_i, the value of weight fraction, w_i, is evaluated by the equation

$$w_i = [H_i / \Sigma H_i] \qquad (3.1.7)$$

The number and weight average molecular weights ($\bar{M}_n$ and $\bar{M}_w$ respectively) were calculated by using the following equations:

$$\bar{M}_n = [1/(\Sigma w_i / M_i)] \qquad (3.1.8)$$

$$\bar{M}_w = \Sigma w_i M_i \qquad (3.1.9)$$

and $$\text{Polydispersity} = [\bar{M}_w/\bar{M}n] \qquad (3.1.10)$$

GPC measurements for higher molecular weight fractions could not be carried out because of their persistent microgel content even after filtration through 0.5 micrometer filter, which clogged the GPC columns.

3.2. Atmospheric Pressure Crystallization Studies

3.2.1. Specimen Preparation

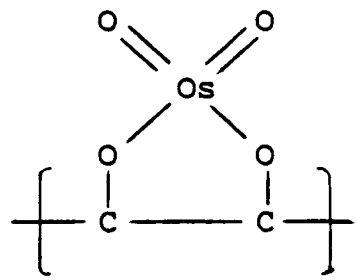
Thin films of natural rubber for transmission electron microscopy (TEM) were prepared by casting a drop of approximately two percent solution onto a grease free distilled water surface. The water surface was created in a petri dish forming a high meniscus to give the needed

surface tension for the drop to spread. After the drop spreads a liquid film forms which rapidly evaporates, leaving behind a thin polymer film on the water surface. The appropriate thickness for microscopy was judged from interference of colors. Golden colored regions have the right thickness (80 - 100 nm) for TEM studies (Peachey 1958). This is the optimum thickness which is as thin as possible for the maximum resolution and contrast and is thick enough to have mechanical stability. The film from this region was collected on 3.0 mm , 400 mesh copper electron microscope grids. The grids were supported by wire gauze filters made of stainless steel and were placed on the bottom surface of the film. The holders containing grids were then vacuum dried to remove excess solvent and water for 20 minutes. Later these grids, covered with thin polymer film were crystallized at preset temperatures ranging from -40^{o} C to $+3^{o}$ C for different periods of time.

3.2.2. Osmium Tetroxide (OsO_4) Staining

Since room temperature is above the melting point of natural rubber spherulites, the crystalline morphology needs to be fixed after the desired crystallization time elapsed. Unsaturated rubbers may be stained selectively by exposure to OsO_4 vapors. This technique yields detailed electron micrographs and was developed by Andrews in the early 1960's (Andrews 1964). The technique is based on the

reaction between OsO_4 and carbon-carbon double bonds producing a complex of the type (Hobbs 1980)



By this fixation technique, the amorphous part of the rubber is stained while the crystalline part is not, due to the difficulty of penetration of a bulky molecule such as OsO_4 into the crystalline regions. Therefore differences between the crystalline and amorphous parts of a specimen are accentuated by staining which also converts the amorphous phase into a glass enhancing the mechanical stability of the film and preventing further crystallization. The penetration is such that the gas can reach in between lamellae permitting lamellar resolution.

OsO_4 crystals were supplied in 0.25 gram glass capsules by Stevens Metallurgical Corporation. These capsules were broken very carefully and placed in a glass jar containing drierite ($CaSO_4$ crystals) which absorbs the humidity. This jar was closed tightly and kept in the freezer at sub zero temperatures. 20 minutes prior to staining the jar was removed from the freezer and allowed to warm to room temperature. Specimens crystallized were exposed to dry OsO_4 vapors in the jar for about 20 seconds.

This stops the crystallization process instantly since the reaction rate of OsO_4 with rubber far exceeds the crystallization rate.

3.2.3. Transmission Electron Microscopy

TEM is widely used to study the detailed morphology of polymers at high levels of resolution. TEM is analogous to visible light microscopy, but it employs an electron beam instead of a light beam. Electromagnetic lenses replace the common glass ones, see Figure 11 which is a schematic representation of a TEM. The condenser lens concentrates the beam of electrons on the specimen whereas the objective and projection lenses form a magnified image of the specimen. Principal focusing is performed on beams which have already interacted with the specimen.

A Siemens Elmiskop 1A ,JEOL JEM 200CX or Philips 300 TEM was used in this study. Samples which were crystallized at preset conditions and stained with OsO_4, were examined using TEM. Electron micrographs were taken of the specimens and the length of lamellae measured for kinetic studies. Besides observing the overall morphology, fine details such as lamellar thickness were also measured from these pictures. The temperature range used was generally between -40 ^{o}C and 0 ^{o}C, in some cases +3 ^{o}C. At 5 ^{o}C intervals, samples were allowed to crystallize at a constant temperature for four different periods of time. The

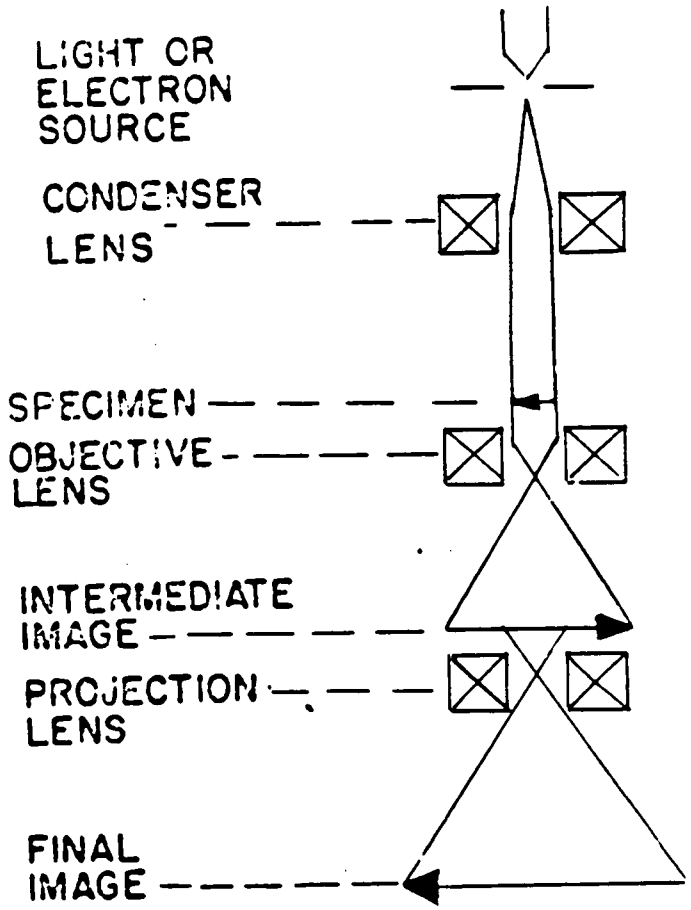


Figure 11 Schematic diagram of a transmission electron microscope.

growth rates were determined by measuring the maximum length attained by a lamella after a fixed crystallization time. The measurement was made from the center of the spherulite to the growth front of lamellae. Plots of maximum lamellar length versus time at a constant temperature were linear (Figure 12). The rate of crystallization was determined from the slope of this line. The growth rates were plotted against the crystallization temperatures and the bell shaped curves were obtained. The same procedure was repeated for different molecular weight fractions at atmospheric pressure as well as under elevated pressures.

3.3. High Pressure Crystallization Studies

3.3.1. Equipment

High pressure crystallization studies were carried out using a modified version of the high pressure generating system developed by Edwards and Phillips (1974). This system is shown in Figure 13 and consisted of a gas cylinder (1), an air driven gas pump (2), a high pressure intensifier (3), an air driven oil pump (4), Bourdon pressure gauges (5)(6)(7), a hand driven oil pump (8), an oil reservoir (9), a piston level sight glass (10), Blow out cross (11)(12), gas and oil vent valves (13)(14),intensifier and cell isolation valves (15)(16) and finally the crystallization

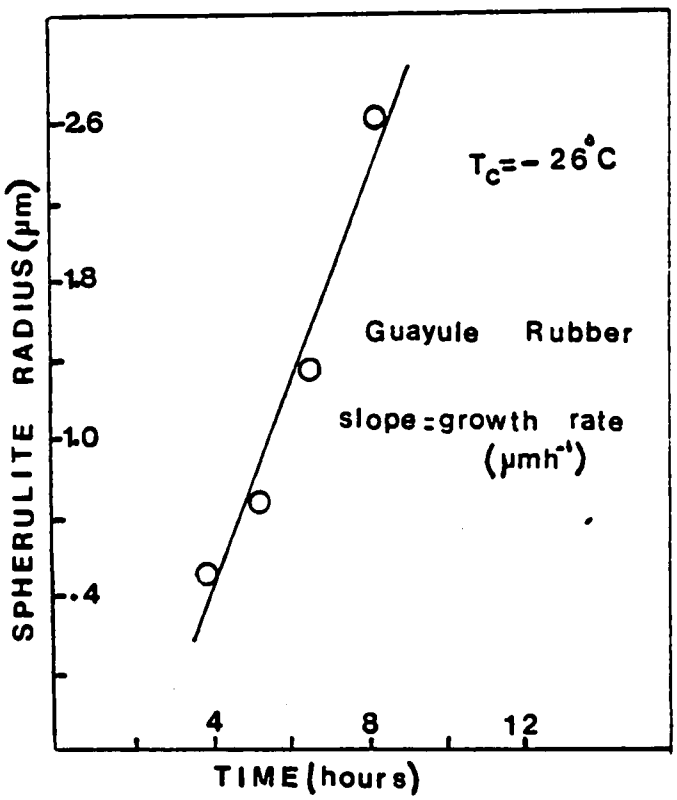


Figure 12 Lamellar growth of guayule rubber at -26 °C.

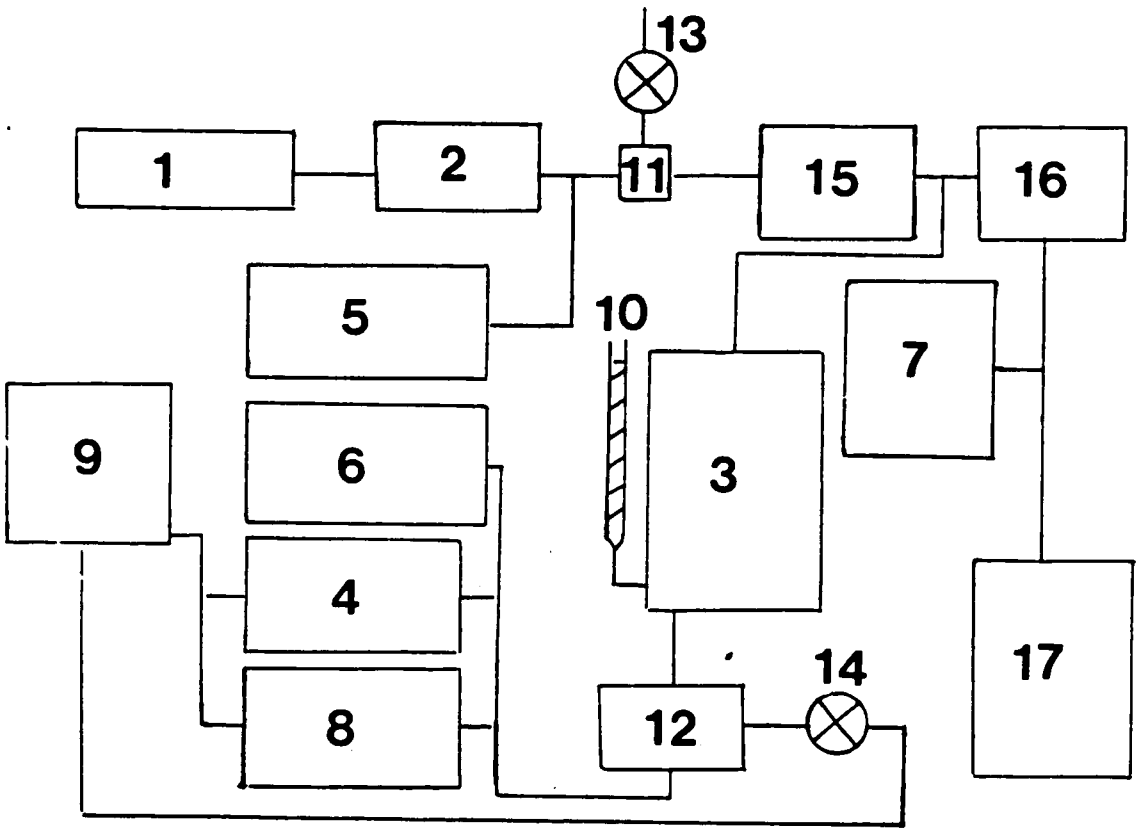


Figure 13 High pressure generating system (schematic).

bomb (17). These components are described in more detail below. The numbers in parentheses refer to Figure 13.

The high pressure system is based on a two stage intensification of argon cylinder gas pressure (1). First an air driven gas pump (2) is used which has a maximum gas discharge pressure of 20 000 psig. The second stage incorporates an air driven oil pump (4) which can compress the initial 1.1 kilobar enabling pressures up to 10 kilobar to be generated using a 10:1 pressure intensifier. Pressure developed in the cell was measured on a Heise pressure gage connected at a tee above the cell. This gage had a full scale reading of seven kilobar and a resolution 0.1 percent of full scale read on a mirrored scale.

The high pressure tubing used was 0.25 inches in outer diameter and had a wall thickness of 0.08 inch.

3.3.2. High Pressure Cell

The high pressure cell used, is shown in detail, in Figure 14. It consisted of a preloading screw (1), brass antiextrusion mitre rings (2), a teflon gasket (3), plug (4), sample holder (5) and the gas inlet (6). The cell was constructed of maraging steel (Vascomax 300 CVM) and was sealed by a Bridgeman unsupported area type seal. The seal consisted of a plug made from a teflon gasket and two brass antiextrusion rings (4)(3)(2). The preloading screw was used to position the plug properly. At the end of a high pressure

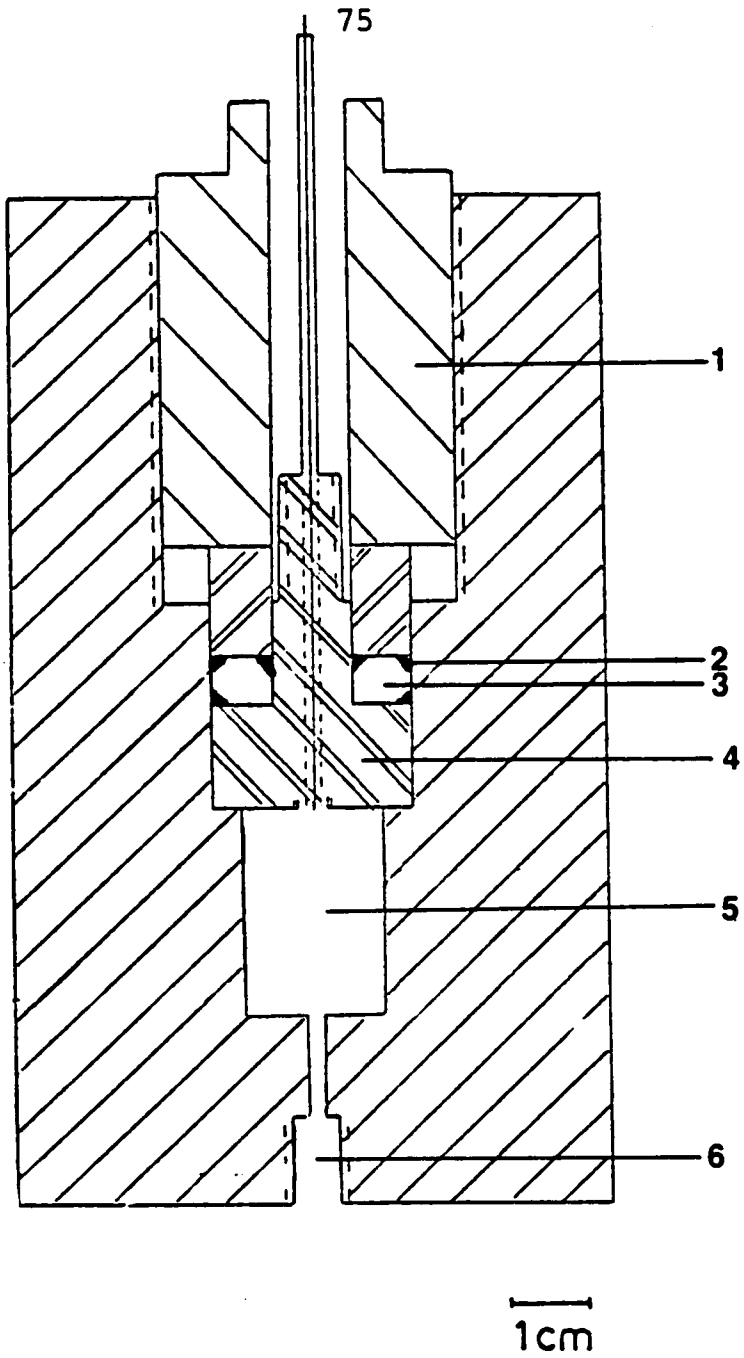


Figure 14 High pressure cell (schematic).

crystallization experiment the cell was disassembled and the plug was withdrawn using the screw thread on it.

The sample holder shown in Figure 15 was used.The material was aluminum which was chosen because of its good heat conducting properties. Six electron microscope grids could be placed at a time on the holder. A lid with appropriate openings for the grids was screwed tightly and the whole assembly was placed into the high pressure cell. First the aluminum sample holder was designed and built in proper dimensions to fill the space in the cell (a cylindrical block with 0.7 inch diameter and one inch height). Then it was cut into two pieces to reduce the metal volume and have a more effective staining of samples on electron microscope grids. If the metal volume is large, most of the OsO_4 vapors are drawn to the cold metal and the thin polymer film on the grids remains unstained.

3.3.3. Temperature Control

The temperature of crystallization was controlled by placing the bomb in a thermostatically controlled, refrigerated circulating bath. For 0^{o} C, an ice-water bath was used as the constant temperature bath. In order to establish the thermal equilibrium the crystallization bomb was allowed to stay 20 minutes in the constant temperature bath prior to the application of high pressure. The constant

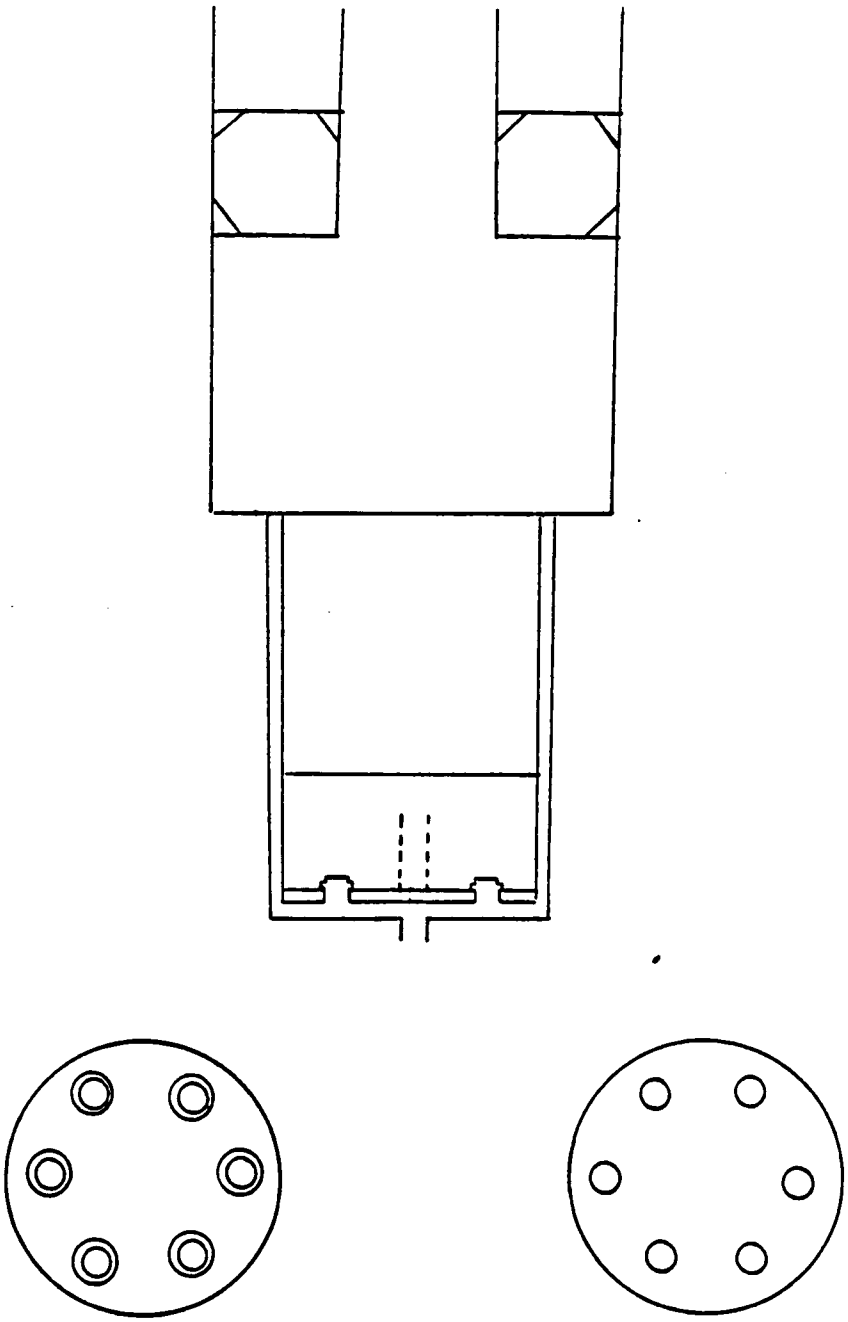


Figure 15 Sample holder used in the high pressure cell.

temperature bath was insulated with two inches thick polystyrene foam.

3.3.4.Experimental Procedure

In this system high pressure was generated by a two stage intensification of argon gas.The cylinder gas pressure was first compressed by using the air driven gas pump, which operated via a standard air line of 5.5 to 7.0 bar. In the first stage, pressures upto 1.1 kilobar were generated. In the second stage a high pressure intensifier was operated by means of a compressed air driven oil pump. In this stage the initial 1.1 kilobar enabling pressure can be compressed upto seven kilobar.

In a typical run, first the electron microscope grids, covered with thin polymer film, were loaded onto the sample holder which was placed into the high pressure cell. The crystallization bomb was then placed in a constant temperature bath and attached to the high pressure generating system. After the system had come to thermal equilibrium, high pressure was applied in less then three minutes.

After the prechosen crystallization time had elapsed, pressure was released carefully. The high pressure cell was then disconnected from the high pressure generating system. The cell was then disassembled quickly at room temperature and the sample holder was placed on top of a

block of dry ice which was held in drierite (drying agent) and covered with a watch glass. The sample holder was then taken to the fume hood and placed in a jar containing dry OsO_4 vapors for two to three minutes for staining as in the atmospheric pressure case. Following the staining step the electron microscope grids were examined in the TEM.

4. RESULTS

4.1. Crystallization of Guayule Rubber

Guayule rubber is a form of natural cis-polyisoprene having linear chains with a gel content which does not exceed a few percent. Crystallization studies were carried out on rubber specimens which were prepared by film casting from two percent hexane solution onto a water surface. An appropriate film thickness of 80-90 nm was judged by a gold interference color in the film (Peachey 1958). Films collected on 400 mesh copper electron microscope grids were crystallized at a constant temperature. After the chosen time of crystallization, samples were stained with OsO_4 vapor and studied using TEM.

The crystallization of guayule rubber which was extracted from the plant on a laboratory scale had been studied earlier (Rensch et al. 1986). Freshly extracted and aged samples showed different morphological features and lamellar growth rates. In this dissertation as a continuation of earlier studies, crystallization kinetics and morphology of freshly prepared specimens which were extracted from the plant in a pilot plant operation were studied.

4.1.1. Lamellar Growth Studies

The growth rates were found by measuring the maximum length attained by the lamellae at a given crystallization time. By repeating for different times the measurement of specimens crystallized at a given temperature, the growth rate can be determined at that specific temperature. The rates were linear until impingement between spherulites occurred. Plots of maximum spherulite radius versus the time of crystallization at -21°C and -5°C are given in Figure 16 as examples where positive intercepts indicate the presence of inhibition times. Linear growth rates were determined from the slopes of the lines at each temperature. The variation of growth rate as a function of crystallization temperature was then plotted as in Figure 17 (the actual rate data are given in the appendix). The figure is a characteristic bell shaped curve of polymer crystal growth showing a maximum at -24°C. At lower temperatures (i.e. below the maximum growth temperature) crystal growth is governed by the mobility of the chains, above the maximum crystallization temperature, the process is controlled by nucleation. A comparison of the α-growth curves of guayule rubber from pilot plant, fresh rubber extracted from the plant on a laboratory scale and the unfractionated hevea rubber shows that (Figure 18) the latter two peak at about -21°C. Pilot plant guayule rubber

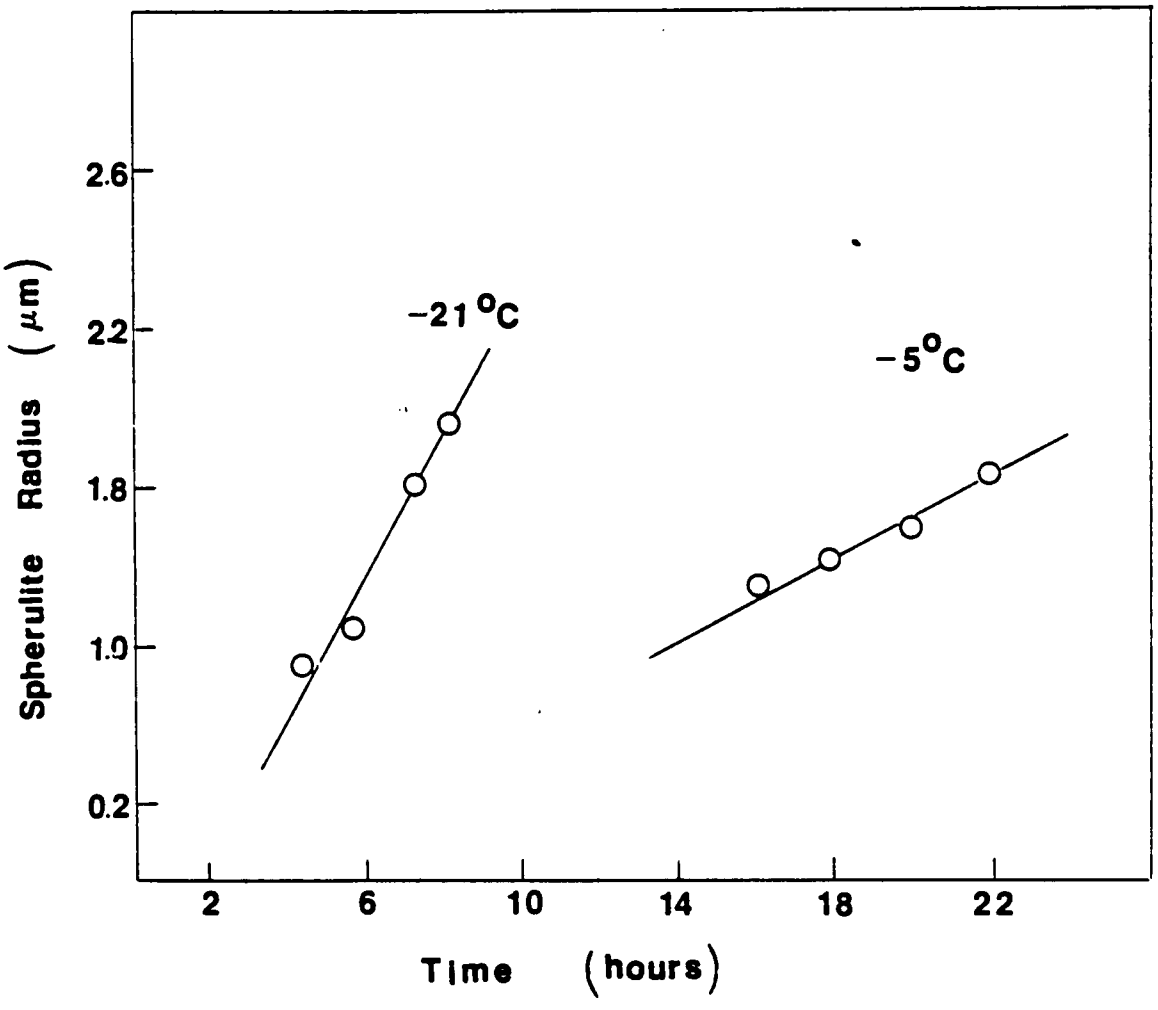


Figure 16 Lamellar growth of guayule rubber at -21 °C and at -5 °C.

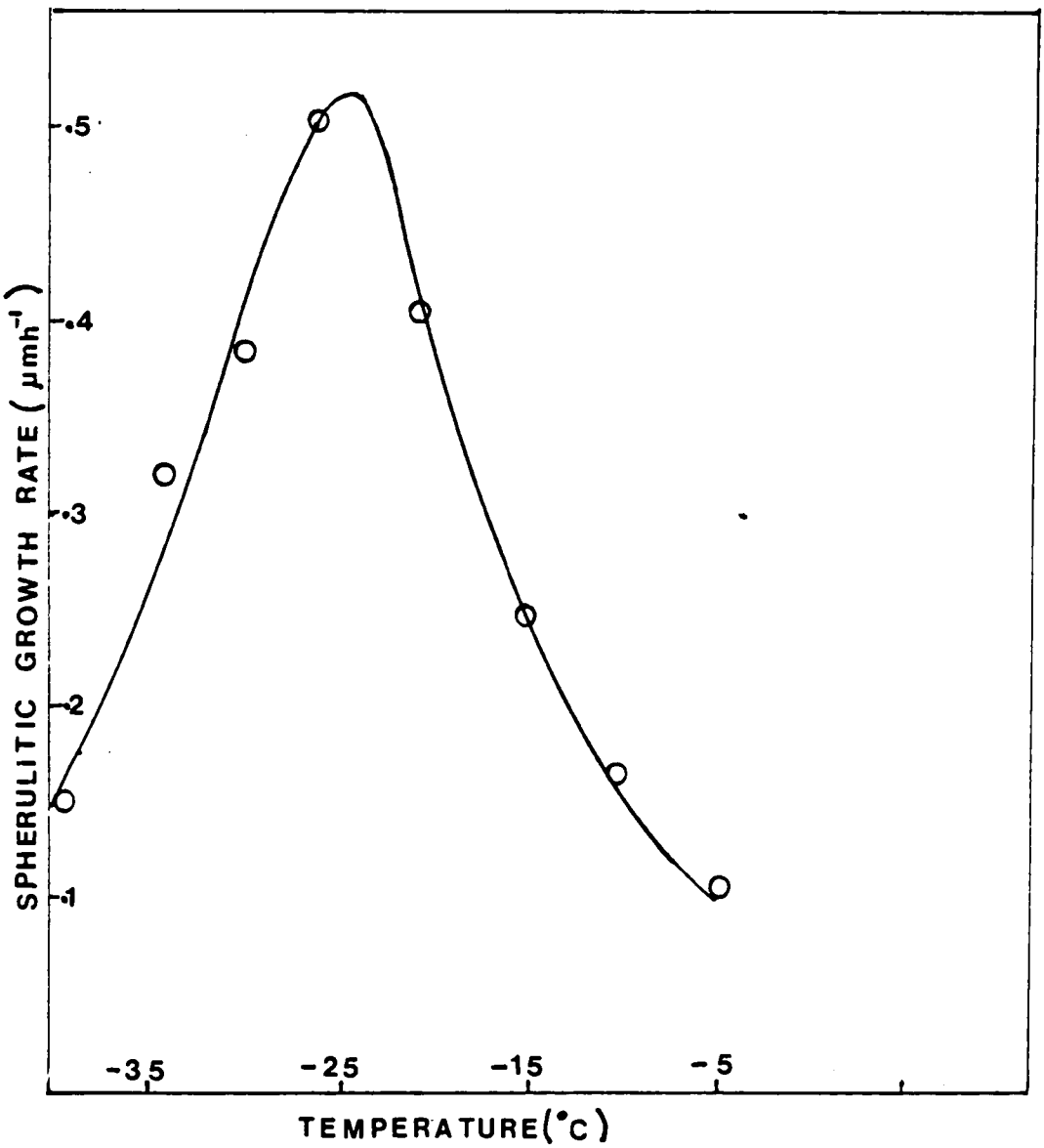


Figure 17 Lamellar growth rate versus crystallization temperature for guayule rubber.

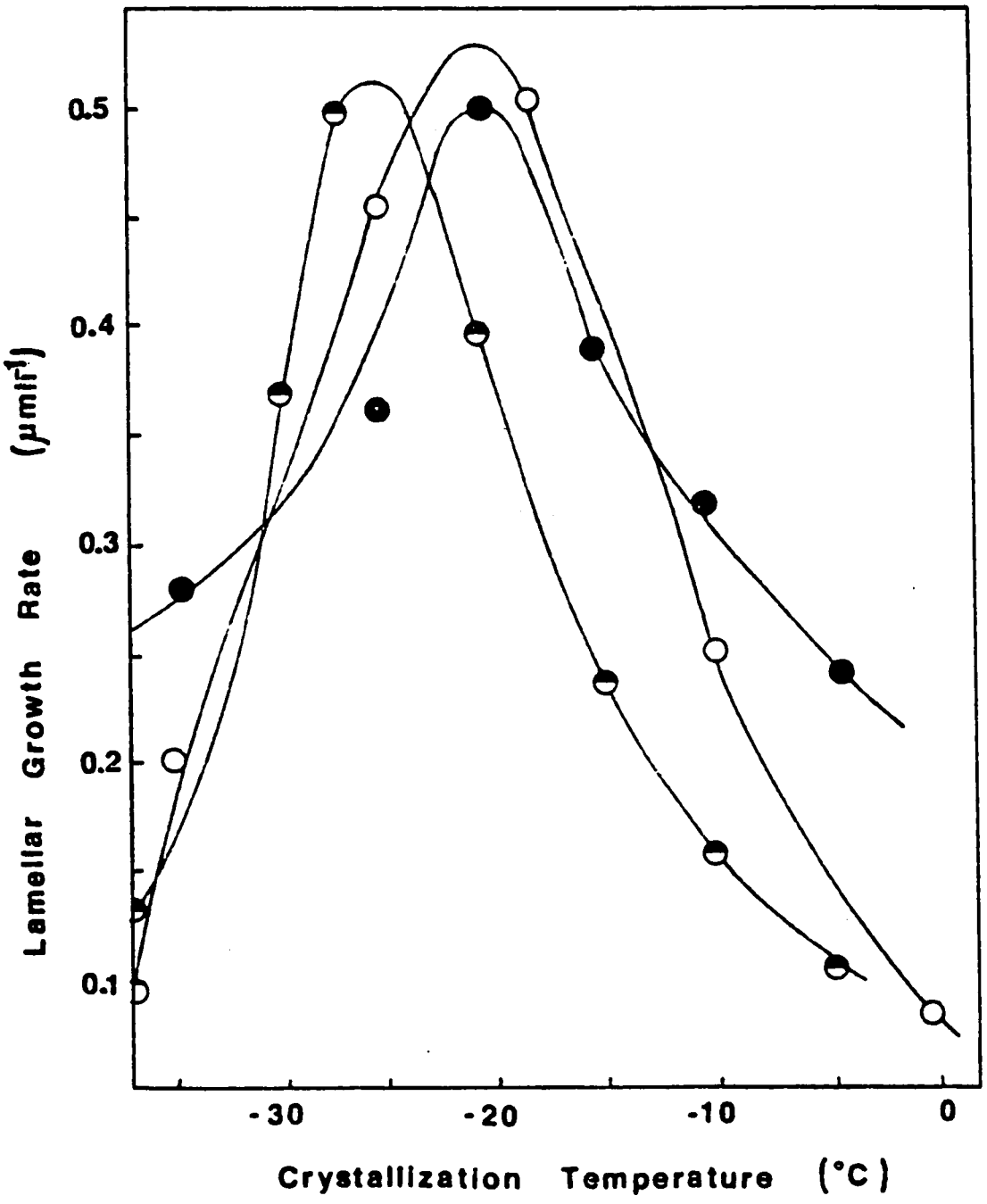


Figure 18 Lamellar growth rate versus crystallization temperature for O-hevea rubber (Andrews 1964), ⊖-guayule rubber from pilot plant, ●-fresh rubber extracted from plant (Rensch et al. 1986).

exhibits a higher peak maximum with a narrower curve and a lower growth rate at low supercoolings than the fresh rubber. It should be noted that a different extraction solvent was used in pilot plant rubber. In earlier studies, organic impurities were extracted using benzene which might also remove the low molecular weight fraction of polymer. For pilot plant rubber in this study, acetone was used as the extraction solvent.

Rubber samples from the plant freshly extracted on a lab scale showed only α growth whereas aged pilot plant rubber exhibited both α and β growth, β crystals having lower growth rates and larger lamellar thicknesses. Lamellar thicknesses were measured from the transmission electron micrographs of OsO_4 stained films. Care was taken to ensure that values corresponded to the completely "edge-on" orientation (Figure 19). The distribution of lamellae is quite narrow as shown in Figure 20. The thicknesses of lamellae at different crystallization temperatures are plotted in Figure 21 together with the thicknesses of the α and β lamellae of aged pilot plant rubber and natsyn (synthetic cis-polyisoprene which contains 2.5 % trans units). It is clear from the figure that the lamellar thickness data are independent of the source of rubber and trans isomer content as would be expected for a copolymer effect (Sanchez 1975).

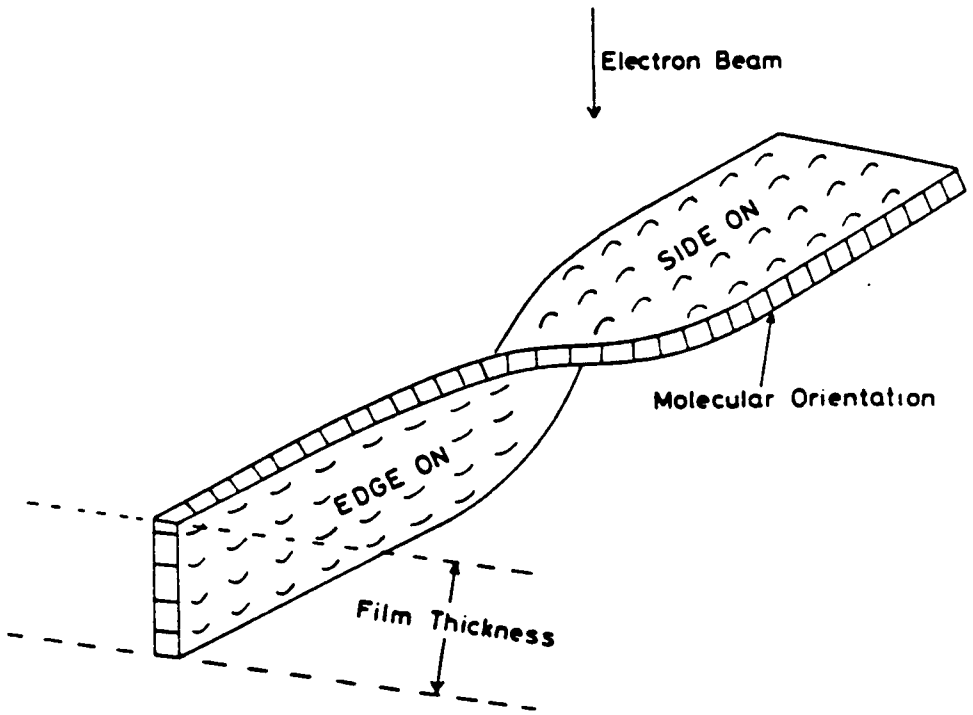


Figure 19 Schematic representation of the "side-on" and "edge-on" orientation of the lamellar crystals with respect to the electron beam.

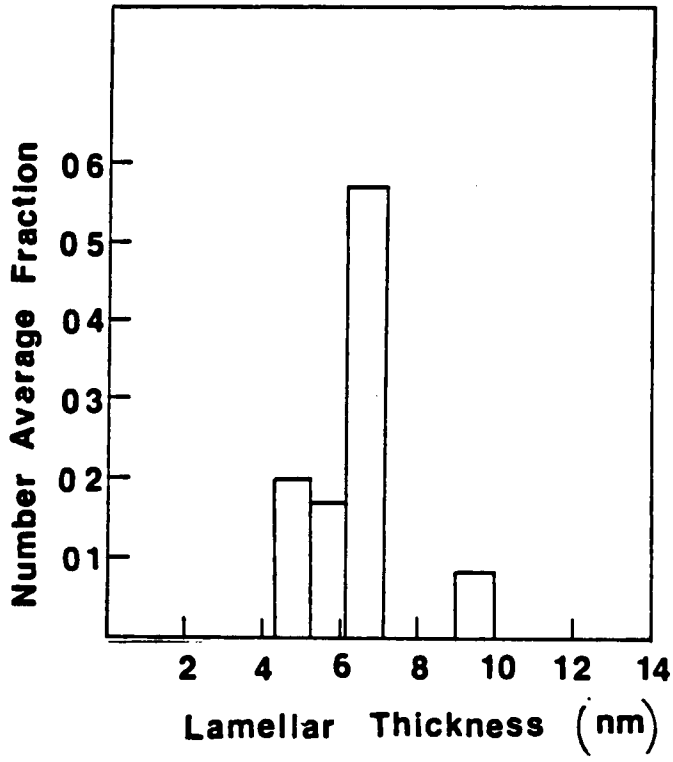


Figure 20 A histogram of lamellar thickness of guayule rubber at -15 °C.

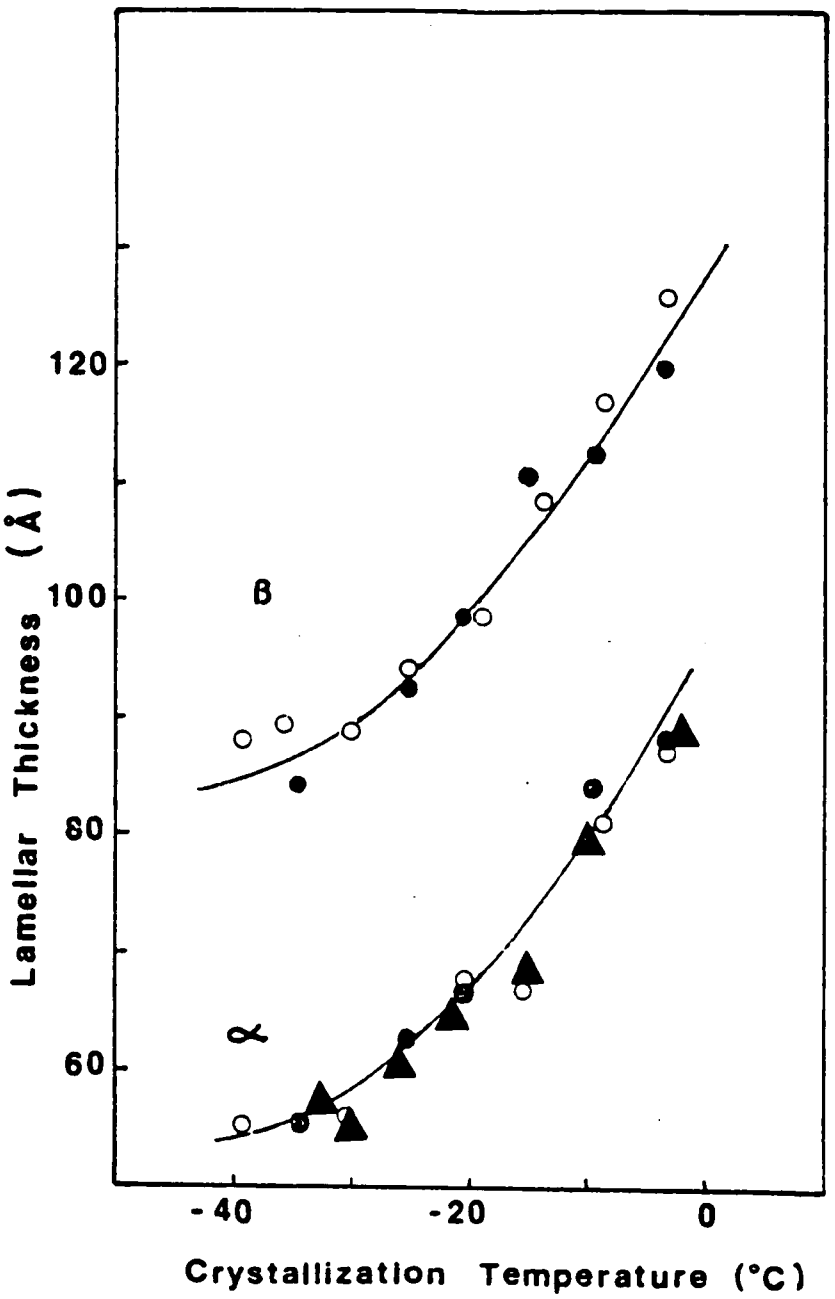


Figure 21 Lamellar thickness as a function of crystallization temperature for α and β lamellae of ●-natsyn (Edwards et al. 1980), O-aged pilot plant guayule rubber (Rensch et al. 1986) and ▲-α lamellae fresh pilot plant guayule rubber.

4.1.2. Morphology

In cis-polyisoprene, two melting peaks have been observed (Kim and Mandelkern 1972, Edwards 1975) indicating two different crystals. One of them is known as the α crystal which occurs for all crystallization conditions and is associated with the growth of crystals utilizing (100) growth faces and having the "a" unit cell parameter oriented along the lamellar length. The second melting peak corresponds to the β crystals which occur at longer crystallization times and have been assumed to be caused by lamellae produced in an in-filling process. In β crystals the growth face is believed to be the (110) face and the "b" unit cell parameter is oriented along the lamellar length. Both α and β crystals have the same crystal structure.

Guayule rubber from the pilot plant mostly showed α growth (Figure 22), β growth being rarely observed. Pictures of β sheaves showed a number of crystallographic branch points (Figure 23). Growing sheaves generally, had a particle near their center (Figure 24). Often this particle is identified as microgel which cannot be extracted during the extraction process carried out prior to crystallization. The growth of lamellae was sometimes in the "side-on" position with circular growth fronts in the equatorial region (Figure 25). The fresh guayule rubber extracted from the plant on a laboratory scale (Rensch et al. 1986) showed a similar mode

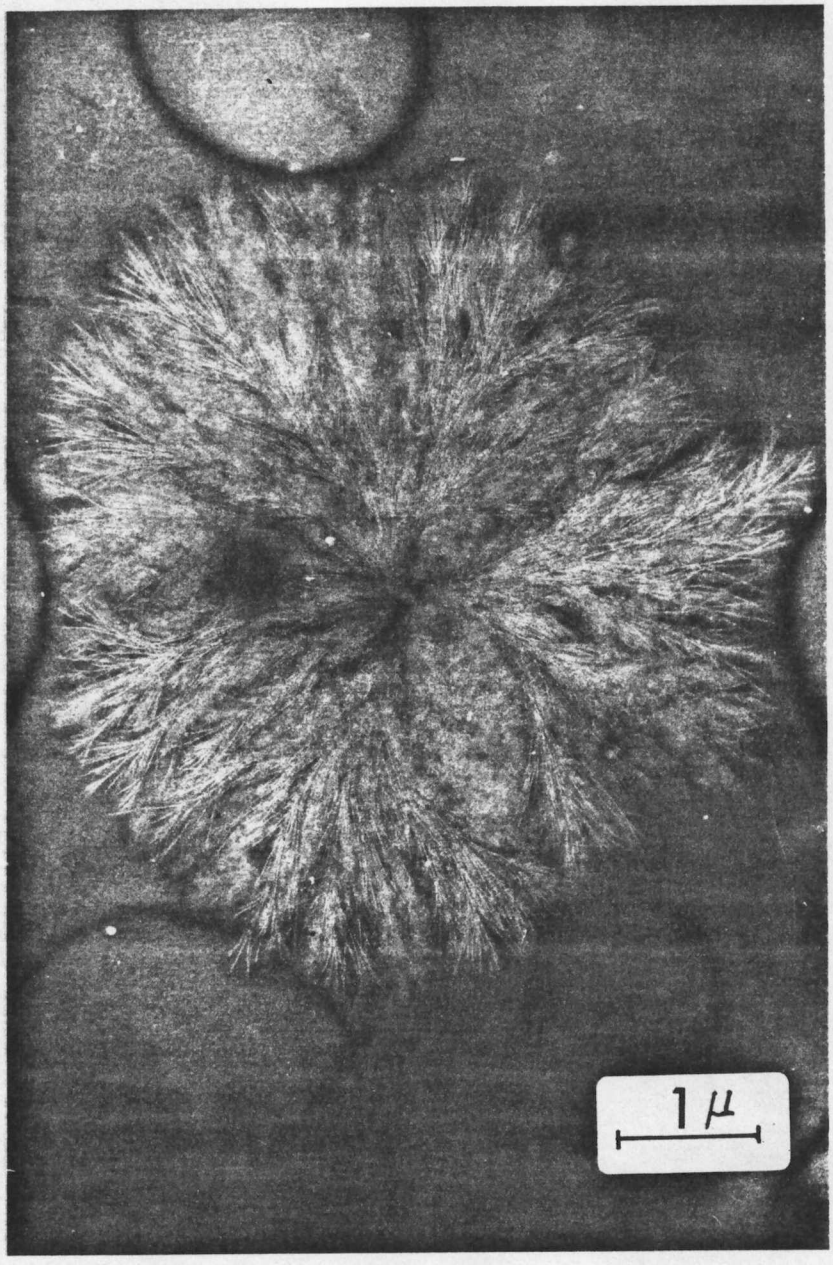


Figure 22 α-spherulite of guayule rubber crystallized at -26 °C.

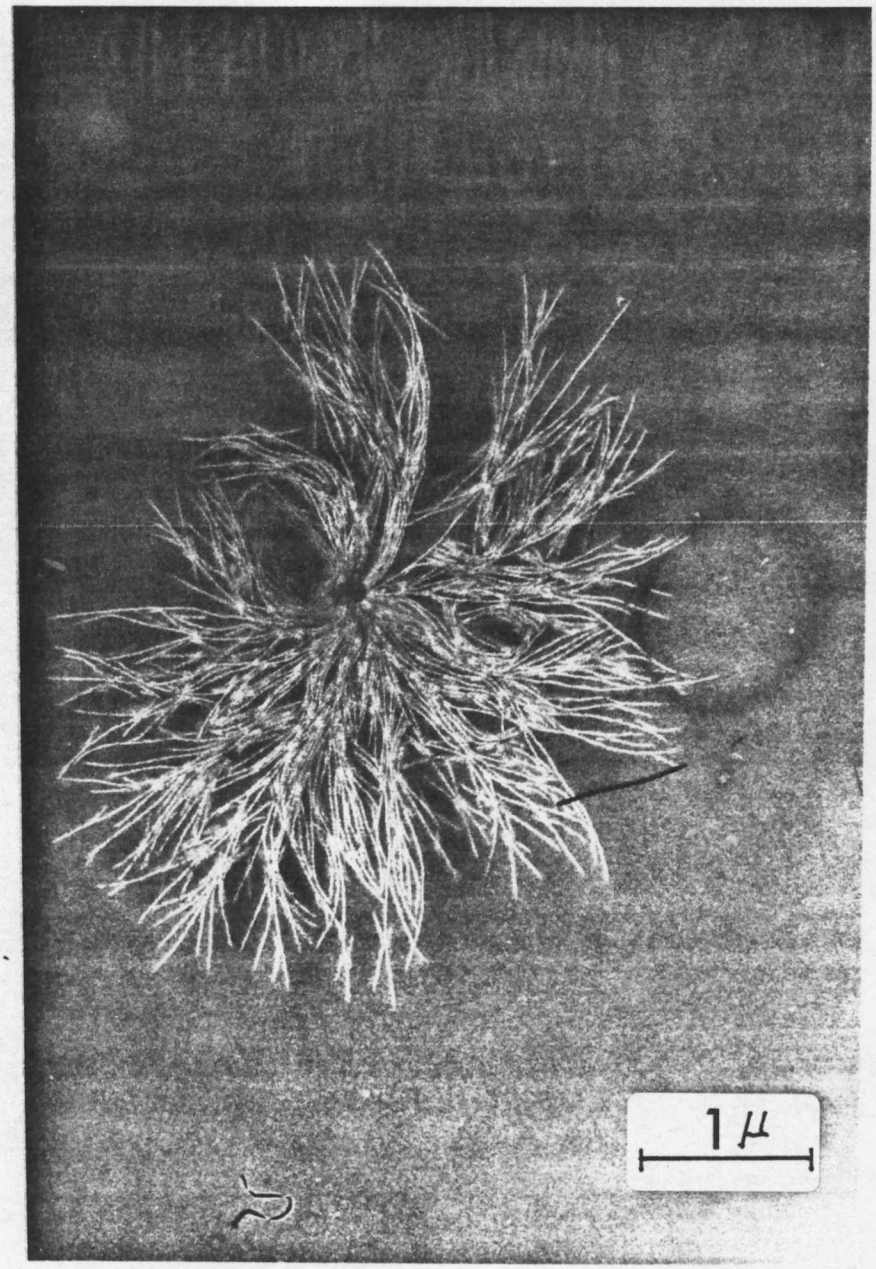


Figure 23 A highly branched β-spherulite in guayule rubber crystallized at -26 °C.

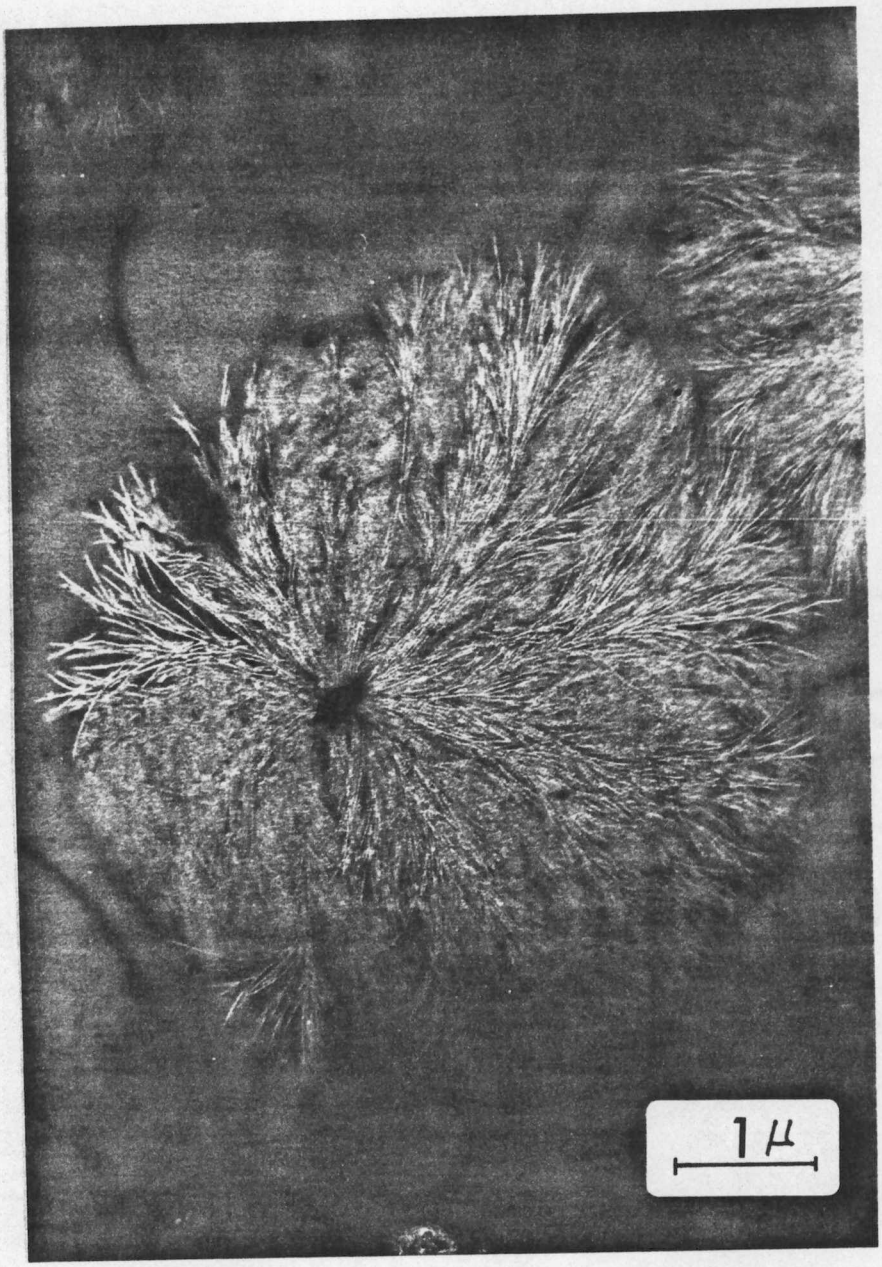


Figure 24 α-spherulite of guayule rubber showing microgel particle at center.

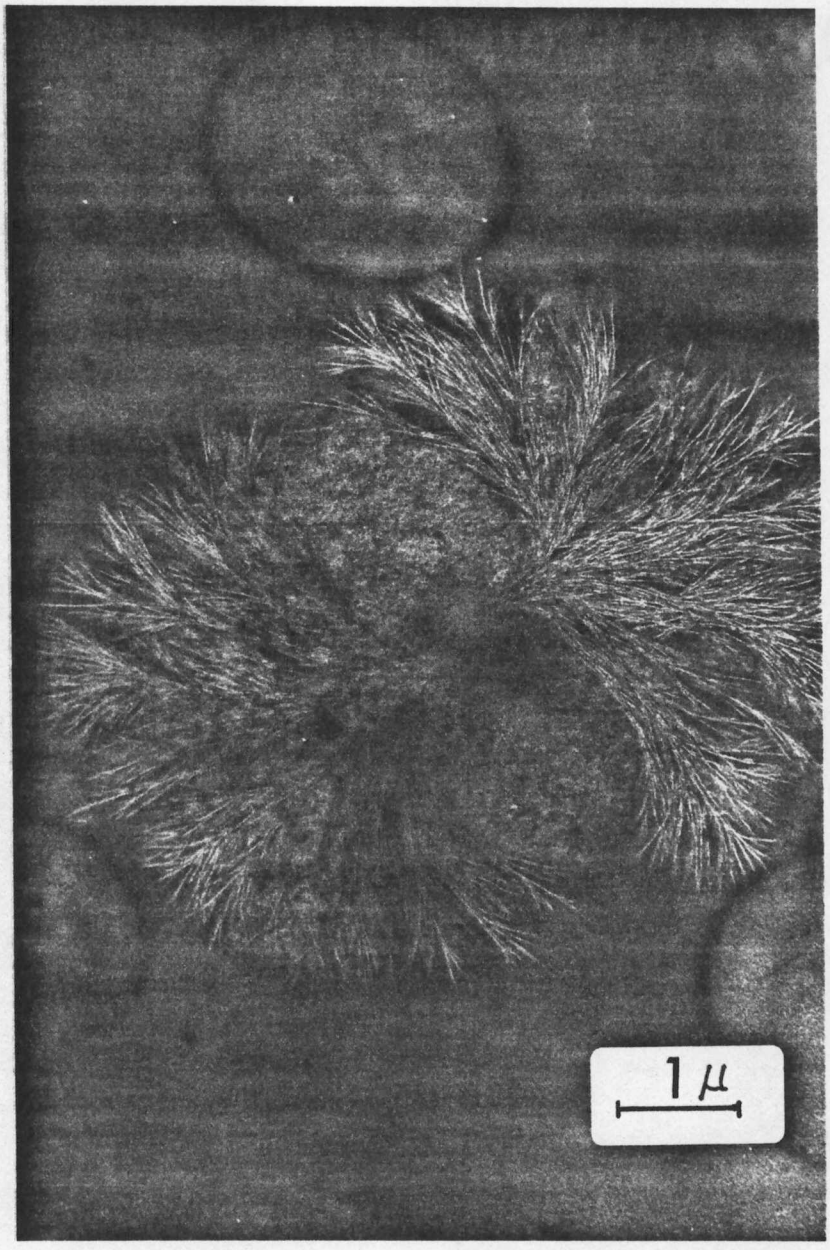


Figure 25 α-spherulite of guayule rubber grown at -26 °C.

of growth leading to rounded hexagonal shapes over long periods of time.

4.2. Studies of Hevea Rubber at Atmospheric Pressure

4.2.1. Fractionation Studies

Fractionation was carried out using a 0.5 % hevea rubber solution in hexane at 26^{o}C using a dropwise addition of non-solvent (1-propanol) under a nitrogen atmosphere and in the dark. In each case the precipitated polymer was collected by siphoning off the supernatant liquid and drying to constant weight at room temperature in vacuo. Details of the fractionation procedure were described in section 3.1.2. Individual fractions obtained are listed in Table 1.

4.2.2. Molecular Weight Studies

Viscosity average molecular weights were determined using a Canon Ubbelohde viscometer for THF solutions at 25^{o}C. The analysis of intrinsic viscosities was discussed in section 3.1.3. The intrinsic viscosity values were converted to viscosity average molecular weights using the Mark-Howink equation. The intrinsic viscosity values as well as the viscosity average molecular weights are listed in Table 2.

Table 1 Fractionation Data

Fraction	Weight (gram)
1	0.1208
2	0.0300
3	0.2133
4	0.1970
5	0.1460
6	0.3392
7	1.0832
8	2.6361
9	0.4103
10	1.3656

Table 2 Molecular Weight Data For Fractions

Fraction	[η]	M_v	M_w/M_n
1	6.53	1.12×10^6	-
2	-	-	-
3	5.50	8.97×10^5	-
4	4.30	6.57×10^5	-
5	3.90	5.80×10^5	-
6	2.52	3.51×10^5	1.37
7	3.85	5.71×10^5	-
8	3.70	5.43×10^5	-
9	2.39	3.13×10^5	1.58
10	0.99	1.02×10^5	1.75
*A	7.91	1.42×10^6	-

* obtained in separate fractionation experiment

Molecular weight distributions of lower molecular weight fractions were determined using GPC (Figures 26, 27,28). Unfortunately the samples of molecular weight half a million and above could not be studied using GPC due to clogging of the columns. The polydispersities of the three fractions are also listed in Table 2. The molecular weight distributions of the fractions are much narrower than that of the original hevea rubber which has a polydispersity of 4-5.

4.2.3. Lamellar Growth Studies

The measurement of growth rates of different molecular weight fractions was carried out as described in section 4.1.1.. The growth of lamellae with time was always linear, for example see Figure 29. All molecular weight fractions exhibited bell shaped growth rate versus temperature curves (Figure 30) with different characteristics (see appendix for a complete listing of all growth rates). The general trend is a decrease in linear growth rate with increasing molecular weight, the peak temperature remaining unchanged. The fraction of molecular weight 543,000 exhibited lower growth rates than the 897,000 molecular weight fraction at high crystallization temperatures (or low undercoolings). The presence of a broad molecular weight distribution might have caused this unexpected trend. Actually an inherent problem with the

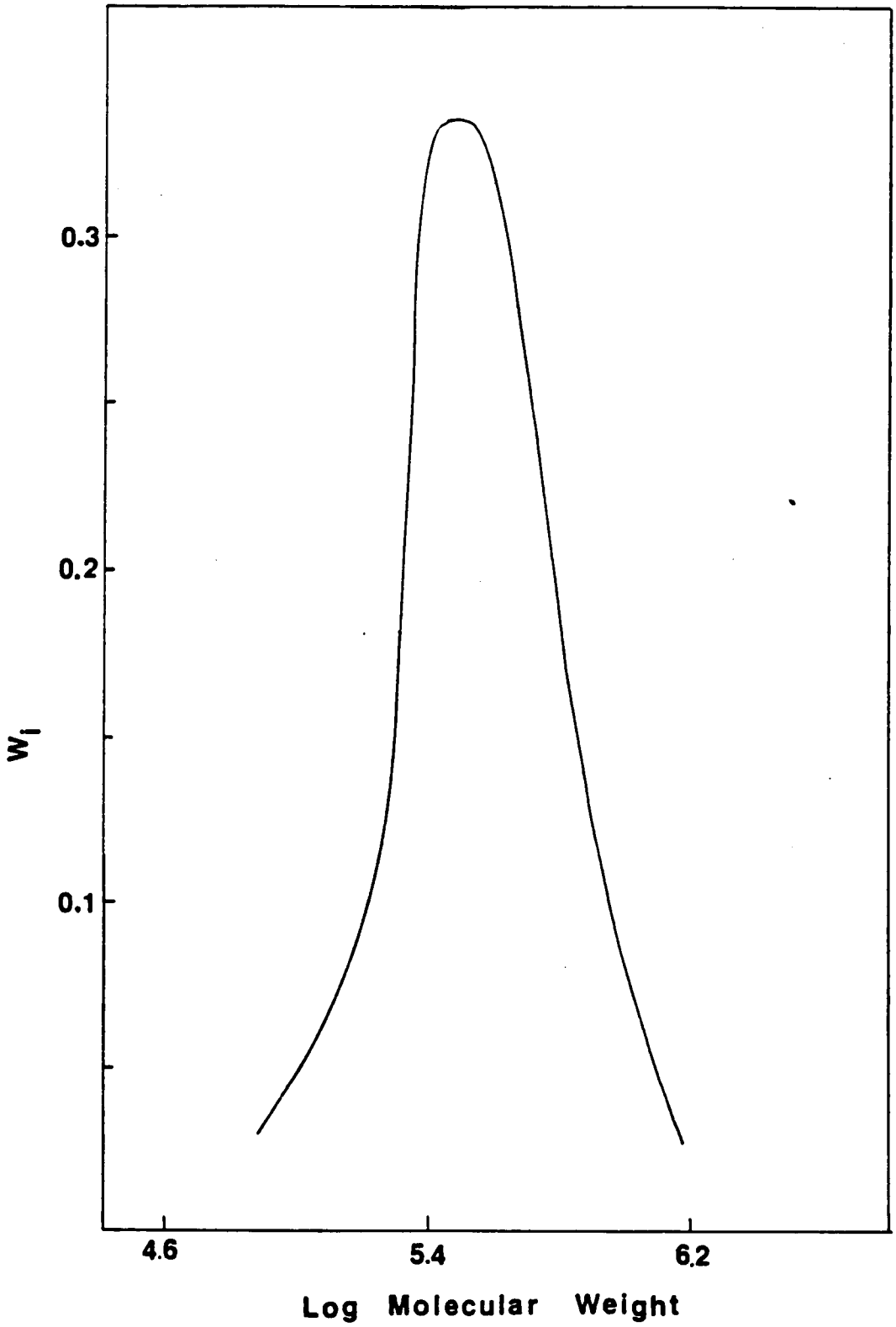


Figure 26 Molecular weight distribution of the hevea rubber fraction of molecular weight 351,000.

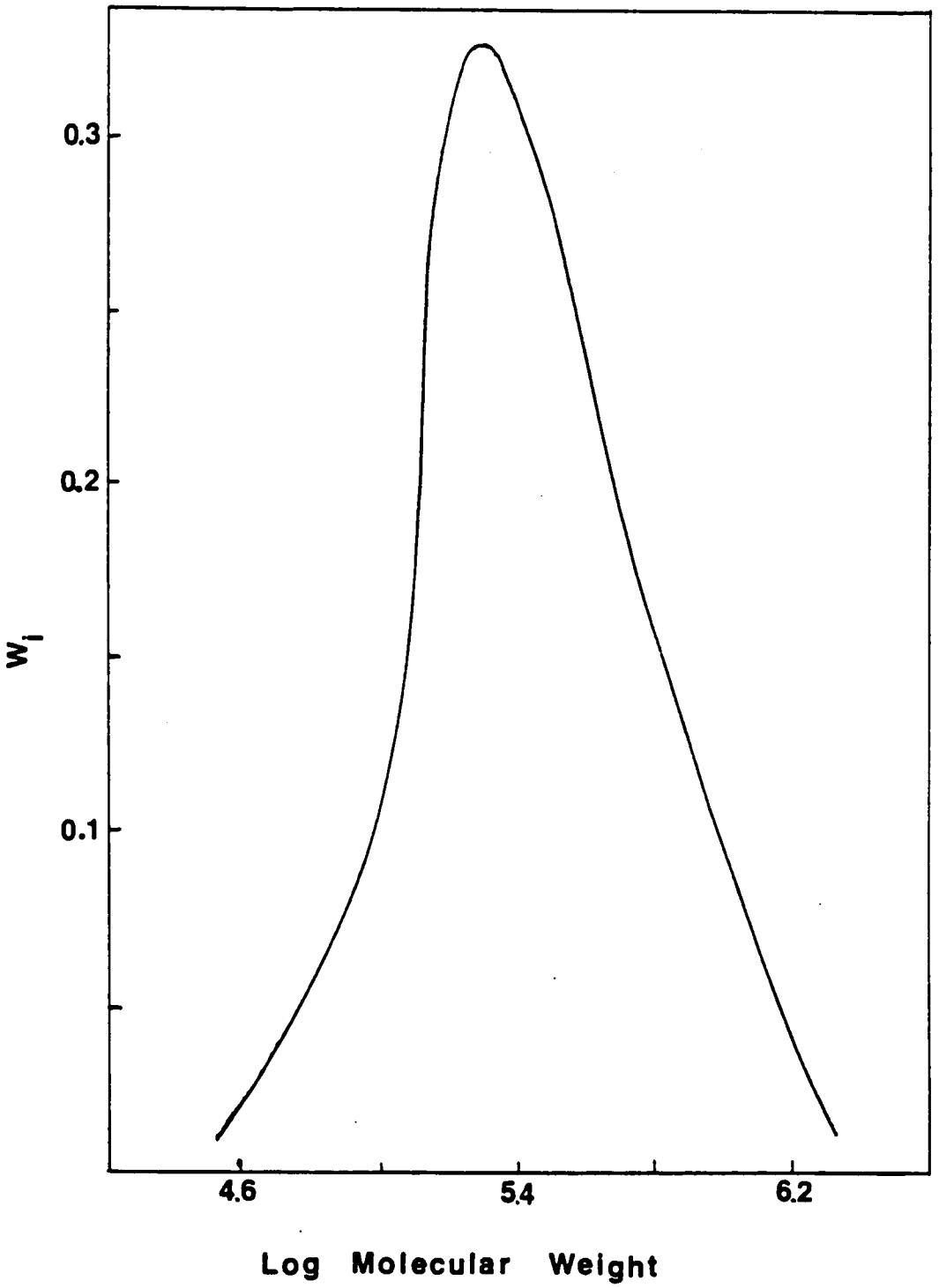


Figure 27 Molecular weight distribution of the hevea rubber fraction of molecular weight 313,000.

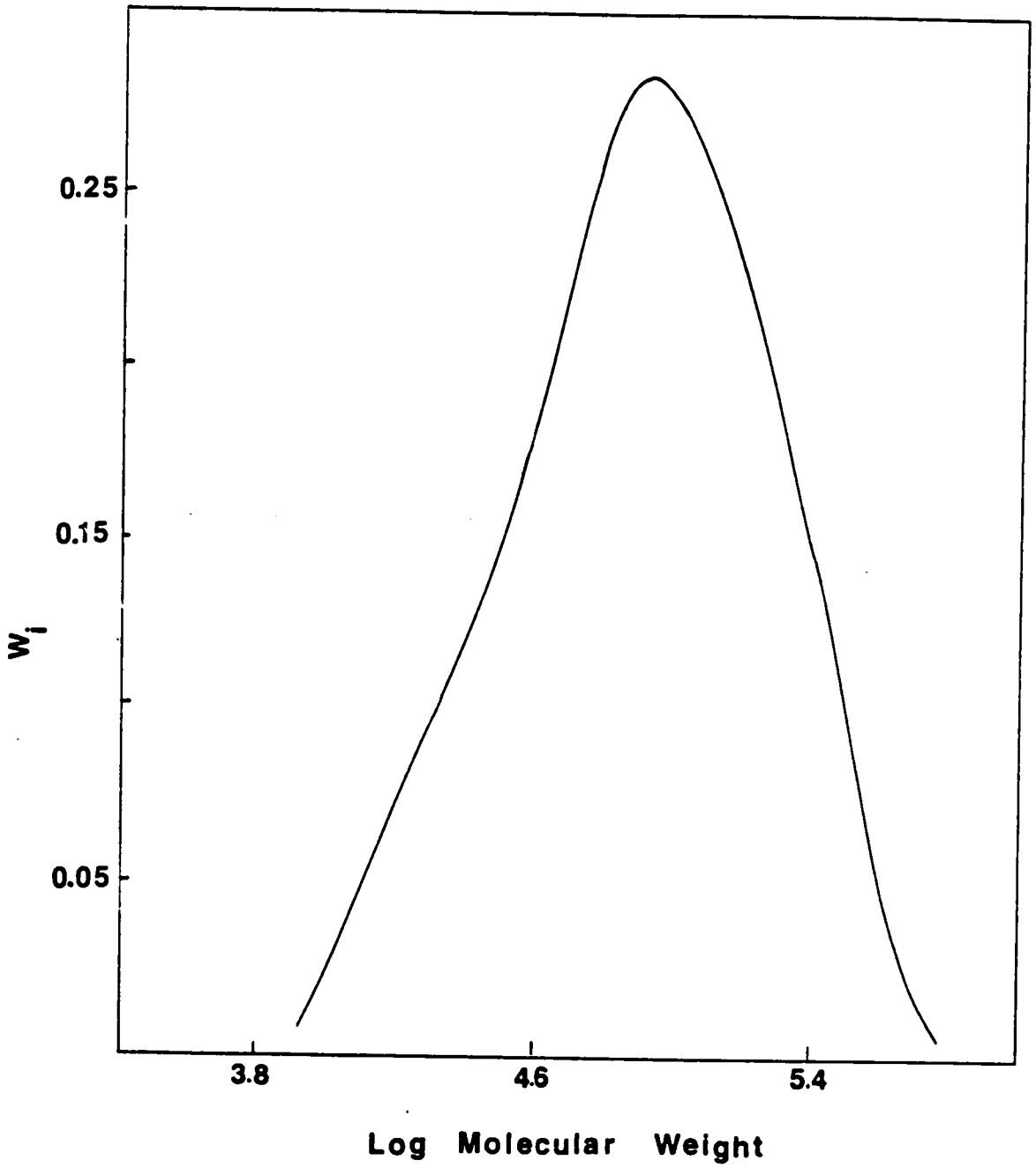


Figure 28 Molecular weight distribution of the hevea rubber fraction of molecular weight 102,000.

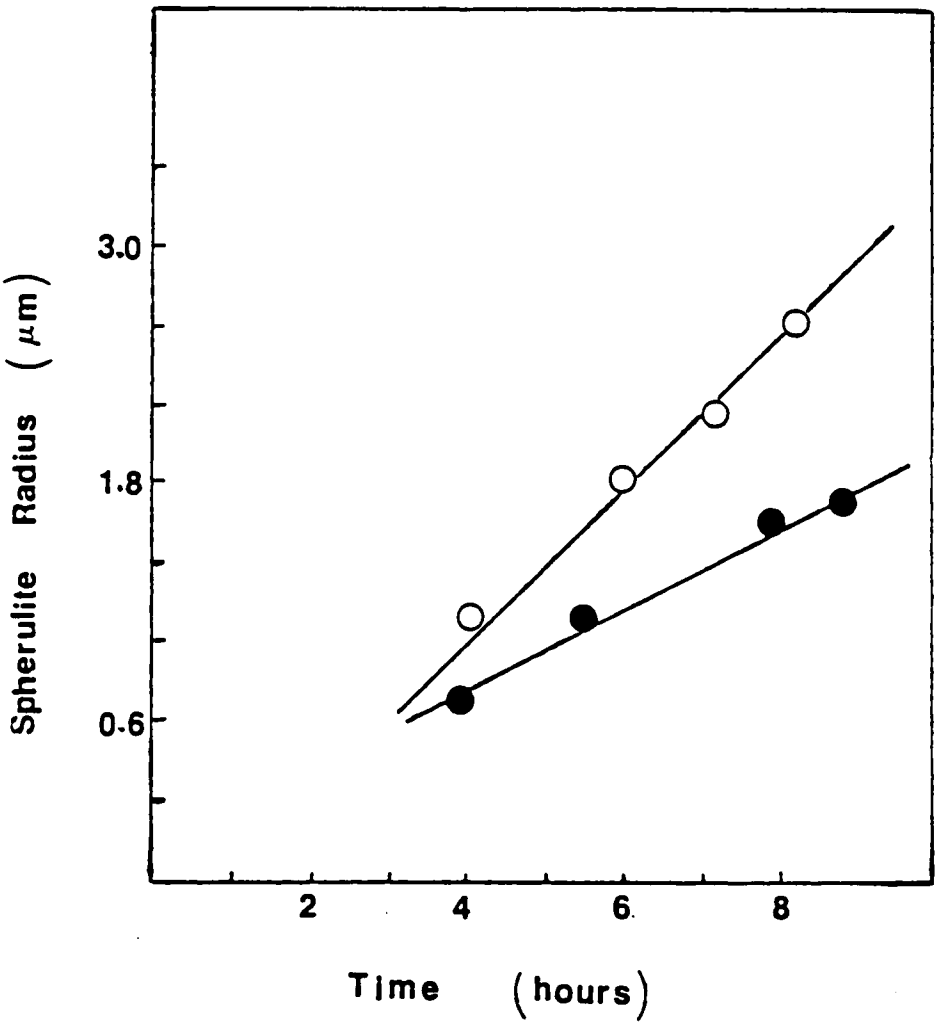


Figure 29 Lamellar growth of hevea rubber fractions with molecular weights O-313,000 and ●-1,421,000 at -20 °C.

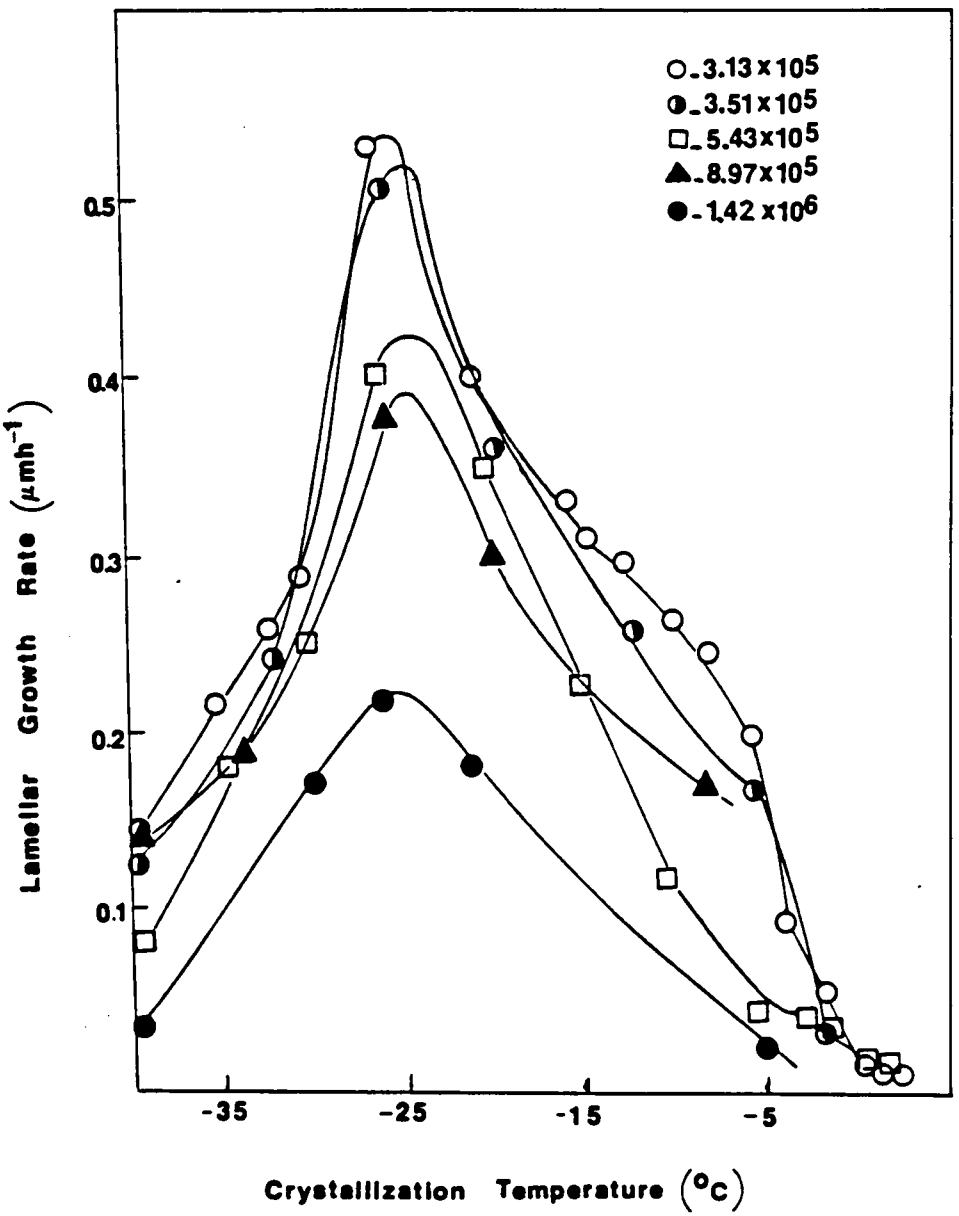


Figure 30 Lamellar growth rate versus crystallization temperature for hevea rubber fractions with the indicated molecular weights.

fractional precipitation method is that each fraction contains an appreciable concentration of lower molecular weight species. Thus the presence of a lower molecular weight polymer in the 897,000 molecular weight fraction could be the reason for this effect.

The growth rates of the fraction of molecular weight 313,000 were studied over wide temperature range (-40°C to +3°C) at small temperature intervals. The result was a very distorted curve (Figure 31). The regions where we see deviations from a smooth bell shaped curve correspond to the temperatures at which changes in crystallization regimes occur. The fraction with 543,000 molecular weight was also studied in more detail for crystallization temperatures ranging from -40°C to +1.4°C (Figure 32). Some distortion in the shape of the curve was observed at -5°C. These growth curves will be considered in more detail in the discussion section.

Lamellar thickness measurements were carried out from the electron micrographs at different crystallization temperatures for different molecular weight fractions. Results are shown in Figure 33, all data being found in the appendix. All samples exhibited increasing lamellar thicknesses with decreasing supercooling as expected. The two lower molecular weight fractions showed a tendency to have thicker lamellae at higher crystallization temperatures. It should be noted that lamellar thickness can

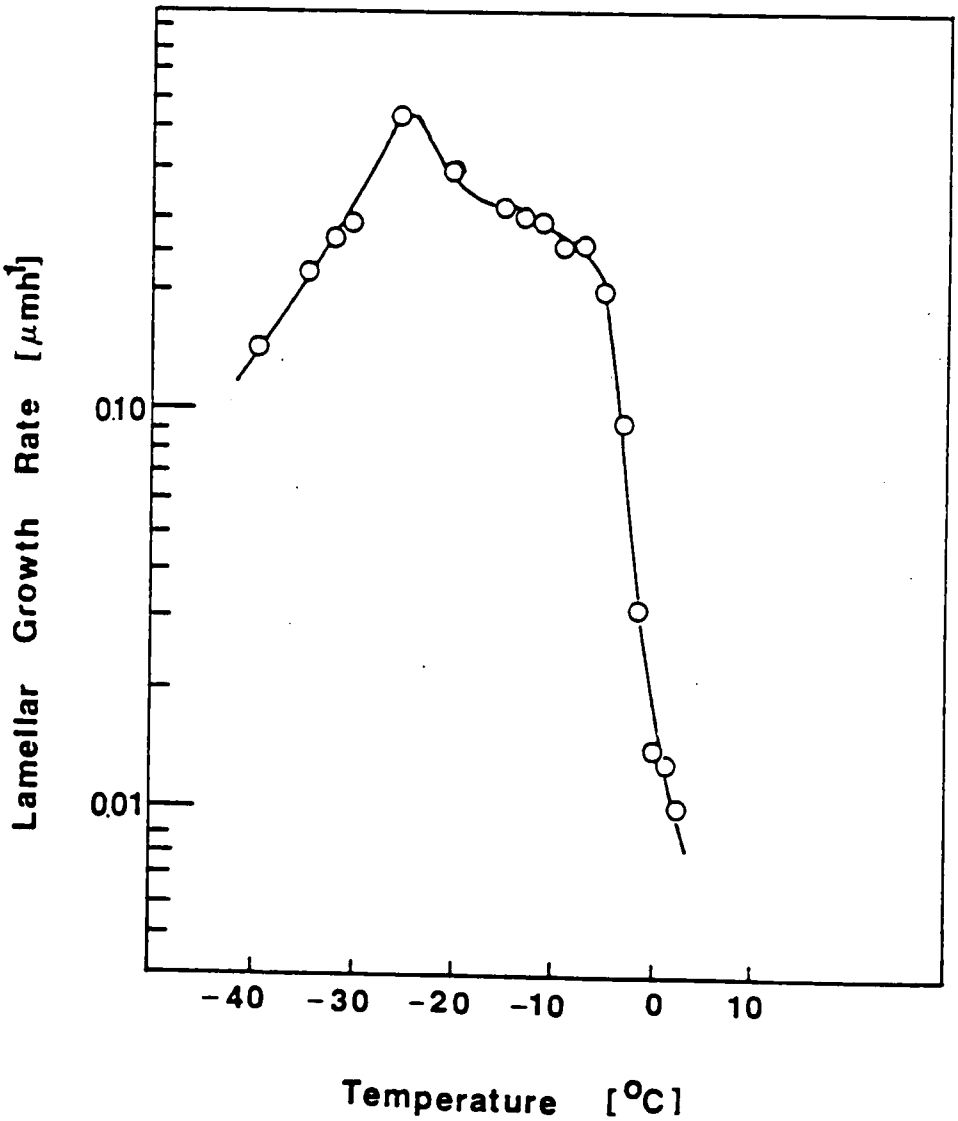


Figure 31 Lamellar growth curve of hevea rubber fraction of molecular weight 313,000.

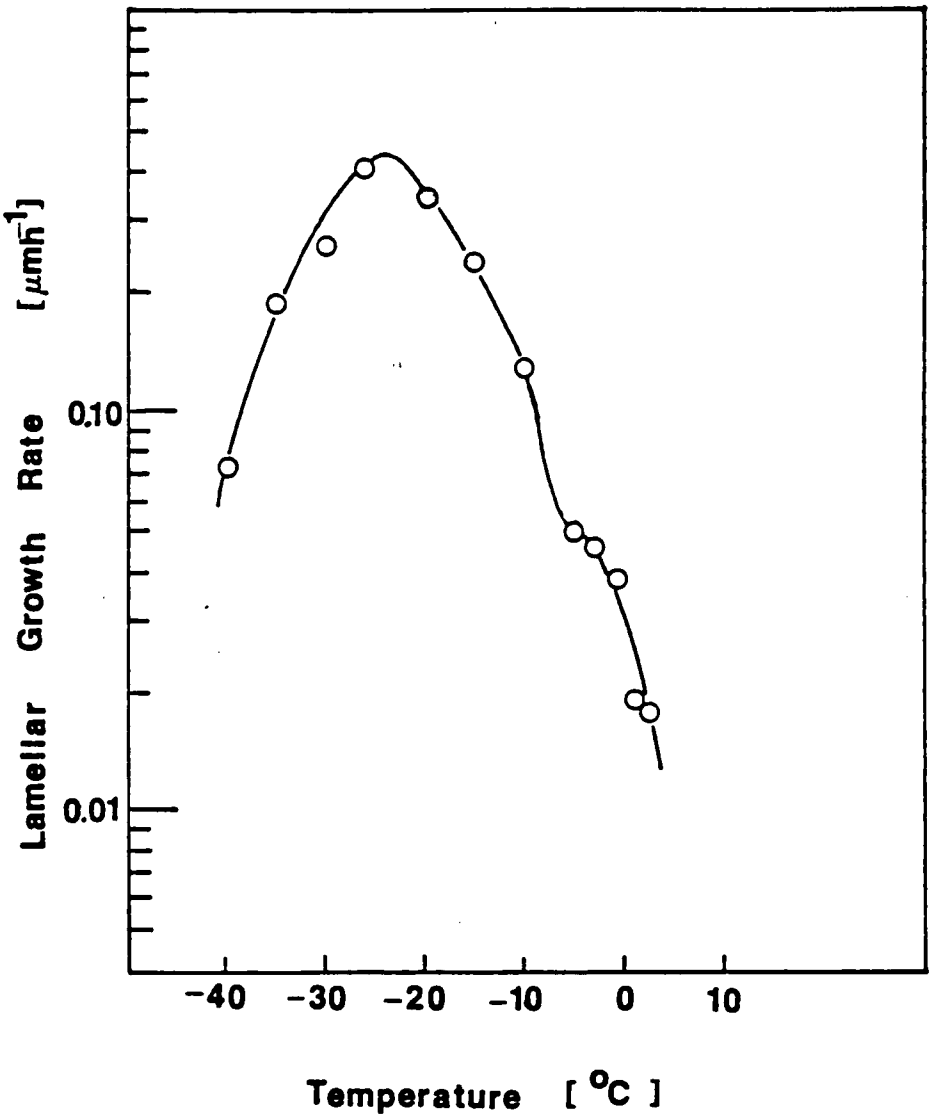


Figure 32 Lamellar growth curve of hevea rubber fraction of molecular weight 543,000.

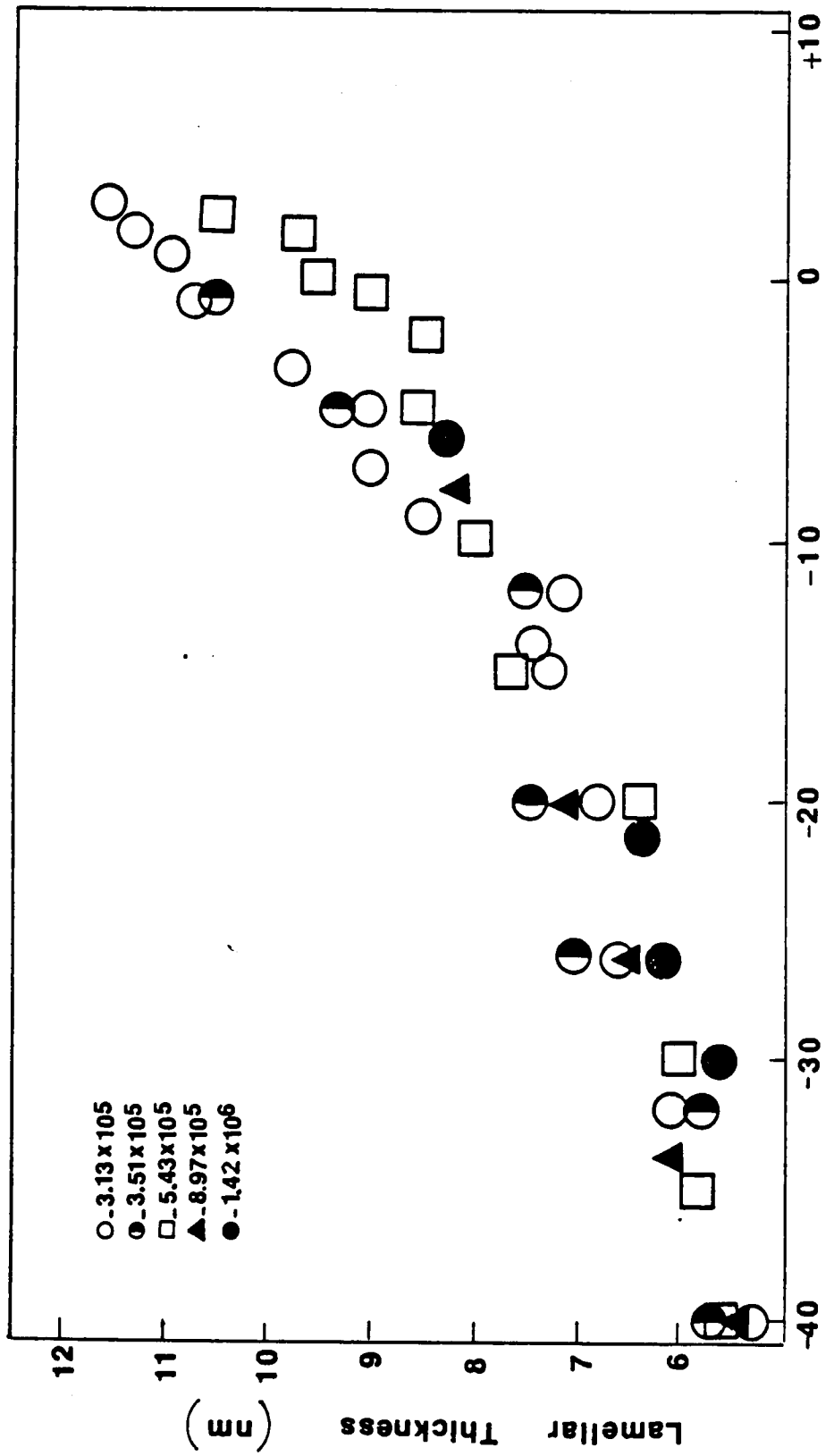


Figure 33 Lamellar thicknesses as a function of crystallization temperature for the hevea rubber fractions of indicated molecular weights.

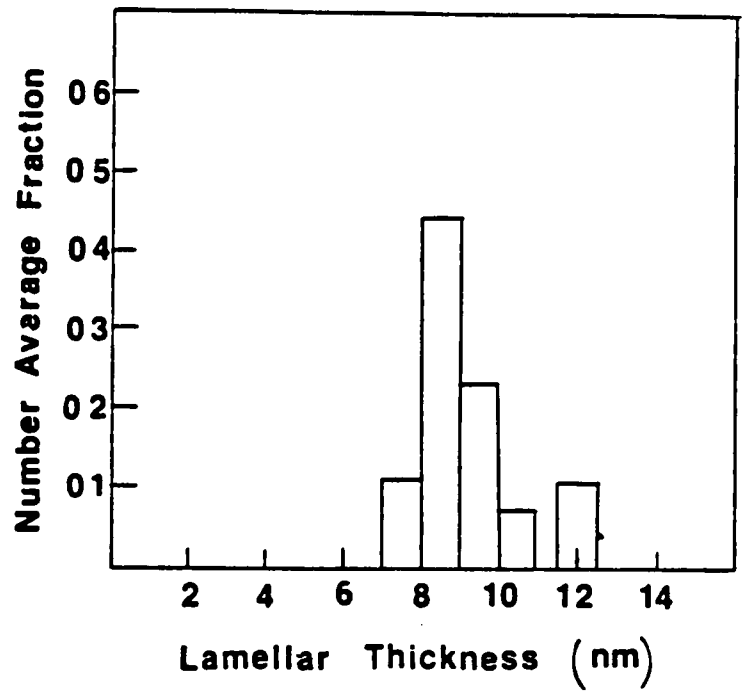
be determined within an error of ±0.5 nm, thus most of the scatter is within the experimental uncertainty (Figure 34).

4.2.4. Morphology

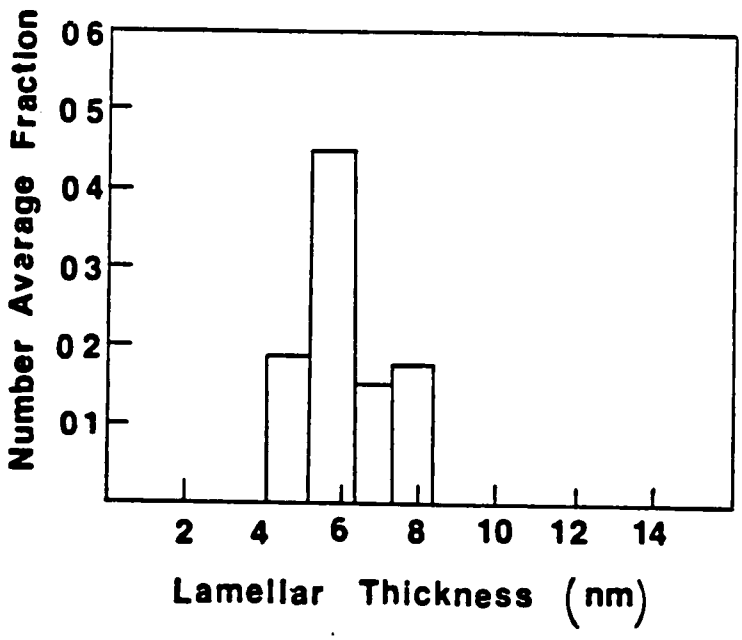
As with many other high polymers, the crystallization of natural rubber is mostly spherulitic in nature. The primary nucleation event may be either homogeneous or heterogeneous in nature. In heterogeneous nucleation, most of the time the nucleation particle is an impurity remaining in an extracted sample of natural rubber or gel particles which are naturally present in the sap of the tree or produced during the coagulation process. In homogeneous nucleation, lamellar crystals can be detected without any central particle.

In hevea rubber, a single lamella or a bunch of lamellae grow into sheaves. Then the lamellae convert into spherulites by splaying and bending back into the equatorial regions. Through both crystallographic and non-crystallographic branching, secondary lamellae are generated and the space in between lamellae is filled.

The morphology of the samples varies depending on the molecular weight and the crystallization temperature. First the morphological observations for the fraction of molecular weight 313,000 over the temperature range studied, will be given; both α spherulites, β spherulites and α-β bimodal spherulites were observed at high undercoolings



a



b

Figure 34 Histograms of lamellar thicknesses of the hevea rubber fractions of (a) molecular weight 543,000 at -2.2 ^{o}C (b) 1,421,000 at -30 ^{o}C.

(Figures 35, 36 and 37 respectively). α-β bimodal spherulites contain both α and β types of lamellae but they are organized into distinct sectors of the spherulite (Phillips and Sorenson 1981). One type of lamella appears to have formed a sheaf with the second type growing as an in-filling process in the equatorial regions of the sheaf. In these spherulites the β lamella grow predominantly in the "edge-on" orientation and the α lamellae in the "side-on" orientation. Around the peak temperature of the growth rate curve mainly spherulites were observed. In Figure 38 growing spherulites which were nucleated close to each other may be seen. As they grew, instead of impinging and generating polyhedra, they interpenetrated each other without having a clear boundary developing between the spherulites, as in Figure 35. In Figure 39 α and β spherulites growing side by side at -12°C are shown. In some regions side-on growth of lamellae are seen. β crystals exhibit a large number of branches and thicker lamellae, another example of a β spherulite being shown in Figure 40. As the temperature of crystallization was increased further, the platelet growth, in which lamellae grow in the "side-on" position, increases (Figures 41 and 42). At -7.3°C darker regions in the growth fronts of lamellae were observed (Figure 43). Darker regions in an OsO_4 stained film correspond to more heavily stained portions which might result from consumption of the crystallizable material in front of lamellae. At

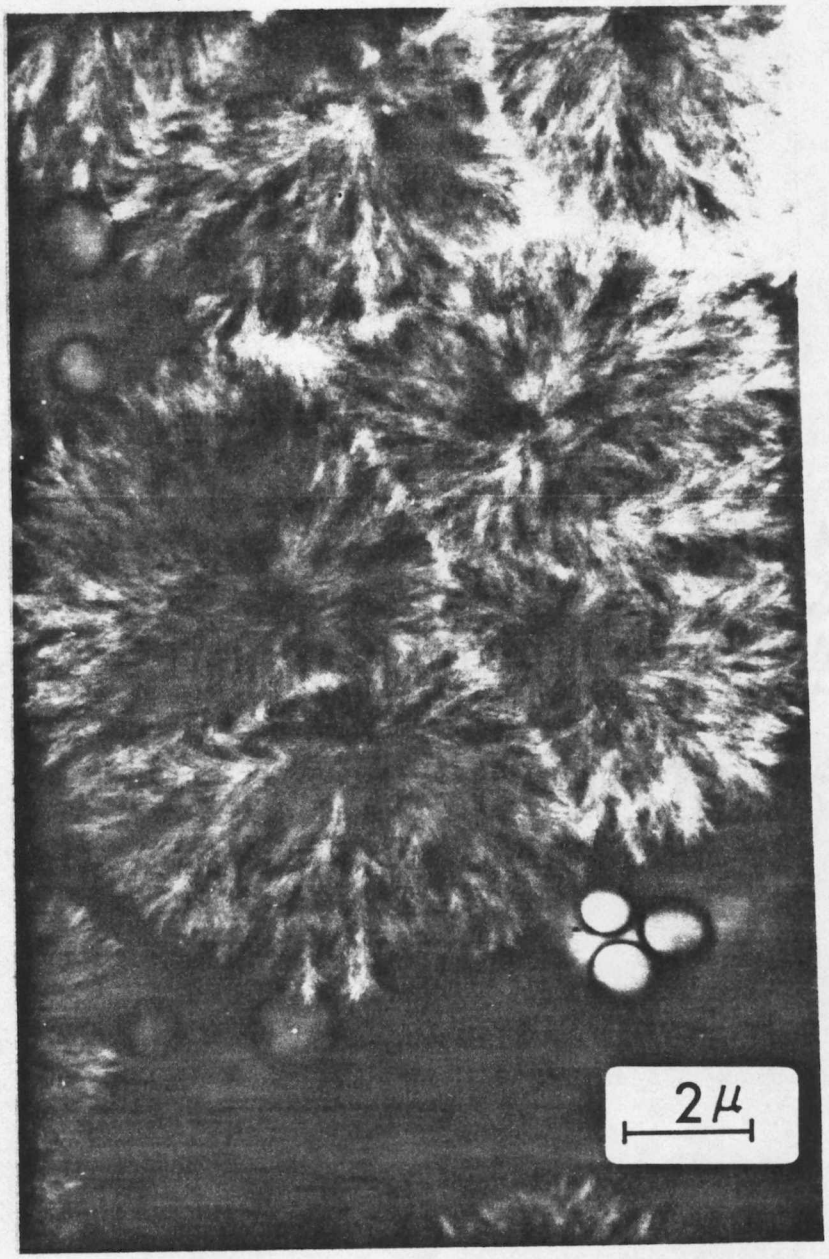


Figure 35 α-spherulites of a hevea rubber fraction of molecular weight 313,000.

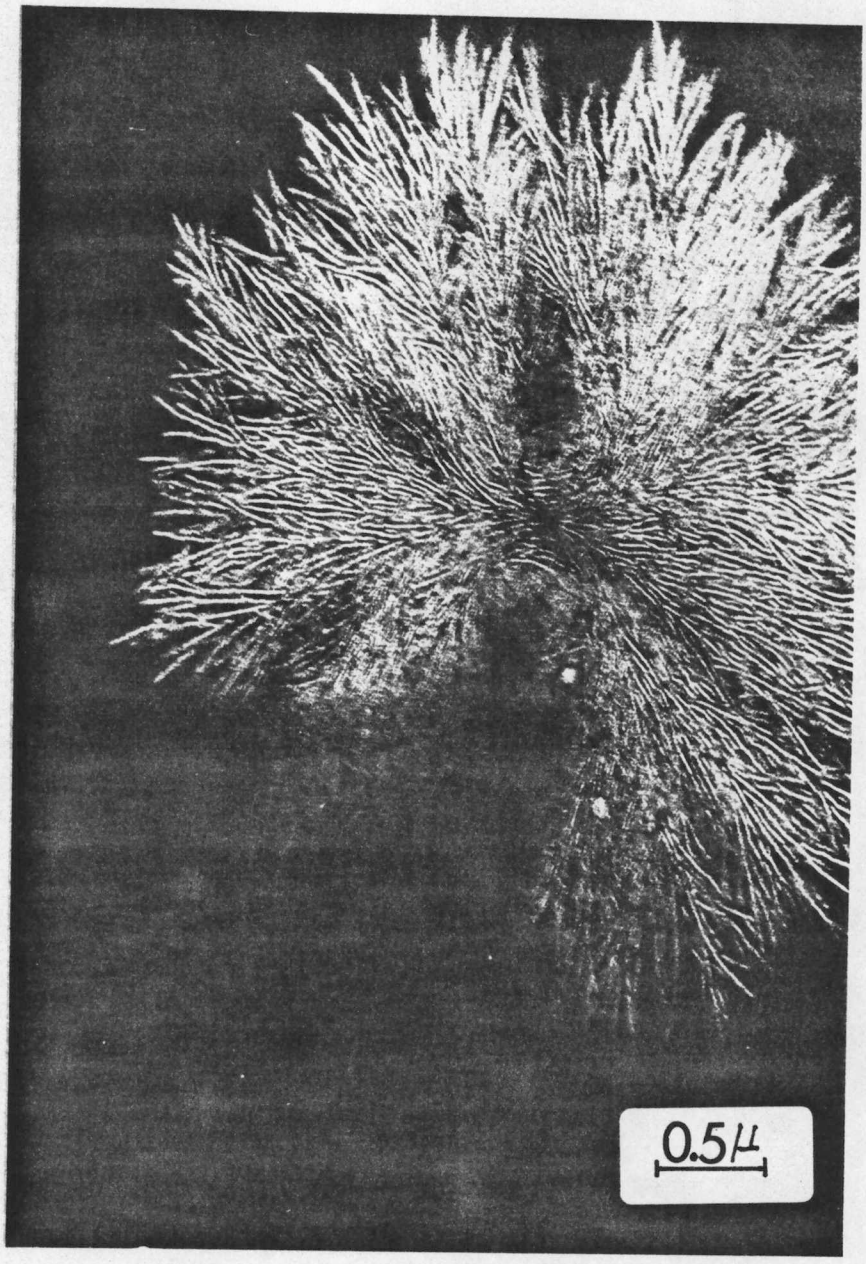


Figure 36 β-spherulite of a hevea rubber fraction of molecular weight 313,000.

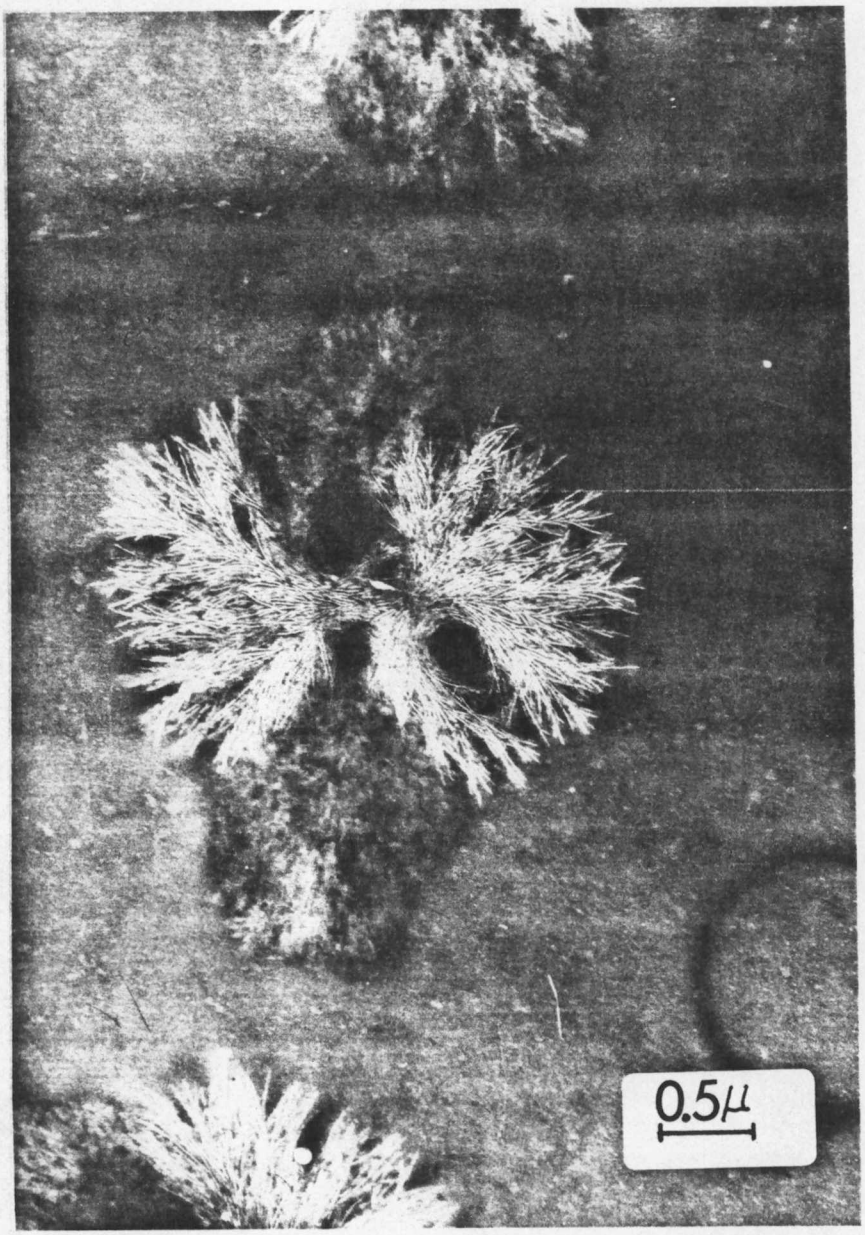


Figure 37 α-β bimodal spherulite of a hevea rubber fraction of molecular weight 313,000 grown at -30 °C.

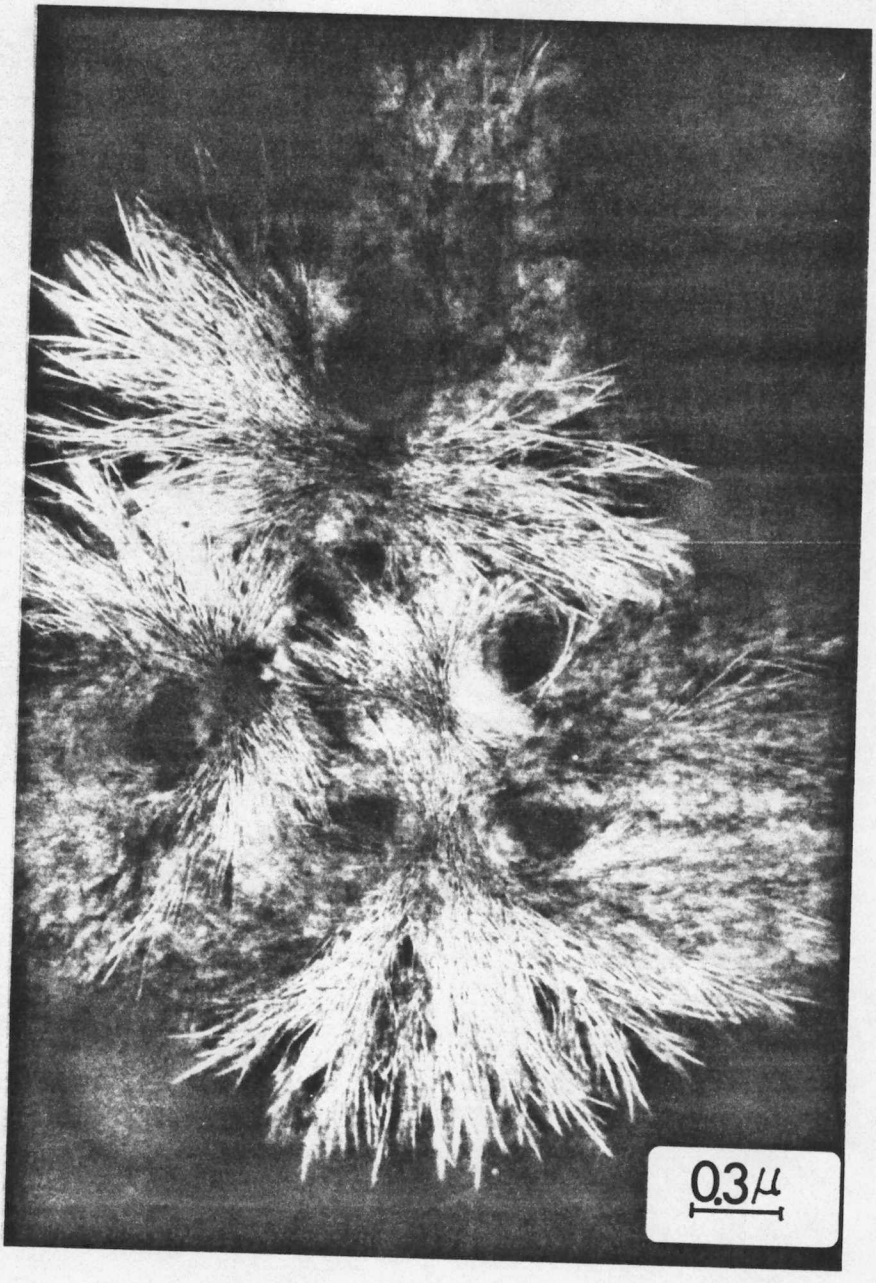


Figure 38 Spherulites of hevea rubber fraction of molecular weight 313,000 growing at -20 °C.

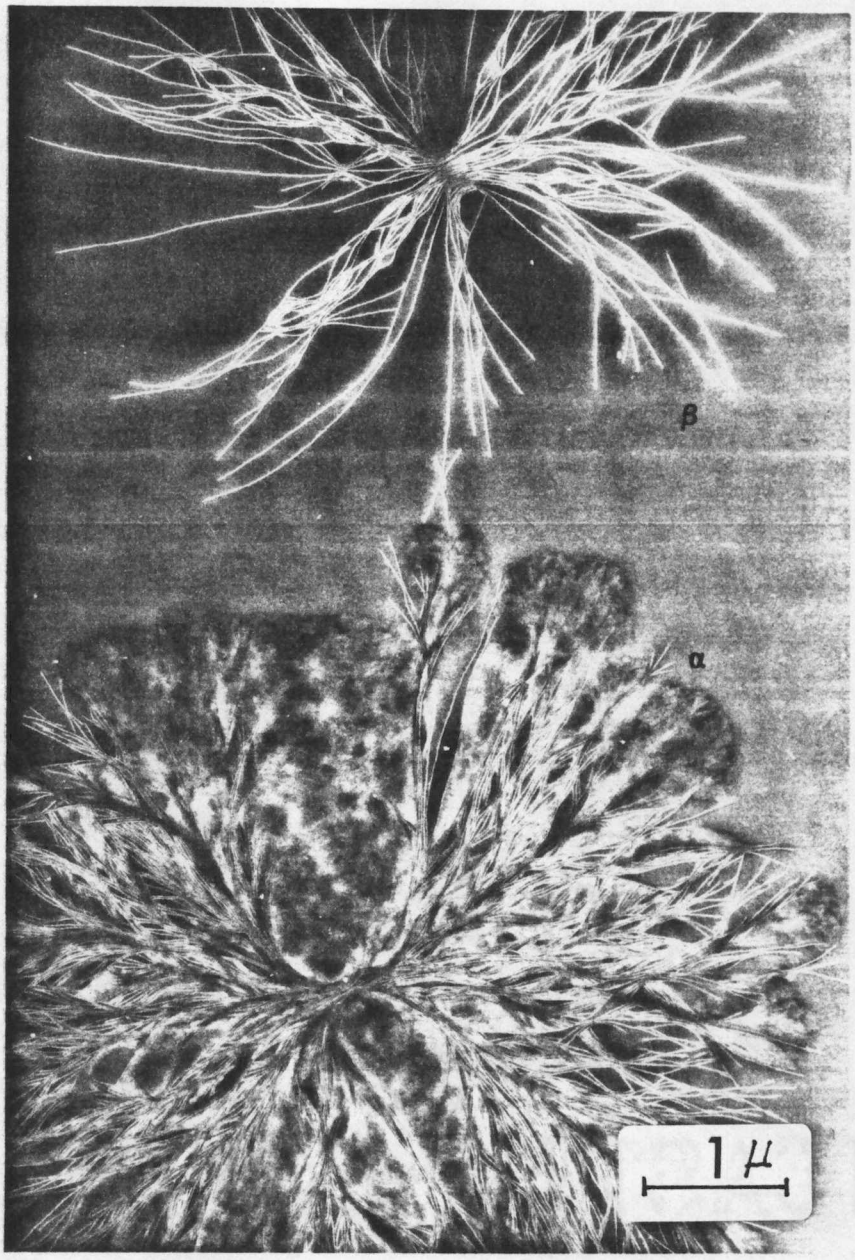


Figure 39 α and β spherulites growing in hevea rubber fraction of molecular weight 313,000.

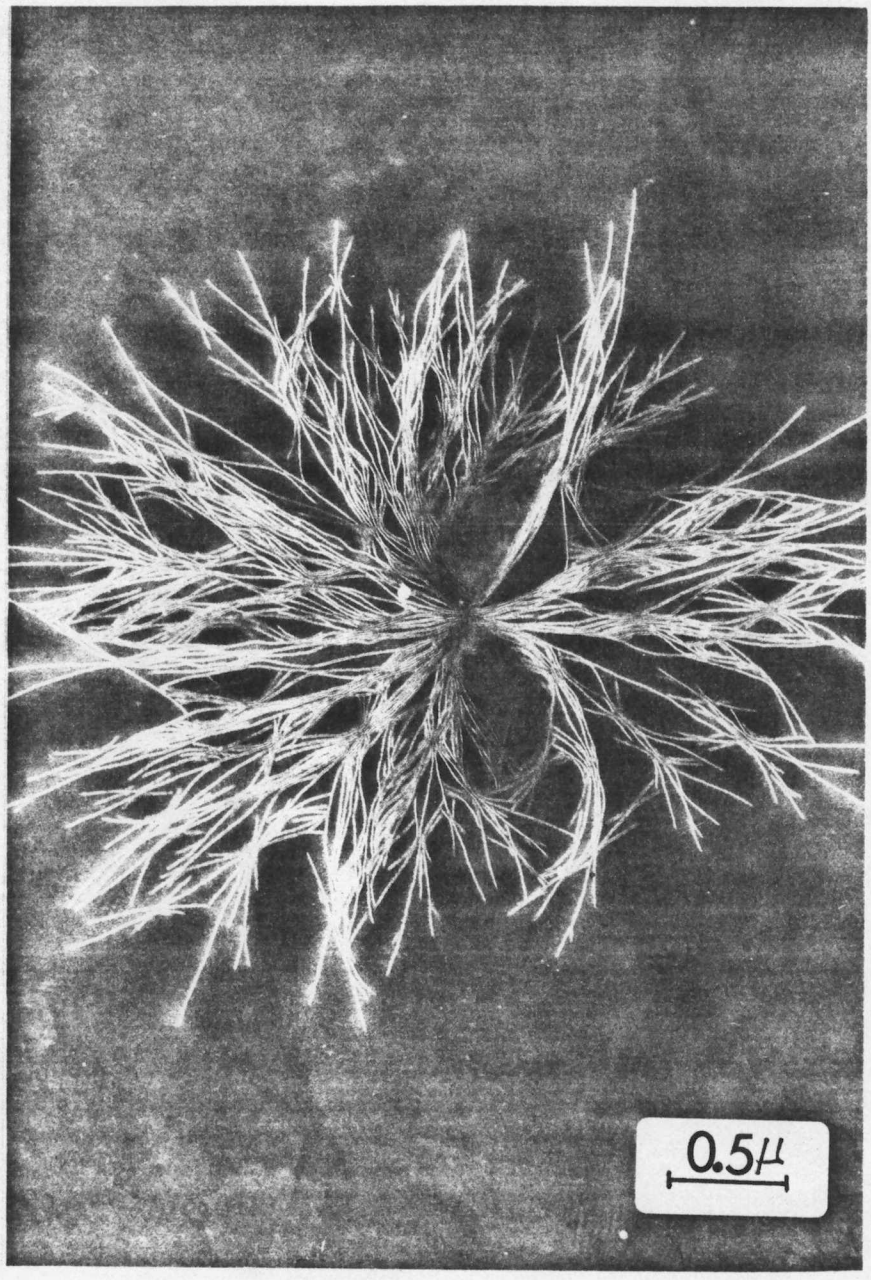


Figure 40 β spherulite growing in a hevea rubber fraction of molecular weight 313,000 at -15 °C.

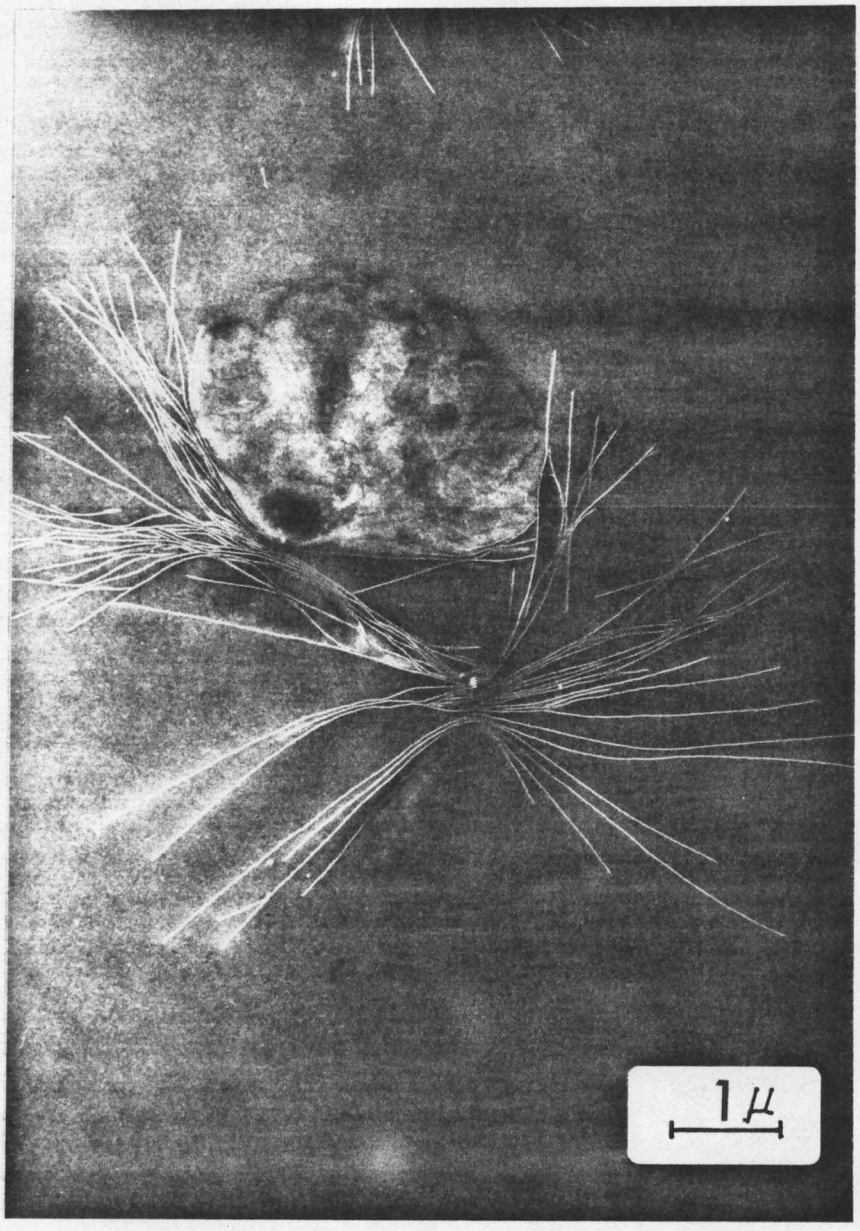


Figure 41 A sheaf showing both the "edge-on" and platelet-like growth of a hevea rubber fraction of molecular weight 313,000 at -5 °C.

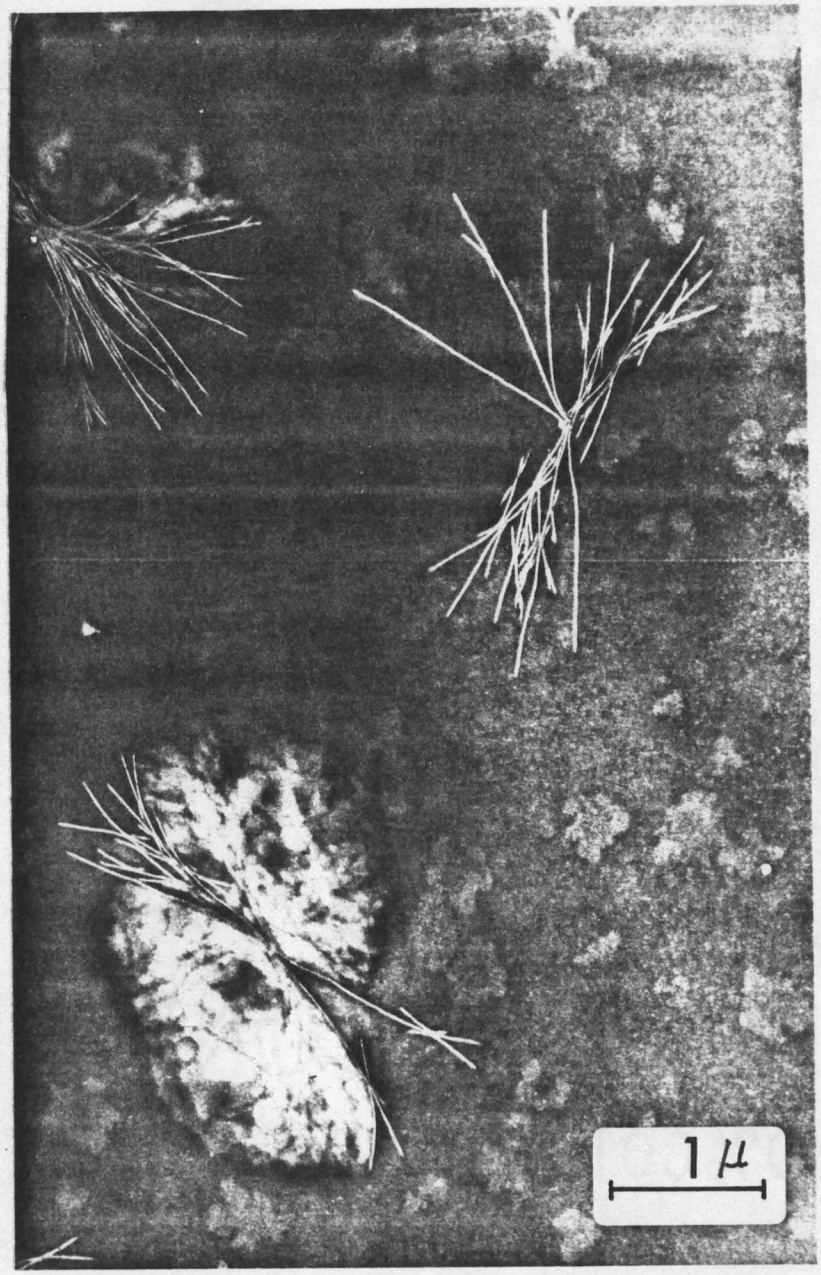


Figure 42 Platelet-like growth observed in a hevea rubber fraction of molecular weight 313,000 at -7.3 °C.

temperatures higher than -8°C single crystals were observed. Their density increased with increasing crystallization temperature and they become dominant at +3°C (Figure 44). These skeletalized single crystals are similar, but better reveal details, than the ones which have been reported earlier for unfractionated hevea rubber crystallized under pressure (Edwards and Phillips 1976). At -3.5°C discontinuities in lamellae were observed (Figure 45). Breaks were sharp and occurred at almost equal distances from each other. Similar behavior has not been reported for any polymer. At +0.8°C platelet growth becomes more pronounced (Figure 46). It is believed that these objects are axialites. In Figure 47 a single crystal and an axialite which were nucleated together may be seen. The circles seen in the pictures are water droplets produced from ice crystals which condensed on the film during crystallization.

The other sample which was studied in more detail than the others was the fraction of molecular weight 543,000. At high undercoolings the morphology did not differ from the fraction of molecular weight 313,000, except in that some sheaf like species, in which equatorial growth is suppressed, are seen (Figure 48). At the temperature of maximum rate of crystallization, sheaves or well grown spherulites were observed depending on the crystallization time (Figures 49 and 50). Figures 51 and 52 show row nucleation occurring adventitiously at -10°C and at -5°C

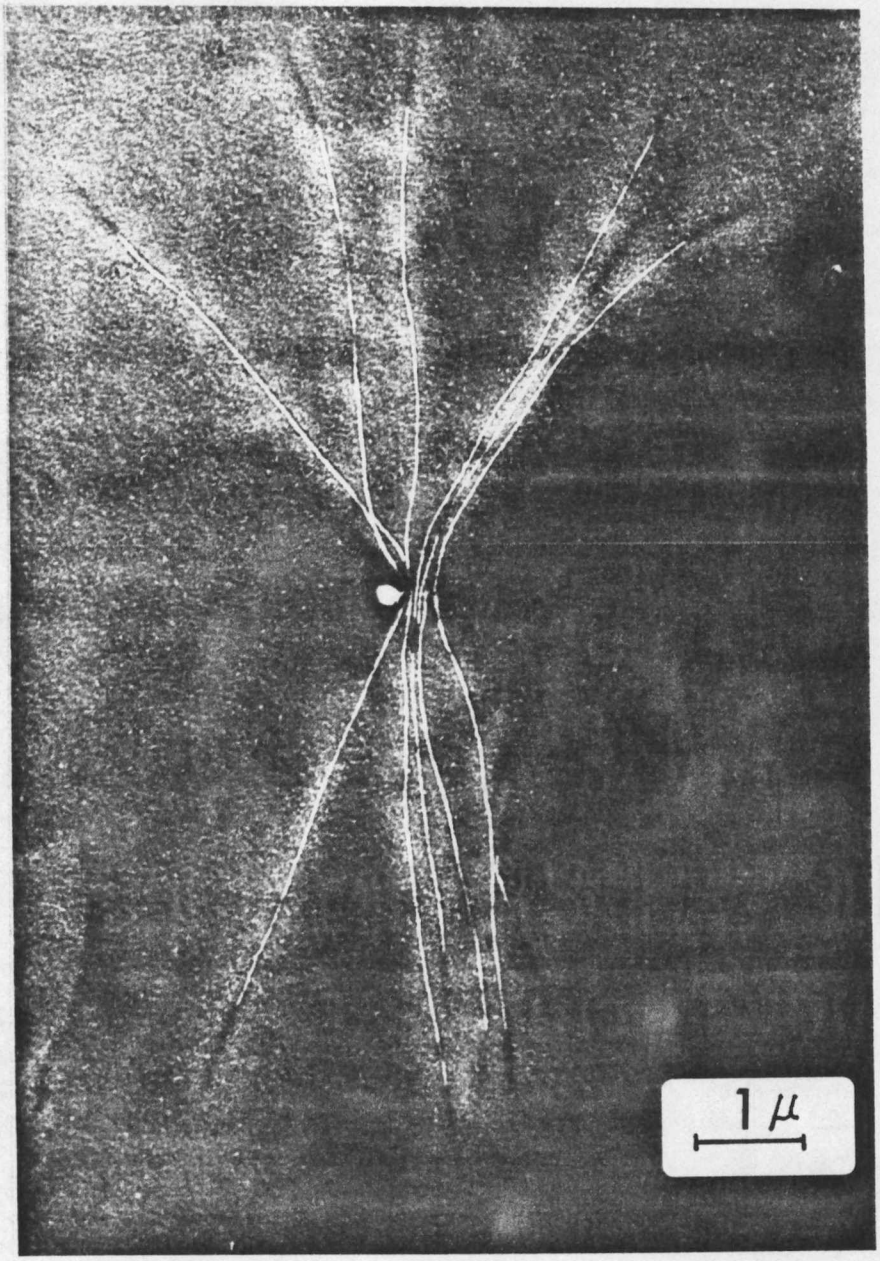


Figure 43 Lamellae observed in a hevea rubber fraction of molecular weight 313,000 at -7.3 °C.

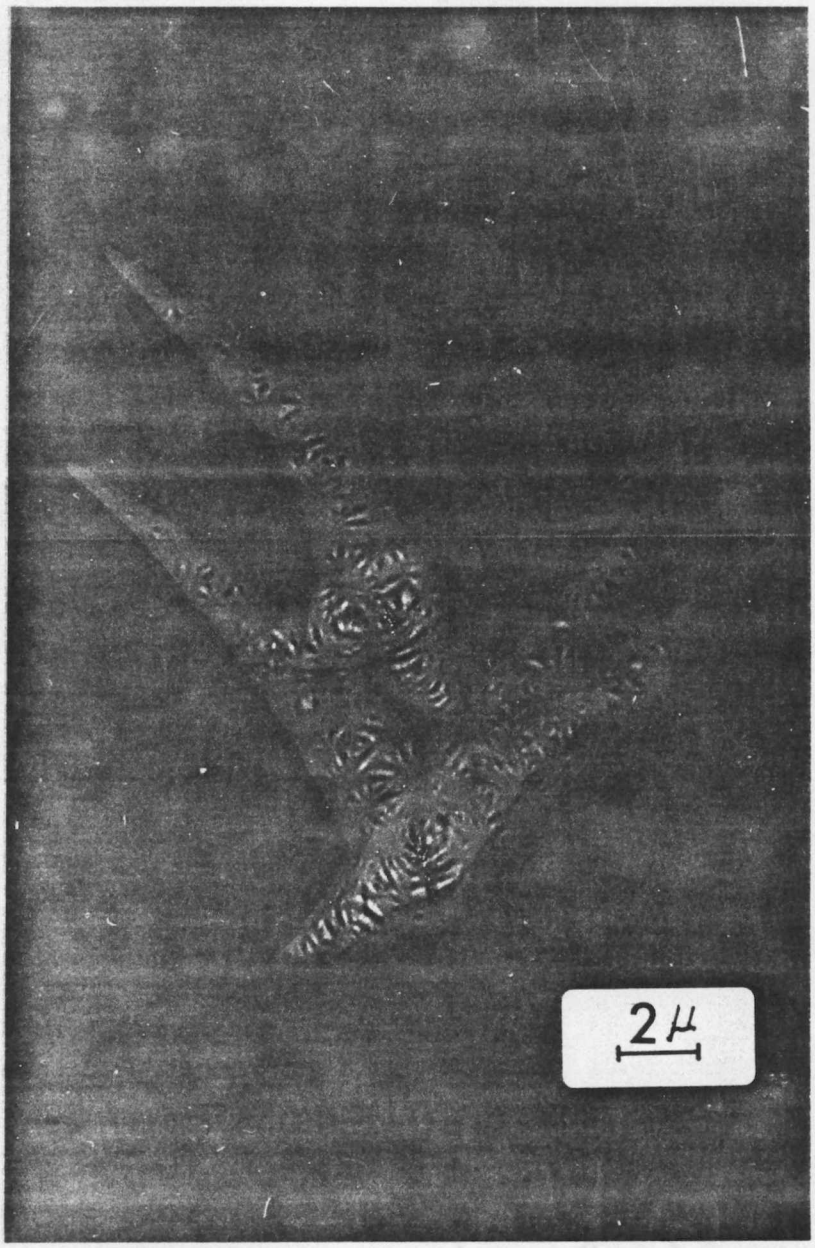


Figure 44 Single crystals observed from hevea rubber fraction of molecular weight 313,000 at +3 °C.

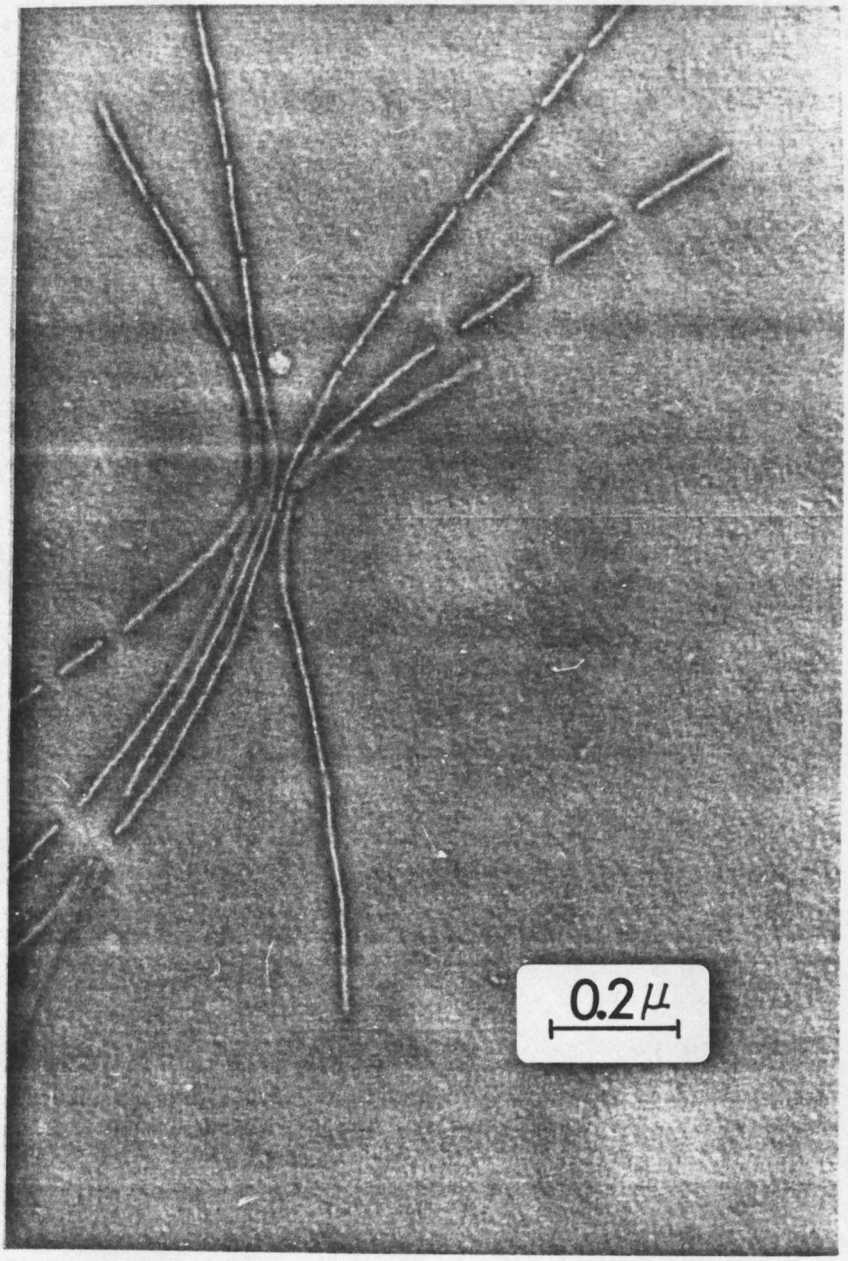


Figure 45 Discontinuities observed in lamellae of a hevea rubber fraction of molecular weight 313,000 at -3.5 °C.



Figure 46 Platelet-like growth observed in a fraction of molecular weight 313,000 at +1.8 °C.

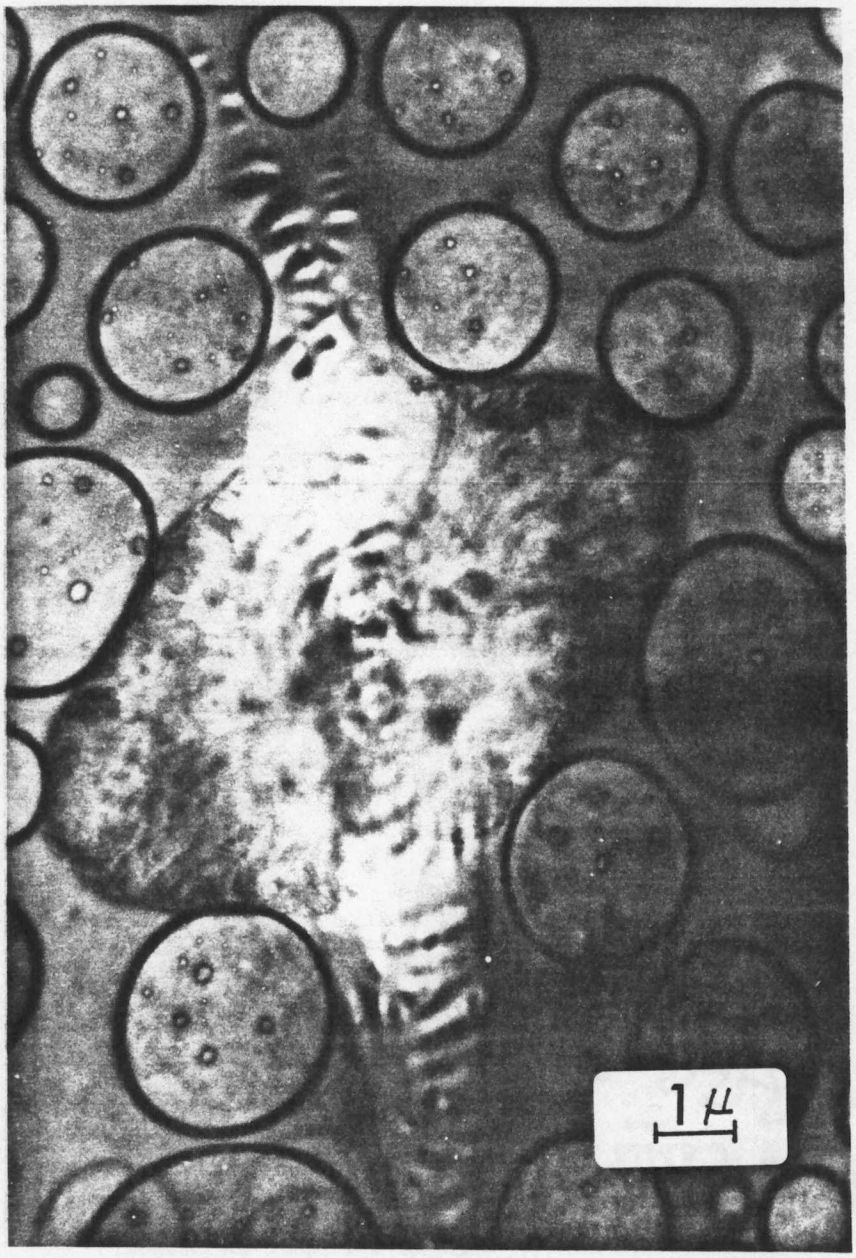


Figure 47 Co-nucleated single crystal and axialite grown at +1.8 °C.



Figure 48 A sheaf-like spherulite in which the equatorial growth process is suppressed in the fraction of molecular weight 543,000 at -40 °C.

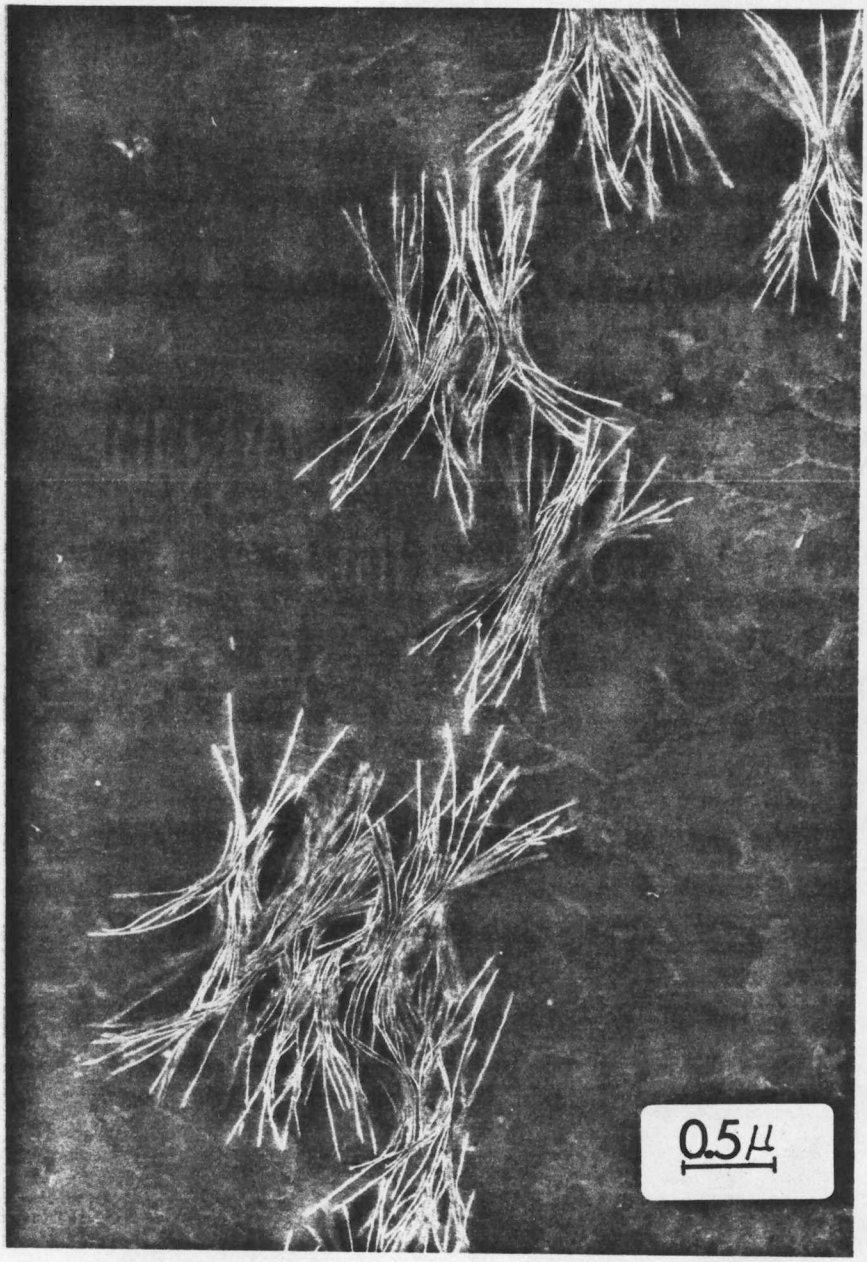


Figure 49 Growing sheaves in a fraction of molecular weight 543,000 at -20 °C.

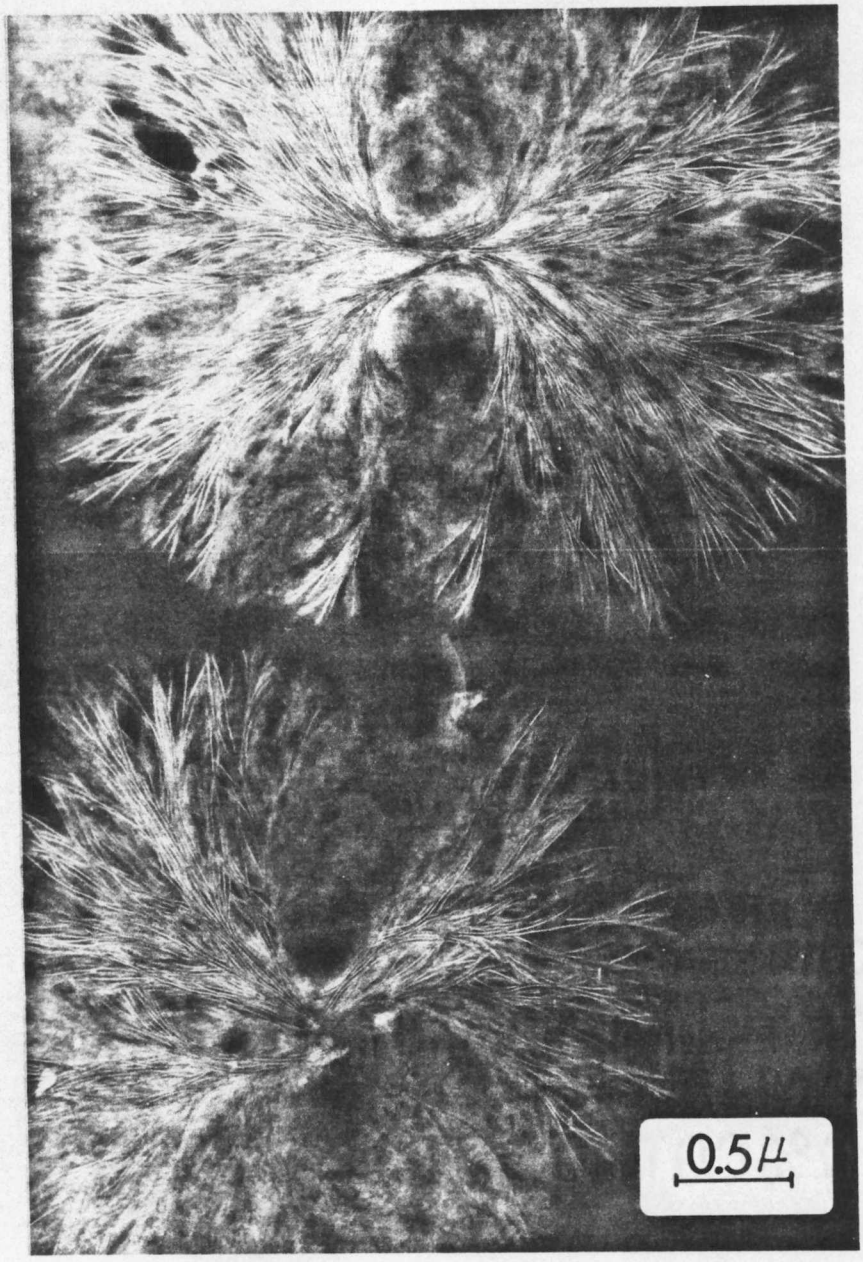


Figure 50 Spherulites in a fraction of molecular weight 543,000 at -20 °C.

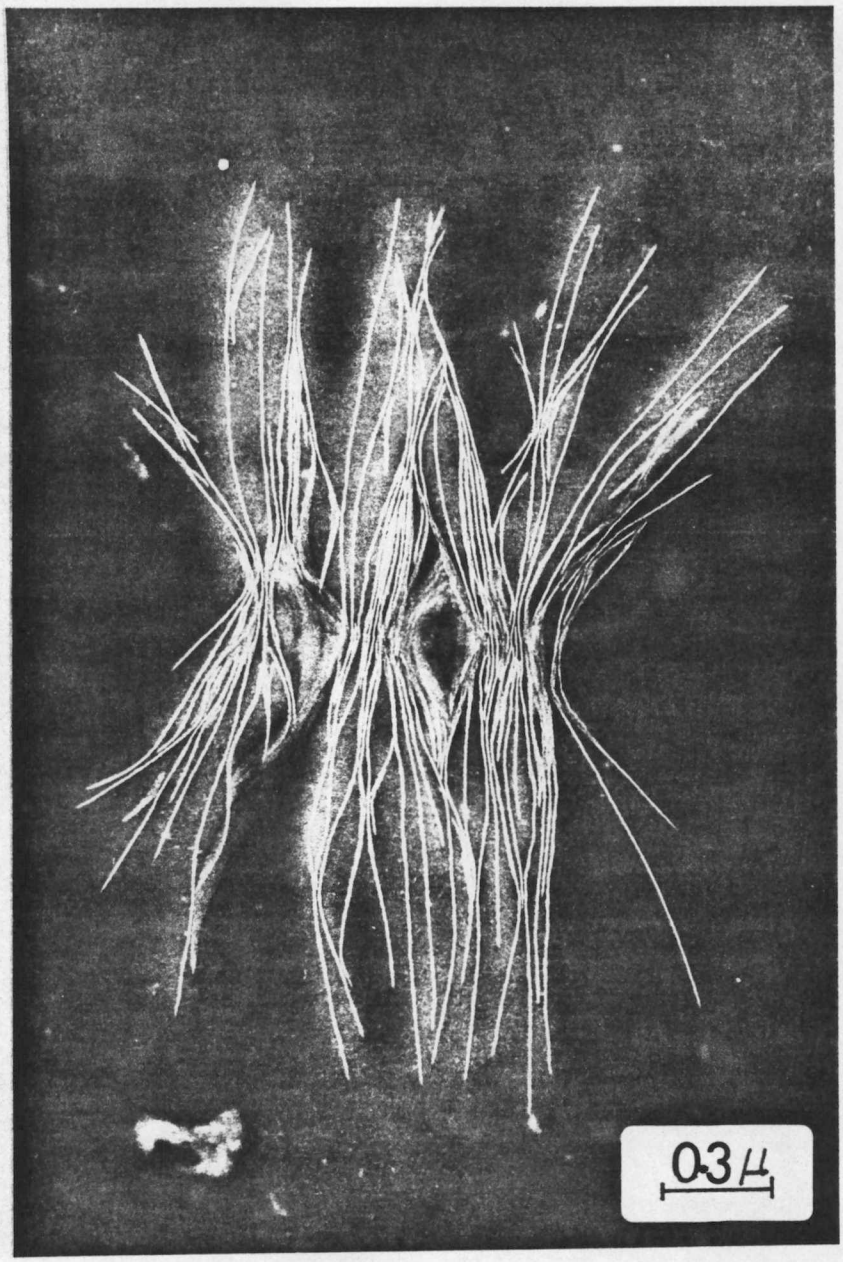


Figure 51 Row-nucleated lamellae in a fraction of molecular weight 543,000 at -10 °C.

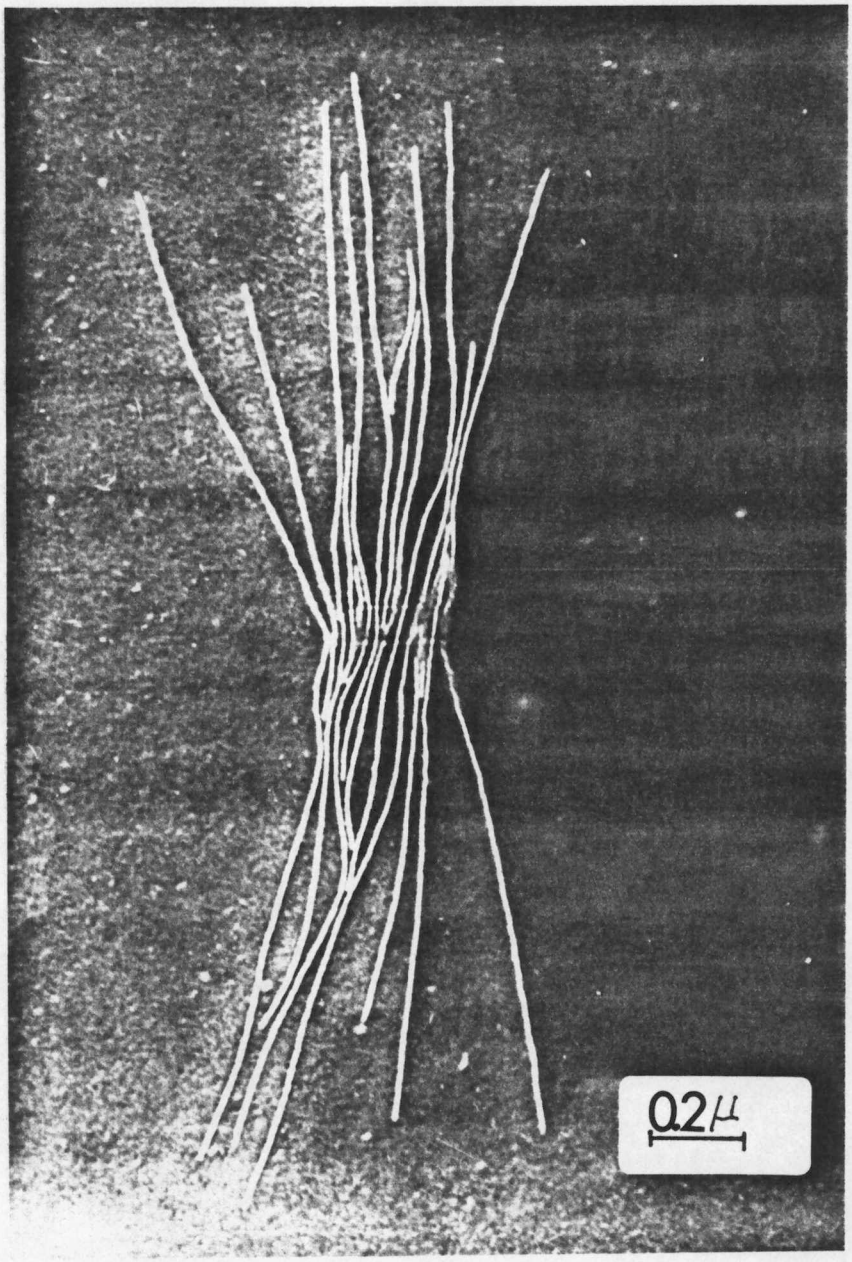


Figure 52 Row-nucleated lamellae in a fraction of molecular weight 543,000 at -5 °C.

respectively. The presence of strain in films has been reported to result in the production of aligned row nucleated structures (Andrews 1964). Above about -5°C platelet growth was observed along with the sheaves growing in the "edge-on" position (Figure 53). Above -0.6°C single crystals were occasionally seen (Figure 54), but their concentrations were much lower than those seen in the fraction of molecular weight 313,000. At +2.2°C "S" shaped lamellae were observed, in Figure 55 a microgel particle is seen to be the nucleation site for such lamellae. In the regions where lamellae cross the water droplets, discontinuities are present. However, it is not clear whether the presence of the water droplets is the cause for the breaks or whether it is only a coincidence. In Figure 56 some lamellae are seen to have almost regular undulations, while others are straight.

The highest molecular weight fraction available was 1,421,000. In this case besides normal spherulites, lozenge shaped crystals were seen at high undercoolings (Figure 57). In the fraction of molecular weight 897,000, at high undercoolings the fractions of α-β bimodal spherulites (Figure 58) and of sheaves with suppressed equatorial growth (Figure 59) were higher than for other samples. No single crystals were observed at any crystallization temperature. At temperatures above -8°C a somewhat lower amount of platelet growth than in the other fractions was observed.

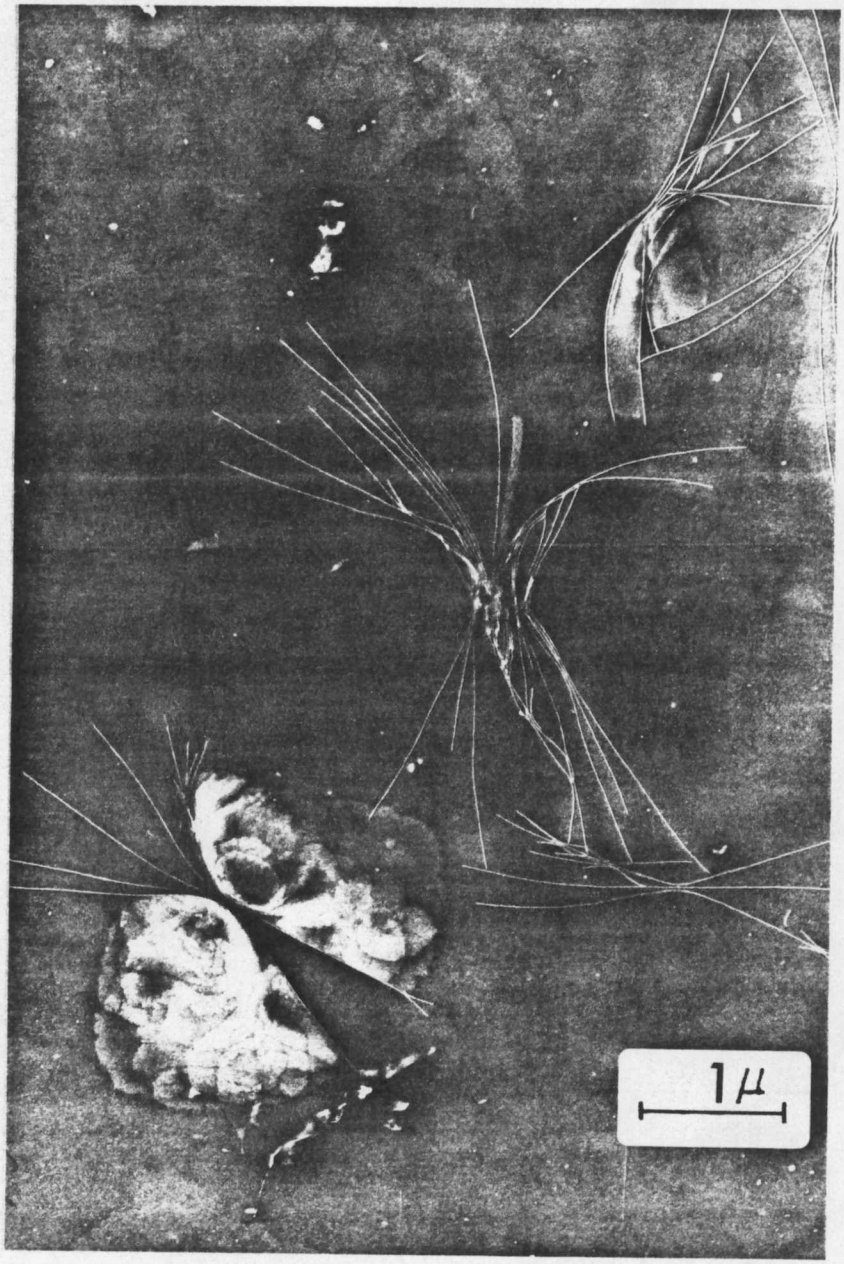


Figure 53 An axialite and lamellae growing in the "edge-on" orientation in a fraction of molecular weight 543,000 at -0.6 °C.

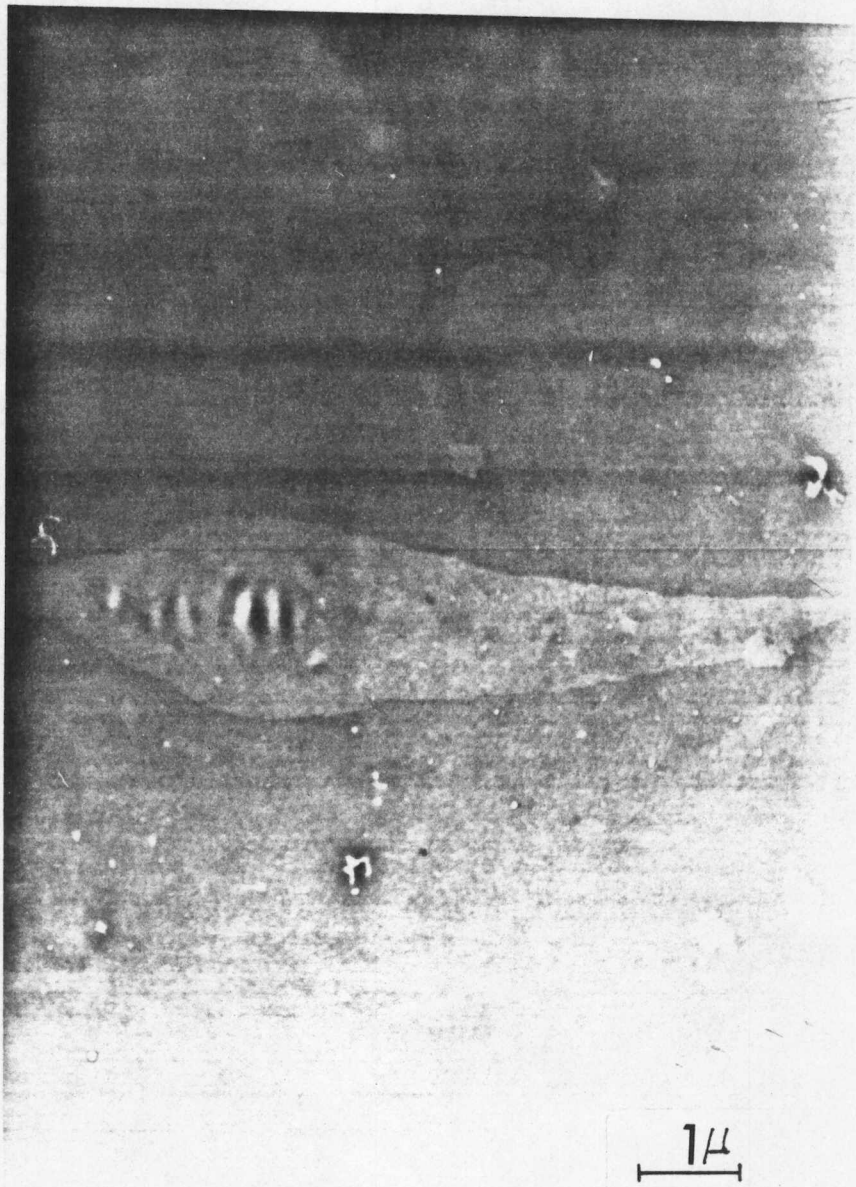


Figure 54 A single crystal growing in a fraction of molecular weight 543,000 at - 0.6 °C.

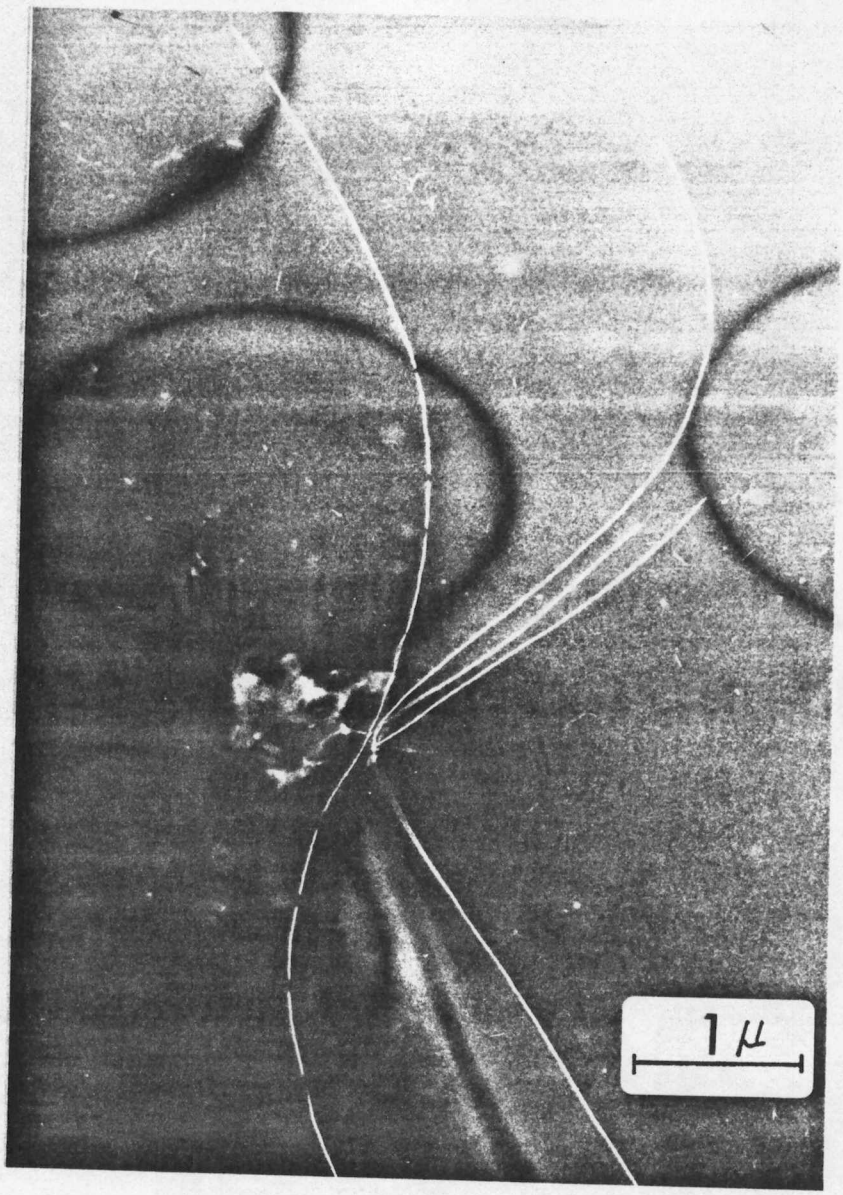


Figure 55 "S" shaped lamella in a fraction of molecular weight 543,000 at +2.2 °C.



Figure 56 Platelet-like growth along with lamellae growing in the "edge-on" orientation in a fraction of molecular weight 543,000 at +2.2 °C.

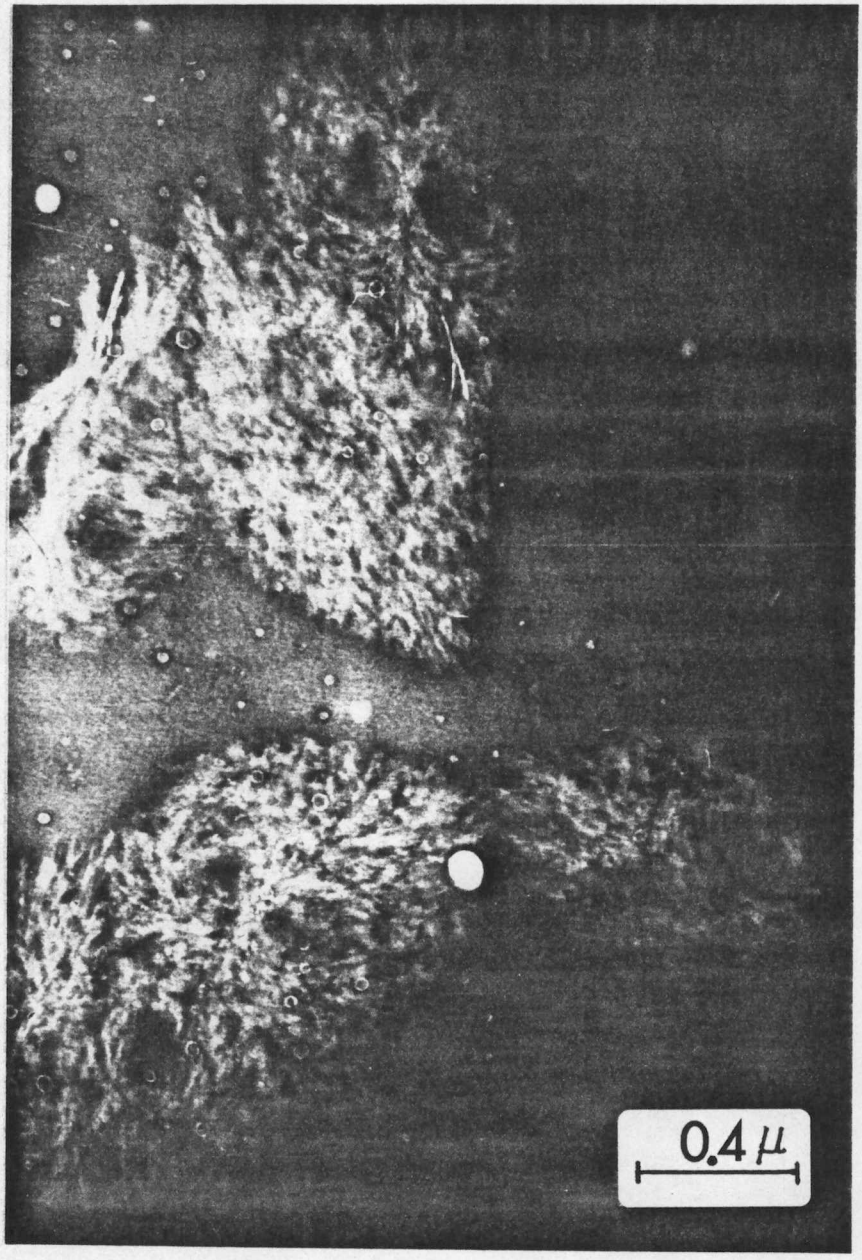


Figure 57 Lozenge shaped crystals in a fraction of molecular weight 1,421,000 at -26 °C.

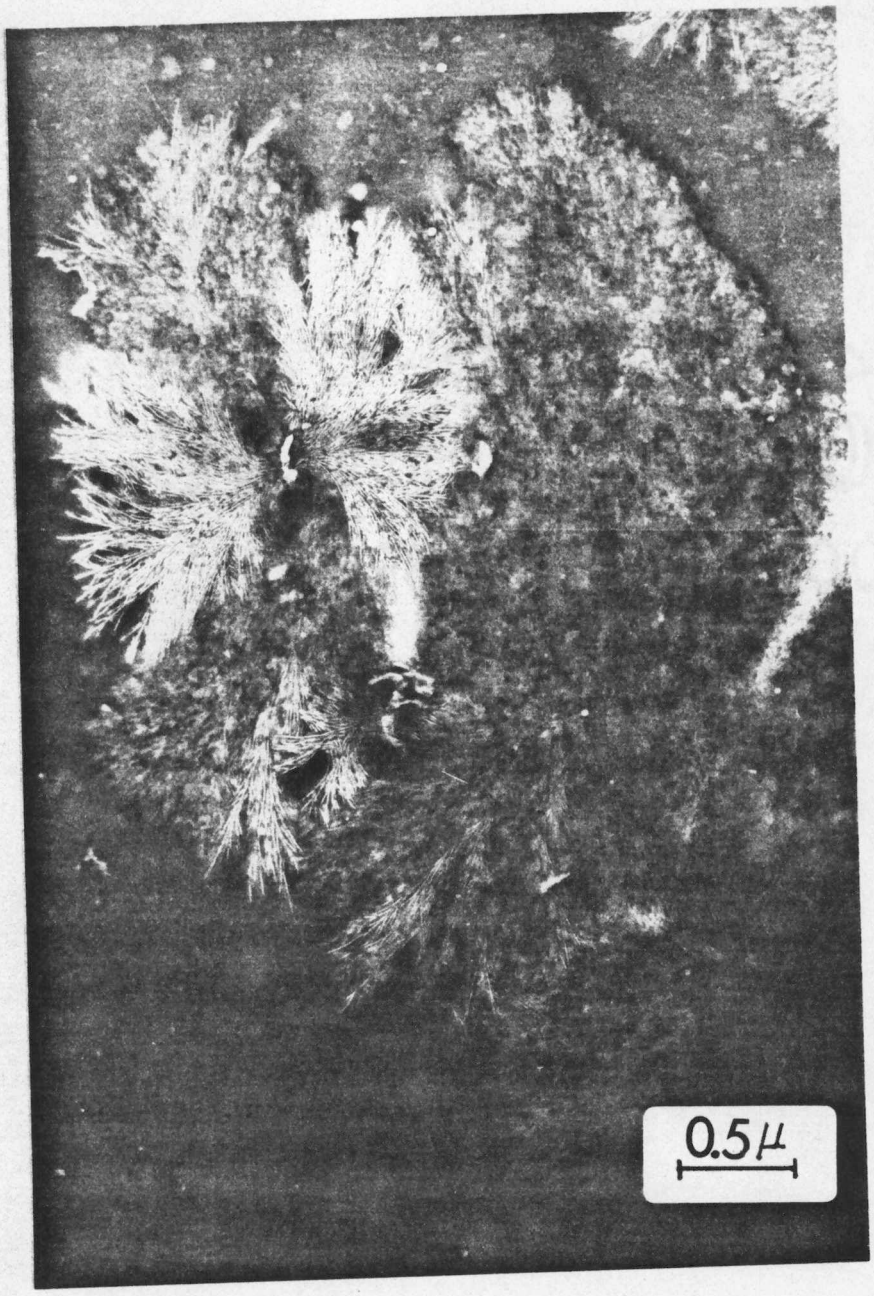


Figure 58 An α-β bimodal spherulite in a fraction of molecular weight 897,000 at -34 °C.

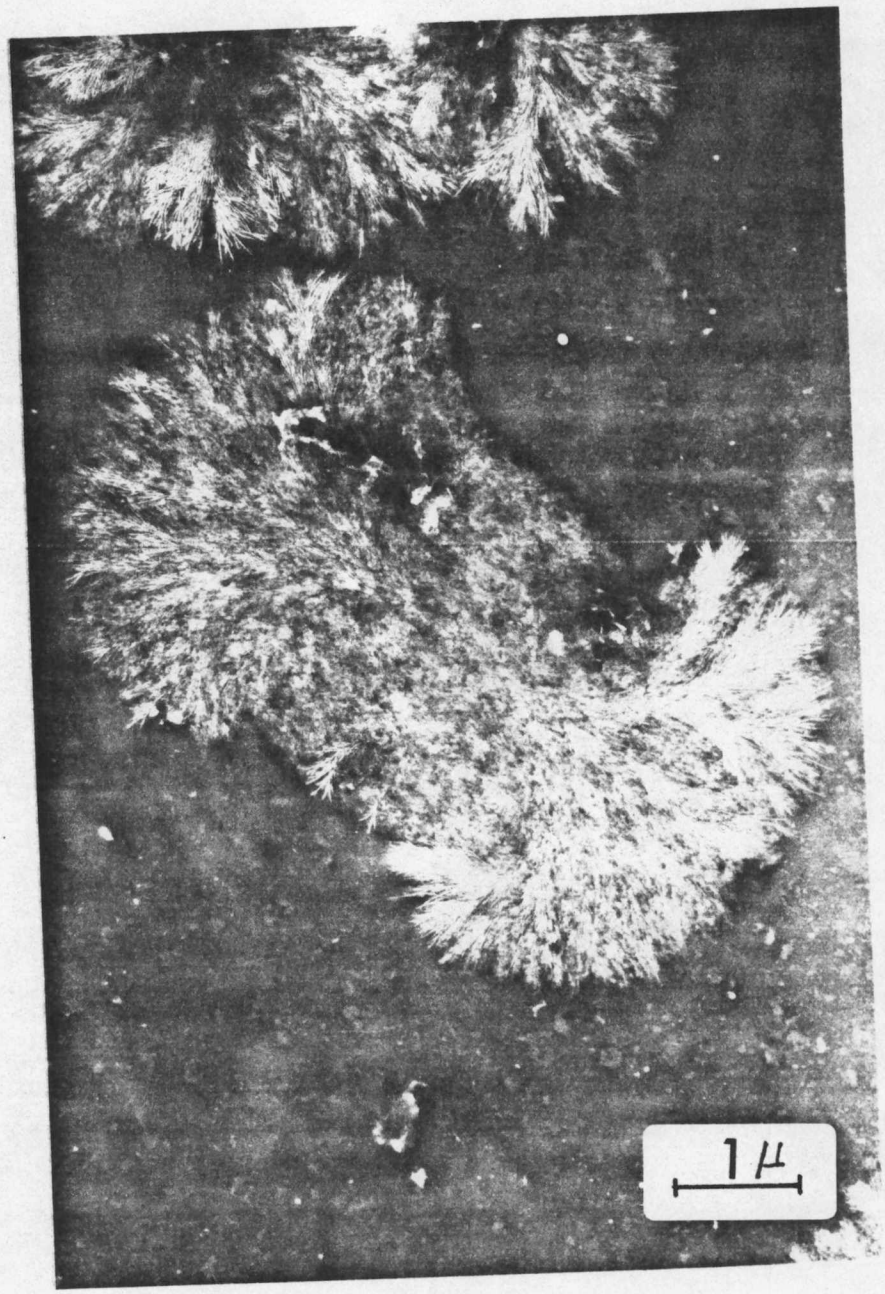


Figure 59 A growing sheaf in which the equatorial growth process is suppressed in a fraction of molecular weight 897,000 at -34 °C.

4.2.5. Branching Studies

Quantitative measurements were made of the branching frequency of two fractions, namely the ones with molecular weights 313,000 and 543,000. In this study, branching frequency was defined as the number of crystallographic branch points per lamella. The variation of branching frequency with crystallization temperature is plotted in Figures 60 and 61 for these two fractions. In Figure 60 the numbers on the graph refer to the regimes in which the fraction crystallized (see discussion section). The regime I - regime III populations appear to part of a continuous curve whereas regime II appears to have a discontinuous rise and decay superposed on the base curve. In Figure 61, the branching frequency versus crystallization temperature of the fraction of molecular weight 543,000 is shown. Here only an upward trend in branching with increasing supercooling is observed.

In linear polyethylene, it was observed (Philpot and Phillips 1986) that branching was caused by the preponderance of screw dislocations at certain undercoolings. High magnification pictures of detailed branching points are given in Figures 62-67. In most of the branch points the secondary lamella exhibits a curved section at the nucleation point. After nucleation, the secondary lamella grows in both directions. The growth rate

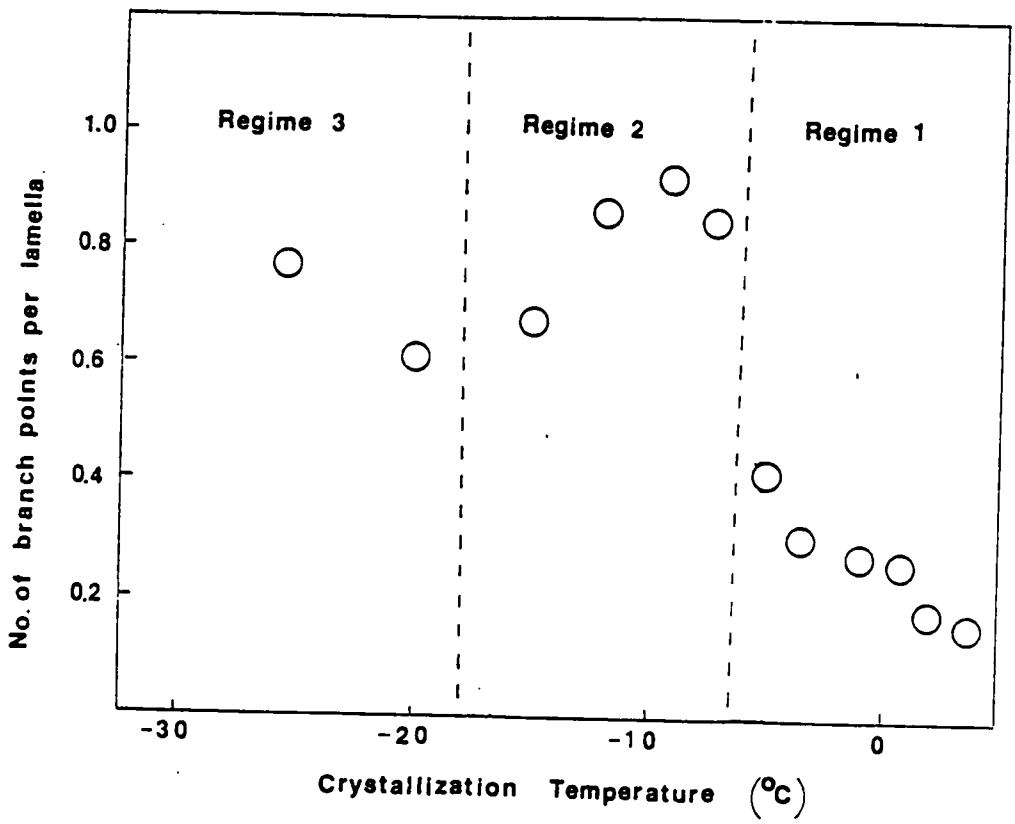


Figure 60 Branching frequency versus temperature of the hevea rubber fraction of molecular weight 313,000.

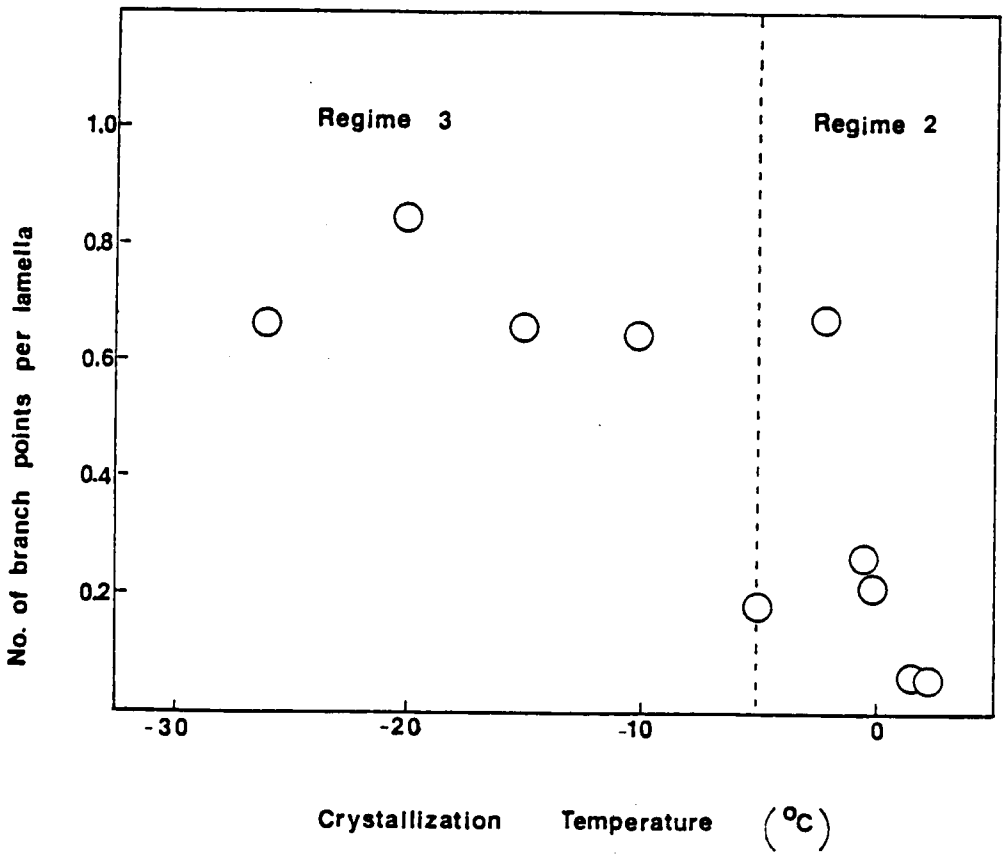


Figure 61 Branching frequency versus temperature of the hevea rubber fraction of molecular weight 543,000.

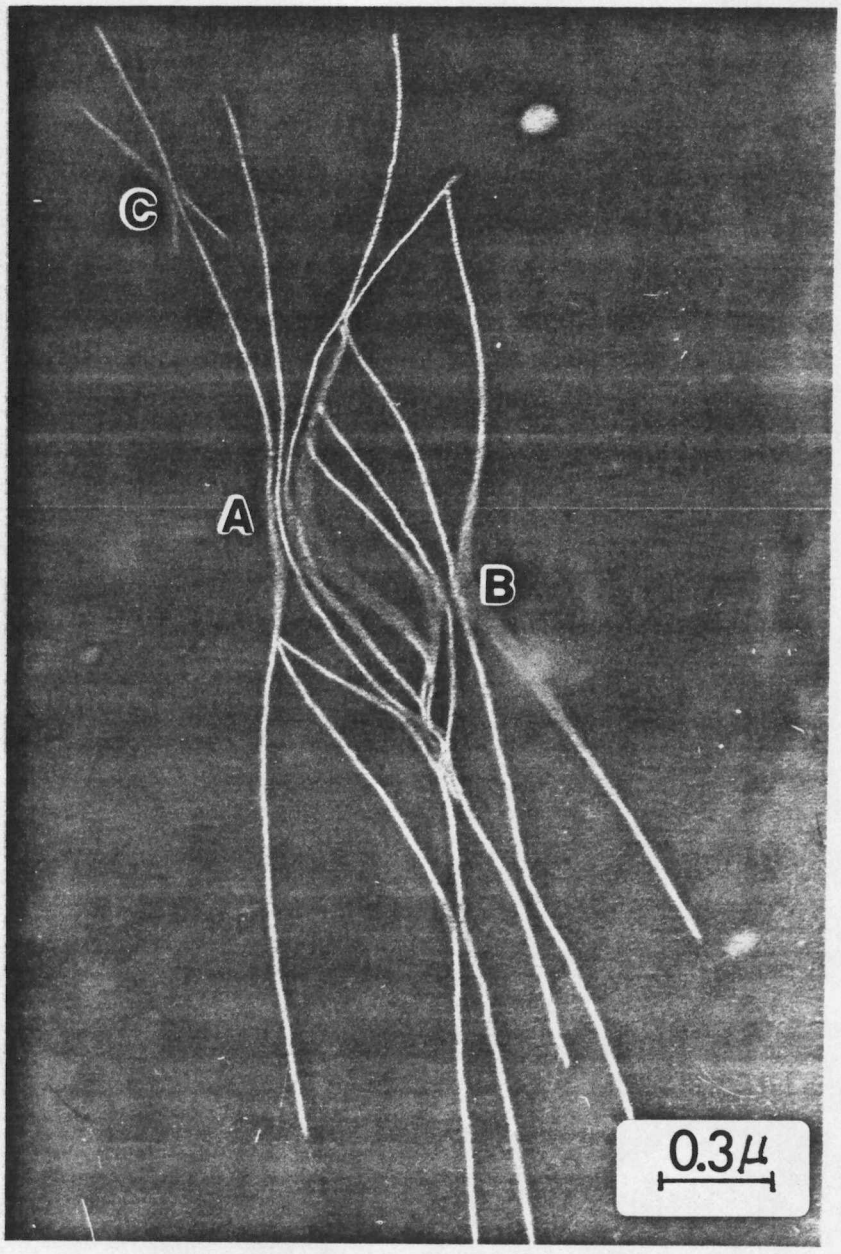


Figure 62 Two growing sheaves in a fraction of molecular weight 543,000 at +1.4 °C.

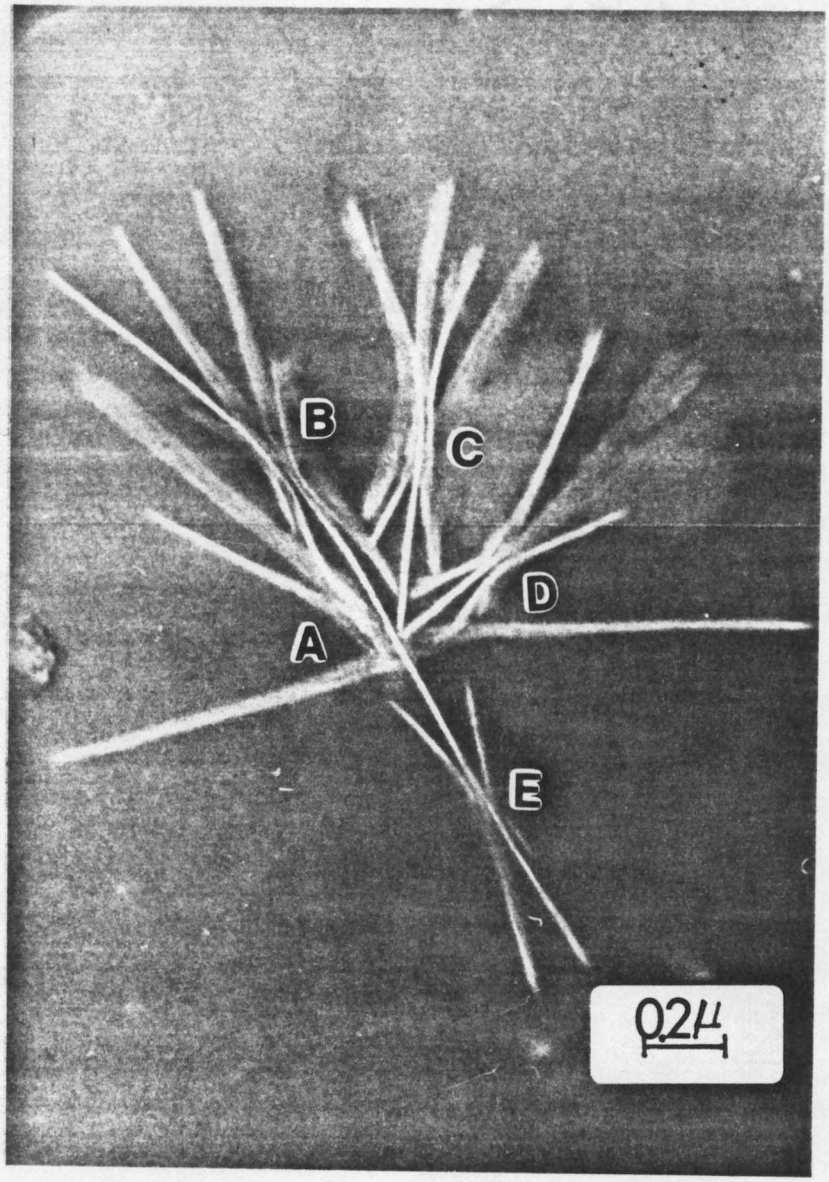


Figure 63 Heterogeneous nucleation in a fraction of molecular weight 543,000 at -2.2 °C.

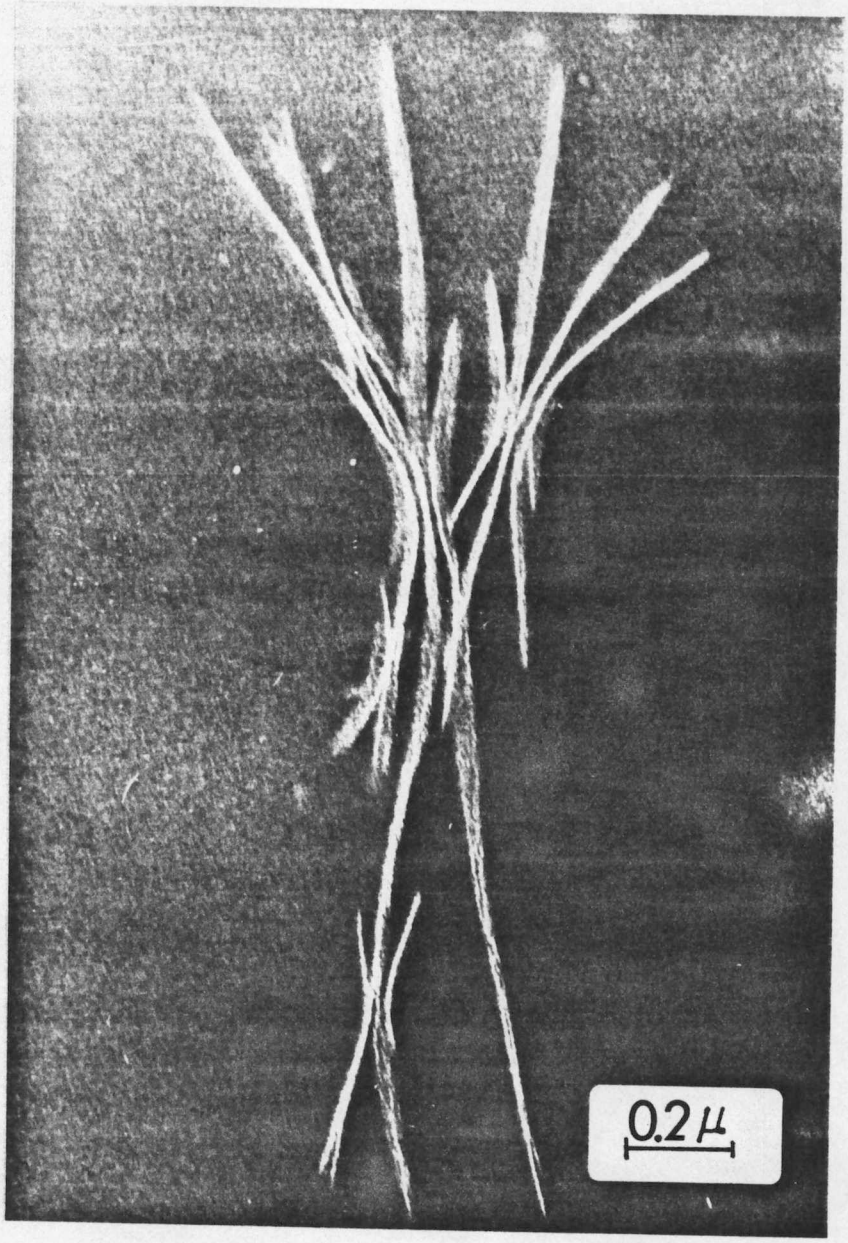


Figure 64 A growing sheaf in a fraction of molecular weight 543,000 showing clear branch points.

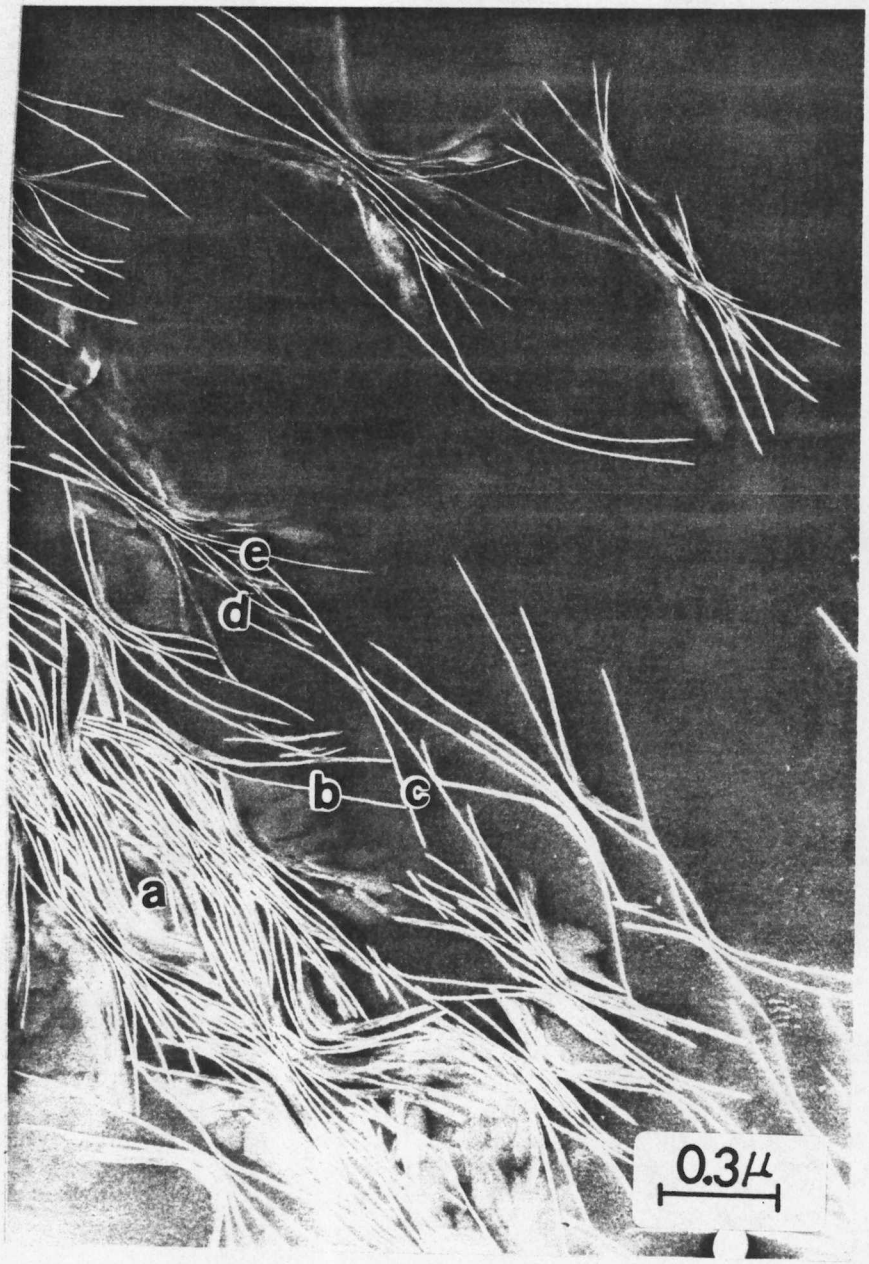


Figure 65 Row nucleation in a fraction of molecular weight 543,000 at -2.2 °C.

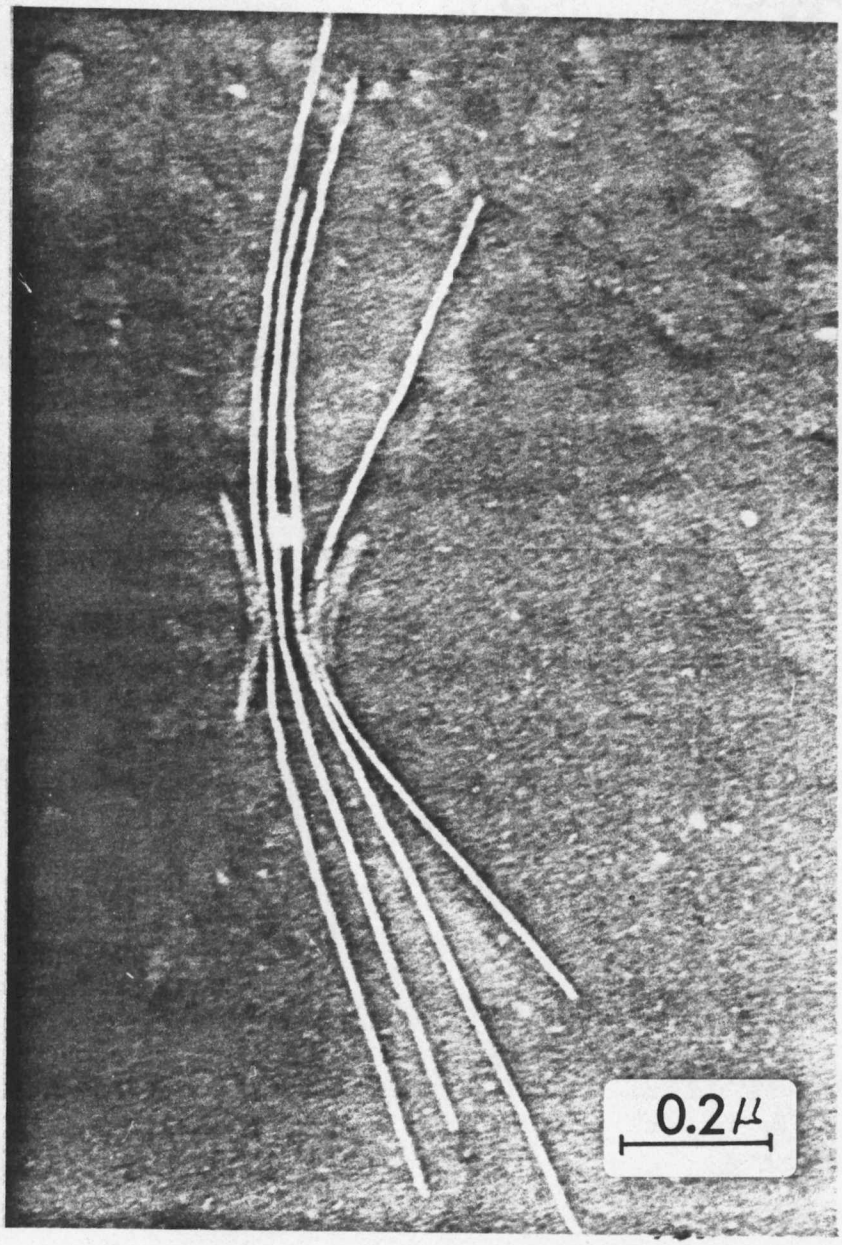


Figure 66 A growing sheaf in a fraction of molecular weight 543,000 at -5 °C.

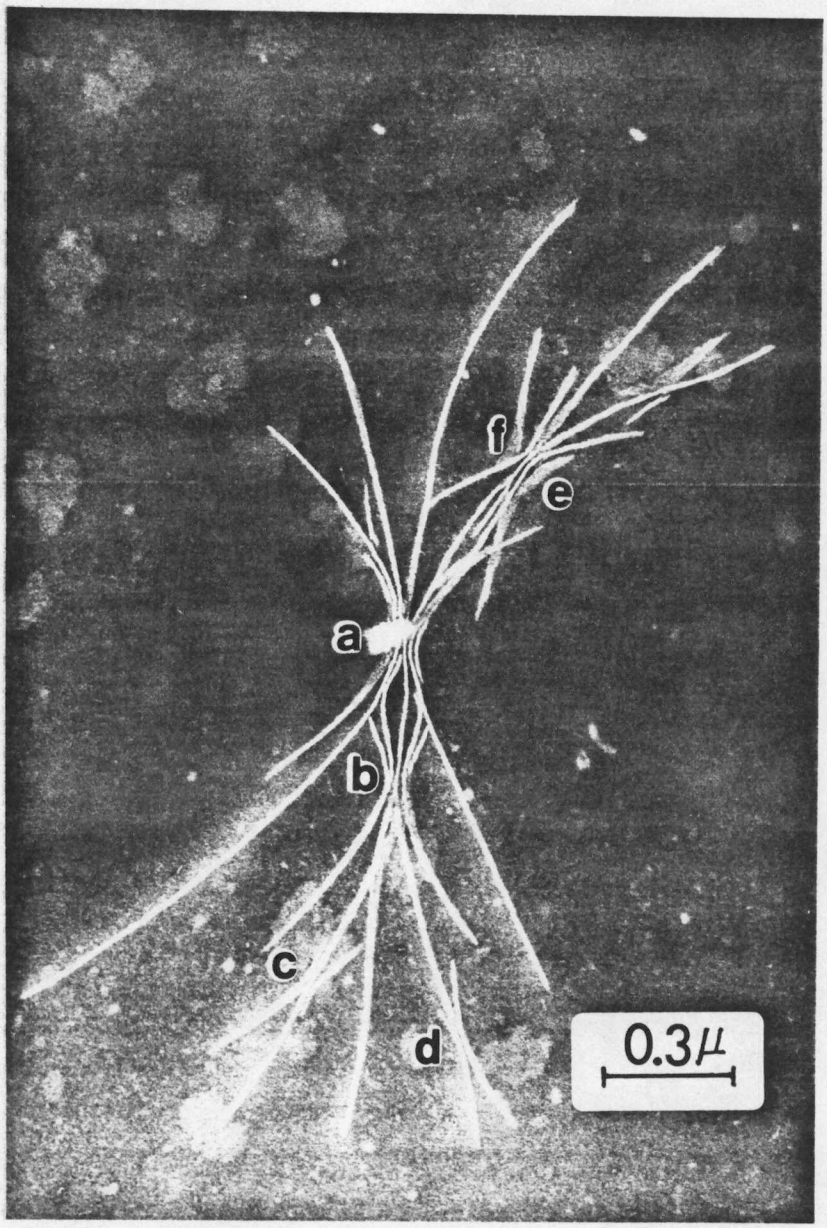


Figure 67 A sheaf nucleated from a microgel in a fraction of molecular weight 897,000 at -5 °C.

in the two directions is not always the same, resulting in asymmetric branches in some cases. The distance between the original and the secondary lamellae increases as they grow.

It is seen that in most of the branches two types of lamellae actually touch each other and the production of connections at the nucleation point can be recognized.

4.3. Crystallization of Hevea Rubber Fractions at 0.5 kilobar

4.3.1. Linear Growth Rate Studies

As in the crystallization studies at atmospheric pressure, the growth rates have been determined by measuring the maximum length attained by lamellae after a fixed crystallization time. A plot of maximum lamellar length versus crystallization time then yielded the growth rate on measurement of the slope.

The crystallization studies were carried out at 0.5 kilobar only for two molecular weight fractions (313,000 543,000). The logarithm of lamellar growth rate versus crystallization temperature at 0.5 kilobar is shown in Figures 68 and 69 together with the atmospheric pressure curves for the molecular weights 351,000 and 543,000 respectively. Growth rates appeared to be higher than in the atmospheric pressure case for both fractions. Phillips and Edwards (1975) reported similar behavior for unfractionated

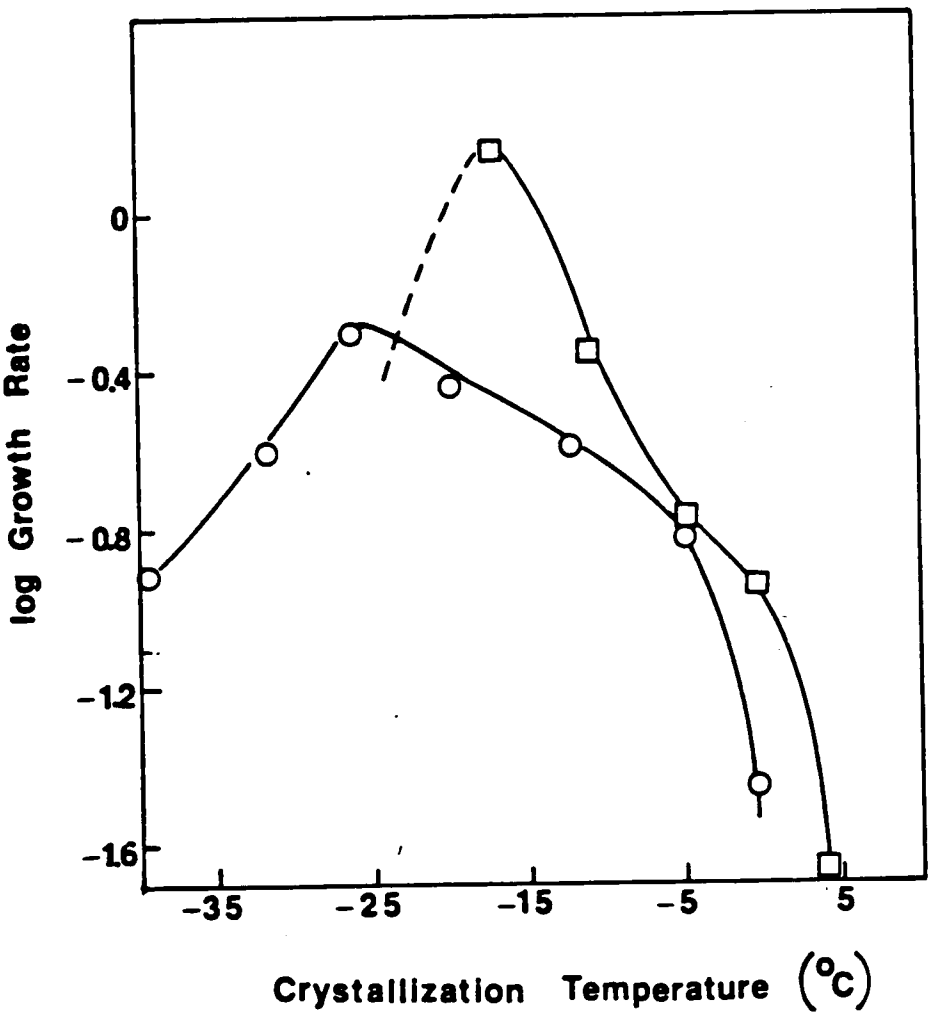


Figure 68 Lamellar growth rates as a function of crystallization temperature at O-atmospheric pressure,□-0.5 kbar for the fraction of molecular weight 351,000.

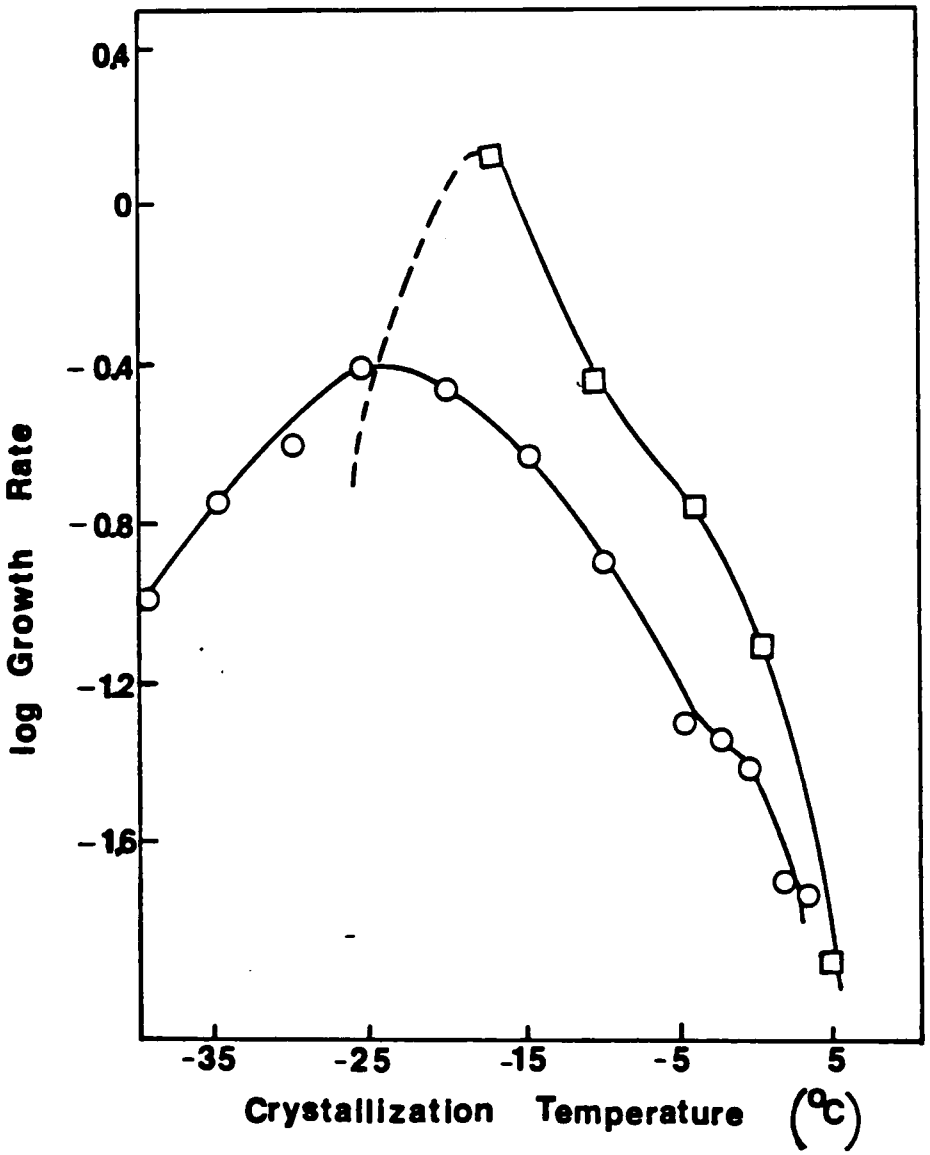


Figure 69 Lamellar growth rates as a function of crystallization temperature at O-atmospheric pressure,□-0.5 kbar for the fraction of molecular weight 543,000.

hevea rubber over a wide pressure range. They found that the growth rate increased gradually up to 1.5 kilobar where a constant value was retained until three kilobar where the high pressure phase began to interfere. For the hevea rubber fractions used in this study, the high pressure phase appeared at all pressures above 0.5 kilobar and prevented lamellar growth. Therefore we were unable to carry out any growth rate studies above 0.5 kilobar.

Lamellar thickness values were obtained from the electron micrographs at different temperatures at 0.5 kilobar for two of the fractions. Results are shown in Figure 70 (all data are listed in the appendix). Both fractions showed increasing lamellar thickness with increasing temperature. Histograms of lamellar thickness distribution at -17 ^{o}C and at +4.2 ^{o}C for the fraction of molecular weight 543,000 are shown in Figures 71,72.

4.3.2. Morphology

As in the atmospheric pressure case, growing lamellae in the form of sheaves were observed. A noticeable difference from the atmospheric pressure growth was the higher number of turned-over lamellae observed (Figure 73). Tapered growth fronts in some lamellae (A) growing in the "side-on" orientation may indicate the possibility of having a different growth plane in the axialitic region. The presence of axialites along with normal sheaves shows the

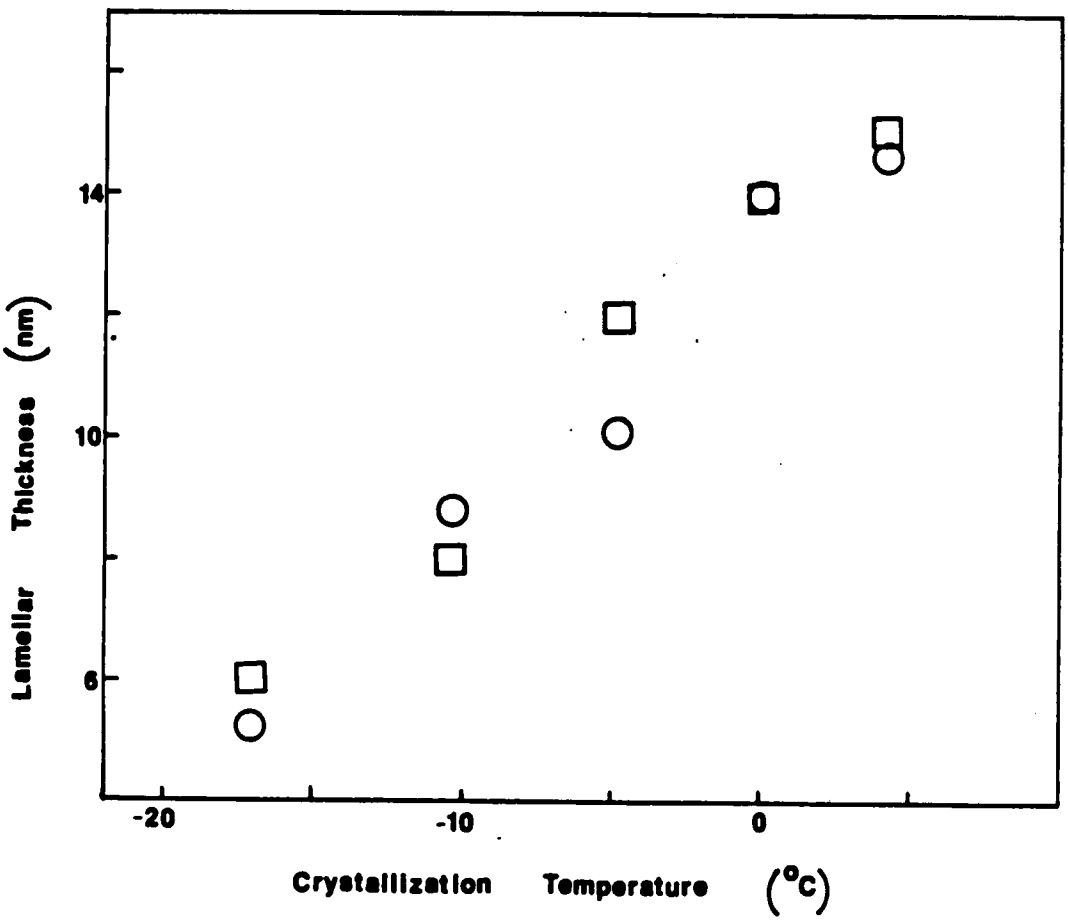


Figure 70 Lamellar thicknesses as a function of crystallization temperature at 0.5 kbar for the fractions of molecular weights O-351,000 and □-543,000.

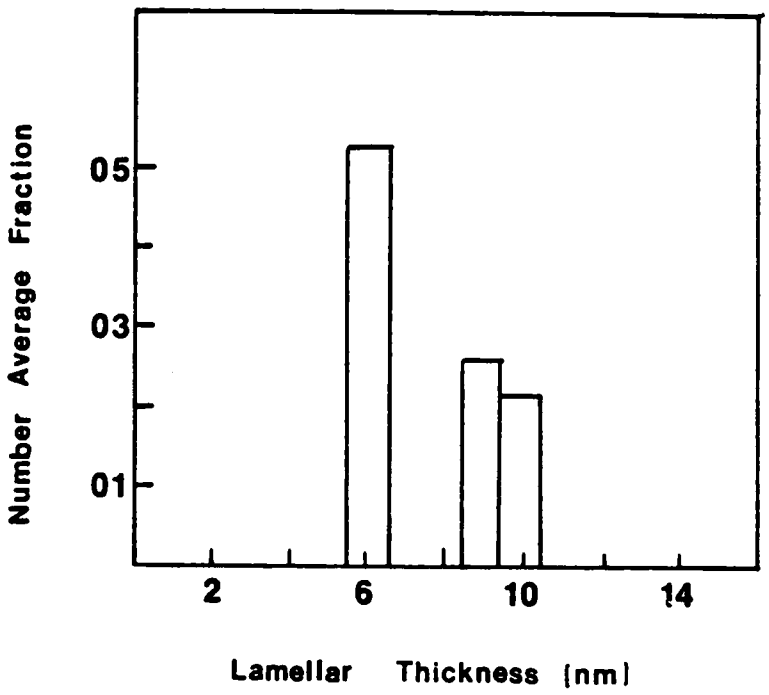


Figure 71 A histogram of lamellar thickness of the fraction of molecular weight 543,000 at -17 ^{o}C and at 0.5 kbar.

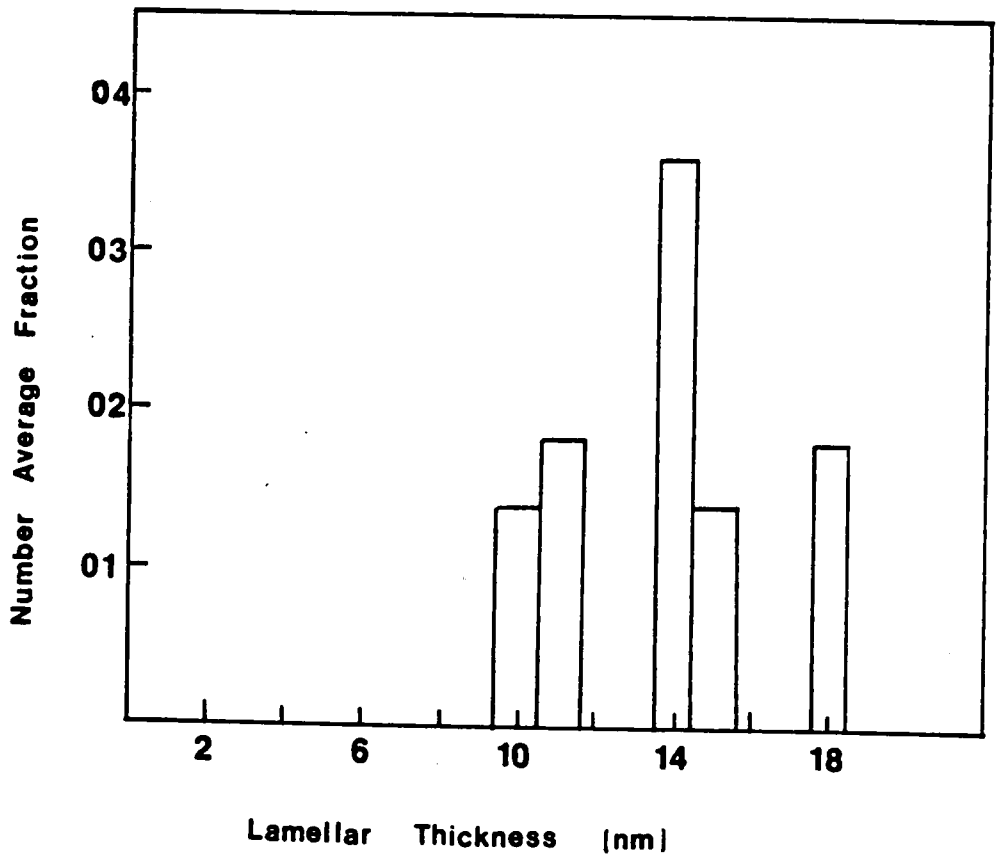


Figure 72 A histogram of lamellar thickness of the fraction of molecular weight 543,000 at +4.2 °C and at 0.5 kbar.



Figure 73 Growing sheaves in a fraction of molecular weight 351,000 at 0 °C and at 0.5 kbar.

existence of fractionated growth. Platelike growth was also seen (Figure 74). In some cases the growth was totally in the platelet form (i.e. regime I) (Figure 75,76). Single crystalline species were observed concurrently with spherulitic growth (Figure 77) which were less skeletalized and less clearly defined than the ones seen at low undercoolings for the lowest molecular weight fraction. Besides these features, some hexagonally oriented structures were observed too (Figure 78).

In earlier studies, spherulitic morphology was observed up to pressures of three kilobar. Above this pressure only randomly oriented high pressure phase was reported. (Edwards and Phillips 1974). In our case the high pressure phase was present at all pressures above 0.5 kilobar (Figure 79). In the high pressure phase ellipsoidal or needle-like crystals were observed, spherulitic nucleation being inhibited by the formation of these species at pressures above 0.5 kilobar. They have very high nucleation densities which increase with increasing pressure (Figures 80,81). The average thickness of these species remains almost constant with crystallization temperature (Figure 82). When nucleation density is plotted against reciprocal average length (Figure 83) an inverse linear relationship is observed showing the conversion of a certain percentage of material into the high pressure phase in

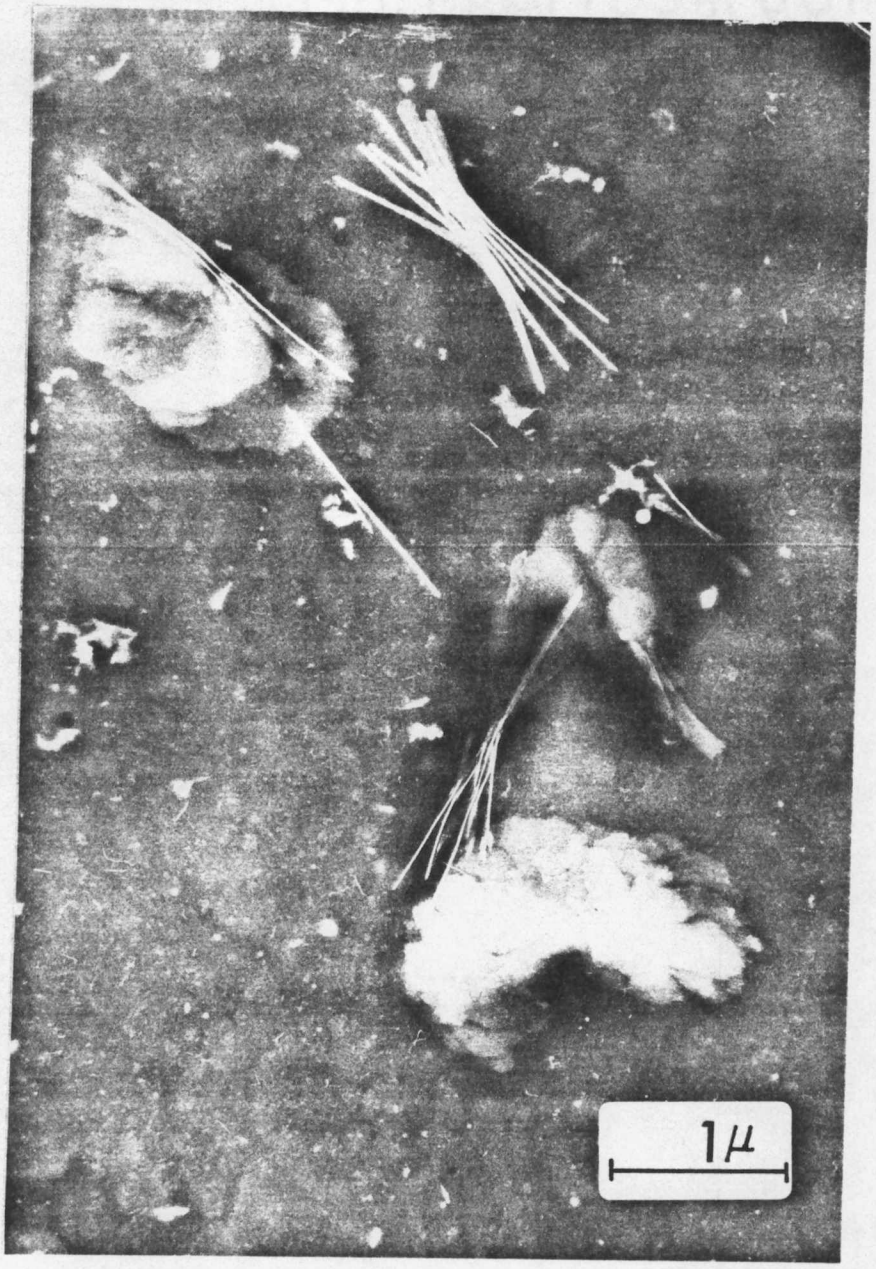


Figure 74 Platelet-like growth in a fraction of molecular weight 351,000 at 0 °C and at 0.5 kbar.



Figure 75 Platelet-like growth observed in a fraction of molecular weight 543,000 at 0 °C and at 0.5 kbar.

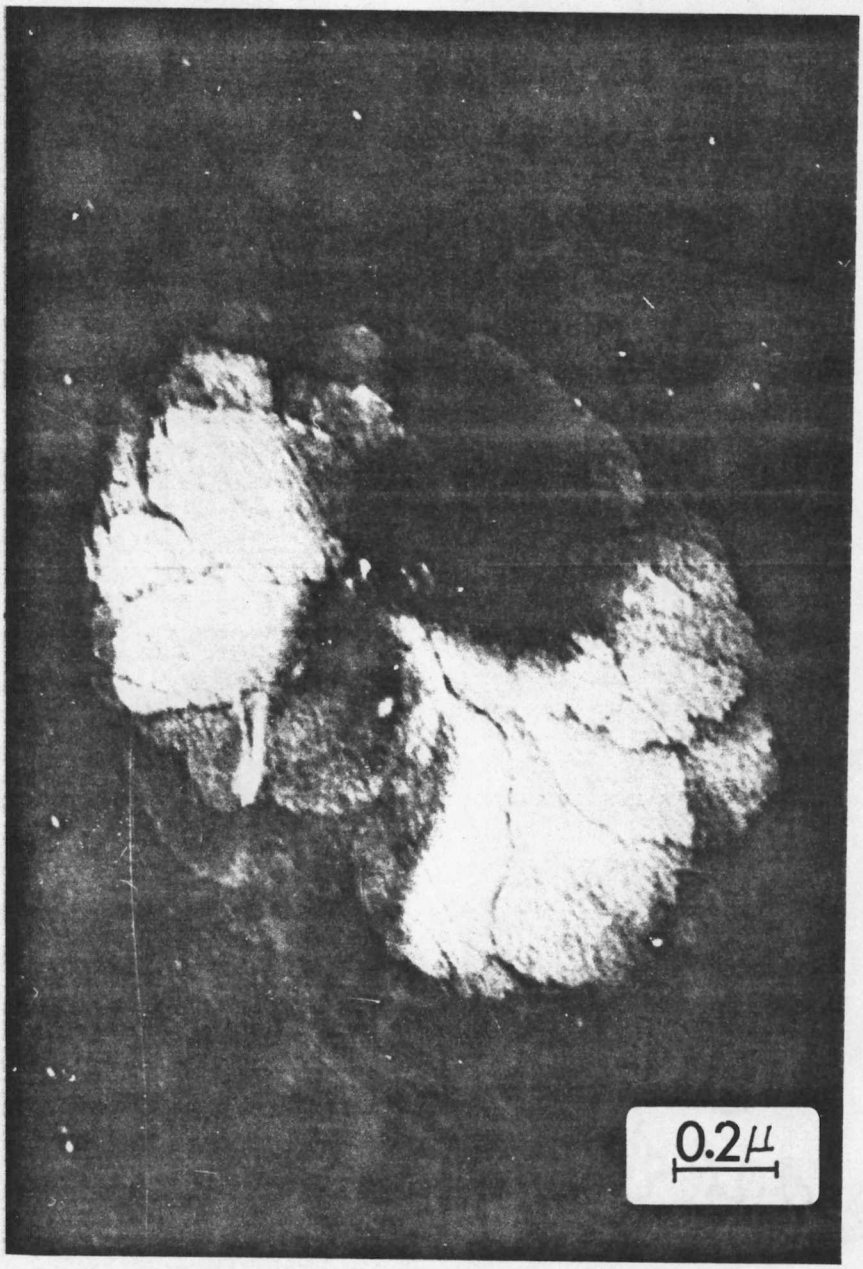


Figure 76 Platelet-like growth in a fraction of molecular weight 543,000 at 0 °C and at 0.5 kbar.



Figure 77 A single crystal in a fraction of molecular weight 351,000 at 0 °C and at 0.5 kbar.

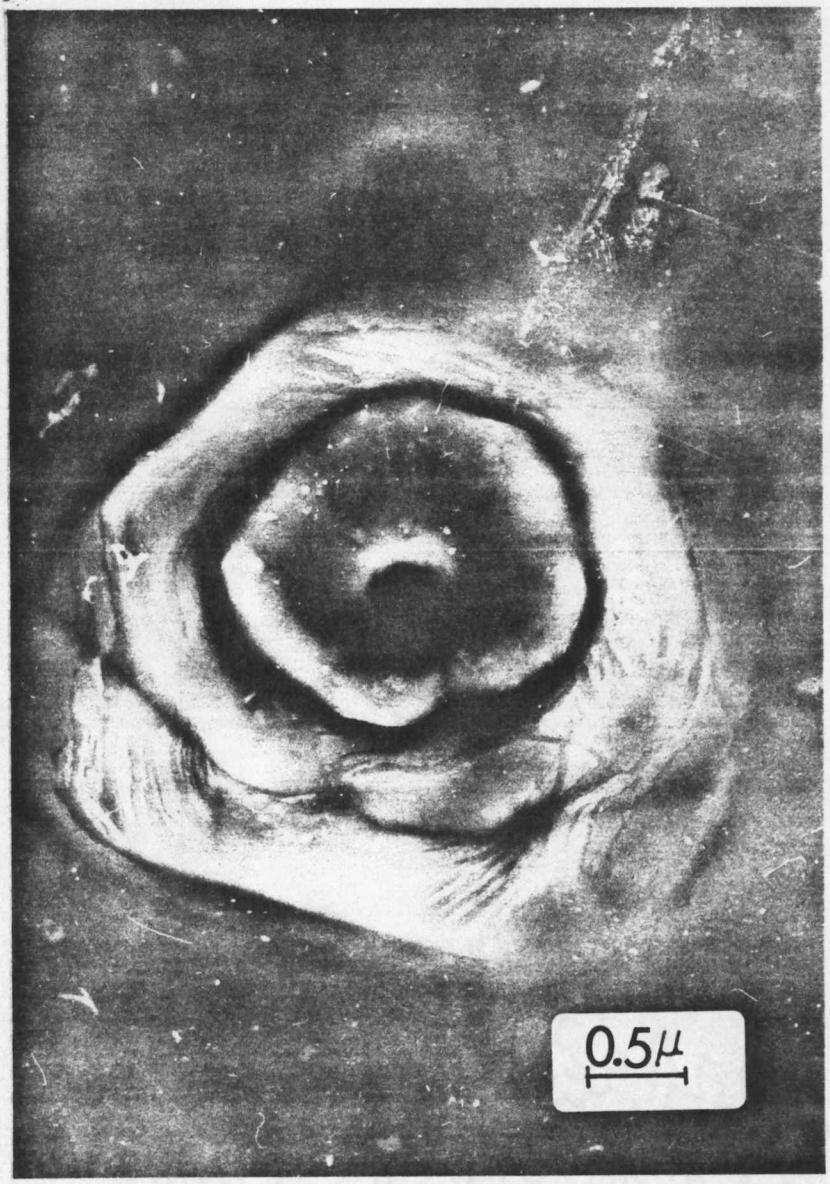


Figure 78 A hexagonally oriented specie in a fraction of molecular weight 543,000 at 0°C and at 0.5 kbar.

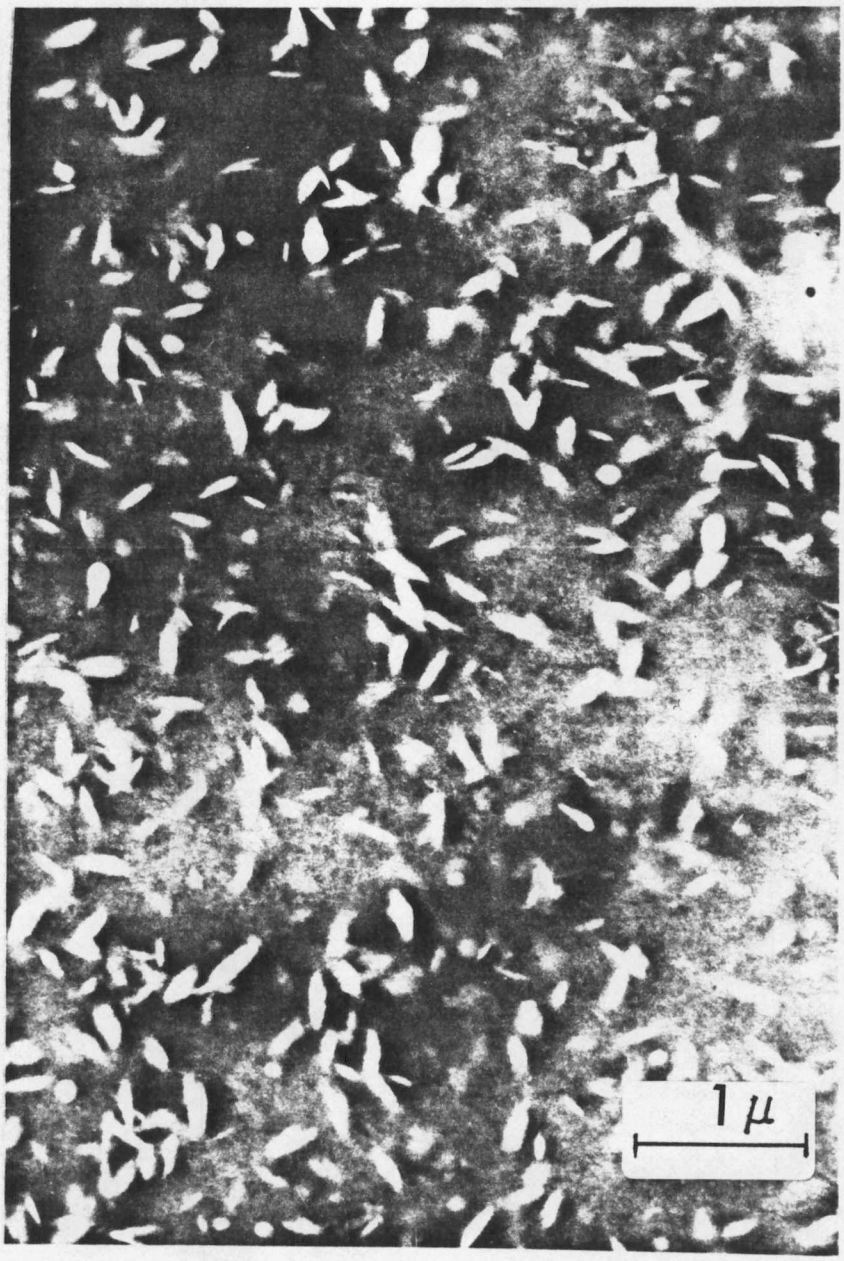


Figure 79 High pressure phase in a fraction of molecular weight 351,000 at 0 °C and at 0.5 kbar.

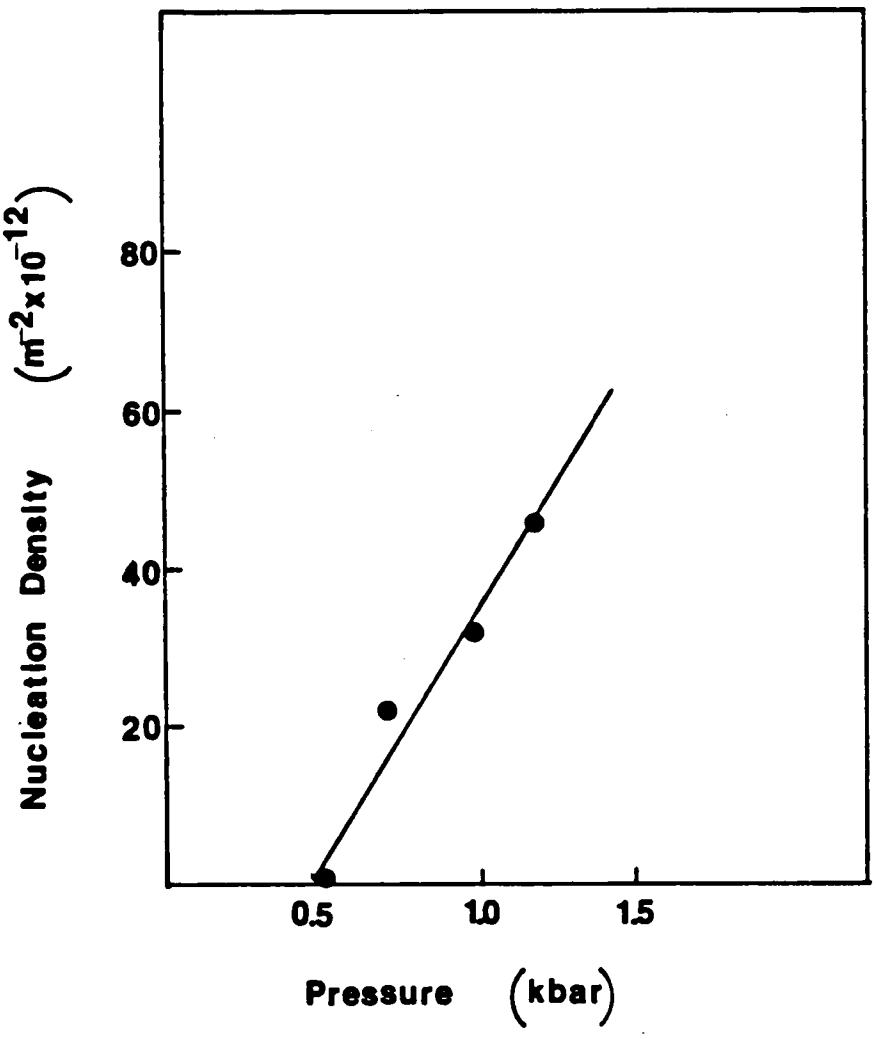


Figure 80 Nucleation density as a function of pressure at 0 °C for the fraction of molecular weight 543,000.

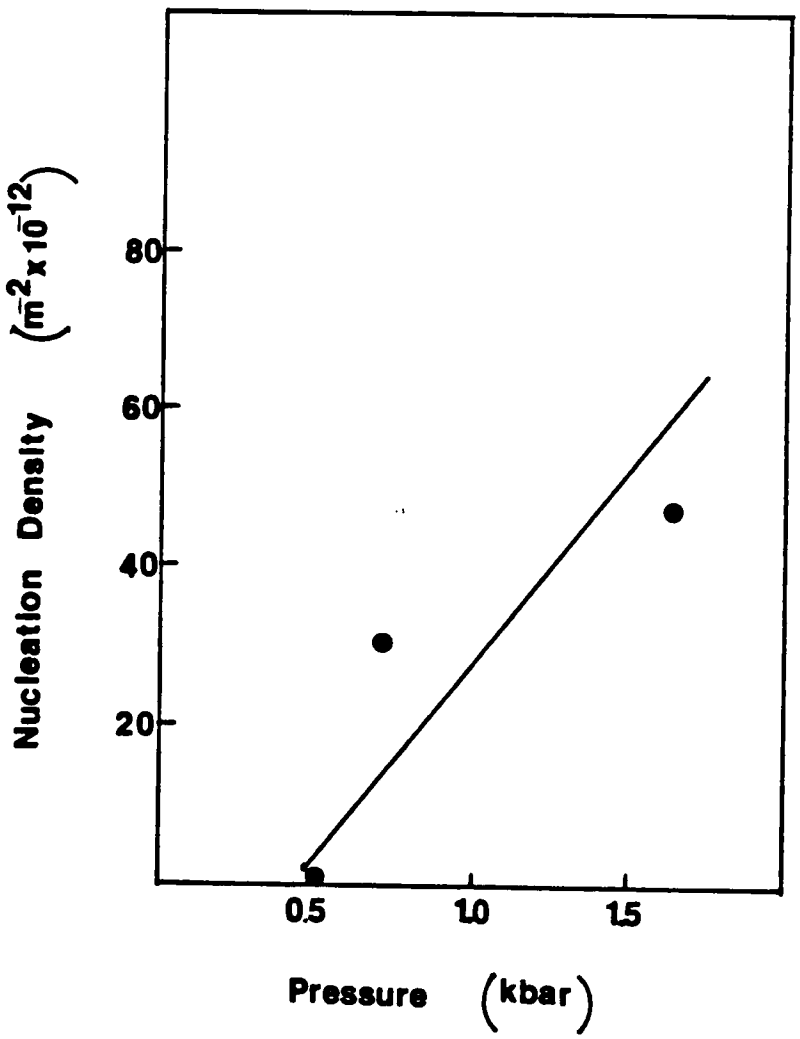


Figure 81 Nucleation density as a function of pressure at 0 °C for the fraction of molecular weight 351,000.

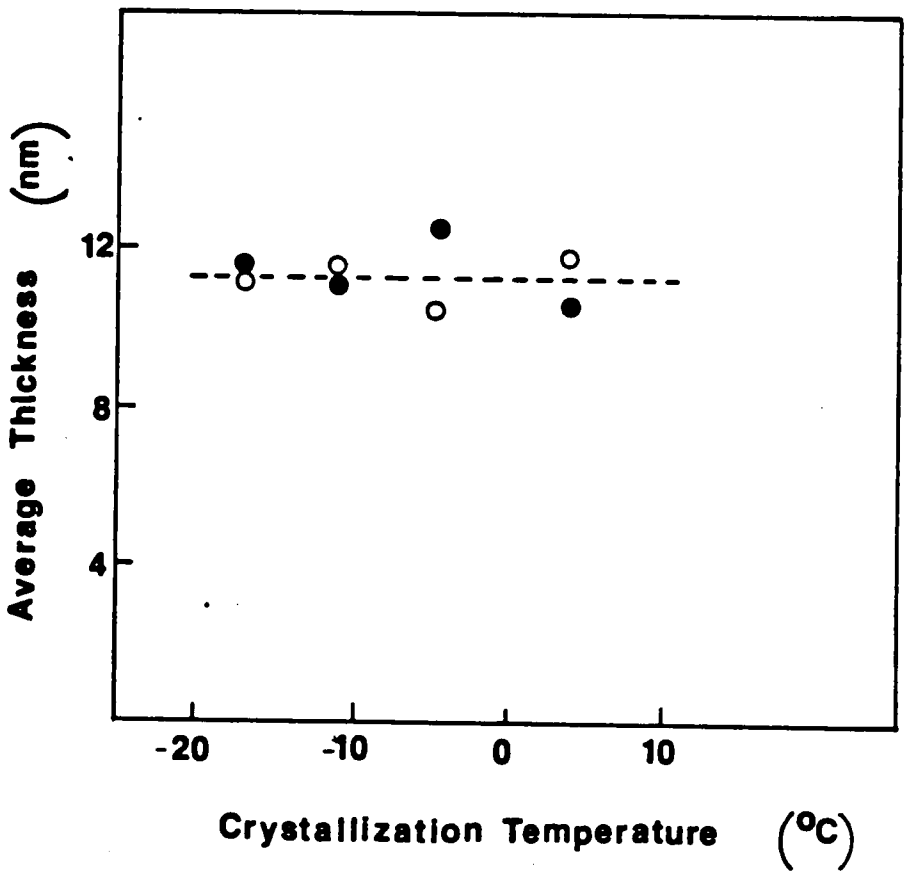


Figure 82 Average crystal thickness as a function of crystallization temperature at 0.5 kbar for the fractions of molecular weights ●-351,000 and O-543,000.

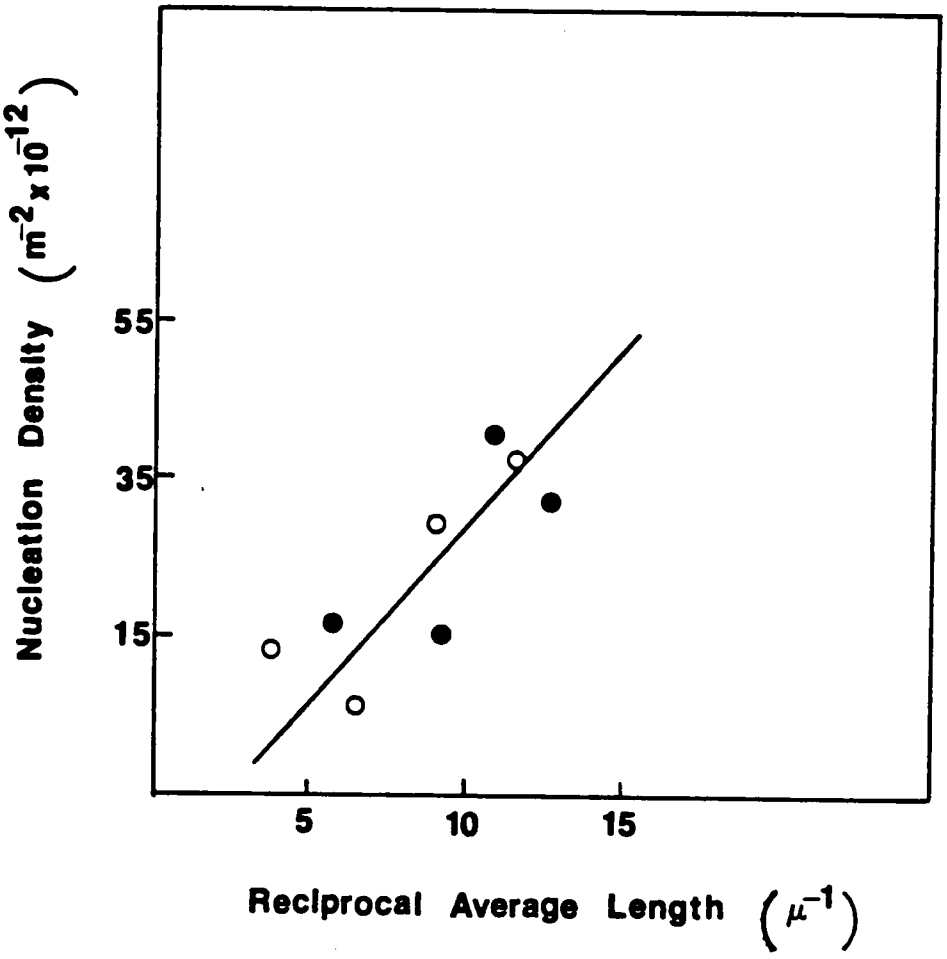


Figure 83 Plot of nucleation density versus the reciprocal average length at 0.5 kbar for the fractions of molecular weights ●-351,000 and○-543,000.

accord with results of Edwards and Phillips (1976) in unfractionated rubber.

5. DISCUSSION

Our kinetic studies with guayule rubber and different molecular weight fractions of natural hevea rubber have resulted in bell shaped growth rate curves. Growth rates were found to be molecular weight dependent. For two fractions the growth rate data at 0.5 kilobar were also obtained. Earlier analysis of unfractionated hevea rubber (Dalal and Phillips 1984) showed the presence of a possible regime III-II transition. In order to investigate this transition further, we analyzed our growth rate data using the Lauritzen-Hoffman theory. In the first part of the discussion the results of kinetic analysis of guayule rubber and hevea rubber fractions at atmospheric pressure, the dependence of regime transitions on molecular weight and molecular weight distribution will be discussed. Then the pressure dependence of regime transitions will be discussed.

In the second part of the discussion, morphological changes observed at various degrees of undercooling for different fractions along with more detailed analyses of lamellar thickness and branching will be discussed. Fold surface free energies which can be obtained from lamellar thickness data will be investigated for their dependence both on molecular weight and undercooling.

5.1 Kinetics

5.1.1. Analyses of Guayule Rubber at Atmospheric Pressure

Guayule Rubber is a form of natural cis-polyisoprene from the plant "parthenium argentatum grey". It is similar to hevea rubber in chemical structure. The main differences between these two rubbers can be summarized as (1) the presence of long chain branching in hevea rubber whereas guayule rubber is linear (2) the high percentage of gel in hevea rubber (>50%) compared to that present in guayule rubber (<5%) and (3) small amounts of epoxy and amino groups in hevea rubber.

Since it has been demonstrated that hevea growth kinetics showed a possible II-III transition (Dalal and Phillips 1984), growth rate data for different guayule specimens have been analyzed to test the applicability of the same concept.

Equation (2.4.17) indicates that according to the Lauritzen-Hoffman theory, the growth rate data should result in a linear plot with the abscissa X and ordinate Y given by;

$$X = 1/(2.303T\Delta Tf) \qquad (5.1.1)$$

$$Y = \log G + U^*/[2.303R(T-T_\infty)] \qquad (5.1.2)$$

The factor 2.303 is ln10 and f is a correction term that is close to unity at high temperatures, but becomes important at high undercoolings where the heat of fusion varies significantly with temperature. It is given as;

$$f = 2T/(T_m^o + T)$$

The parameters K_g and G_o in the equation (2.4.17) are given by the slope and the intercept respectively.

The analyses of growth rate data for unfractionated Guayule Rubber are shown in Figure 84 where curve (a) was generated using the experimentally determined input parameters; T_m^o =308.7 K, U^* =17.2 kJ/mole and T_∞ = 150.7 K (Dalal 1982). The values of U^* and T_∞ are almost equal to the universal values. It is clear from Figure 84-a, that the data points do not lie on a single straight line. There are two straight line segments with markedly different slopes. The break in the curve occurs at X = 3.53×10^{-5} K^{-2} corresponding to a crystallization temperature (T_c) of -17.5 ^oC and the ratio of the two slopes is 1.87. Curve (b) in Figure 84 was generated using the empirical input parameters for U^* and T_∞ which were proposed by Hoffman et al. (1976). They have reported that for most of the polymers they studied, empirical values (U^* = 6.28 kJ/mole and $T_\infty = T_g - 30$) gave a better fit to the kinetics data than the universal ones. They suggested that this was because crystallization occurred from an adsorbed layer of macromolecules rather

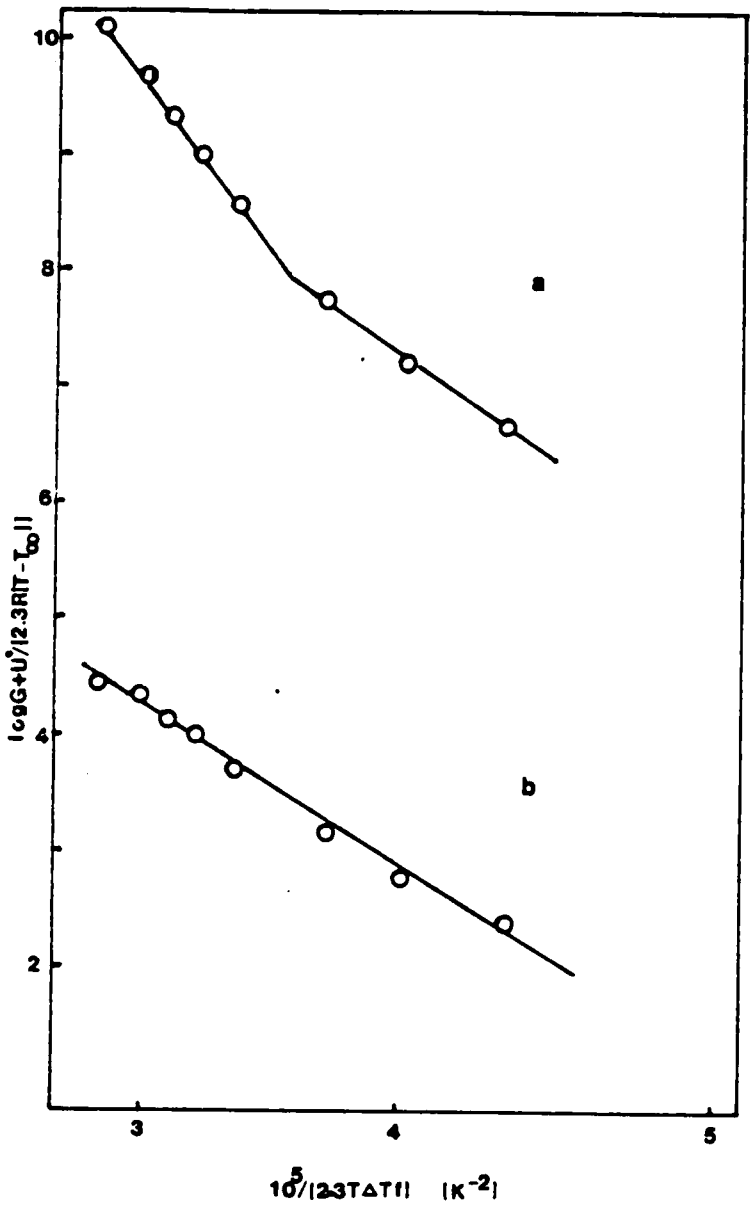


Figure 84 Plots of kinetics data of guayule rubber at atmospheric pressure (a)experimental values U^* = 17.2kJ/mol, T_∞ = 150.7 K;(b)U^* = 6.28 kJ/mol and T_∞ = 171 K.

than directly from the bulk amorphous region, and that the adsorbed layer had relaxation parameters different from those of the bulk. Using empirical values of U^* and T_∞ brought the points closer to a single straight line. However, in Figure 84-a the presence of two linear segments is unmistakable and is due to a transition from regime III to regime II. Regime III-II transitions have been reported in polyoxymethylene (Hoffman 1983), cis-polyisoprene from hevea (Dalal and Phillips 1984), polypropylene (Clark and Hoffman 1984) and polyphenylene sulphide (Lovinger et al. 1985). Pelzbauer and Galeski (1972) analyzed their growth rate data on polyoxymethylene using universal values and obtained a slope ratio of two. Later Hoffman re-analyzed the same data using the activation energy for reptation of polyethylene and an experimentally determined T_m^o. He obtained a slope ratio of 1.983. The data of unfractionated hevea rubber yielded a slope ratio of 1.65 and the deviation from the expected value of two was explained by a possible change in the amount of non-adjacent reentry in regime III region. In guayule rubber the slope ratio being closer to two may be explained by the presence of linear chains. Hevea rubber contains long chain branches which might inhibit the chains' ability to translate over large distances. Actually it is now recognized that the molecular weight distribution present in the unfractionated guayule rubber is the main reason for the slope ratios being far from two, because our

studies with fractionated samples yielded slope ratios closer to two (see later). A broad molecular weight distribution may smear the regime transitions and produce lower slope ratios.

At high undercoolings the first exponential in equation (2.4.17) which contains the contribution of the diffusional process to the growth rate, controls the crystallization process. So at these low temperatures (i.e regime III region), the slope of the line is very sensitive to the choice of the U^* value. A comparison of the results of kinetic analyses of different guayule rubber specimens (Figure 85) (Rensch et al. 1986) shows that regime III slopes are different in different samples but that the slopes of the regime II region do not change significantly. Since we know that σ_e values are the same for these polymers from the lamellar thickness data (Rensch et al. 1986), an alternative conclusion could be that the exact value of U^* is different for these samples resulting in unclear regime transitions in some of them.

The information obtained from the analysis of kinetic data is tabulated in Table 3. The analyses with experimental values resulted in reasonable σ_e values for the choices of regimes III and II. But in the analyses with the empirical values, the σ_e value obtained is very low if regime III is assumed. A regime II approximation yields the σ_e value usually found in cis-polyisoprene. In the

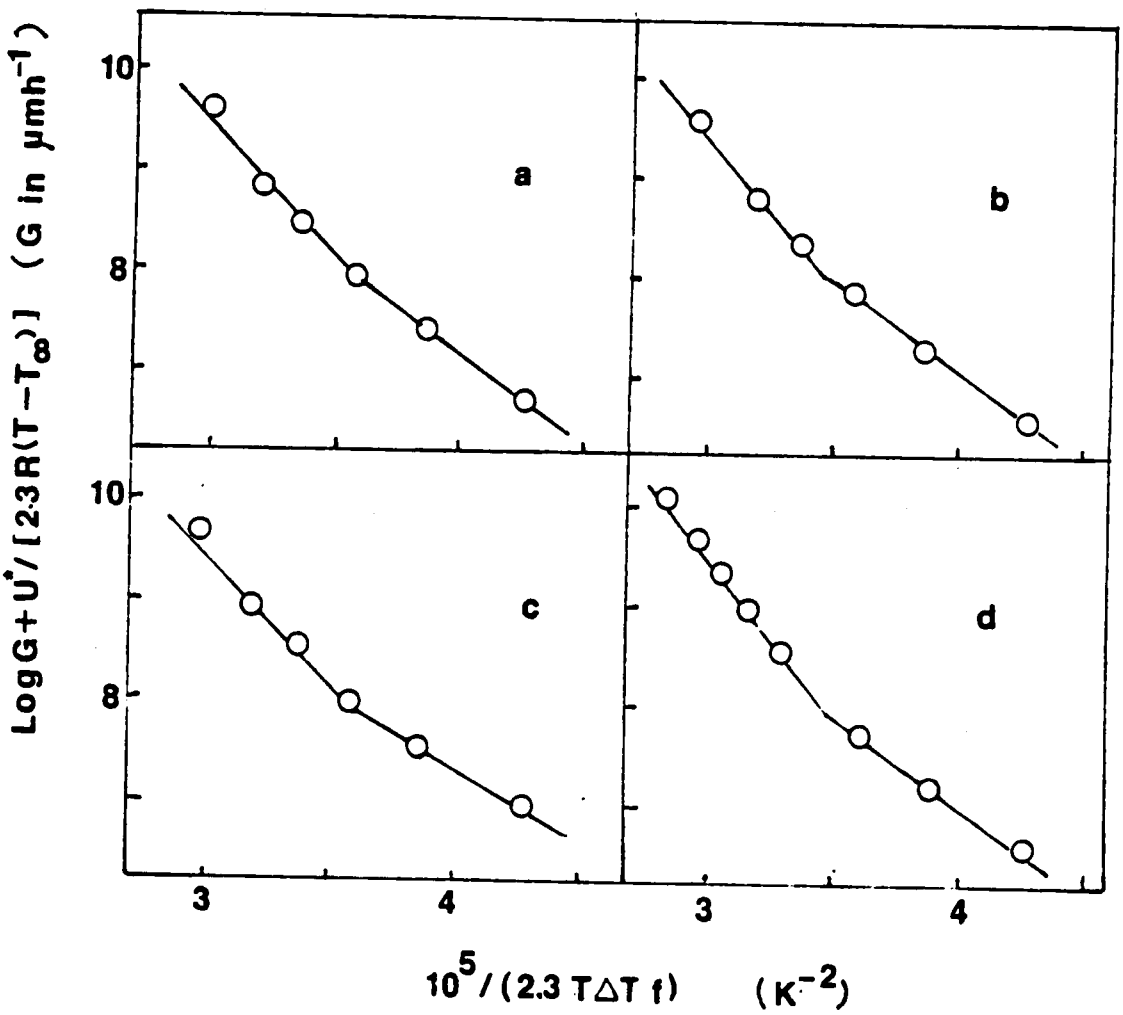


Figure 85 Plots of kinetics data of (a)α-lamellae of aged pilot plant,(b)β-lamellae of aged pilot plant,(c)α-lamellae of fresh guayule rubber and (d)α-lamellae of fresh pilot plant.

Table 3 Analyses of Atmospheric Pressure Kinetics Data of Unfractionated Guayule Rubber.

T_m^o (K)	U^* (kJ/mole)	T_∞ (K)	Lines Allowed	$K_g x10^{-5}$ (K^2)	Regime Assumed	$\sigma\sigma_e x10^4$ (J^2/m^4)	$\sigma_e x10^2$ (J/m^2)
308.7	17.2	150.7	two	3.19	III	3.66	2.61
				1.71	II	3.93	2.81
308.7	6.28	171	one	1.52	III	1.75	1.25
					II	3.49	2.49

calculation of σ_e, the well established value of 0.014 J/m^2 for σ was used.

5.1.2. Analysis of Hevea Rubber Fractions at Atmospheric Pressure

After the presence of a regime III-II transition in cis-polyisoprene from hevea rubber had been detected (Dalal and Phillips 1984), an investigation of the effect of molecular weight and molecular weight distribution on this transition was required to understand better the details of crystallization in this polymer. Earlier studies had not been extended to sufficiently low undercoolings for regime I crystallization to be detected. In this study we carried out detailed studies at low undercoolings, for the lowest molecular fraction we have, to check on the presence or absence of regime I kinetics. So first the kinetic data on hevea rubber fractions will be analyzed to settle these points.

Analysis of crystallization kinetics data has been carried out using secondary nucleation theory as described in section 5.1.1. In the first treatment values of U^* = 17.2 kJ/mole and T_∞ = 150.7 K, corresponding to independently determined WLF analyses, were used. In the second, empirical values of U^* = 6.28 kJ/mole and T_∞ = 171 K which were suggested by Hoffman were used. In both cases the experimentally determined melting point of 308.7 K was used.

Analyses of the data have resulted in the detection of three different types of behavior over the temperature range of crystallization considered. First, for the fractions of molecular weights 897,000 and above only one straight line was obtained for both sets of input parameters (Figures 86,87) indicating the presence of only regime III growth. A second type of plot is presented in Figure 88, which was obtained for the fraction of molecular weight 543,000. Here it can be seen that the regime III-II transition occurs at -5 ^{o}C with a slope ratio of 1.92. In Figure 88-b a similar break occurs at -5 ^{o}C but with a slope ratio of 1.55 which is far from the expected value of two. The third type of result we obtained from the analyses was the presence of all three regimes together in a single polymer. This type of behavior was observed for only two fractions, those with molecular weights 313,000 and 357,000 (Figures 89,90). The fraction with molecular weight 313,000 was studied in more detail. A regime III-II transition at -18.1 ^{o}C and a I-II transition at -5 ^{o}C are clearly distinguishable (Figure 89). The slope ratio for the regime III-II transition is 1.97 and for the regime I-II transition is 1.86. The transitions may also be seen in the curves generated using the empirical input parameters (Figures 89-b). However, here the slope ratios are 1.43 and 2.45 for the regime III-II and regime I-II transitions respectively. It is clear that the

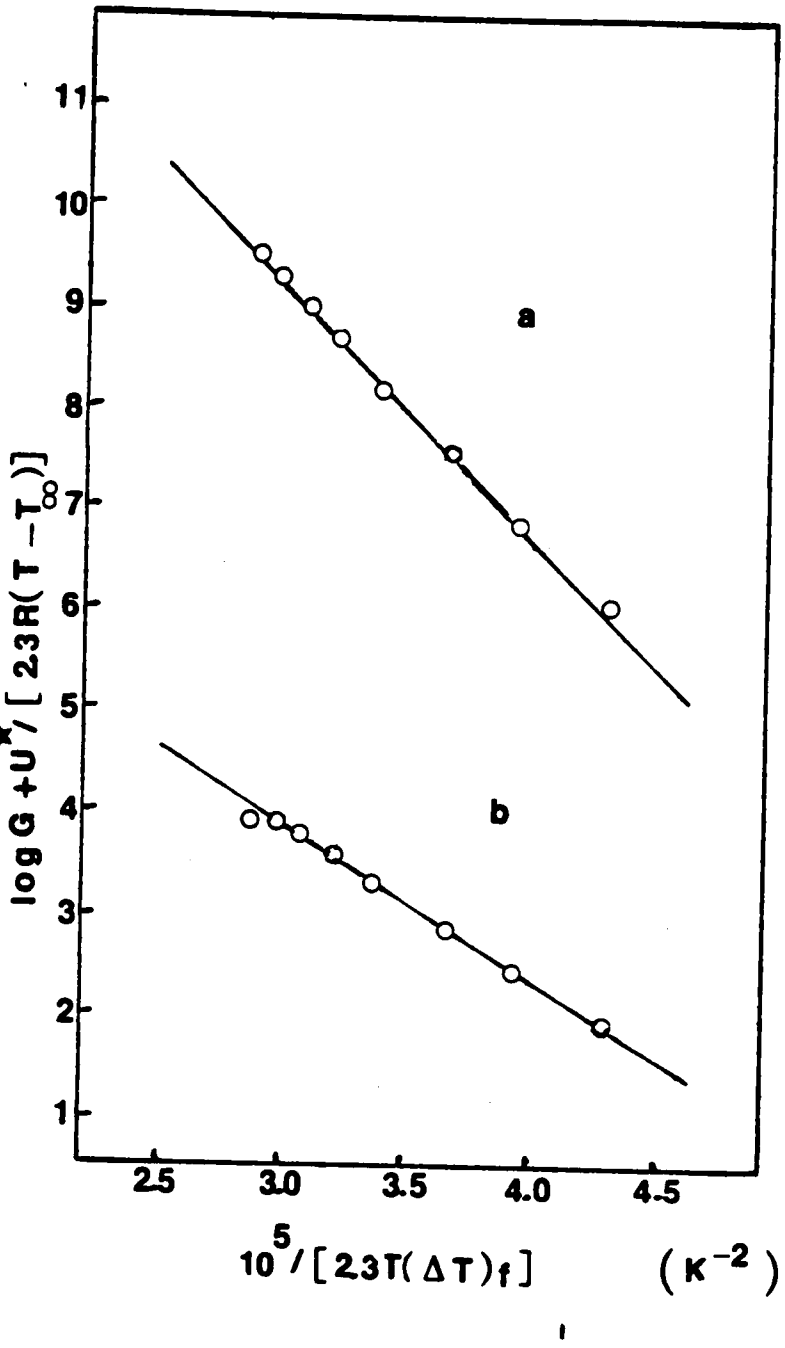


Figure 86 Plots of kinetics data of hevea rubber fraction of molecular weight 1,421,000 at atmospheric pressure (a)experimental values U^* = 17.2kJ/mol, T_∞ = 150.7 K;(b)U^* = 6.28 kJ/mol and T_∞ = 171 K.

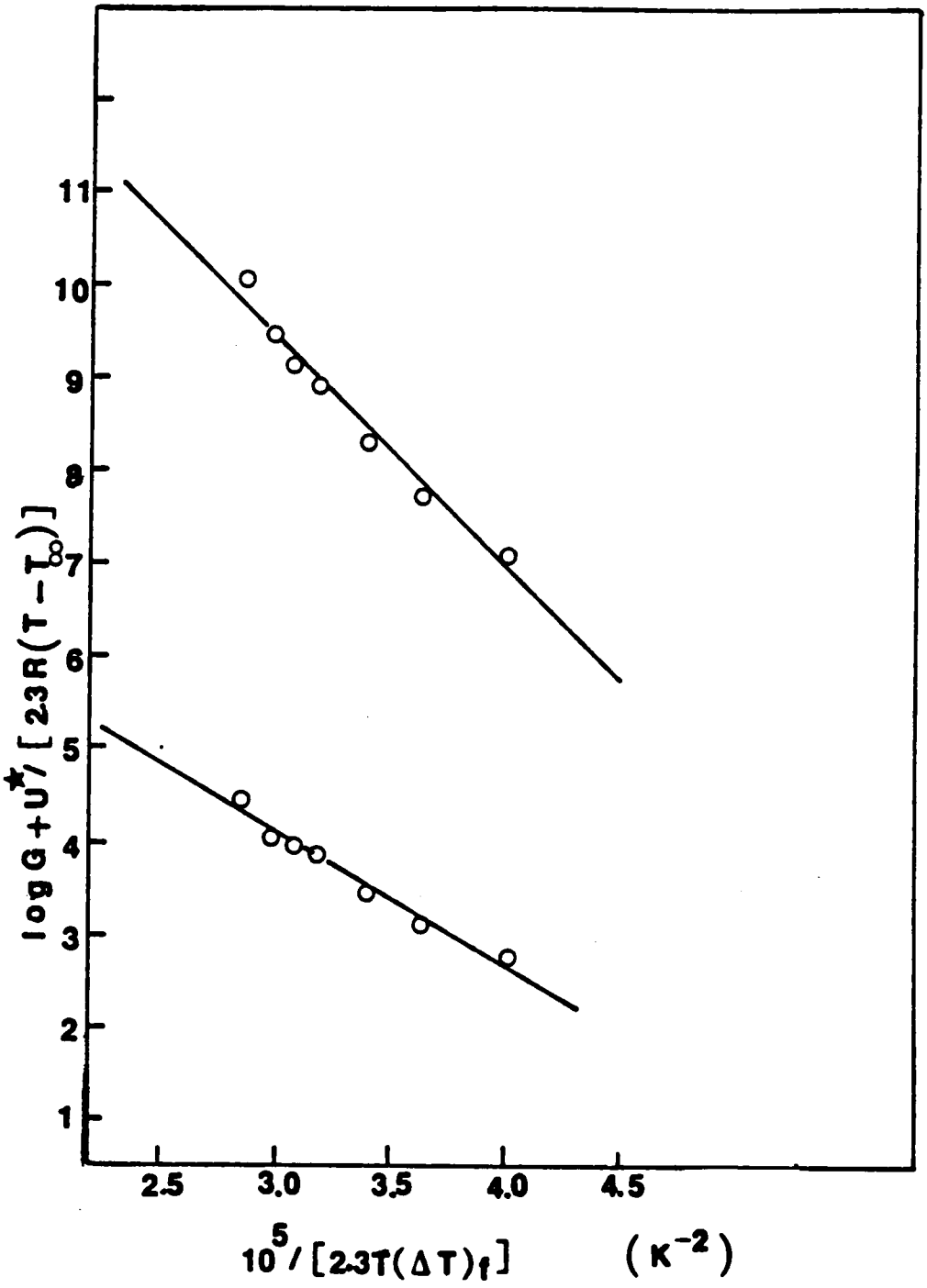


Figure 87 Plots of kinetics data of hevea rubber fraction of molecular weight 897,000 at atmospheric pressure (a)experimental values U^* = 17.2kJ/mol, T_∞ = 150.7 K;(b)U^* = 6.28 kJ/mol and T_∞ = 171 K.

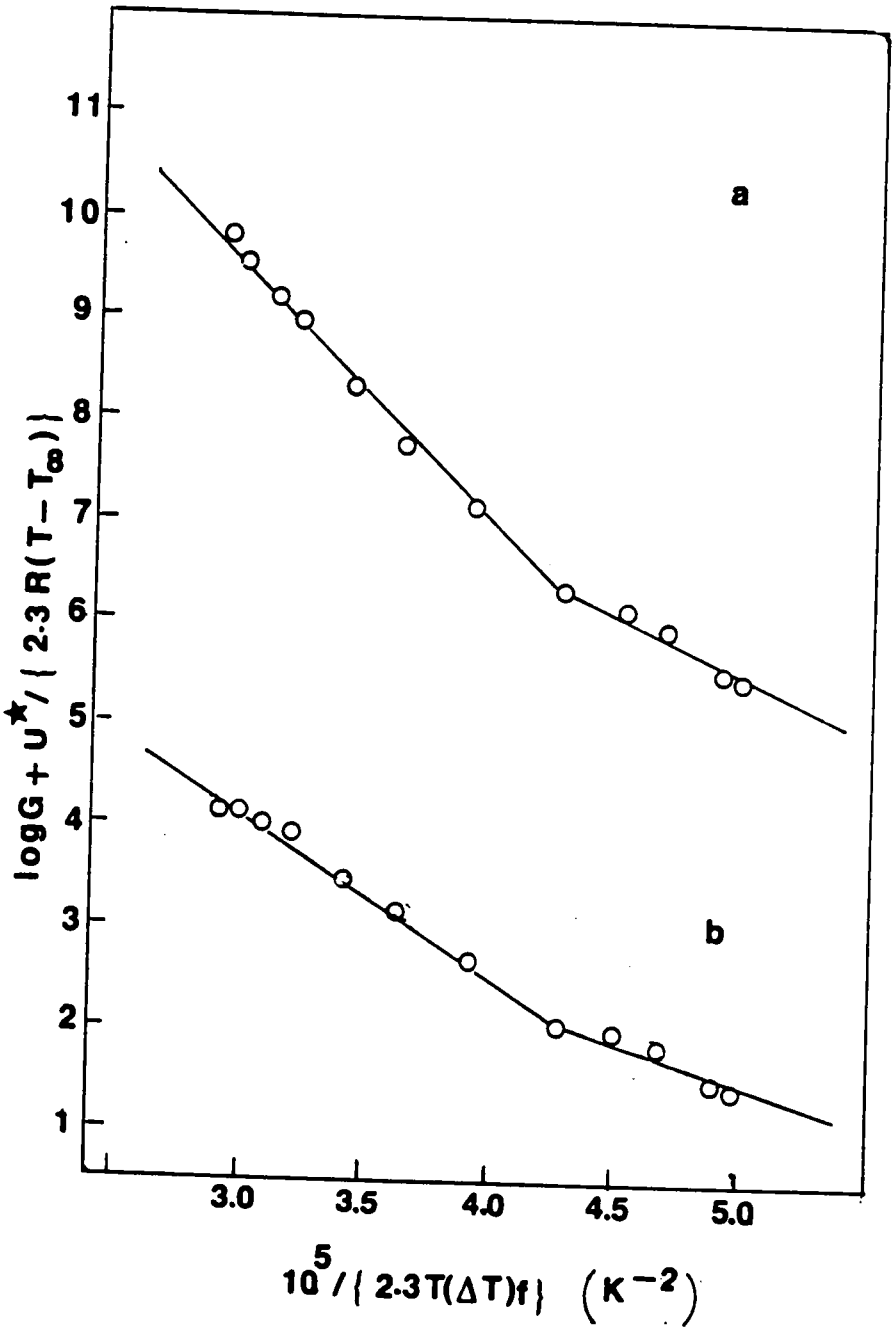


Figure 88 Plots of kinetics data of hevea rubber fraction of molecular weight 543,000 at atmospheric pressure (a)experimental values U^* = 17.2kJ/mol, T_∞ = 150.7 K;(b)U^* = 6.28 kJ/mol and T_∞ = 171 K.

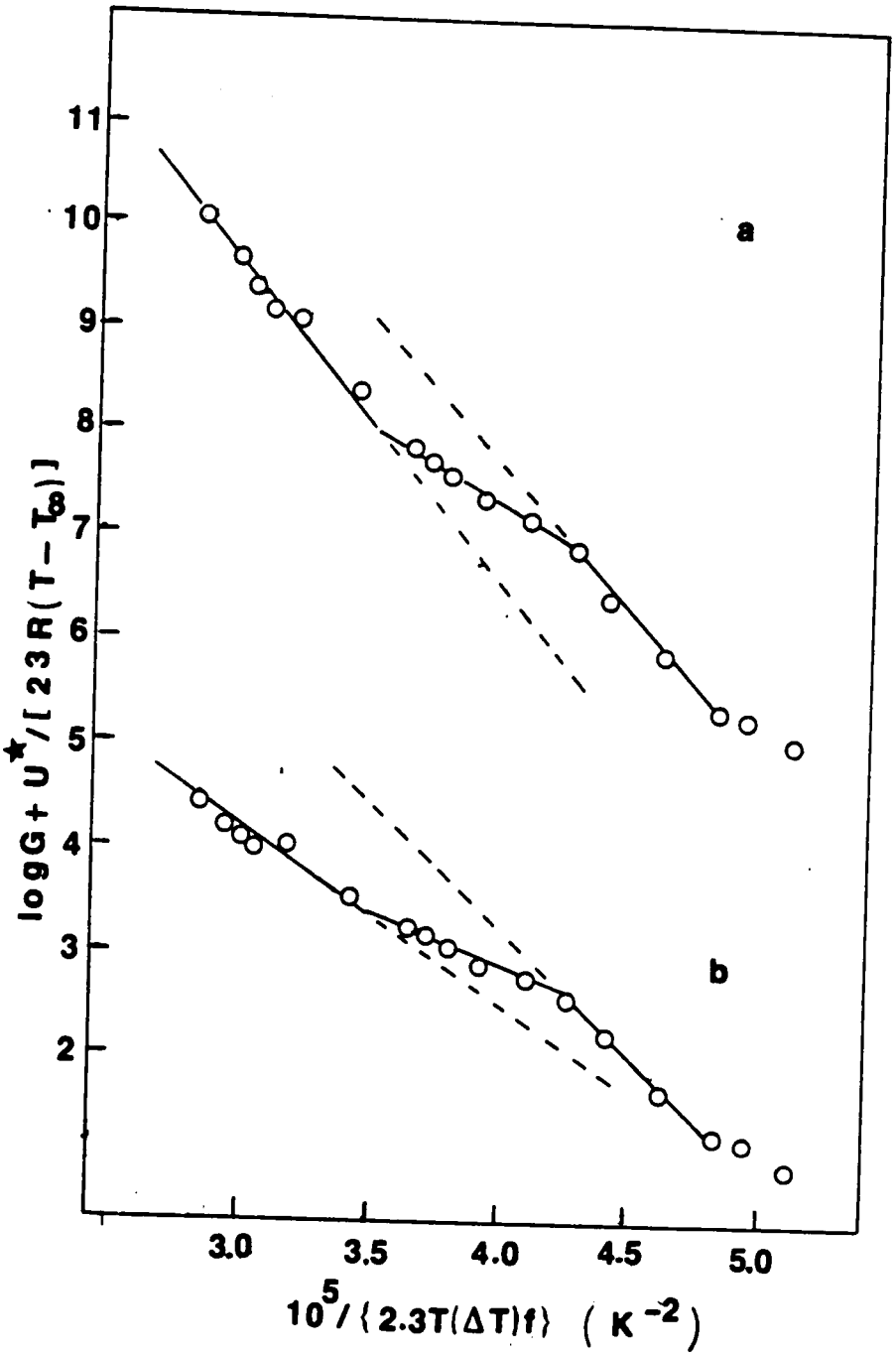


Figure 89 Plots of kinetics data of hevea rubber fraction of molecular weight 313,000 at atmospheric pressure (a)experimental values U^* = 17.2kJ/mol, T_∞ = 150.7 K;(b)U^* = 6.28 kJ/mol and T_∞ = 171 K.

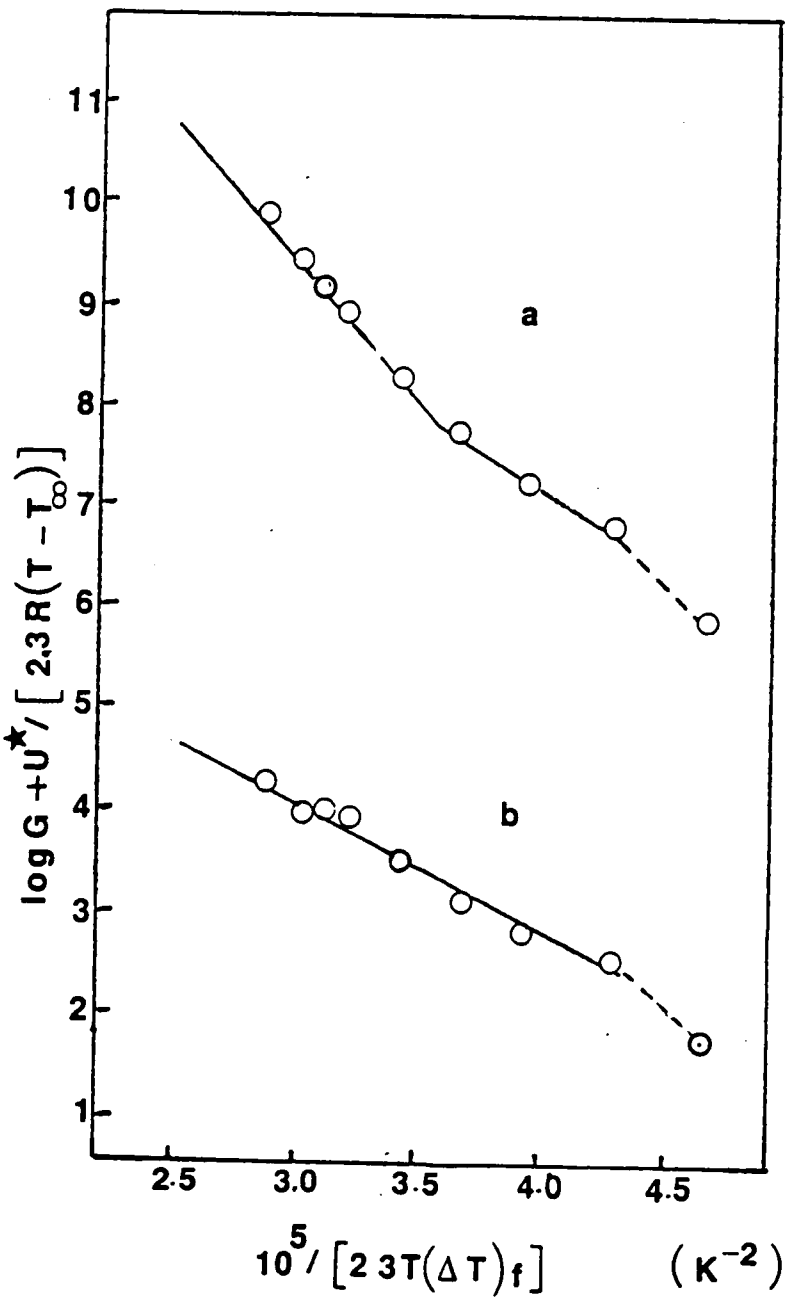


Figure 90 Plots of kinetics data of hevea rubber fraction of molecular weight 351,000 at atmospheric pressure (a)experimental values U^* = 17.2kJ/mol, T_∞ = 150.7 K;(b)U^* = 6.28 kJ/mol and T_∞ = 171 K.

experimentally determined input parameters result in slope ratios closer to the theoretical values of two.

The two points corresponding to the highest crystallization temperatures do not fit on the regime I line. This may occur as a result of fractionation during crystallization. At these temperatures, we see an increased amount of single crystal formation. Since the single crystals will be formed from the lowest molecular weight species, the remaining material will have a higher molecular weight than average and may follow regime II kinetics. This effect is expected to intensify as the fraction of single crystals increases, resulting in the points which deviate from the regime I line. This can explain the regime I-II slope ratio of 1.86 being lower than two. At lower temperatures the fractionation effect will still be present to some extent but not as pronounced as at the high temperature end, resulting in a straight line with a lower slope in the regime region.

Cooper and Manley (1975) have reported a deviation from linearity of logG versus $10^4/T\Delta T$ curves at the highest crystallization temperatures for polyethylene fractions crystallized from solution. Their kinetics data did not reveal pure regime II growth. At higher temperatures a non-linearity, which was attributed to a diffuse regime I-II transition, was observed. Later Point et al. (1986) tried to reproduce the growth rate data of Cooper and Manley.

Although most of their points correlated with each other, their data led to a straight line fit over the full range of crystallization temperatures.

In a recent paper, Point et al.(1986) reported a decrease in the growth rate of polyethylene crystals grown from dilute solution when crystallization proceeds further. In order to investigate the effect of fractionation during crystallization, they crystallized polyethylene from dilute solution at different temperatures. After an appropriate period of time, each crystallization suspension was filtered at the crystallization temperature. Both the precipitate and the polymer in the remaining solution were analyzed using GPC. The crystallized fraction contained a low molecular weight fraction. Then, they concluded that because of this fractionation the growth rate decreases more rapidly as crystallization progresses than is predicted on the basis of the decrease in concentration. In our case it was impossible to carry out a similar procedure to check fractionation effects, because the crystallization was carried out in the bulk. In our case in order to investigate the effect of fractionation, fractions with narrower molecular weight distributions are needed. If a fraction of the same molecular weight with a low polydispersity does not exhibit that curvature, it may be concluded that fractionation is responsible for the deviation from straight line behavior.

Recently Hoffman (1985) proposed a model in which a gradual reversion takes place leading to mixed regime I and regime II, or only regime II above the I-II transition temperature. In this model, substrate length is treated as the length between defects having the capacity to inhibit surface completion. The defects are described as resembling the greek letter Ω (omega) in their most extended state (Figure 91). He suggested that in order to have a regime I-II transition an equilibrium defect distribution should be present and the mean lifetime of a stabilized omega defect of critical size should be longer than the mean time associated with nucleation and completion of the substrate. It is possible for this condition to fail at some temperature above the I-II transition point causing a gradual reversion to mixed regime I and II. This may be considered as another possible explanation for the curvature obtained at the high crystallization temperatures (Figure 89).

A third possible explanation for the deviation from linearity at temperatures closer to the melting point is a model proposed by Goldenfeld (1984). He suggests a cross-over from regime I to regime II as a function of time. According to his model, as a crystal grows in regime I, the radial dimensions grow rapidly and the lateral growth rate becomes so small that regime I kinetics are no longer applicable and regime II kinetics will be valid. However, in

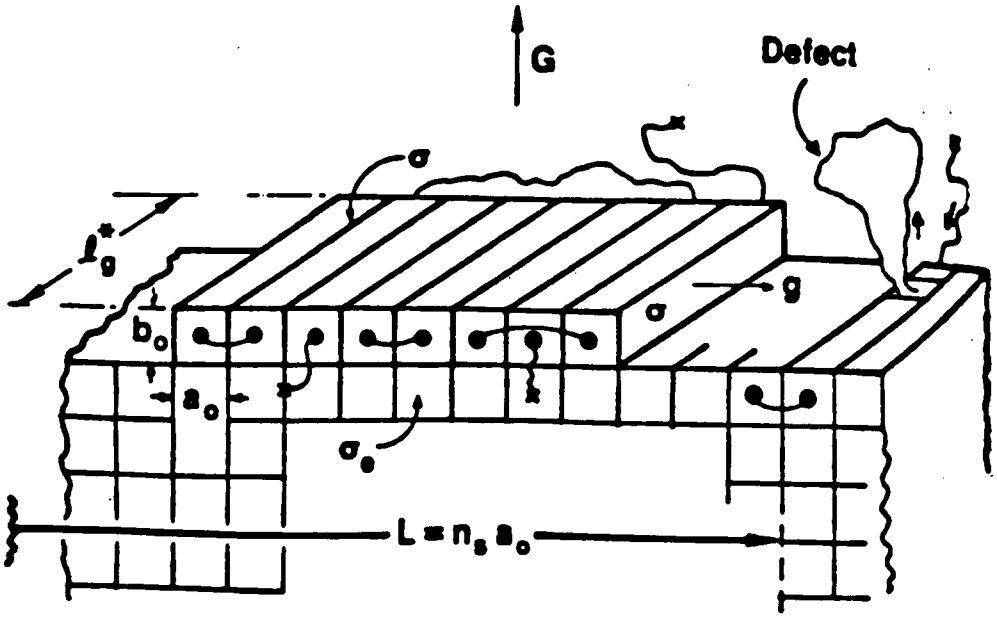


Figure 91 A diagram illustrating the omega defect schematically (from Hoffman 1985).

the Goldenfeld explanation the reversion from regime II to regime I occurs as a function of time. Temperature dependence of this aspect has not been investigated theoretically.

The Lauritzen-Hoffman regime test described in section (2.4.7) was applied to the growth rate data of the fraction of molecular weight 3.13×10^5 in the regime I and regime II regions. It produced $(L/a)_I$ values between $8.\times10^3$ and 2×10^5 when we used values of 33 and 31 which are the high and low limits of of regime I for the first exponential term in equation (2.4.31). For convenience, the first exponential in equation (2.4.31) will be referred as Q hereafter. The factor Q may be taken as 10^3 for all polymers (Hoffman et al. 1976). Choice of the $Q = 10^3$ approximation gave $(L/a)_I$ values between 1.57×10^3 and 2.1×10^4. According to the regime test, $(L/a)_I$ values greater than 10^2 are considered to be in regime I. For the regime II region $(L/a)_{II}$ values between 2.3×10^4 and 2.3×10^5 resulted with the use of Q values calculated for cis-polyisoprene. Use of the "universal" Q value of 10^3 resulted in $(L/a)_{II}$ between 4.5×10^3 and 4.1×10^4. These values are too high for regime II, because according to this test $(L/a)_{II}$ is expected to be less than 10^2. When the empirical U^* and T_∞ values of 6.28 kJ/mole and 171 K were used, relatively lower values were obtained but they were still outside of the regime II range.

All the results are tabulated in Table 4 for a better comparison.

Since this test was devised to distinguish regime I from regime II and has not been extended to the regime III region we did not test our regime III kinetics data. But it is clear that the regime test is not applicable to cis-polyisoprene. Actually it is not a commonly used test for regime transitions, only a few authors have attempted to use this procedure.

At this point it is worth considering equation (2.4.17) in more detail in order to understand the nature of the regime II-III transition. The first exponential in this equation is the mobility term and includes the activation energy of the diffusion or transport process by which the molecular section goes from the melt to the crystal (U^*), as well as T_∞ which is the theoretical temperature where all motion associated with viscous flow stops. It is worth considering the influence of these parameters on the value of $y = \log G + U^*/ R(T-T_\infty)$ which is the y-axis used for kinetic analysis. Variation in the growth rate (G) over the temperature range used, affects the value of the y-axis by less than two units. If we consider the effect of the second term on y, we see that it is responsible for a change of from 7 to 11 units over the temperature range -40 ^oC to +3 ^oC. The effect of transport parameters become more pronounced as the temperature of crystallization is lowered.

Table 4 Results of Lauritzen-Hoffman Regime Test for the Fraction of Molecular Weight 313,000 in Regime I and Regime II Regions.

U^* (kJ/mole)	T_∞ (K)	T_c (K)	Q	$(L/a)_I$	$(L/a)_{II}$
17.20	150.7	268	10^3	1.57×10^3	-
17.20	150.7	276	10^3	2.10×10^4	-
17.20	150.7	268	33.4	8.5×10^3	-
17.20	150.7	276	30.6	1.2×10^5	-
6.28	171.0	268	10^3	3.46×10^2	-
6.28	171.0	276	10^3	3.37×10^3	-
6.28	171.0	268	33.4	1.89×10^3	-
6.28	171.0	276	30.6	1.93×10^4	-
17.20	150.7	258	10^3	-	4.5×10^3
17.20	150.7	268	10^3	-	4.1×10^4
17.20	150.7	258	38.8	-	2.3×10^4
17.20	150.7	268	33.9	-	2.2×10^5
6.28	171.0	258	10^3	-	1.1×10^2
6.28	171.0	268	10^3	-	4.7×10^2
6.28	171.0	258	38.8	-	5.5×10^2
6.28	171.0	268	33.9	-	2.6×10^3

For example a change of 10 ^{o}C from -40 ^{o}C to -30 ^{o}C lowers the y value by 1.3 units whereas, an identical temperature change from -7 ^{o}C to +3 ^{o}C changes the y value by 0.6 units. This shows clearly the relative importance of the parameters U^* and T_∞, especially in the vicinity of the regime II-III transition. It is clear that the choice of correct values of U^* and T_∞ is critical. A wrong choice of these parameters can smear the regime transitions. The question of using the appropriate input parameters has been investigated in the literature, the main concern being only a better straight line fit of the kinetics data. In the Kovacs and Suzuki (1970) approach, the transport parameters are analyzed on the basis of the WLF equation. Here first a reasonable value is given to U^* and then T_∞ is given successive values. The technique involves fitting of data to a straight line and the value of U^* at which linearity is found, is calculated. A second approach has been suggested by Hoffman which involves using the empirical values U^* and $T_\infty = T_g - 30$ which gives a good linear fit for some polymers. The reasoning behind his approach is that the layer from which crystallization occurs may have different relaxation parameters from the bulk. In our case the use of empirical values resulted in a single line for some fractions (Figures 86-b, p.176, 87-b, p.177, 90-b, p.180), but fractions with molecular weights 3.13×10^5 and 5.43×10^5 showed the breaks (Figures 88-b, p.178 and 89-b, p.179). The fold surface free

energies ,σ_e, obtained from kinetics data are shown in Tables 5-6 in which it may be seen that the values of σ_e are reasonable if the regime assumed is II for analysis with empirical values. However, in this case it is impossible to explain the three straight line segments of Figure 89-b. If we assume they are regime III, II and I regions, the resulting σ_e`s are very low. Therefore it is clear that the empirical values do not work for cis-polyisoprene. The use of experimentally determined U^* and T_∞ values (which are very close to the WLF parameters) in kinetic analysis gave good fits with unmistakable regime transitions. The existence of regime transitions is supported by morphological changes at the regime I-II transition (see section 5.2.1).

It is now well established that the selection of the input parameters U^* and T_∞ is very important in the interpretation of kinetics data. This importance increases at higher undercoolings where we have the regime III-II transition. Therefore it is reasonable to assume that the regime III-II transition is controlled by kinetic factors rather than thermodynamic factors. We already know from studies on polyethylene (Phillips and Tseng 1985) that the regime I-II transition, which occurs nearer to the melting point, is controlled by thermodynamic factors. High pressure studies for polyethylene showed that the change of the I-II transition temperature with pressure paralleled the change

Table 5 Analyses of Atmospheric Pressure Kinetic Data of Lower Molecular Weight Fractions With Indicated Molecular Weights.

T_m^o (K)	U^* (kJ/mole)	T_∞ (K)	Lines Allowed	$K_g x10^5$ (K^2)	Regime Assumed	$\sigma\sigma_e x10^4$ (J^2/m^4)	$\sigma_e x10^2$ (J/m^2)
			M_v = 313,000				
308.7	17.2	150.7	three	2.87	III	3.29	2.35
				1.46	II	3.35	2.39
				2.71	I	3.11	2.22
308.7	6.28	171	three	1.39	III	1.59	1.14
				0.97	II	2.23	1.59
				2.38	I	2.73	1.95
			M_v = 351,515				
308.7	17.2	150.7	three	2.80	III	3.21	2.29
				1.50	II	3.44	2.46
				2.63	I	3.02	2.16
308.7	17.2	171	one	1.28	III	1.47	1.05
					II	2.94	2.10

Table 6 Analyses of Atmospheric Pressure Kinetic Data of Higher Molecular Weight Fractions With Indicated Molecular Weights.

T_m^o (K)	U^* (kJ/mole)	T_∞ (K)	Lines Allowed	$K_g x10^5$ (K^2)	Regime Assumed	$\sigma\sigma_e x10^4$ (J^2/m^4)	σ_e (J/m^2)
			M_v = 543,000				
308.7	17.2	150.7	two	2.46	III	2.82	2.01
				1.28	II	2.94	2.10
308.7	6.28	171.0	two	1.55	III	1.78	1.27
				0.99	II	2.27	1.62
			M_v = 897,000				
308.7	17.2	150.7	one	2.47	III	2.84	2.03
308.7	6.28	171	one	1.43	III	1.64	1.17
					II	3.28	2.34
			M_v = 1,421,000				
308.7	17.2	150.7	one	2.48	III	2.85	2.04
308.7	6.28	171	one	1.52	III	1.75	1.25
					II	3.49	2.49

of equilibrium melting point with pressure. Because of the reasons mentioned earlier, we could not obtain detailed growth rate data at high pressures. Data obtained at 0.5 kilobar for two fractions and the unfractionated cis-polyisoprene (Phillips and Edwards 1975) are analyzed in section 5.1.3. The analysis supports the prediction of a kinetic transition.

5.1.3. Analyses of Hevea Rubber Fractions at 0.5 Kilobar

Analyses of growth rate data at 0.5 kilobar according to Secondary Nucleation theory were carried out to determine the pressure dependence of the regime transitions in two fractions. In polyethylene, the pressure dependence of the regime I-II transition has been reported to follow that of the equilibrium melting point (Phillips and Tseng 1985). The regime I-II transition point at 0.5 kilobar is expected to shift to higher temperatures where the crystallization rate is extremely slow. Therefore in this work, only the pressure dependence of III-II transition will be investigated to test the hypothesis that it may be a kinetic transition (see section 5.1.2.).

Growth rate data obtained at 0.5 kilobar for two different molecular weight fractions as well as the data of Phillips and Edwards (1975) on the unfractionated polymer were analyzed using equation (2.4.17). The input parameters at 0.5 kilobar were obtained from the work of Dalal (1983)

as: U^* = 18.01 kJ/mole, T_m^o = 321.8 K and T_∞ = 157 K. The heat of fusion, Δh_f, was assumed to be invariant with pressure and the atmospheric pressure value of 6.4×10^7 J/m^3 was used. The growth rate data for the fractions at 0.5 kilobar were not extensive enough to define exactly the regime transition temperature. For this reason, first lamellar thickness data at 0.5 kilobar measured from transmission electron micrographs were plotted against $1/f(\Delta T)$ to obtain the fold surface free energies, σ_e, (see section 5.2.2). Then using these σ_e values, expected K_g values were calculated. Thus the slopes for all three regimes were calculated using equations (2.4.28) and (2.4.29) assuming that σ (lateral surface free energy) is independent of pressure and has the value of 0.014 J/m^2. When the lines with expected slopes were drawn, regime III-II transitions at -8 ^oC and +1 ^oC for fractions of molecular weights 3.57×10^5 and 5.43×10^5 respectively were observed (Figures 92,93). Analyses of growth rate data of the unfractionated polymer (Phillips and Edwards 1975) yielded a regime III-II transition at -2 ^oC with a slope ratio 1.81 (Figure 94). Fold surface free energies for the fractions were found to be much higher than for the unfractionated polymer. A comparison of σ_e values is given in Table 7. In fact we observed other differences between the high pressure crystallization behavior of the fractions and of the unfractionated rubber used in earlier studies. We were not

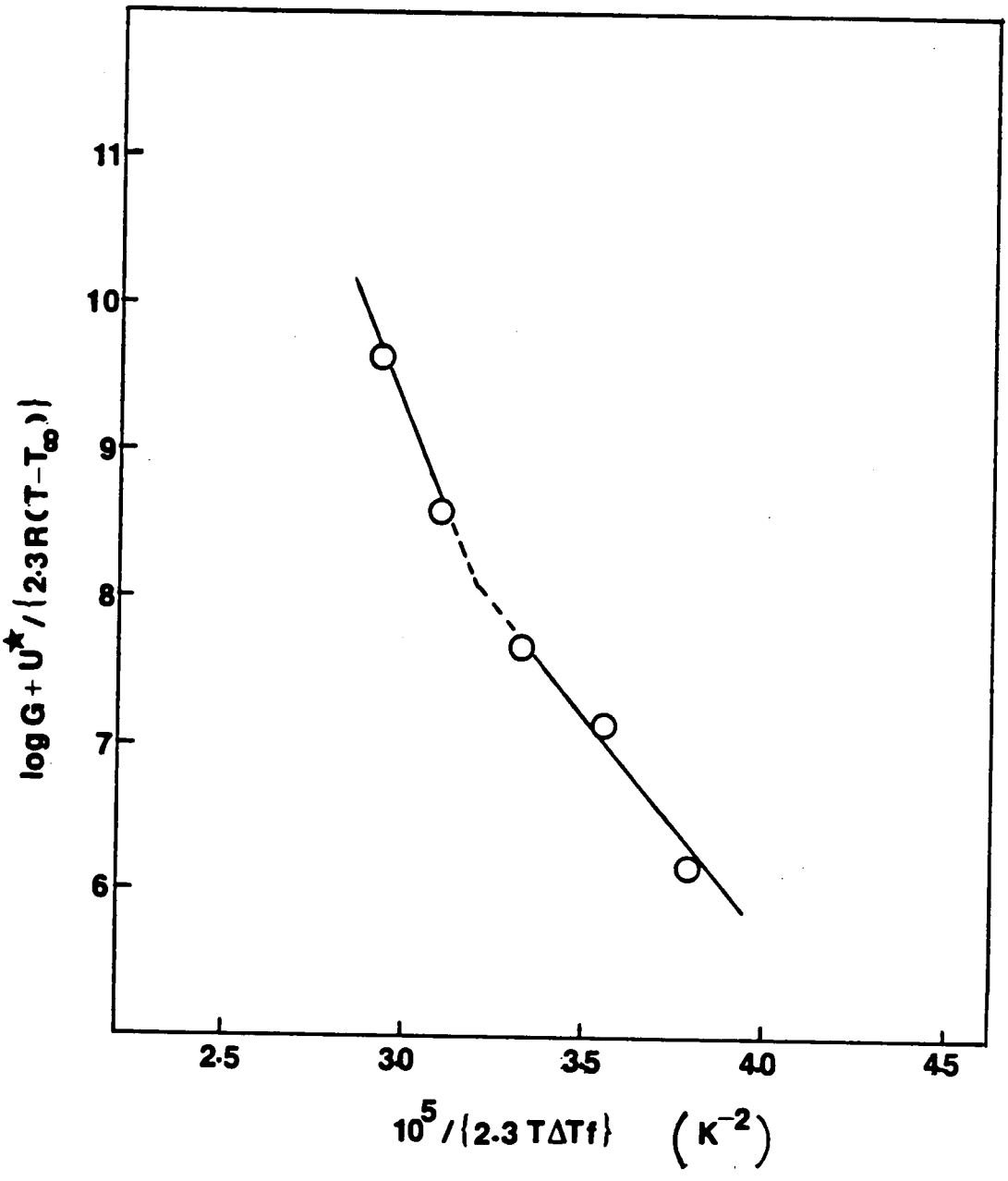


Figure 92 Plot of kinetics data of hevea rubber fraction of molecular weight 351,000 at 0.5 kbar.

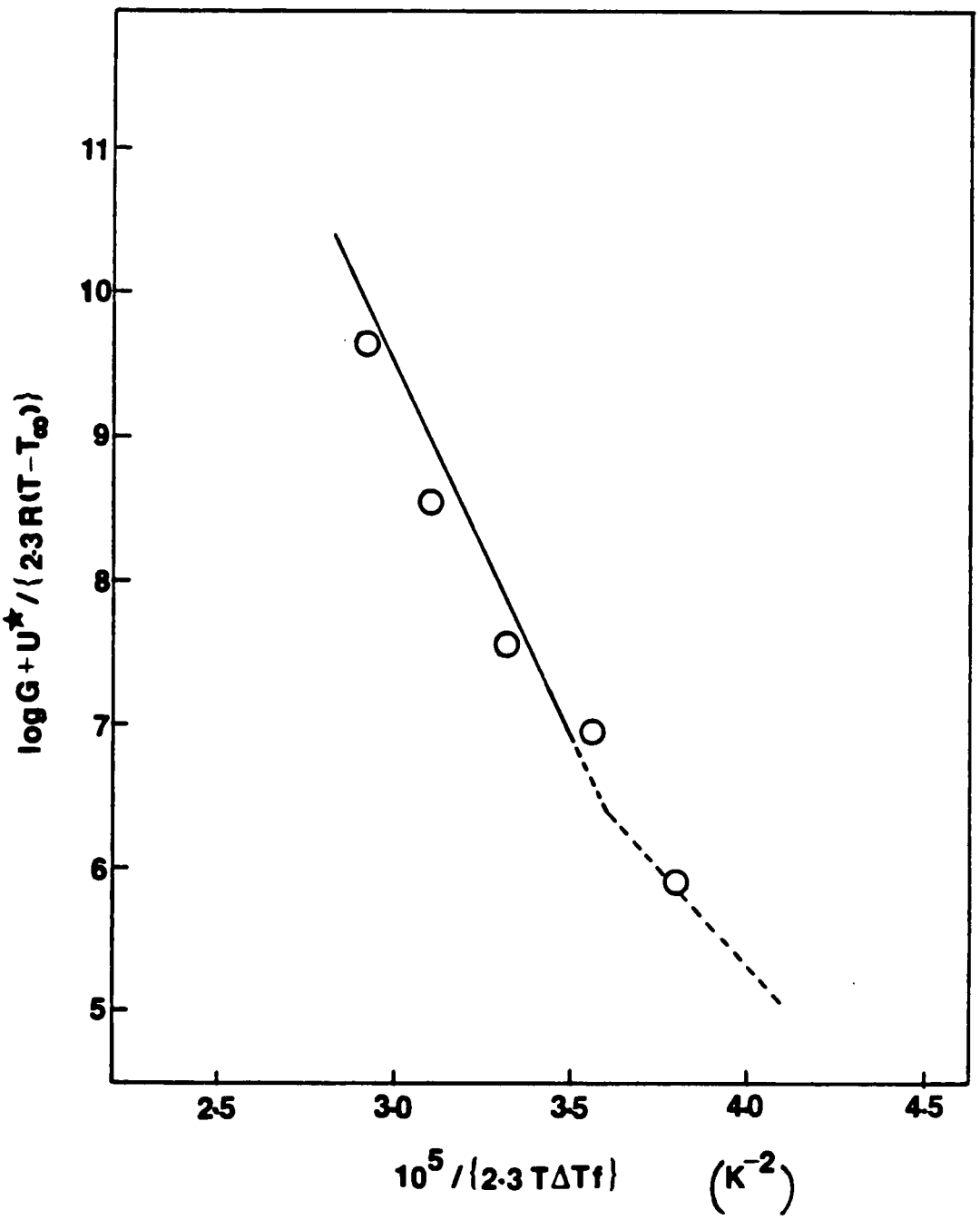


Figure 93 Plot of kinetics data of hevea rubber fraction of molecular weight 543,000 at 0.5 kbar.

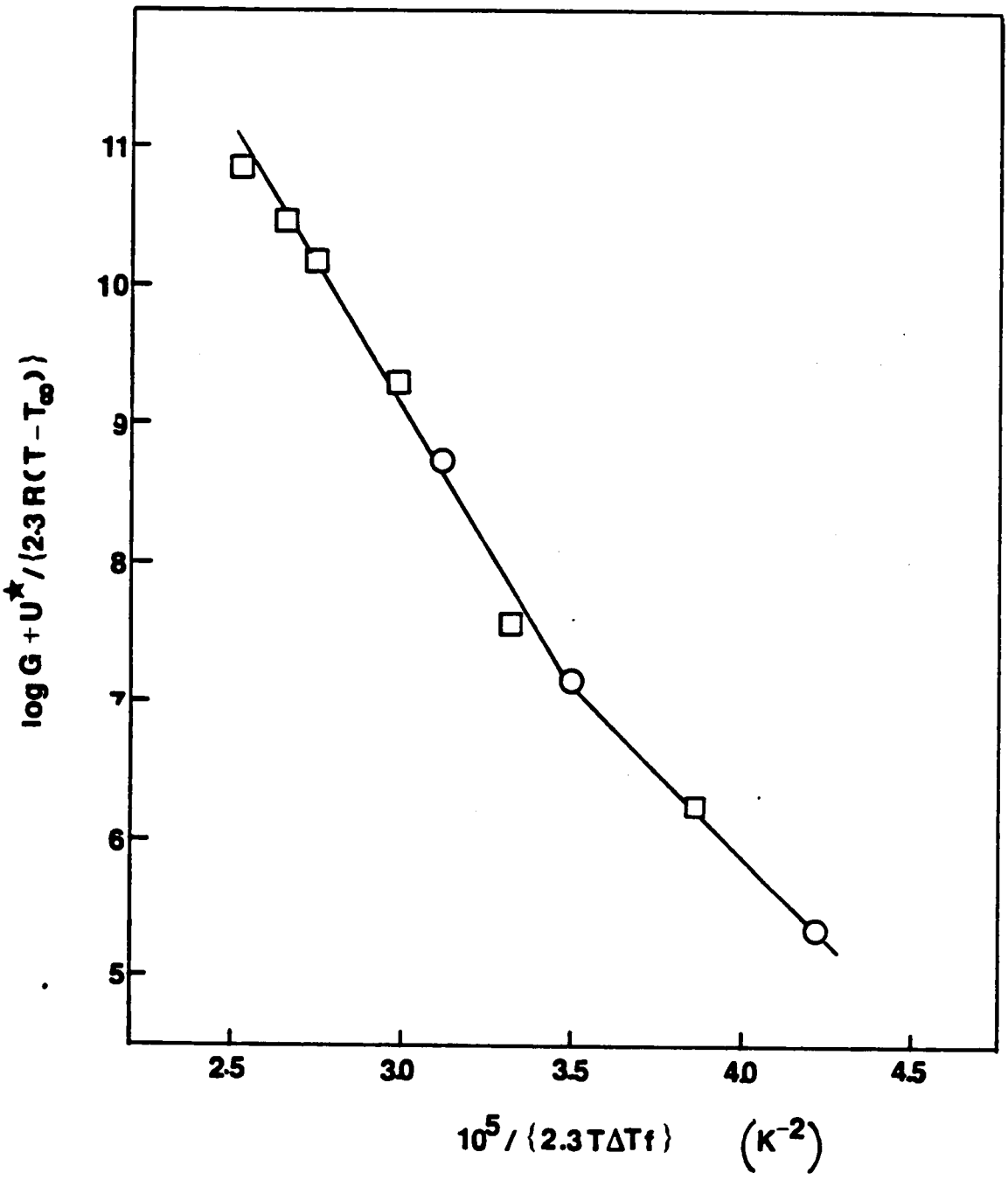


Figure 94 Plot of kinetics data of unfractionated hevea rubber (Phillips and Edwards 1975) at 0.5 kbar □-interpolated points.

Table 7 The Change of σ_e With Pressure

P (kbar)	σ_e (J/m^2) $M_v=3.57\times10^5$	$M_v=5.43\times10^5$	Unfractionated
0.001	0.0242	0.0194	0.0240
0.500	0.0479	0,0430	0.0220

able to see any lamellar morphology at pressures above 0.5 kilobar, but in earlier studies lamellar growth rate data were reported for pressures of up to three kilobar. This suggests a difference in the materials used. Actually both materials were natural cis-polyisoprene and were supplied from the same source. Both are Malaysian rubber. The collection processes of the two rubbers from the plant were a little different. The one used earlier was an example of Standard Malaysian Rubber and was processed more carefully than the one we have used. Thus it can be expected that there will have been more degradation in the one used throughout this work. Since polyisoprenes can easily crosslink with the parts of the same chain resulting in gel formation, our polymer is expected to have higher branching and gel contents. In fact gel percentage in the earlier material did not exceed 30 % whereas it was over 50 % in our case.

In earlier studies σ_e was found to increase with pressure in unfractionated cis-polyisoprene but was invariant in polyethylene. Similar effects occur for our material but at lower pressures than for the other material in terms of producing the high pressure phase and having higher fold surface free energies.

Dalal (1982) proposed a model involving volume reduction in adjacent reentrant folds, for the sudden change of σ_e with pressure at about one kilobar. The absence of

such a change at atmospheric pressure was attributed to a large energy barrier between these two conformations which was overcome at high pressures. The same mechanism may be operating here too. Actually their lamellar thickness analyses were carried out with limited data which might have masked the sudden increase at 0.5 kilobar. In this study we have more data points to calculate the fold surface free energy. Because of this we were able to detect the sudden increase at 0.5 kilobar.

The regime III-II transition temperatures at atmospheric pressure and at 0.5 kilobar are listed in Table 8. The work of Dalal and Phillips (1983-a) showed that the change of equilibrium melting point followed the polynomial

$$T_m^o(P) = 35.5 + 27.0P - 1.49P^2 \qquad (5.1.3)$$

with $dT_m^o/dP = 28\ ^oC/\text{kilobar}$

and the change of glass transition temperature with pressure was given by the polynomial (Dalal and Phillips 1983-b)

$$T_g(P) = -72 + 17.78P - 0.673\ P^2 \qquad (5.1.4)$$

with $dT_g/dP = 18.4\ ^oC/\text{kilobar}$.

From Table 8 it is seen that the change of regime III-II transition is closer to the change in glass transition temperature with pressure than that of the equilibrium

Table 8 The Change of the Regime III-II Transition Temperature With Pressure

Molecular Weight	III-II Transition Temperature p = 0.001 kbar	p = 0.5 kbar	% change/kbar
357,000	-17.2 °C	-8.0 °C	18
543,000	-5.0 °C	+1.0 °C	12
Unfractionated cis-polyisoprene	-13.9 °C	-13.9 °C	24

melting point. With more data at higher pressures the effect of pressure on the III-II transition point could be better defined. We were unable to do this because of the complete absence of spherulitic growth at pressures higher than 0.5 kilobar. The point at 0.5 kilobar still gives evidence supportive to the hypothesis that the III-II transition is kinetically controlled.

Since we could not extend our growth rate studies to higher temperatures due to the very long crystallization times (several weeks) involved, no comment can be made on the nature of the I-II transition based on our data. But in the paper reporting the effect of pressure on spherulitic growth of unfractionated hevea rubber (Phillips and Edwards 1975), the presence of single crystals was mentioned. A boundary curve was drawn beyond which they observed single crystalline species. In our atmospheric pressure crystallization studies, we observed single crystals in the regime I region. Therefore the dashed line drawn for single crystals can be considered as reflecting the change of the regime I-II transition with pressure (Figure 95). In fact the middle straight line portion of the curve is parallel to the change of equilibrium melting point with pressure suggesting that the regime I-II transition in cis-polyisoprene is thermodynamically controlled as in the polyethylene case (Tseng and Phillips 1984).

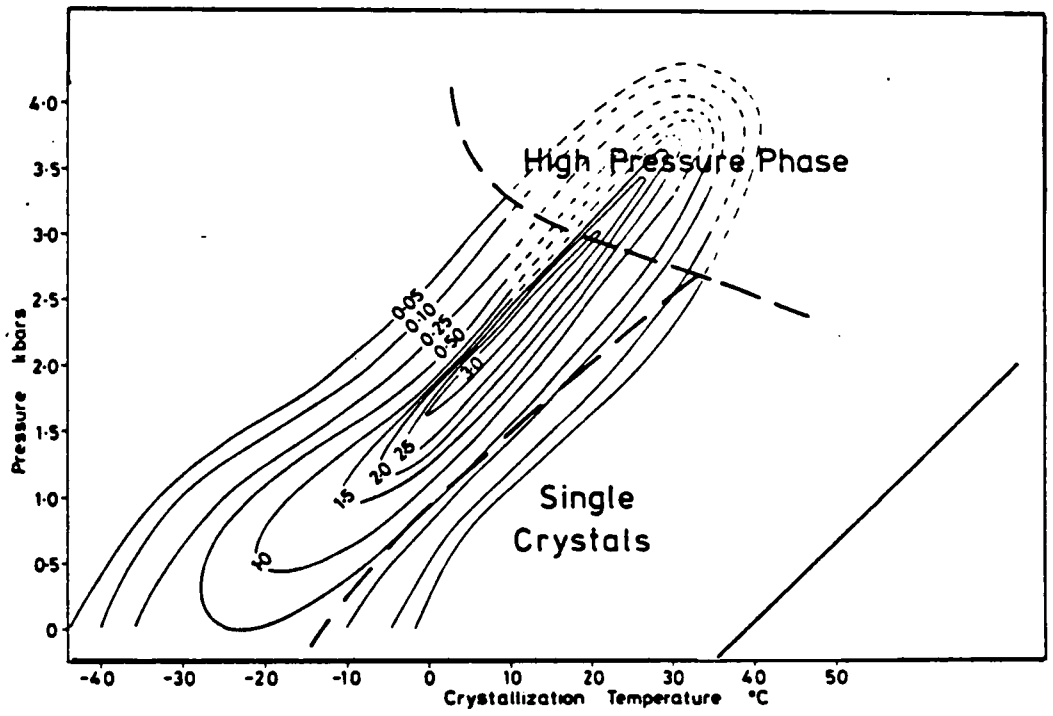


Figure 95 Growth rate contours for cis-polyisoprene (from Phillips and Edwards 1975) and the change of equilibrium melting temperature (T_m^o) with pressure (Dalal 1982).

5.2. Morphology

Morphology of natural cis-polyisoprene from hevea rubber at atmospheric pressure and high pressures has been examined (Andrews 1962, Edwards and Phillips 1975) using transmission electron microscopy of osmium tetroxide stained thin films. At atmospheric pressure, the crystallization was found to be spherulitic. At high pressures three different morphological species occurred, namely: spherulites, single crystals and ellipsoidal high pressure phase at pressures in excess of 2.5 kilobar.

Fold surface free energy values from lamellar thickness data for the unfractionated polymer yielded a sudden increase at one kilobar then remained approximately constant. This fact was explained in terms of a pressure induced change in the fold conformation (Dalal 1982).

Branching in unfractionated cis-polyisoprene has been defined to be non-crystallographic which is a procedure for the generation of new lamellae. In some cases the presence of tie chains at branch points has also been reported (Phillips and Edwards 1976).

In this section these subjects will be discussed for the fractions to investigate the effect of molecular weight and molecular weight distribution on these concepts.

5.2.1. General Morphology

In addition to the typical spherulitic morphology of cis-polyisoprene, other species were observed depending on the crystallization regime followed. For the fraction of molecular weight 3.13×10^5 at low crystallization temperatures (i.e. between -40 ^{o}C and -18 ^{o}C) regime III kinetics were followed. Between the crystallization temperatures of -18 ^{o}C and -5 ^{o}C regime II crystallization was seen. In both regimes III and II spherulites were virtually the only morphological entities encountered. An interesting change in morphology around the regime I-II transition point of the fraction of molecular weight 313,000 is found in the discontinuities observed in the lamellae (Figure 45, p.121). The discontinuities look sharp and occur at almost equal intervals. Such effects have not been reported before. Partial melting of lamellae may result in such discontinuities causing OsO_4 to stain melted portions, the overall result being the mottled appearance of lamellae. But in such a case they are not expected to be sharp, one would expect rather diffuse changes. Secondly, since these changes occur at higher crystallization temperatures where we expect more thickening a relationship between thickening and the formation of holes may be considered. Lamellar thickening may produce such holes in the lamellae during the rearrangement process, if additional crystallizable material is not drawn into the crystal.

Above -5 ^{o}C , in the regime I region, two different species could be detected. First species that look like spherulites, but in which lamellae grow in the "side-on" orientation rather than the usual "edge-on" orientation were observed. Similar species were also reported to occur in trans-polyisoprene (Davies and Ong 1977). We believe these are axialites and the growth rates in the regime I region were measured using these species. In the regime I region it is possible to observe fractionated growth, in which we have complete side-on growth together with the wide ribbons which are normally observed at higher undercoolings (Figure 96). This in fact demonstrates fractionated growth at high temperatures. Fractions used in our experiments do not have a very narrow molecular weight distribution (M_w/M_n=1.5). The presence of this distribution results in different modes of growth occurring concurrently. As the crystallization temperature is increased, fractionation is expected to be more effective due to the longer periods of time required for crystallization.

Secondly, at crystallization temperatures of -7 ^{o}C and above, single crystalline species occurred. These crystals are skeletalized and grow much faster than the normally observed spherulites (Figures 97,98). In earlier studies of unfractionated polymer this type of species was only observed at elevated pressures. The crystals grow preferentially along one crystal direction and contain

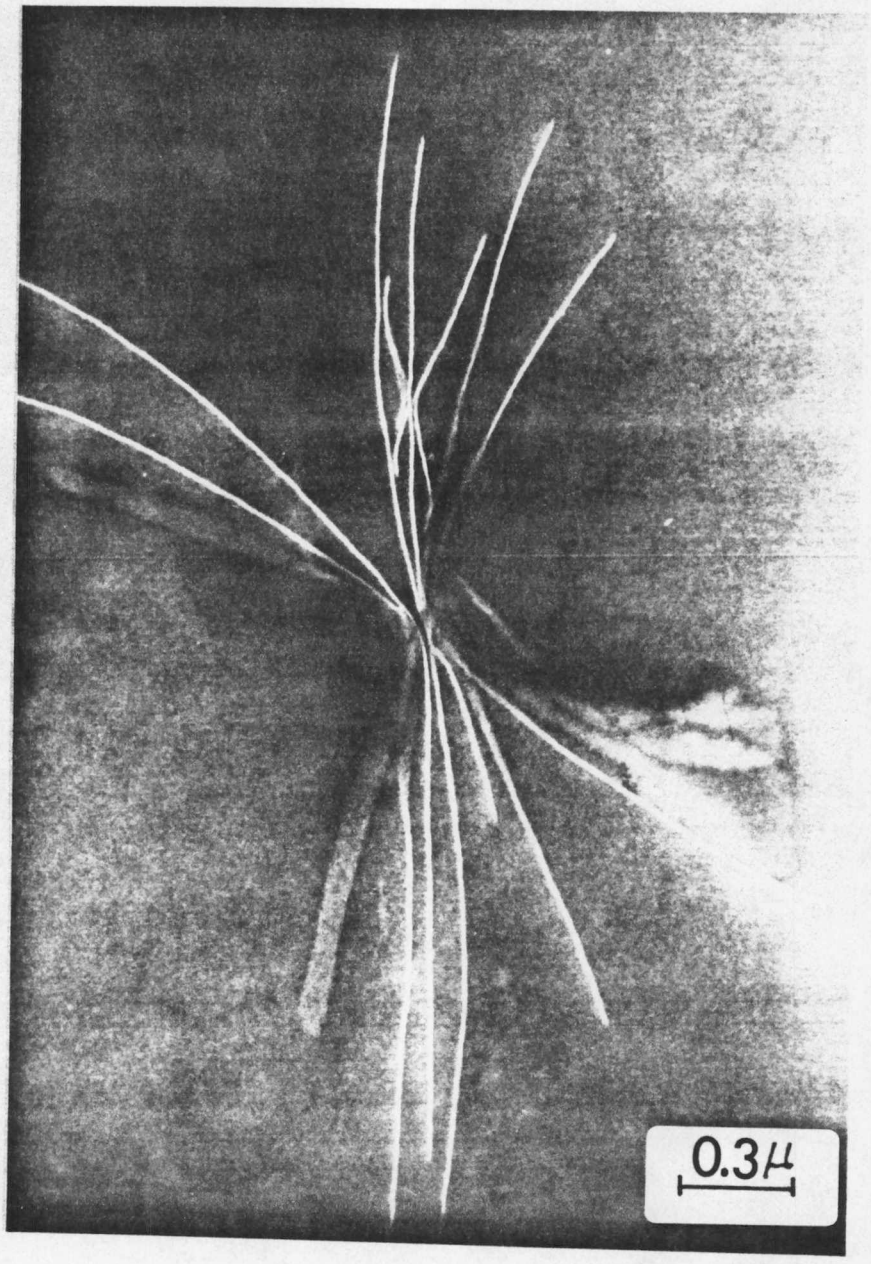


Figure 96 Fractionated growth in regime I region at -5 °C.

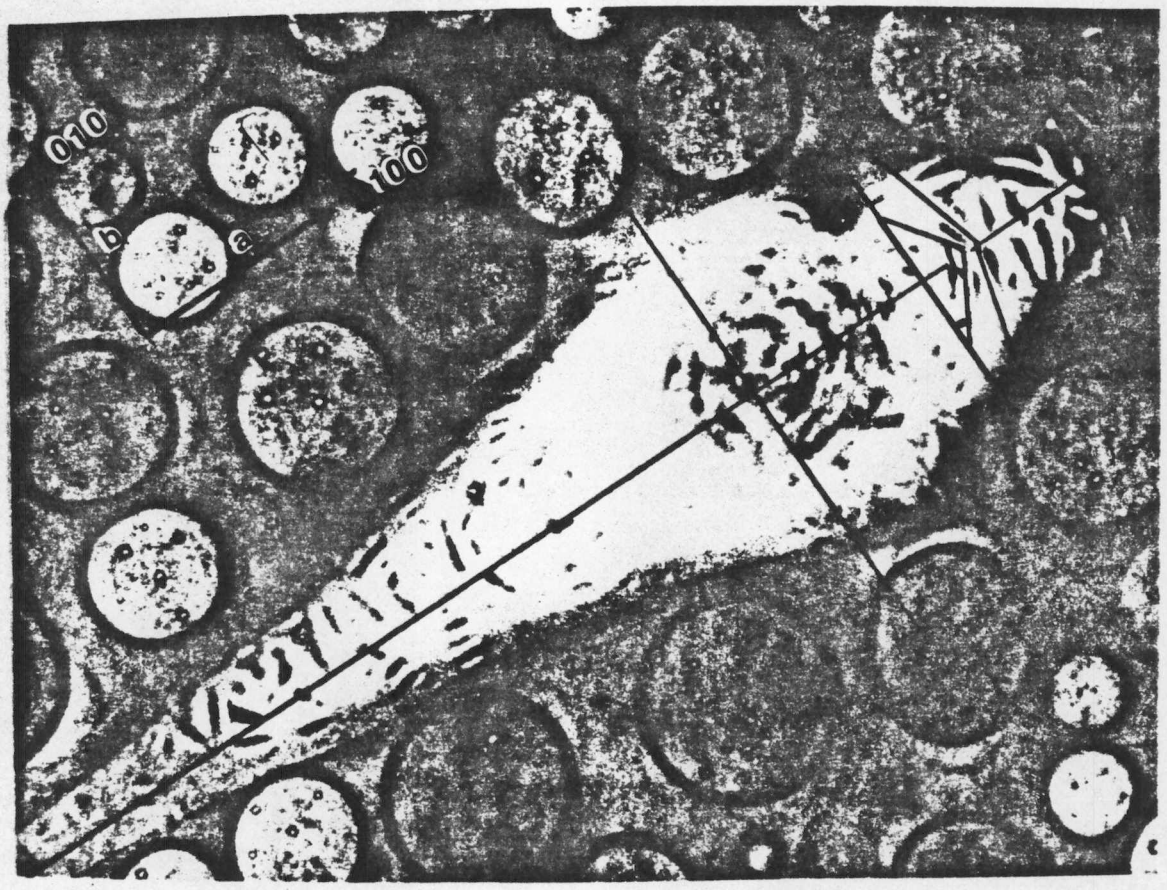


Figure 97 A single crystal growing in a fraction of molecular weight 313,000 at +1.8 °C.

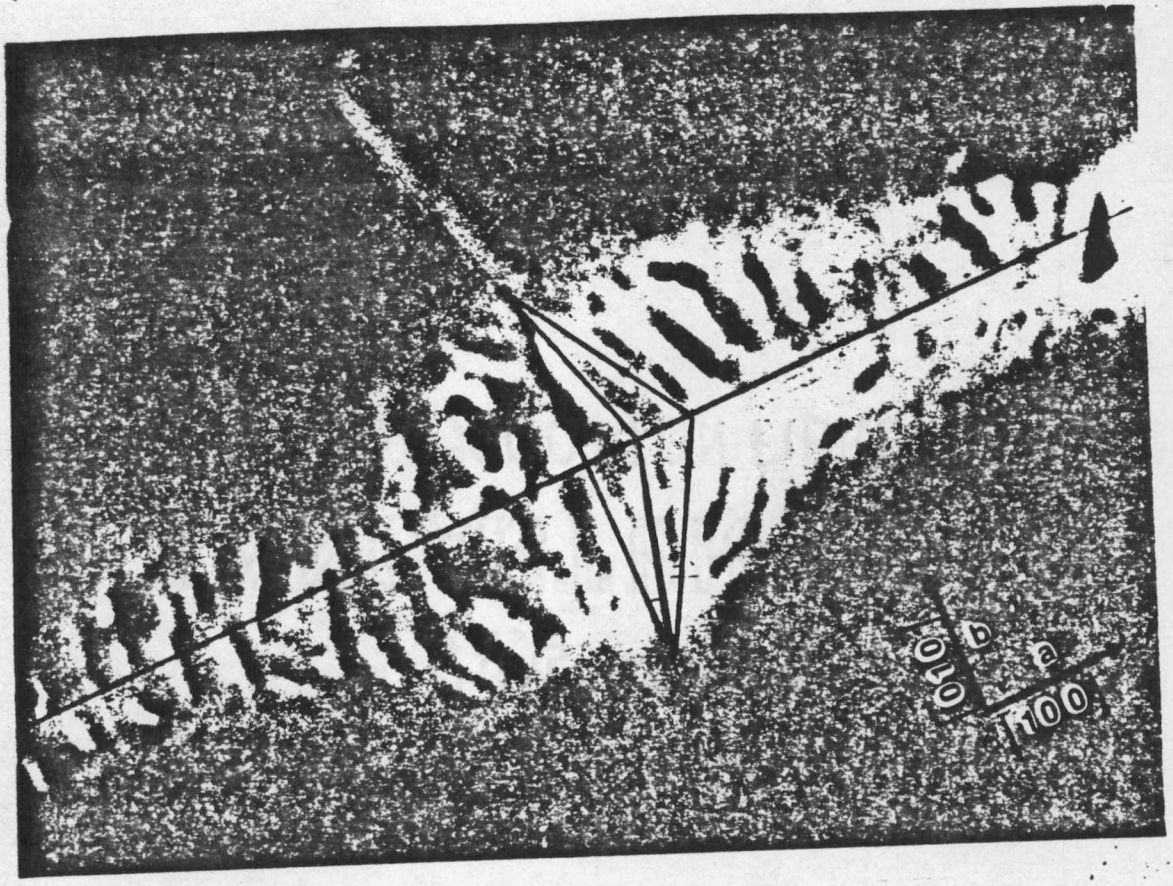


Figure 98 A single crystal in a fraction of molecular weight 313,000 at +1.8 °C.

corrugations in the backbone which are similar to those observed in polyethylene (Reneker and Geil 1960). Earlier attempts to index the planes of corrugations in cis-polyisoprene has failed because of the lack of contrast between the crystals and the amorphous background. Electron diffraction patterns of these crystals (Phillips and Edwards 1976) showed several orders of reflection with both arced and single crystal patterns. Multiple orders of reflection show that some planes within the crystal are tilted with respect to the incident beam. Their analyses of the diffraction patterns showed that they have a crystal structure identical to spherulites, the "a" direction corresponding to the longer axis of the crystal (Edwards and Phillips 1976).

Transmission electron micrographs of the crystals grown from cis-polyisoprene fractions at atmospheric pressure were good enough to permit measurement of the angles between the corrugations and the growth axes. There were two sets of corrugations observable (Figures 97,98). The angles of intersection of corrugations with the "a" and "b" axes (long and short diagonals) of the crystal matched quite well with the intersection of (110) and (130) planes with the same axes. The formation of corrugations suggest that these crystals are not flat. The crystals might have grown as hollow pyramids and collapsed on melting during heating to room temperature. However from our pictures it

can be distinguished that there is more than one hollow pyramid in each of the skeletalized large crystals. Attempts to index and define each hollow pyramid failed. Partly due to the lack of contrast in some places and also because of the curving of the crystals it proved impossible to measure the angle of intersection between the planes and the diagonals of the crystal.

Crystallization studies at 0.5 kilobar showed that the morphology was mainly lamellar along with frequent occurrence of single crystals at low undercoolings. At pressures in excess of 0.5 kilobar ellipsoidal or needle-like species were the only species present (Figure 79, p.160). Similar observations have been reported (Edwards and Phillips 1975) for pressures above 2.5 kilobar in unfractionated cis-polyisoprene. The structure is called the high pressure phase, has no preferred crystal orientation and has a very high nucleation density (Figure 79, p.160). In this study with fractions, we observed the high pressure phase at a much lower pressure than in the unfractionated polymer. As was discussed in section 5.1.3 our polymer has a higher gel content and the relation between a high gel content and formation of the high pressure phase at lower pressures may explain the nature of this phase. Probably what we have at high pressures is gelation crystallization which is a small scale crystallization process. Although the gel was removed from the original material by filtration,

certain amounts of highly branched material may still be present. If the nucleation and growth of lamellar crystals is inhibited at sufficiently high pressures, the chains may be pulled together by entanglements into a localized uniaxial arrangement resulting in these needle-like crystals.

5.2.2. Lamellar Width

The lamellar width was found to increase with crystallization temperature (Figures 99, 100), the data having been obtained by measuring the width of the lamellae in the "side-on" orientation from the micrographs. The errors involved in measuring the lamellar widths are greater than those of lamellar thickness, because of the preferred "edge-on" orientation of lamellae. Lamellae rarely turn over and in many cases it is not clear whether a complete turn-over has occurred or not. Also lamellar widths at constant temperature show a wide distribution which increases the error involved in the measurement (Figure 101). In our analyses we used the average lamellar width at each temperature. The change of lamellar width with temperature for two of the fractions is given in Figures 99, 100. If we consider the width of lamellae growing in the "side-on" orientation in the regime I region, it will be off of the scale of this plot, since the width of such a lamella is about 200 nm at -5 ^{o}C for the fraction of molecular weight

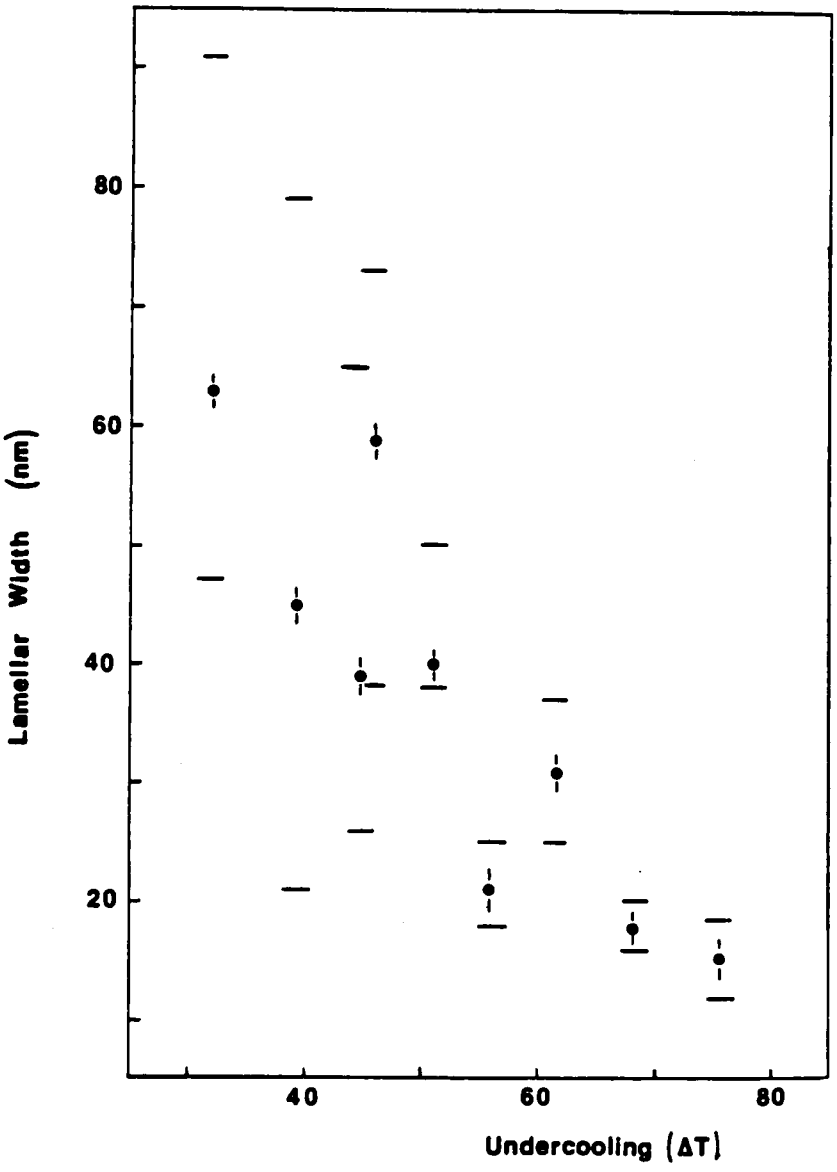


Figure 99 Plot of average lamellar width as a function of undercooling in a fraction of molecular weight 313,000 (parallel lines represent the highest and lowest values measured).

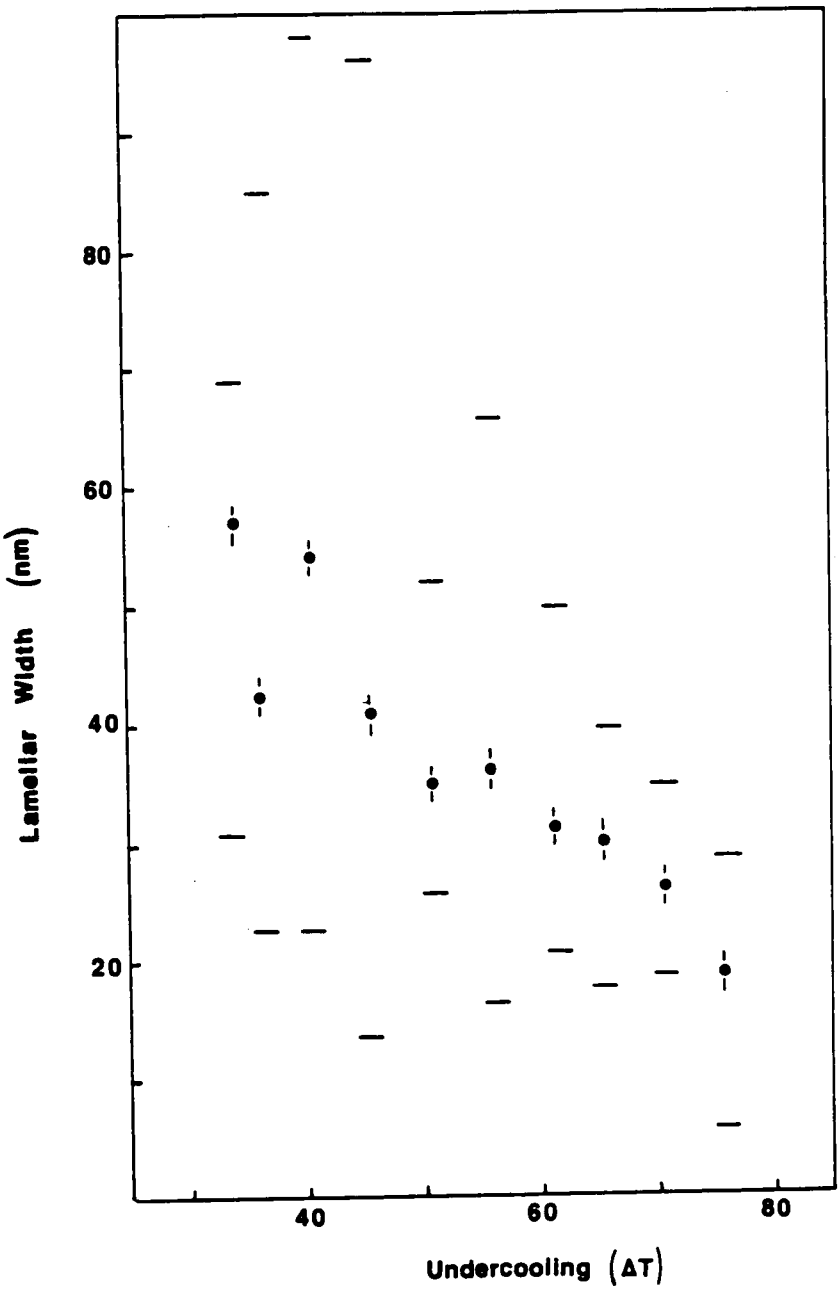


Figure 100 Plot of average lamellar width as a function of undercooling in a fraction of molecular weight 543,000 (parallel lines represent the highest and lowest values measured).

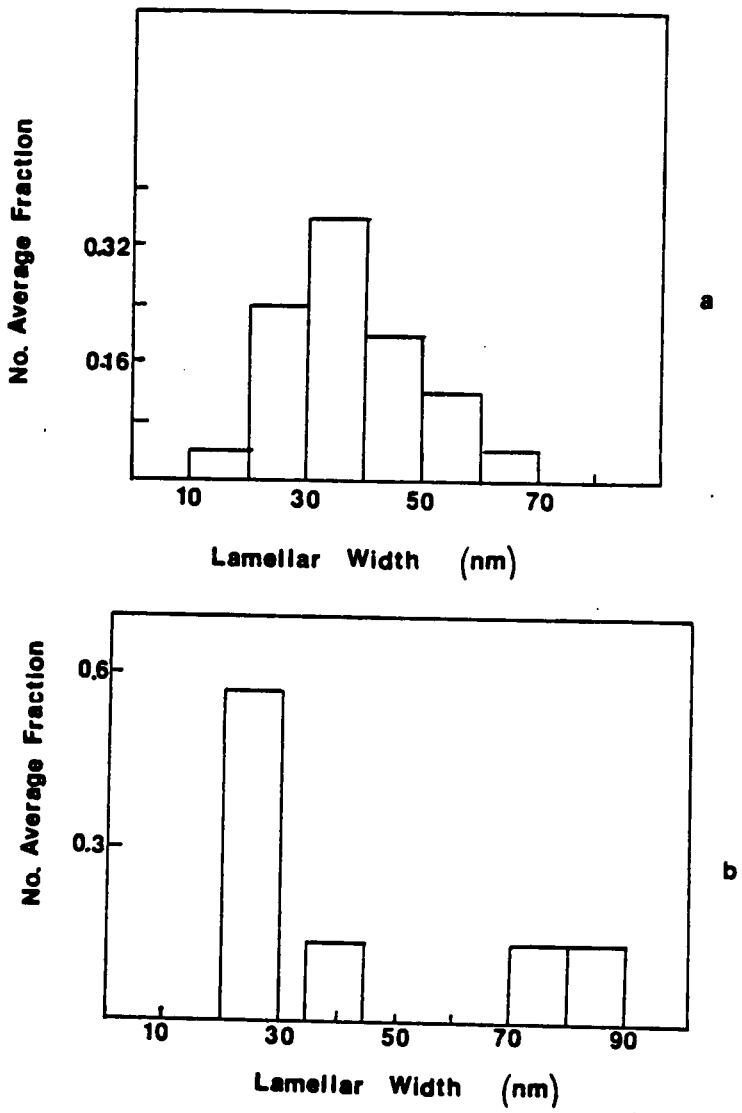


Figure 101 Histograms of lamellar width in a fraction of molecular weight 543,000 at (a) -20°C (b)-0.6°C

313,000. The values we have in this region are the widths of ribbon-like lamellae.

The dependence of lamellar width on temperature has not been explored theoretically. The only experimental data which has been reported so far on this dependence is the work of Bassett et al. (1981-b). They reported a slight increase in lamellar width with temperature in polyethylene fractions. But they have not analyzed their data in detail. We have more extensive data of lamellar widths at different crystallization temperatures. Since it is known that in cis-polyisoprene lamellar thickness varies with crystallization temperature ,T_c, following a second degree polynomial (Dalal 1983), and linearly with $1/f\Delta T$ according to equation (2.5.4), we tried curve fitting of T_c,ΔT and $1/\Delta T$ dependences of lamellar width for two fractions. The resulting equations for the fractions of molecular weights 543,000 and 313,000 respectively are;

$$L.W. = 51.05 + 0.84\ T_c + 2.21\times10^{-3}\ T_c^2 \qquad (5.2.1)$$

where L.W.(lamellar width) is in nanometers and T_c is in ^oC and the correlation coefficient is 93%.

$$L.W. = 60.08 + 2.01\ T_c + 2.29\times10^{-2}\ T_c^2 \qquad (5.2.2)$$

correlation coefficient is 94%.

$$L.W. = 77.65 - 0.75\,\Delta T \qquad (5.2.3)$$

with a correlation coefficient of 93 %.

$$L.W. = 97.64 - 1.15\,\Delta T \qquad (5.2.4)$$

with a correlation coefficient of 88%.

$$L.W. = -1.25 + 1.92\times10^{3}(1/\Delta T) \qquad (5.2.5)$$

with a correlation coefficient of 92%.

$$L.W. = -25.16 + 3.05\times10^{3}(1/\Delta T) \qquad (5.2.6)$$

with a correlation coefficient of 94%.

The introduction of the correction term "f" did not improve the fits. Lamellar width seems to change with temperature as lamellar thickness does, but shows poorer fits. This may be related to the error involved in measurements of lamellar width, because of the wide distribution occurs in lamellar width. In the case of lamellar thickness, the slope of the straight line obtained from lamellar thickness vs $1/f\Delta T$ plot is equal to $2\sigma_e T_m^{o}/\Delta h_f$. One would expect lamellar width to be a function of lateral surface free energy, σ, rather than σ_e. If this is the case, then we will have different σ values for different molecular weight fractions, but σ is not expected to be a function of molecular weight. Therefore, the lamellar width data of two fractions were combined to see

if a better fit could be obtained. The resulting correlation coefficient of the straight line of lamellar width vs $1/\Delta T$ is 90%, which is no better than those of the two separate fractions. Since it is not known how lamellar width depends on σ exactly, we were unable to check the σ values from our equations. Lateral surface free energy values obtained, assuming equation (2.5.4) is valid for σ dependence of lamellar width, were 10-20 times higher than the known value of 0.014 kJ/mol of σ. The analysis of Bassett's data (1981-b) for polyethylene fractions resulted in extremely high σ values which are 10^4 times higher than the σ value of polyethylene.

5.2.3. Lamellar Thickness

Lamellar thickness "l" is a strong function of crystallization temperature and increases with increasing temperature. The lamellar thickness data of different molecular weight fractions of hevea rubber are shown in Figure 33, p.106. Lamellar thicknesses are seen to increase with decreasing undercooling as expected.

It is now well established that lamellar thickness and undercooling (ΔT) are related in the form:

$$l = (2\sigma_e T_m^{\circ} / \Delta h_f \Delta T) + \gamma \delta l \qquad (5.2.7)$$

where σ_e is the fold surface free energy, T_m^o is the equilibrium melting point, Δh_f is the heat of fusion per unit volume of the crystal and γ is the thickening ratio. The quantity "δl" is the additional thickness required for the crystal to grow at a finite rate.

σ_e is claimed to have a slight temperature dependence (Hoffman et al. 1976) according to the equation;

$$\sigma_e = \sigma_{e1} (1+y\Delta T) \qquad (5.2.8)$$

where σ_{e1} is the fold surface free energy near T_m^o and y is a small positive number. The factor "f" is introduced to correct the non-linearity in the heat of fusion at large undercoolings. By combining all these modifications, the lamellar thickness "l" is given as;

$$l = (2\sigma_{e1}T_m^o /\Delta h_f)(1/\Delta Tf) + (2\sigma_{e1}\gamma T_m^o \gamma/\Delta h_f)\gamma\delta l \qquad (5.2.9)$$

The equation can be reduced to the general form of

$$l = (c_1/f\Delta T) + c_2 \qquad (5.2.10)$$

In order for c_2 to be constant the parameter ψ in equation (2.4.8) must be very low.

The approximate value of σ_e may be obtained by using equation (5.2.10) and the value of c_1. Figures 102 and

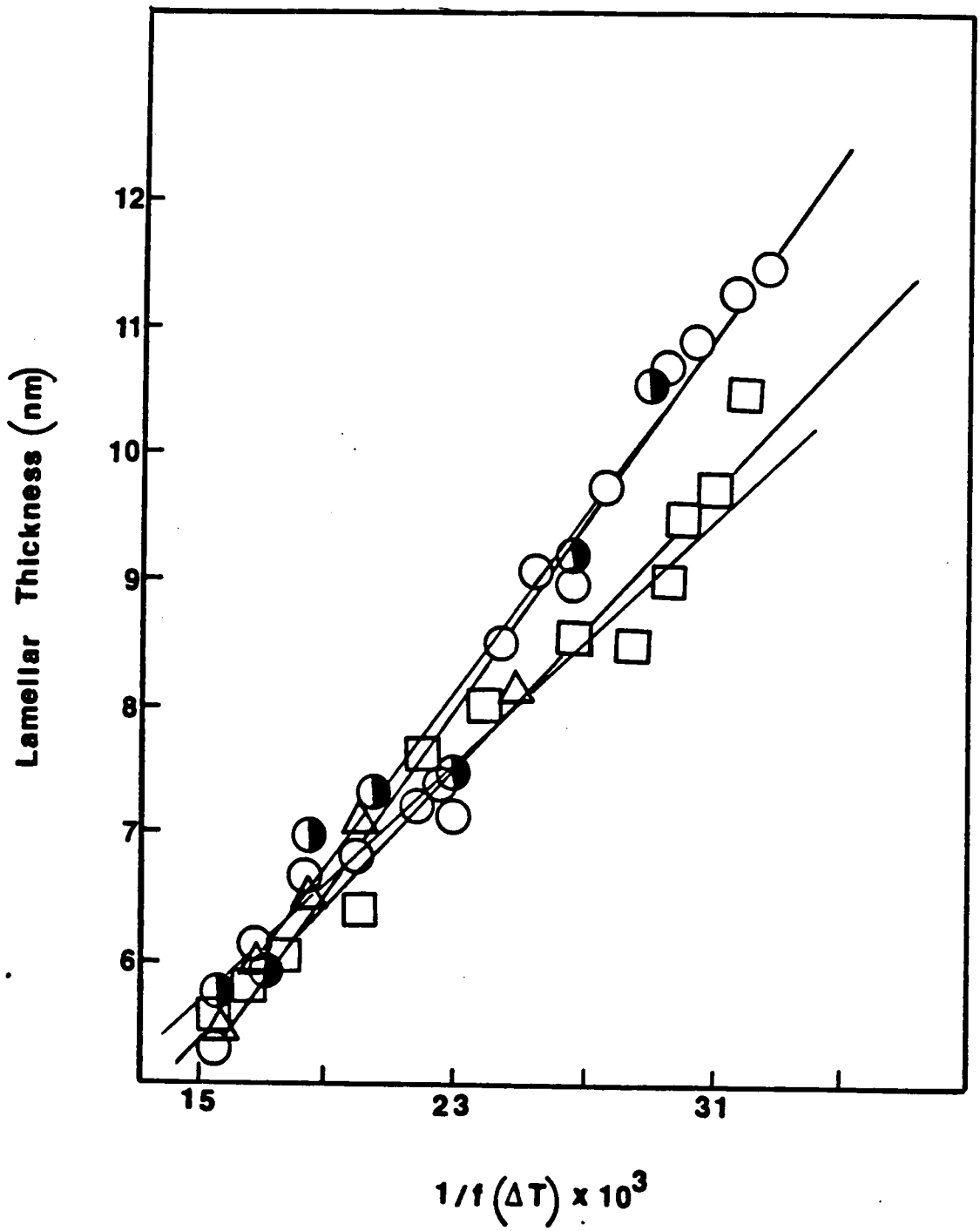


Figure 102 Plots of lamellar thickness versus $1/f\Delta T \times 10^3$ for the hevea rubber fractions of molecular weights O-313,000, ◑-351,000,□-543,000 and ▲-897,000.

103 show plots of "l" versus $1/(f\Delta T)$ which were drawn using the data of Figures (33,70, p.106,150). Figures 104-107 show histograms for some fractions at different temperatures. It may be seen that at higher crystallization temperatures a relatively wider lamellar thickness distribution is present due to the presence of thicker lamellae at these temperatures. An increase in lamellar thickness with time has been reported in polyethylene (Fischer and Schmidt 1962) at atmospheric pressure. In cis-polyisoprene the thickening effect is not important at shorter crystallization times (i.e at lower temperatures), but at high temperatures crystallization times are very long (days to weeks) and thickening is more important. We also know that the lower molecular weight fraction crystallizes in regime I at high crystallization temperatures and the higher molecular weight fraction may contain a certain amount of low molecular weight material due to its molecular weight distribution. This low molecular weight polymer may crystallize in regime I. So the ability to thicken at these temperatures may be related to regime I growth. In the regime I region the number of branches is low (Figure 60, p.138) and the thickening is not limited by too many lamellae competing for the available space. On the other hand, at high undercoolings most of the crystallizable material in between the lamellae is consumed for branching and thickening is suppressed. From the morphological changes occurring in the

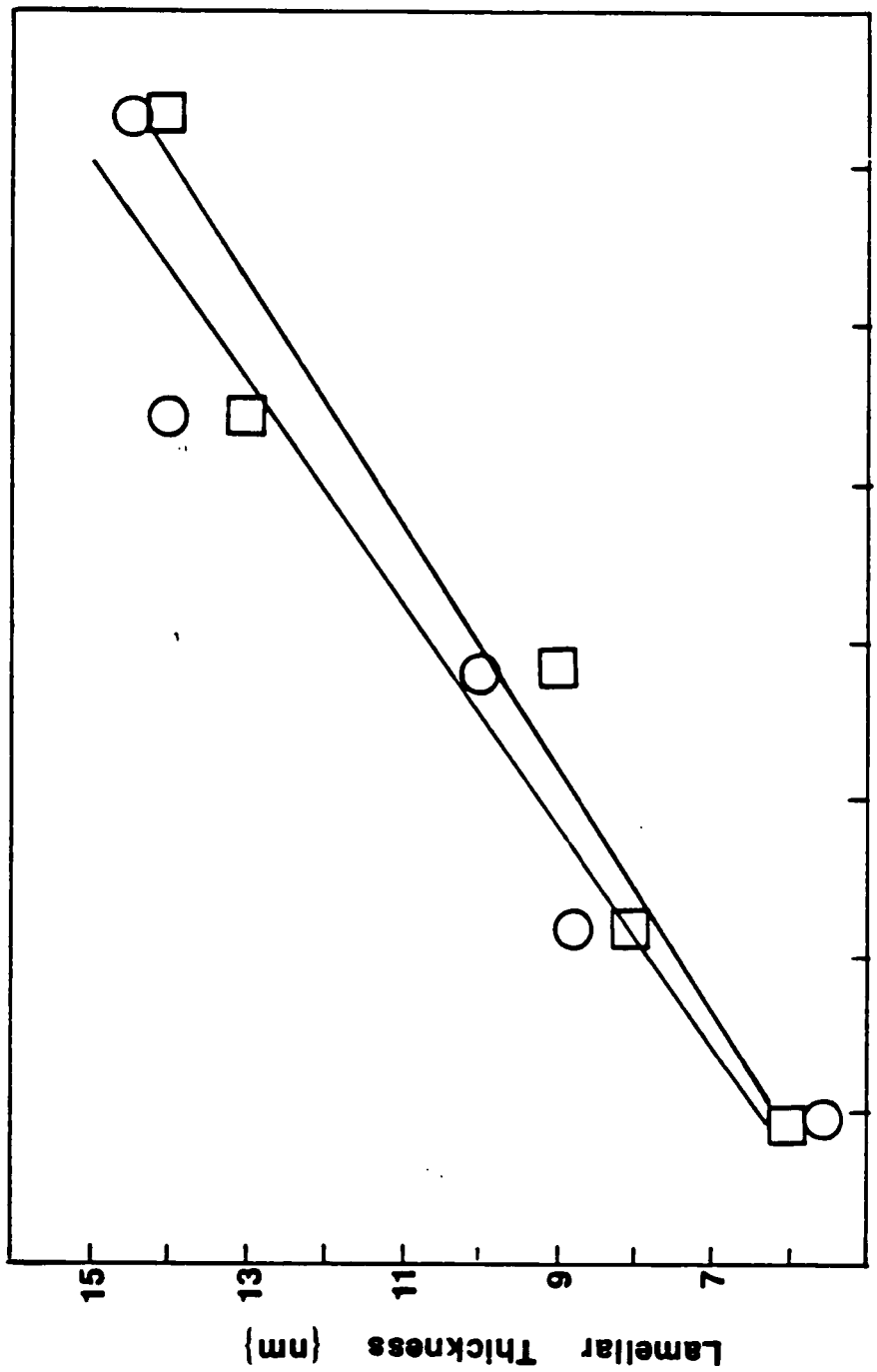


Figure 103 Plots of lamellar thickness versus $1/f\Delta Tx10^3$ at 0.5 kbar for the hevea rubber fractions of molecular weights O-351,000 and □-543,000.

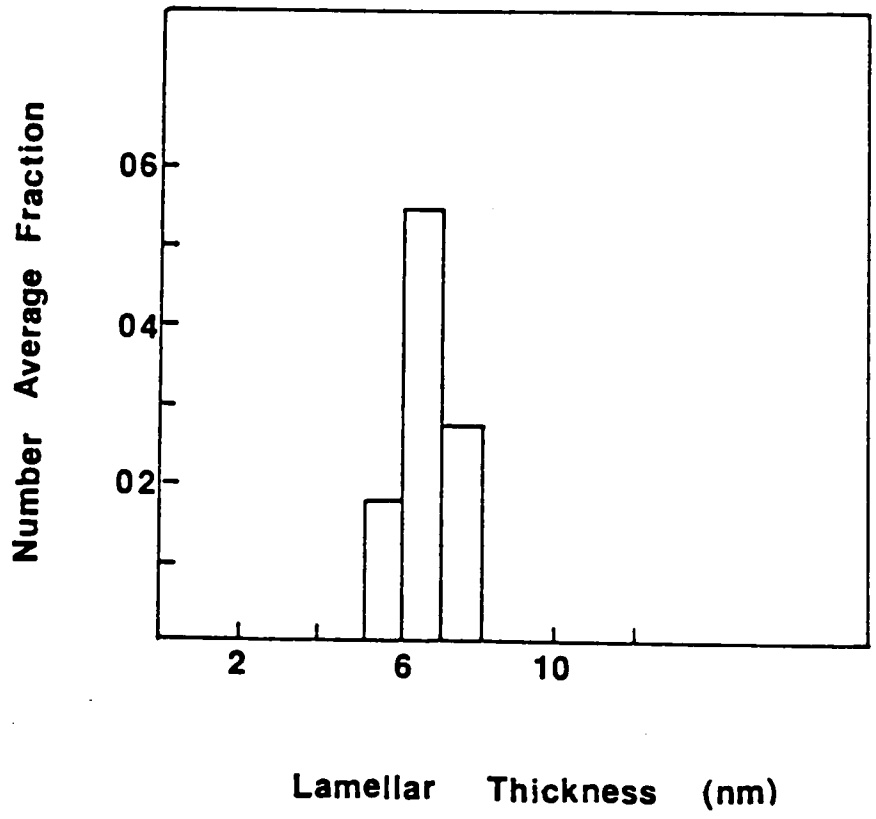


Figure 104 A histogram of lamellar thickness of hevea rubber fraction of molecular weight 313,000 at -26 ^{o}C and at atmospheric pressure.

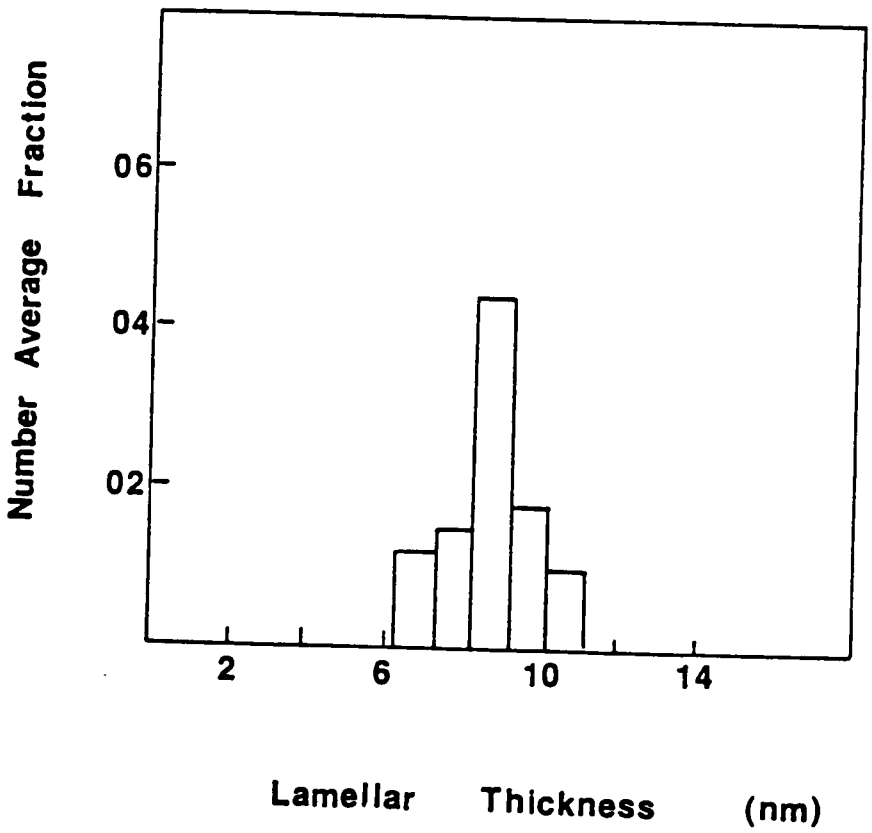


Figure 105 A histogram of lamellar thickness of hevea rubber fraction of molecular weight 543,000 at -0.6 °C and at atmospheric pressure.

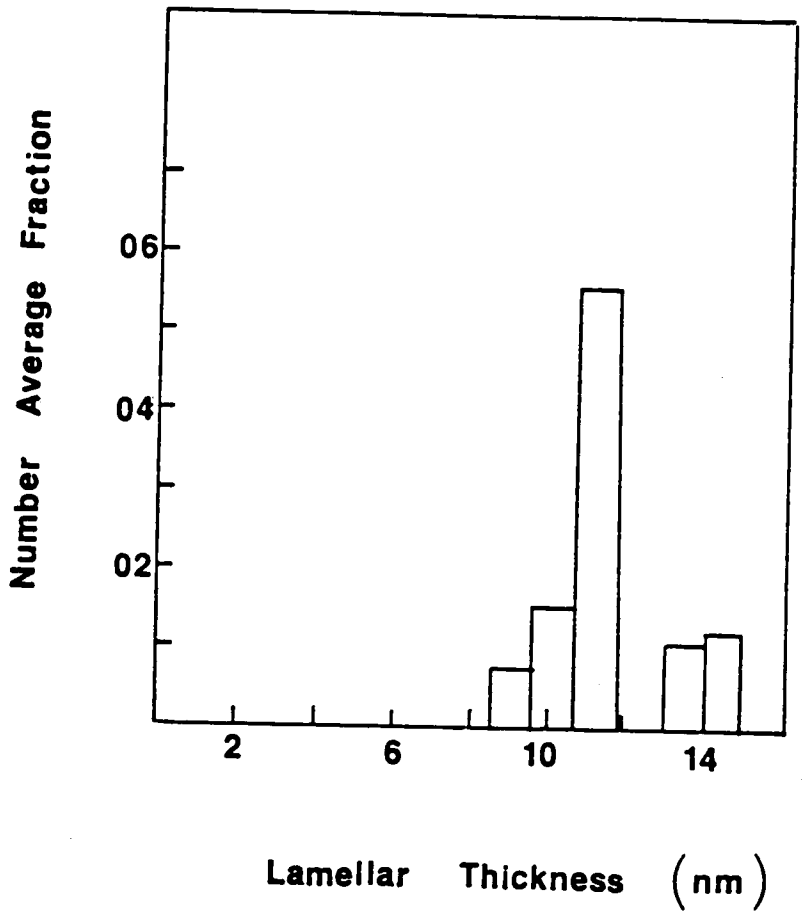


Figure 106 A histogram of lamellar thickness of hevea rubber fraction of molecular weight 313,000 at +1.8 ^{o}C and at atmospheric pressure.

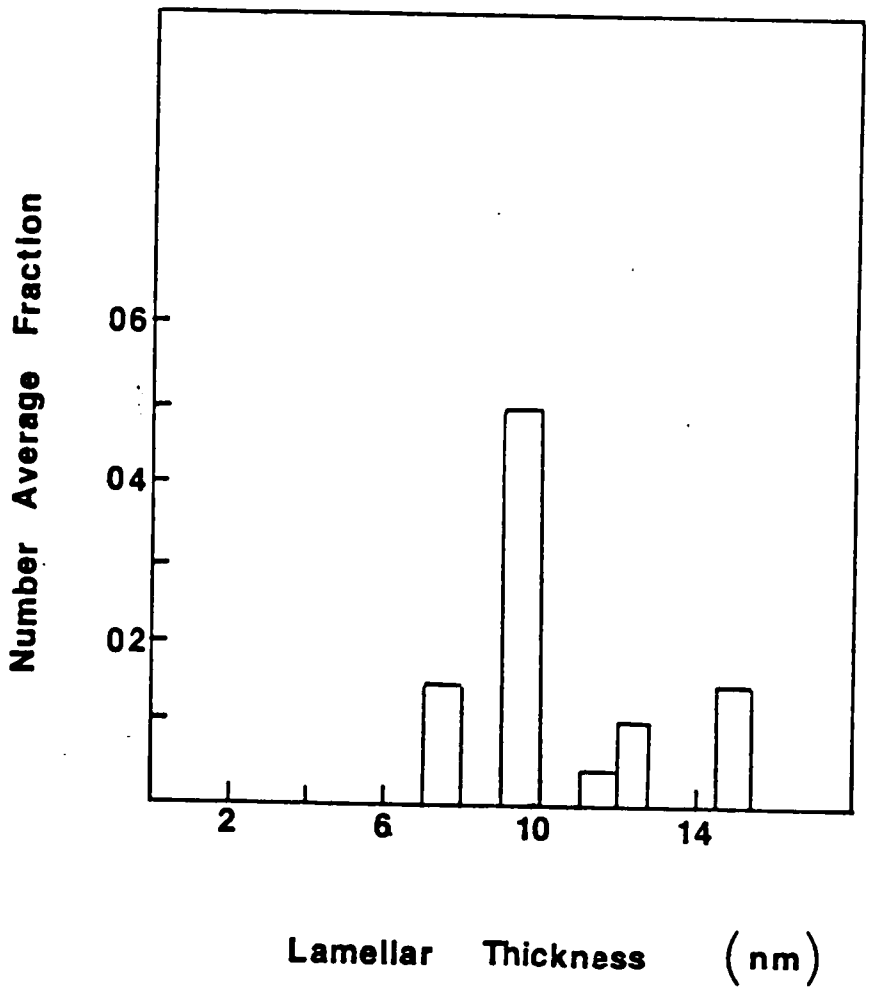


Figure 107 A histogram of lamellar thickness of hevea rubber fraction of molecular weight 543,000 at +1.4 ^{o}C and at atmospheric pressure.

regime I region it is known that single crystals and axialites are the regime I species. The lamellar thicknesses in these axialites were measured to check whether they correspond to the thicker crystals produced at high crystallization temperatures. In fact most of the lamellae in these axialitic species had higher lamellar thicknesses than average, demonstrating a relationship between regime I growth and thickening. Molecular weight effects may also be deduced from a comparison of the behavior of two molecular weight fractions. It can be seen that the lower molecular weight one produces thicker crystals than the higher molecular weight one at comparable undercoolings (Figures 106 and 107). According to Kawai et al. (1971) the higher molecular weight species start to crystallize at high undercoolings giving rise to comparatively thin crystals. Lower molecular weight material starts to crystallize at lower degrees of undercoolings, resulting in formation of thicker crystals. Here what is seen is probably due to a combination of effects of molecular weight, crystallization regime and long crystallization time.

Lamellar thickness is expected to increase with increasing pressure due to the increase of equilibrium melting point T_m^o (Equation 2.5.4.). The pressure dependence of solution grown polyethylene crystals was analyzed by Wunderlich (1963) and a slight linear increase in lamellar thickness with pressure was reported. The pressure

dependence of melt crystallized polyethylene was found to be similar to that of solution grown crystals, up to three kilobar. A very broad lamellar thickness distribution was reported at pressures in excess of three kilobar (Wunderlich and Arakawa 1964). An increase in lamellar thickness with time in polyethylene under high pressure was also reported (Rees and Bassett 1971).

The histograms of two of the fractions at 0.5 kilobar and different crystallization temperatures (Figures 71,72, p.151,152 and 108-115) exhibited significantly different lamellar thickness distributions especially towards the higher temperatures in which longer crystallization times are required. The step thicknesses of these crystals also increased with crystallization temperature. Here, thicker crystals do not correspond to axialitic crystals. This indicates that pressure induced thickening is more effective on normal lamellar crystals than those of the axialitic species.

From the slopes of the plots of "l" versus $1/(f\Delta T)$, σ_e values for different molecular weight fractions at atmospheric pressure and at 0.5 kilobar can be calculated. Atmospheric pressure results are shown in Table 9. The input parameters used in the calculation of σ_e values are $\Delta h_f = 6.4 \times 10^7$ kJ/mole and $\gamma = 1.46$ (Dalal 1982). Fold surface free energies calculated from lamellar thickness data are comparable to those obtained from kinetics data

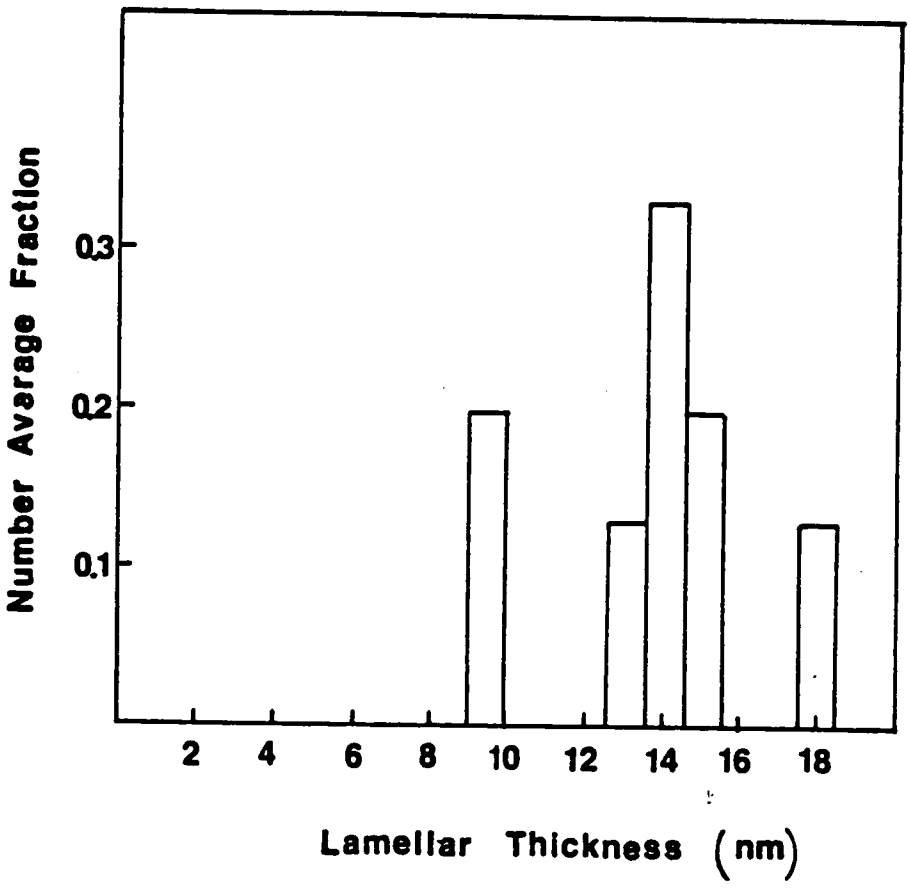


Figure 108 A histogram of lamellar thickness of hevea rubber fraction of molecular weight 351,000 at +4.2 ^{o}C and at 0.5 kbar.

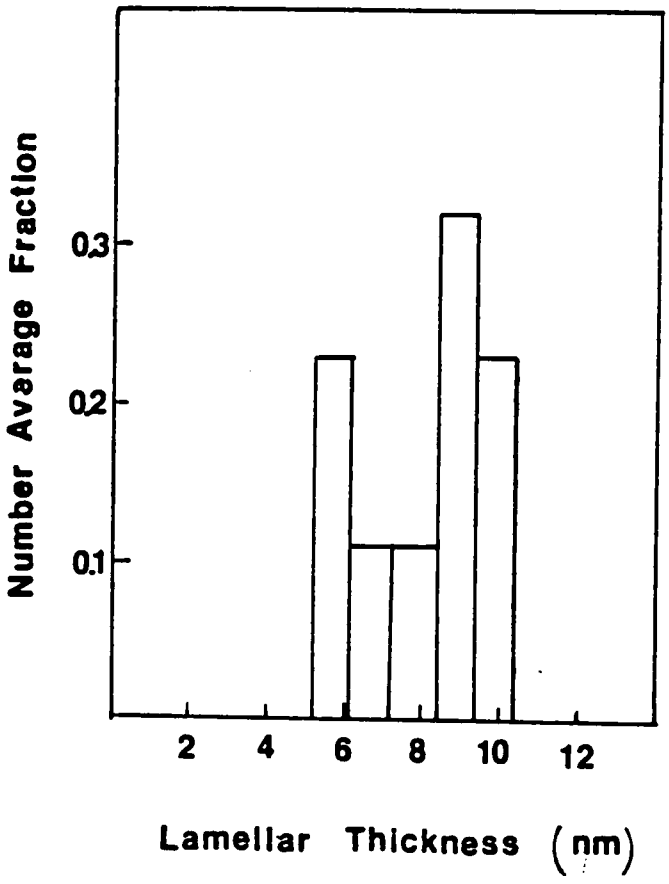


Figure 109 A histogram of lamellar thickness of hevea rubber fraction of molecular weight 351,000 at -11 ^{o}C and at 0.5 kbar.

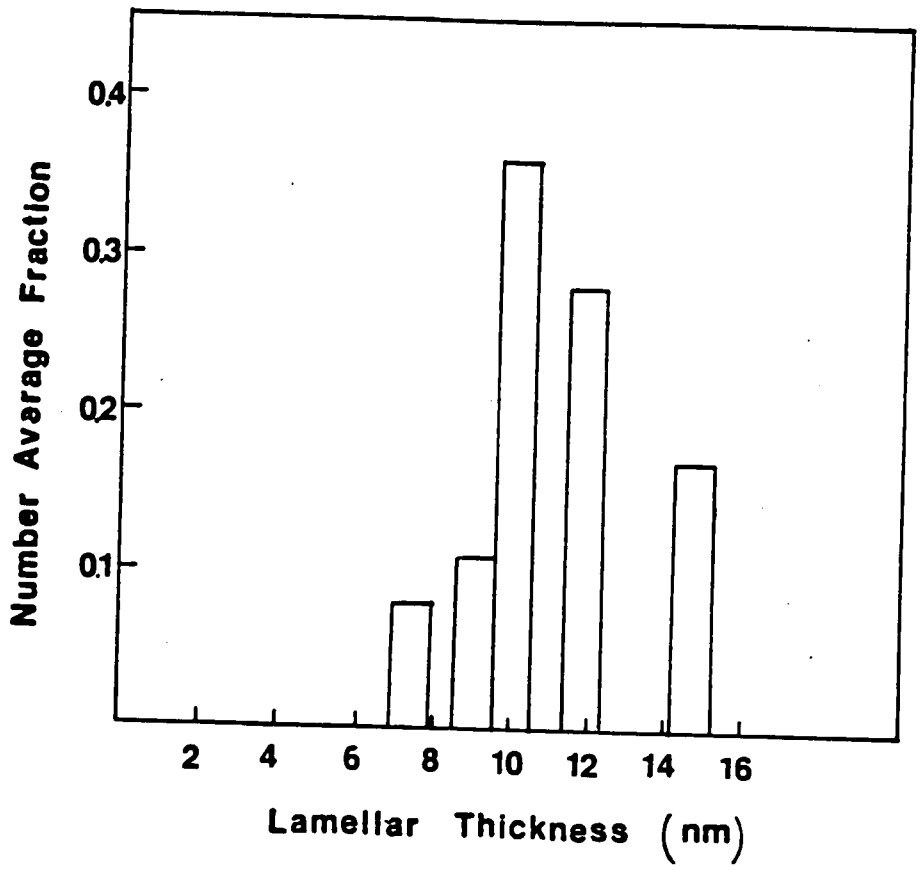


Figure 110 A histogram of lamellar thickness of hevea rubber fraction of molecular weight 351,000 at -4.8 ^{o}C and at 0.5 kbar.

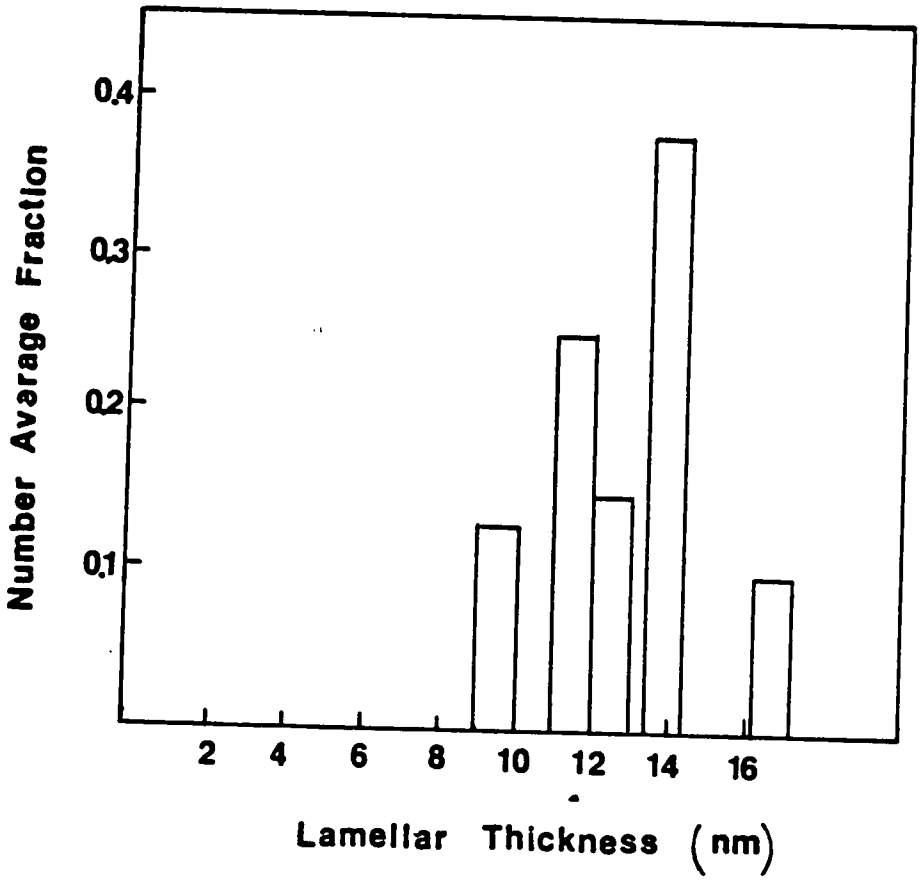


Figure 111 A histogram of lamellar thickness of hevea rubber fraction of molecular weight 351,000 at 0 ^{o}C and at 0.5 kbar.

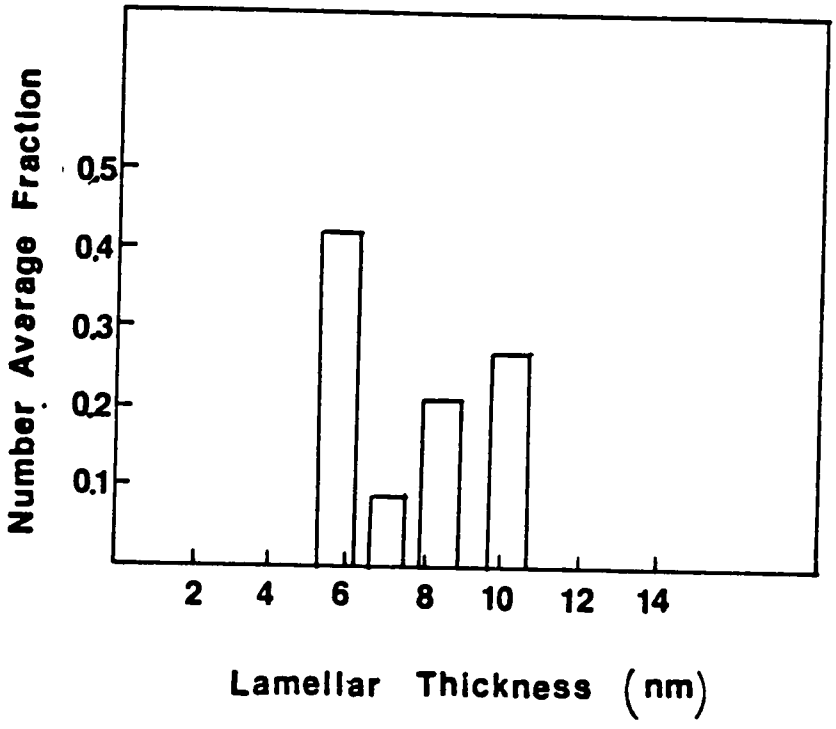


Figure 112 A histogram of lamellar thickness of hevea rubber fraction of molecular weight 351,000 at -17 ^{o}C and at 0.5 kbar.

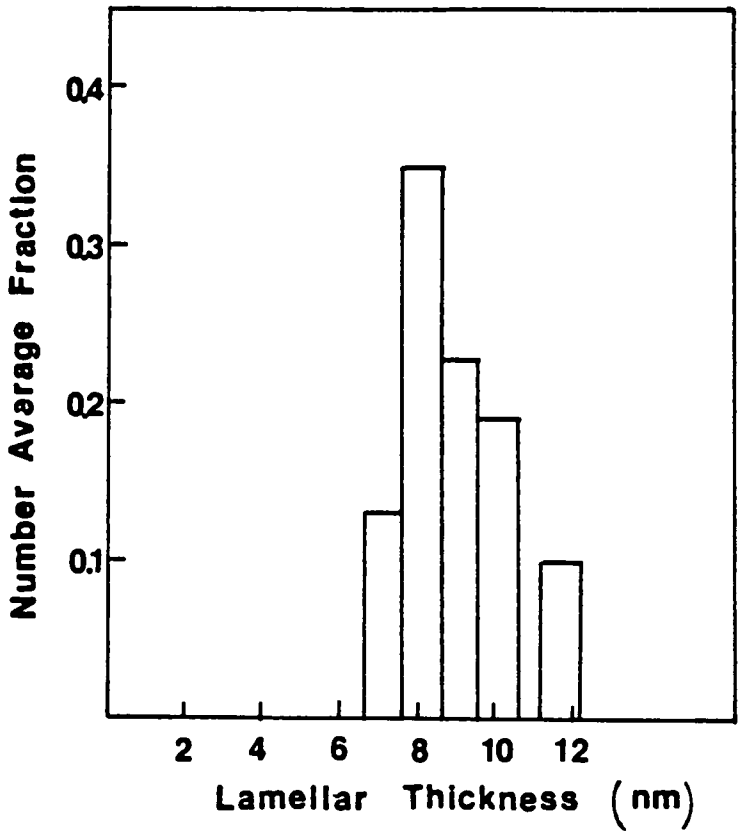


Figure 113 A histogram of lamellar thickness of hevea rubber fraction of molecular weight 543,000 at -11 ^{o}C and at 0.5 kbar.

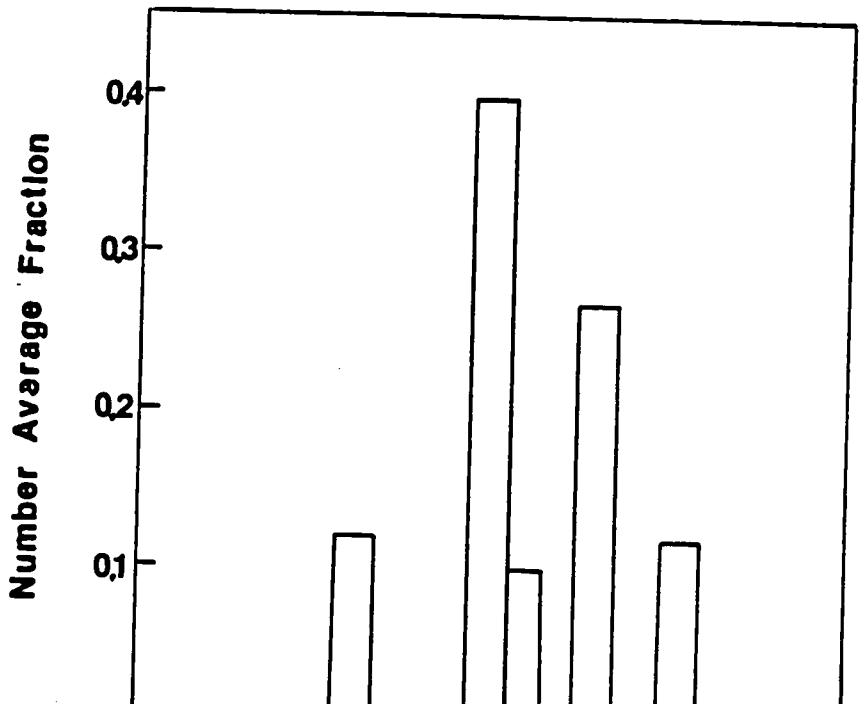


Figure 114 A histogram of lamellar thickness of hevea rubber fraction of molecular weight 543,000 at -4.8 ^{o}C and at 0.5 kbar.

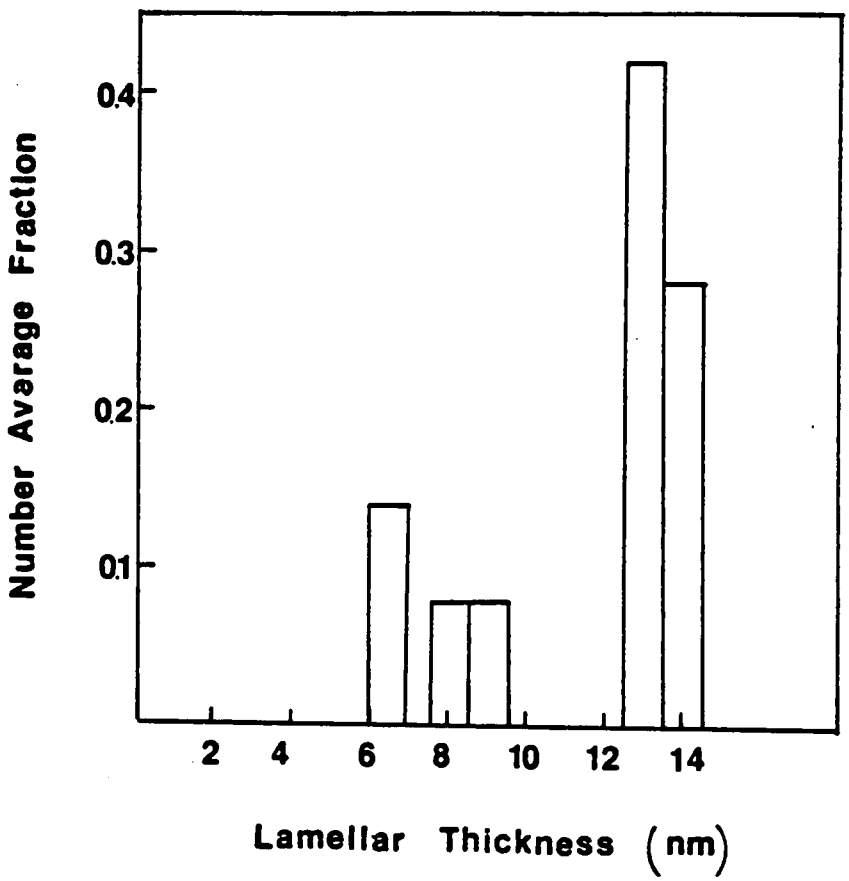


Figure 115 A histogram of lamellar thickness of hevea rubber fraction of molecular weight 543,000 at 0 ^{o}C and at 0.5 kbar.

Table 9 The Change of σ_e With Molecular Weight

Molecular Weight	$\sigma_e(J/m^2)$
313,000	0.0262
351,000	0.0242
543,000	0.0194
897,000	0.0195
1,421,000	0.0192

(Tables 5-6, p.190-191). It is clear that the two lowest molecular weight fractions showing all three regimes have the highest fold surface free energies and that above a molecular weight of 543,000 σ_e stays constant. This effect may be due to a higher percentage of adjacent reentrant folds in the regime I region. If this assumption were true, the σ_e values for the regime I region obtained from kinetic analysis should have been higher than those of regime II and III (Table 5, p.190). But we see that it is not the case. In order to check the regime dependence of σ_e further, we analyzed the lamellar thickness versus $1/f\Delta T$ data for two fractions in more detail. For this purpose we divided the straight lines in Figure 102 (p. 219) in to two or three straight line segments, the intersection points of the segments being the regime transition temperatures. In this way, from the slopes of each region, σ_e values for the different regimes could be calculated. Results are presented in Table 10. σ_e values for regimes I and II appeared to be higher than those of regime III which may be explained by the presence of a higher fraction of non-adjacent reentry and loose loops in regime III. The correlation coefficients for the three line segments did not show a better fit than a single line plot. This may be due to an insufficient number of data points in each region. The higher values of σ_e found in the regime III region from the kinetic analysis can be explained by the slope ratio of I-II transition. This value

Table 10 . Analyses of Lamellar Thickness Data

Molecular Weight	Regime	$\sigma_e(J/m^2)$	Correlation Coefficient
313,000	III	0.0233	0.94
	II	0.0320	0.93
	I	0.0330	0.96
543,000	III	0.0203	0.98
	II	0.0259	0.91

was found to be equal to 1.86. If we manipulate the input parameters so that the regime I-II slope ratio would equal two, then $\sigma_e(I)$ would be higher in accord with the results obtained from the analyses of lamellar thickness.

5.2.4. Branching

Spherulites are polycrystalline aggregates formed from a single nucleus in rather viscous systems. Crystal orientation in spherulites is independent of the orientation in the original nucleus, but is determined by the form of overall growth of the polycrystalline aggregate. In the course of growth of a spherulite branching occurs and, after that, growth proceeds at the same rate in all directions. Branching can be either non-crystallographic or crystallographic. In the first case, as the spherulite grows branching occurs to fill the available space between lamellae and it is not necessary to have contact between them. Regular crystallographic branching leads to preferred growth in particular directions, not to a uniform growth in all directions. In this case, branches are connected to the original lamellae through crystalline material. Figures 62-67 (p. 140-145) are transmission electron micrographs which contain many branch points. In Figure 62 (p.140) probably there were two nucleation centers (A, B). The growth of lamellae growing from A stopped when they met with other lamellae originating from B. There is a branch point at C

from which the growth of secondary lamella did not proceed at equal rates in both directions. In Figure 63 (p.141) possible nucleation on an impurity (A) resulted in growth of lamellae in all directions. It is interesting that branch points B, C, D and E are all at equal distances from the point of nucleation (A). In Figure 65 (p.143), in region, A, row nucleation may be seen. There are also many branch points e.g. a, b, c, d, e. Finally in Figure 67 (p.145) we see a growing sheaf originated from an impurity (a) most likely a microgel particle which is naturally present in the plant and was not removed by filtration. Branch points may be seen at points b, c, d, e and f. All of these figures (62-67, p.140-145) show clear branch points demonstrating that secondary lamellae at the branch point are curved, are in the "side-on" orientation and grow at a small angle to the original lamella. This may be due to the concentration gradient of the crystallizable material present. It is reasonable to expect to have more crystallizable material in the regions far away from the lamellae. The amount may be very limited in regions around growing lamella, so once a secondary lamella is nucleated it prefers to grow at an angle. Measurement of the angles between primary and secondary lamella from the micrographs of the fractions showed that the angles vary from 15 to 35 degrees. This suggest that the type of branching we have may not be crystallographic. Although our high magnification pictures

show a connection between them, it is still not clear whether they are really connected through the crystal or only a tie chain connecting them. Keith et al (1966) were able to show that the intercrystalline links between polyethylene lamellae grown from a blend of polyethylene with n-paraffins were 30-300 A^{o} thick and 15,000 ^{o}A in length. The links observed in cis-polyisoprene are only about 10-20 A^{o} thick. So it is possible that the tie chains on the growing lamella may act as nucleation sites in cis-polyisoprene. As lamellae grow some non-crystallized material such as low molecular weight fraction polymer or other organic impurities are segregated. Later after the consumption of the easily crystallizable material, the segregated material may start to crystallize on the already existing tie chains (Phillips and Edwards 1976). Then the branching frequency may be expected to increase with increasing concentration of tie chains. It is known that high undercooling has an increasing effect on the probability of non-adjacent reentry (Hoffman et al. 1976). In Figure 60 (p.138) it may be seen that for the fraction of molecular weight 313,000 the general trend is the increase of branching frequency with supercooling which was superposed with a peak in the regime II region. In polyethylene similar behavior, i.e. an increase in branching below the regime I-II transition and a decrease in branching where the helicoidal twisting appears has been observed

(Philpot and Phillips 1986). For the higher molecular weight fraction an upward trend in the branching with increasing supercooling is observed although there is a considerable increase in branching near the II-III transition temperature (Figure 61, p.139).

In order to investigate the branching process in more detail, we tilted the specimen with respect to the electron beam by different amounts and observed the contact point. Upon tilting crystals, the "edge-on" orientation changed to the "side-on" orientation, accompanied by a change in the crystal thickness and the contrast. Figure 116 shows the effect of tilting on the orientation of lamella and the branch point. The secondary lamella is curved at the branch point and we are able to see the contact point. This is probably an example of a branch nucleated on a tie chain, as described above. A schematic diagram of the possible changes upon tilting in Figure 116 is given in Figure 117. Figure 117-a corresponds to the untilted state of the specimen where we see two secondary lamellae (A,B) nucleated on tie chains. For the lamella "B", the tie chain may be seen more clearly. Upon tilting (Figure 117 b-d) the gradual changes may be followed in accord with Figure 116. Figure 118 contains more branch points of different types. Some of them (a, b) look like the ones described in the previous figure. But in addition to this type, at points c and d we see branches in the form of a possible splitting of original

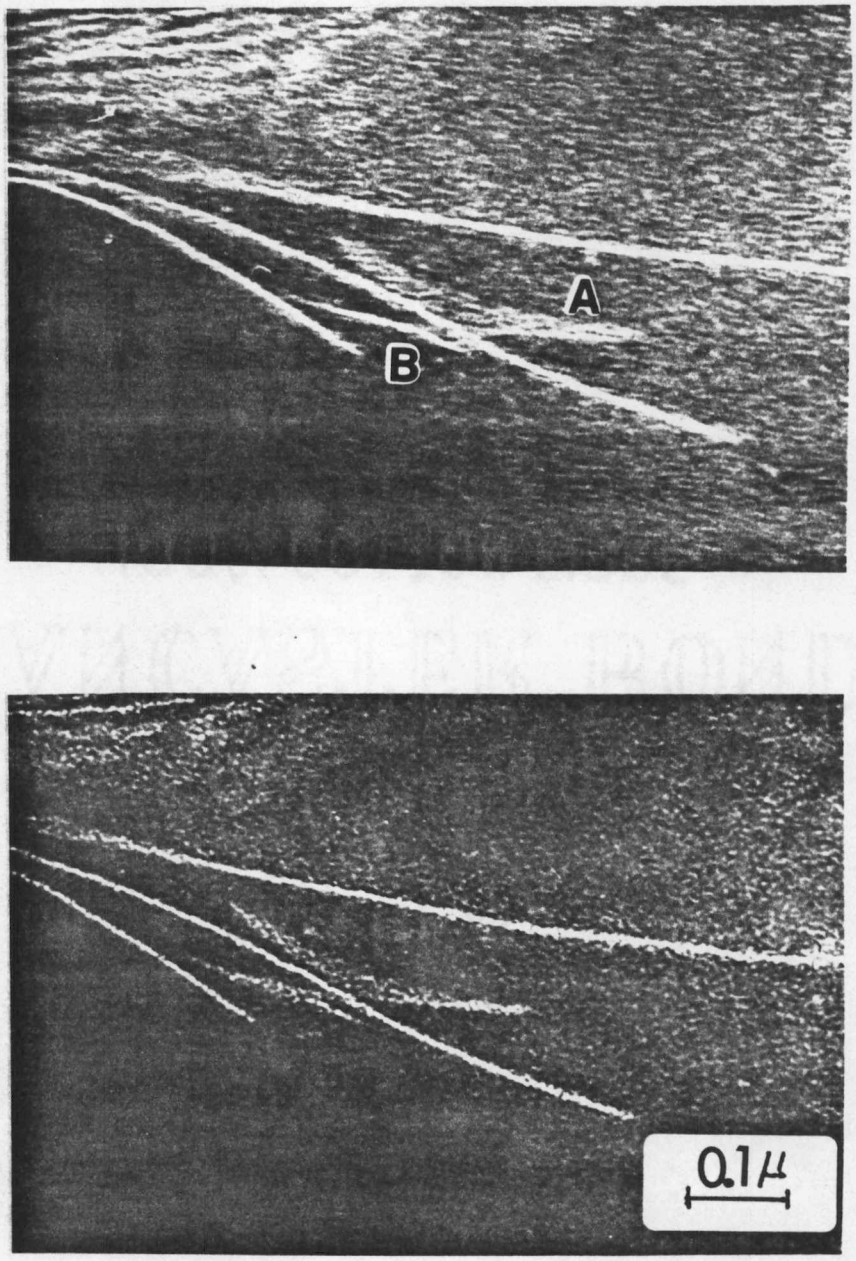
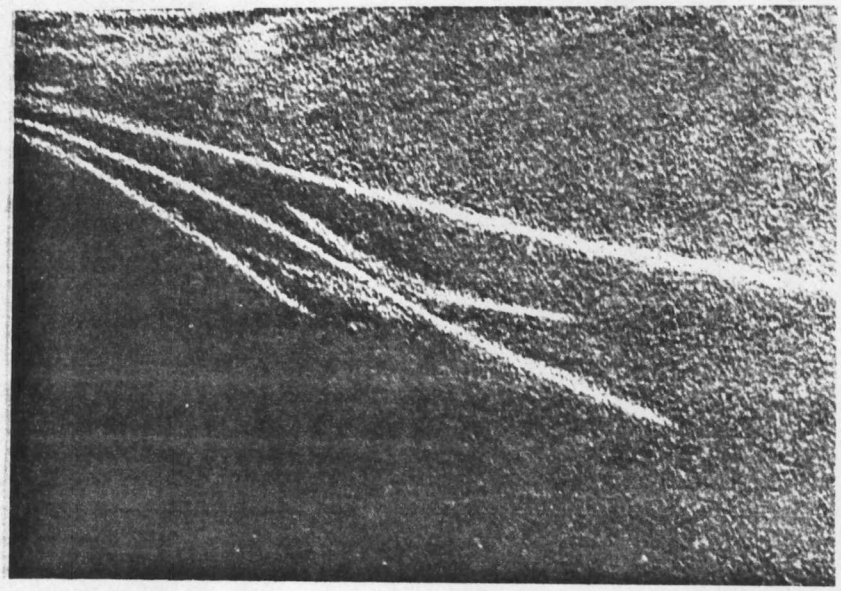
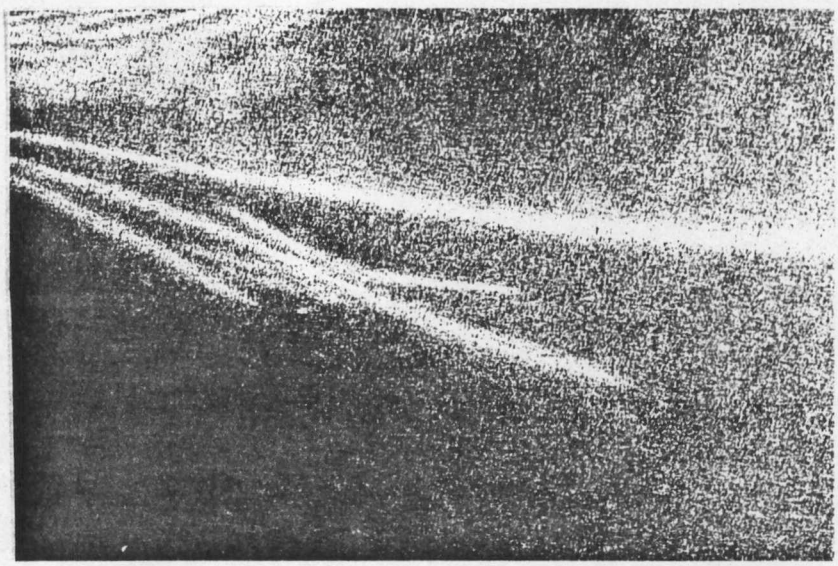


Figure 116 (a) A high magnification picture showing a branch point in a fraction of molecular weight 543,000 at -15 °C (b) shows the same area as in (a) but tilted 12° with respect to the electron beam



c



d

Figure 116 Continued

(c)tilted 24° (d)tilted 32°

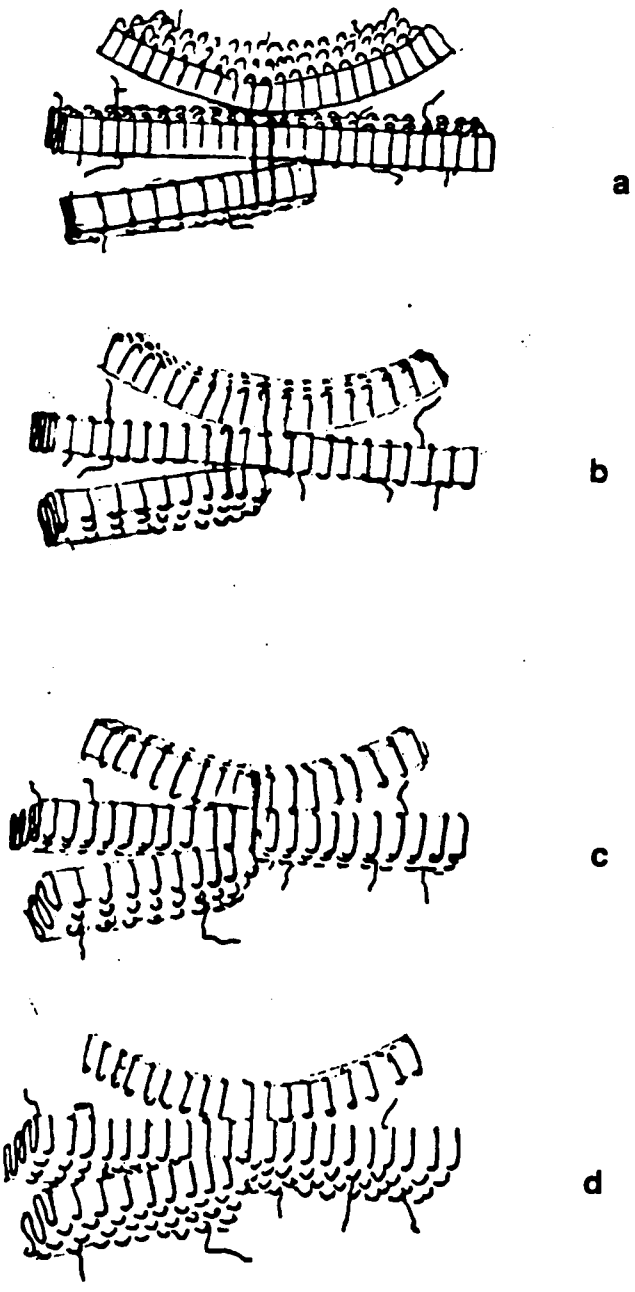


Figure 117 Schematic representation of figure 116.

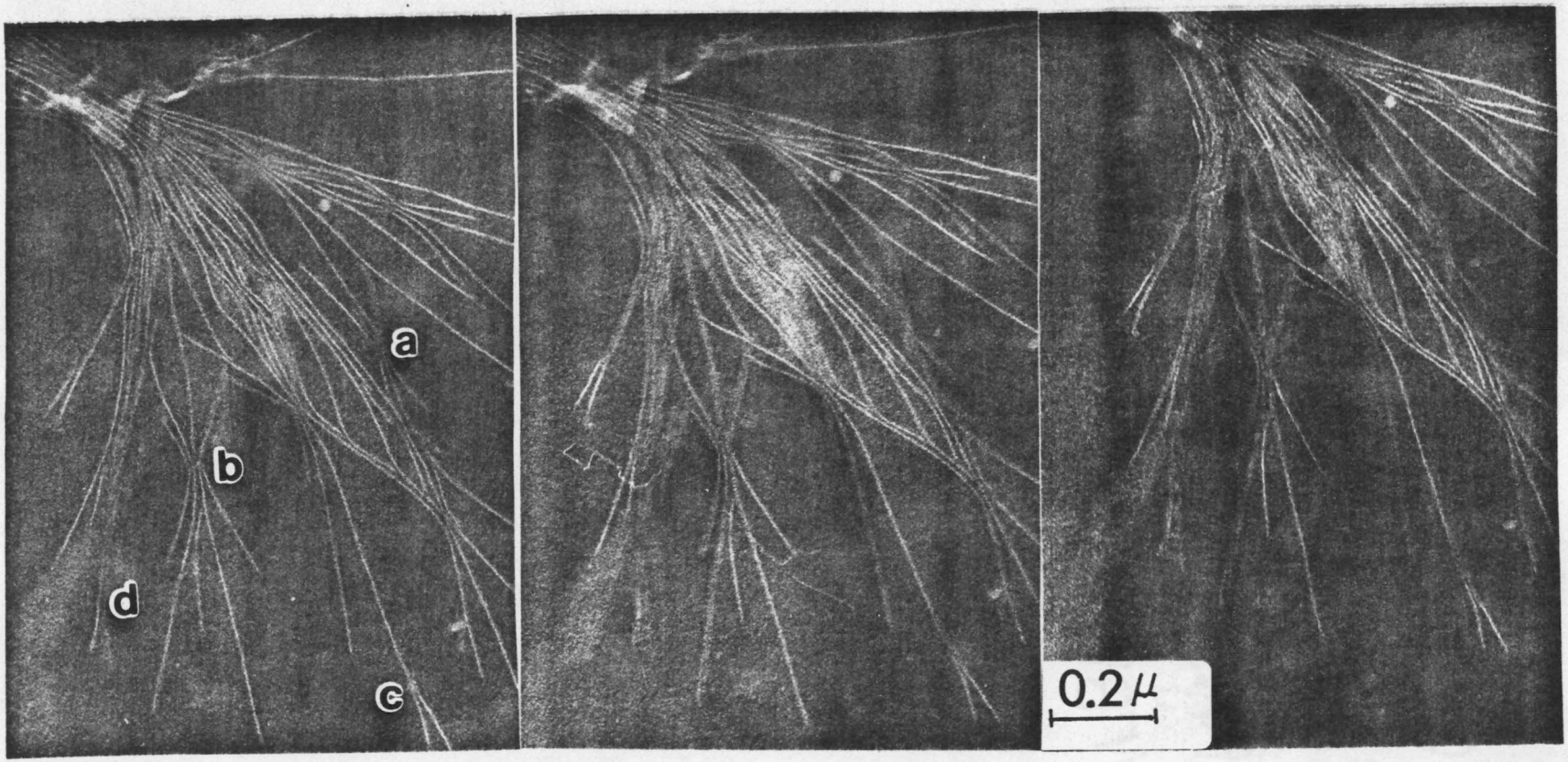
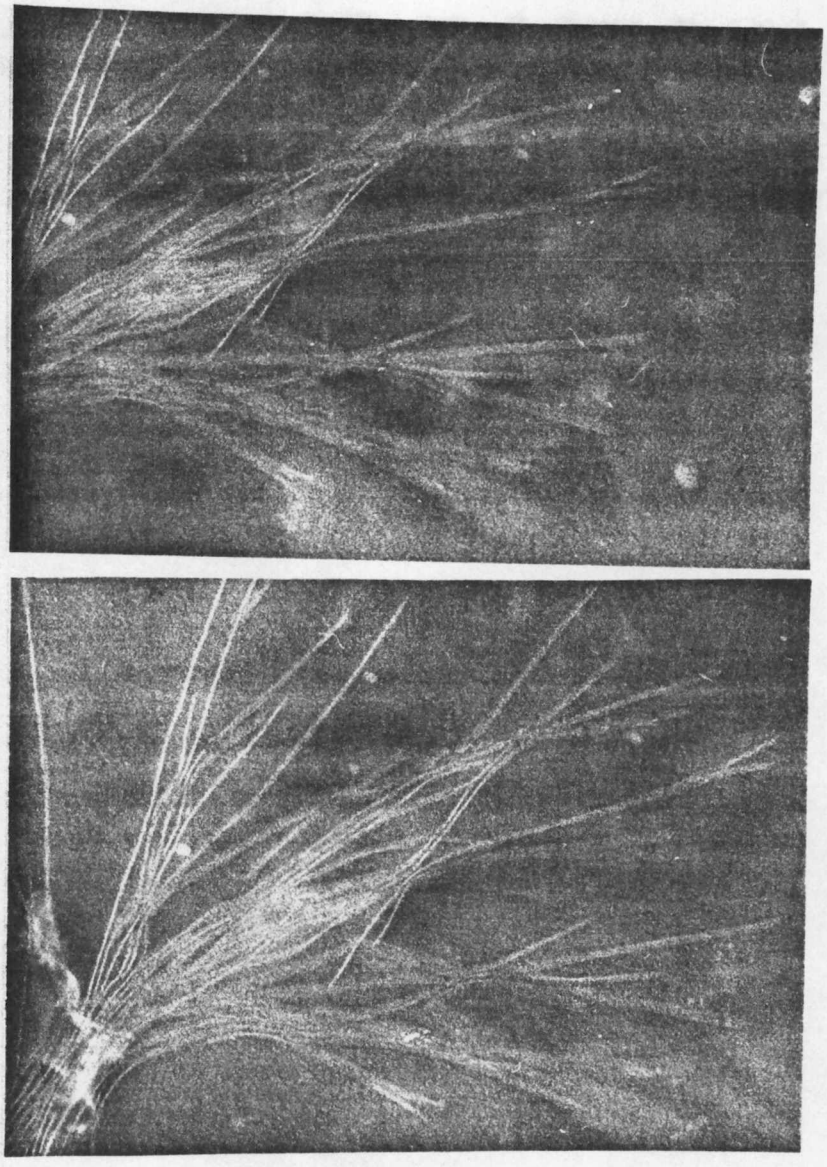


Figure 118 (a) A Picture showing a branch point in a fraction of molecular weight 543,000 at -10 ^{o}C (b) shows the same area as in (a) but tilted 12^{o} with respect to the electron beam (c)tilted 18^{o}



d e

Figure 118 Continued
(d)tilted 30° (e) tilted by 36°.

lamella into two parts. Higher magnification pictures showing the branch point "c" are given in Figure 119. In Figure 119-e splitting in the "side-on" orientation may be seen clearly. Keith et al. (1966) postulated that the presence of impurities which cannot diffuse away because of the high viscosity of polymer melts, may lead to the divergence of two growth fronts as illustrated schematically in Figure 120. This may be the mechanism operating for this type of branches.

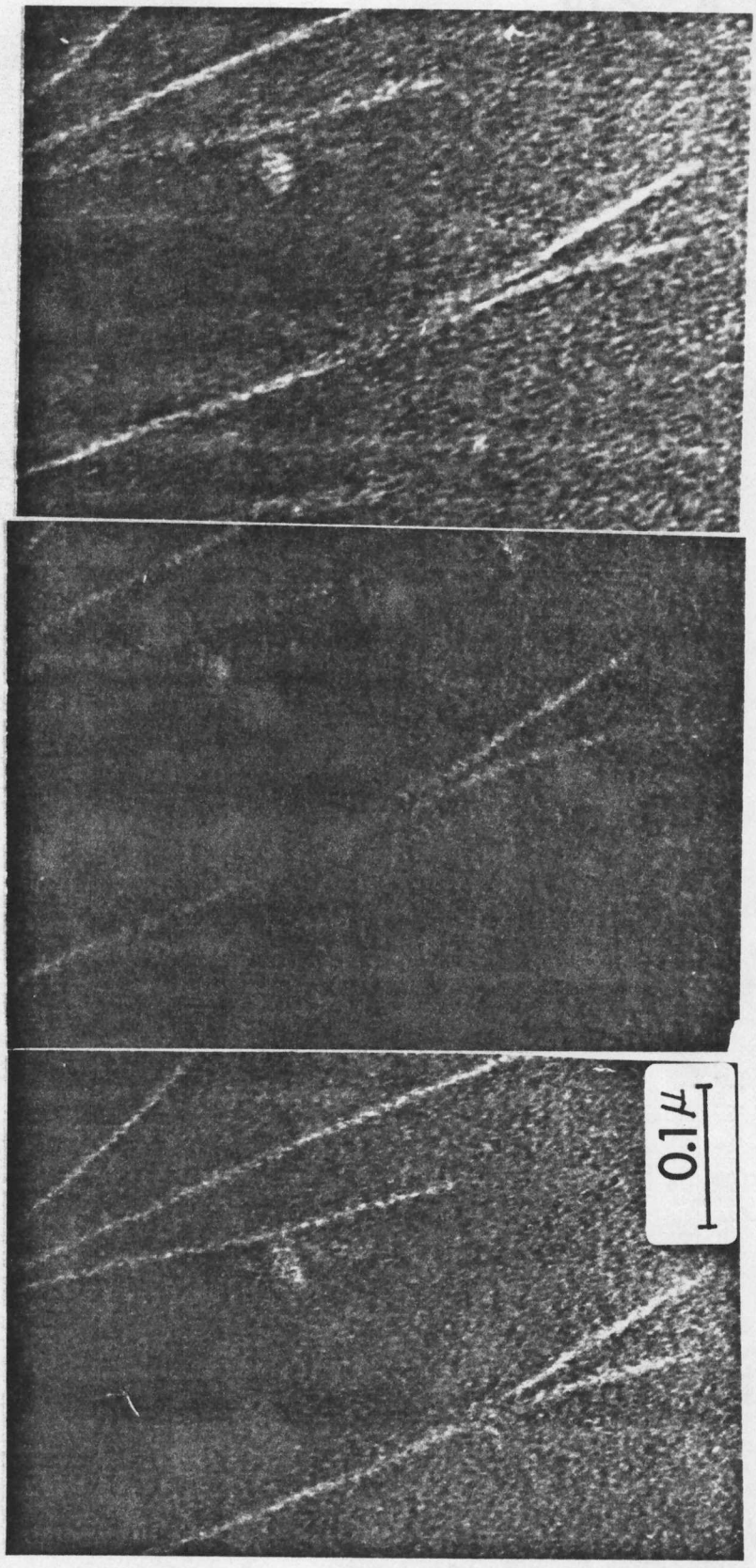
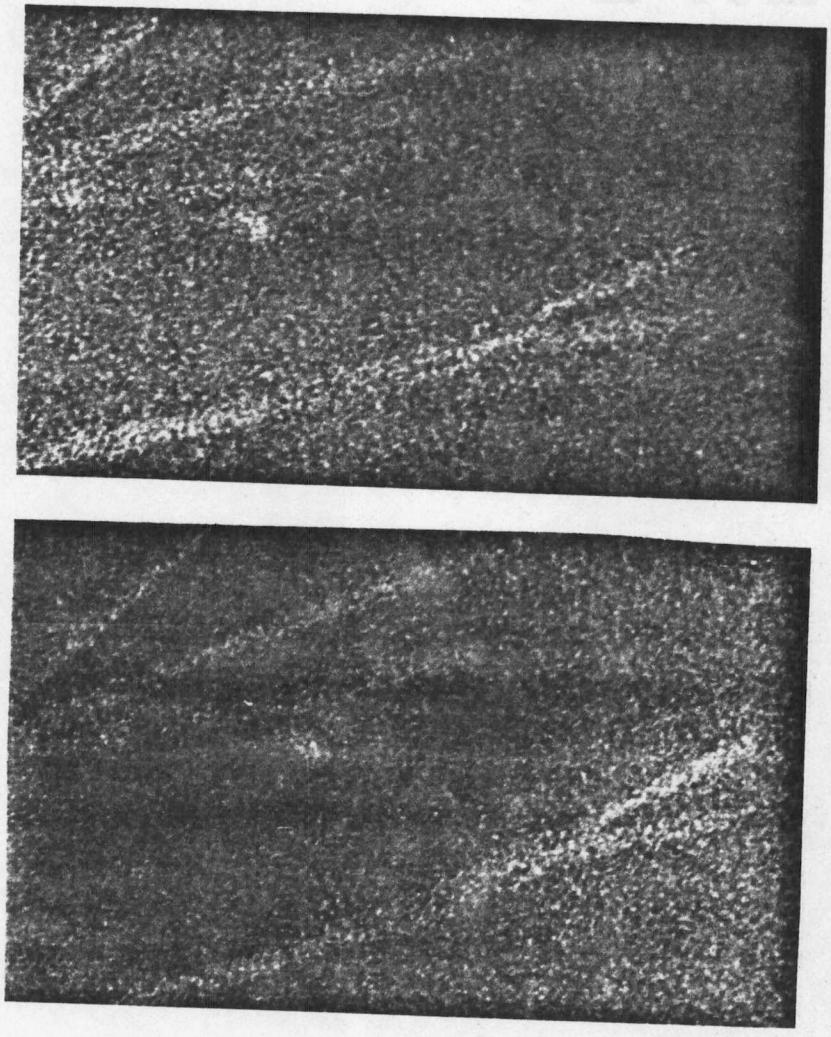


Figure 119 A high magnification picture showing the point "C" in figure 118 in more detail.



d e

Figure 119 Continued

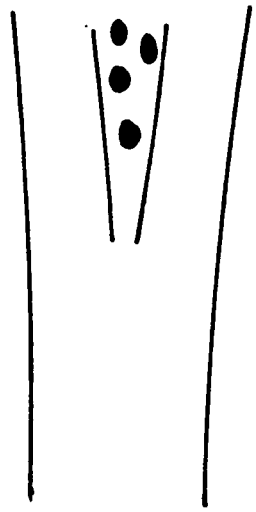


Figure 120 Impurites causing crystal branching.

6. CONCLUSIONS

6.1. Crystallization Regimes

The atmospheric pressure growth rate data of unfractionated guayule rubber and different molecular weight fractions of hevea rubber were analyzed in terms of secondary nucleation theory. The use of WLF transport values resulted in successful kinetic analysis of the growth rate data of cis-polyisoprene. Relatively low molecular weight fractions showed all three regimes whereas the moderate and higher molecular weight fractions showed only two or one regime(s) respectively. This is the first observation of all three regimes in one polymer and is the first definitive evidence produced for regime theory.

Unfractionated guayule rubber also showed a regime III-II transition. The slope ratios of the fractions were close to two (in hevea the value was 1.65) indicating the importance of having a polymer with a narrow molecular weight distribution for crystallization kinetics studies.

Growth rate studies at 0.5 kilobar showed regime III-II transitions for both fractions 313,000 and 543,000. The change of the temperature of the regime III-II transition with pressure is closer to the change of glass

transition temperature with pressure, showing the possibility of the III-II transition being mobility controlled.

6.2. Lamellar Thickening

Lamellar thickening was observed in fractions at atmospheric pressure and at 0.5 kilobar. The phenomenon is believed to be time, molecular weight and crystallization regime dependent.

6.3. Fold Surface Free Energies

At atmospheric pressure fold surface free energy, σ_e, showed a dependence on molecular weight. The two lowest molecular weight fractions gave the highest fold surface free energies. Other fractions exhibited an almost constant value of σ_e.

A sudden increase in σ_e at 0.5 kilobar was observed. In earlier studies a similar sudden increase at one kilobar has been reported. The explanation of two different fold conformations (Dalal 1983) may still be valid here.

6.4. General Morphology

Morphological changes have been observed at the regime I-II transition point. In the regime I region fractionated growth due to long crystallization times gave rise to the concurrent formation of spherulites, axialites and single crystals.

6.5. Branching

Branching was found to be a major function of crystallization temperature. An increase in branching frequency was observed at temperatures below the I-II transition providing additional evidence for the existence of the transition.

6.6. Lamellar Width

Lamellar width was found to increase with increasing temperature. A linear relationship between lamellar thickness and the reciprocal undercooling seemed to fit the data quite well.

7. SUGGESTIONS FOR FURTHER WORK

7.1. Effect of Molecular Weight Distribution

Although we have used fractions with relatively narrow molecular weight distributions (MWD), the effect of MWD still remains questionable in some cases. The deviation observed from the straight line behavior in the regime I region of the fraction with molecular weight 313,000 can be further investigated. A sharp fraction of the same molecular weight may be studied in the same temperature region. If this sample does not show a similar deviation then the deviation can be attributed to the MWD of the sample. If the deviation is generated a second time than it may provide evidence for the validity of Hoffman's "omega defect" theory.

7.2. Regime Reversion

The deviation from linearity in the kinetic curves of the low molecular weight fraction at high temperatures may also be checked for regime reversion. Goldenfeld's theory of regime reversion (I$\rightarrow$II) may be tested if the time dependence of this behavior can be studied. If crystallization studies at a constant temperature for a

number of different time intervals in the region of curvature is carried out, the time dependence can be found. Then it may be concluded whether or not it is a time dependent reversion of regime I into the steady state regime II region.

7.3. High Temperature Crystallization

It was shown that the fraction with molecular weight 543,000 had a regime transition at -5 ^{o}C which is about 13 ^{o}C higher than that of the fraction of molecular weight 313,000. Therefore, crystallization studies of higher molecular weight fractions at temperatures close to the melting point may be carried out to check for the presence of a regime II-III transition.

7.4. The Influence of Regime Transitions on Mechanical Properties

Regime transition temperatures are expected to influence mechanical properties due to the changes produced in fold surface structure, tie-chain concentration and molecular weight fractionation effects. The crystallization behavior of another polymer (e.g. polypropylene) can be investigated for regime behavior and the relation between mechanical properties and regimes may be studied.

7.5. Effect of Trans Units on Regime Transition

Natsyn is synthetic cis-polyisoprene, which contains 2.5 % trans units as a microstructural impurity. Crystallization kinetics of Natsyn fractions can be studied to investigate the effect of copolymer content on regime transitions.

7.6. Pressure Effects

Natsyn has been reported to show no high pressure phase. Therefore the dependence of the regime transition temperature on pressure could be analyzed more thoroughly in fractions of this polymer.

LIST OF REFERENCES

LIST OF REFERENCES

Andrews E.H., Proc. Roy. Soc. (London), A277, 562 (1964).

Baer E. and Kardos J.L., J. Polym. Sci., A3, 2827 (1965).

Bank M.I. and Krimm S., J. Polym. Sci., Polym. Symp., No 53, 347 (1975).

Bassett D.C. and Turner B., Nature (Phys. Sci.), 240, 146 (1972).

Bassett D.C. and Turner B., Phil. Mag., 29, 925 (1974).

Bassett D.C. in "Principles of Polymer Morphology", The Alden Press, Oxford, 1981-a, p.19.

Bassett D.C and Hodge A.M., Proc. Roy. Soc. (London), A377, 61 (1981)-b.

Clark E.J. and Hoffman J.D., Macromolecules, 17, 885 (1984).

Cooper M. and Manley R., Macromolecules, 8, 219 (1975).

Dalal E.N.,Ph.D Dissertation, Univ. of Utah, 1983.

Dalal E.N. and Phillips P.J., Macromolecules, 16, 1754 (1983-a).

Dalal E.N. and Phillips P.J., Macromolecules, 16, 890 (1983-b).

Dalal E.N. and Phillips P.J., J. Polym. Sci., Polym. Lett. Ed., 22, 7 (1984).

Davies C.K.L. and Ong E.L,, J. Mat. Sci., 12, 2165 (1977).

Davies C.K.L. and Cucarella M.C.M., J. Mat. Sci., 15, 1547 (1980)-a.

Davies C.K.L. and Cucarella M.C.M., J. Mat. Sci., 15, 1557 (1980)-b.

De Gennes P.G., J. Chem. Phys., 55, 572 (1971).

De Gennes P.G., Macromolecules, 9, 591 (1976).

Devoy C. and Mandelkern L., J. Poly. Sci.,A2, 1, 1883 (1969).

DiMarzio E.A., Guttman C.M. and Hoffman J.D., Faraday Discuss. Chem. Soc., 68, 210 (1979).

Doolittle A.K., J. Appl. Phys., 22, 1471 (1951).

Edwards B.C. and Phillips P.J., Polymer, 15, 491 (1974).

Edwards B.C., J. Polym. Sci., Polym. Phys. Ed. ,13, 1387 (1975).

Edwards B.C. and Phillips P.J., J. Mat. Sci., 10, 1233 (1975)-a.

Edwards B.C. and Phillips P.J., J. Polym. Sci., Polym. Phys. Ed., 13, 2117 (1975)-b.

Edwards B.C. and Phillips P.J., J. Polym. Sci., Polym. Phys. Ed., 14, 391 (1976).

Edwards B.C., Phillips P.J. and Sorenson D., J. Polym. Sci. Polym. Phys. Ed., 18, 1737 (1980).

Ergoz E., Fatou J.G. and Mandelkern L., Macromolecules, 5, 147 (1972).

Fatou J.G. and Mandelkern L. J. Phy. Chem., 69, 417 (1965).

Fischer E.W., Z.Naturforsch, 12a, 753 (1957).

Fischer E.W. and Schmidt G.F. Angew Chem., 74, 511 (1962).

Flory P.J., J. Am. Chem. Soc., 84, 2857 (1962).

Flory P.J. and Yoon D.Y., Nature, 272, 226 (1978).

Fox T.G. and Flory P.J., J. Appl. Phys., 21, 581 (1960).

Frank F.C. and Tosi M., Proc. Roy. Soc.(London), A263, 323 (1961).

Geil P.H., Anderson F.R., Wunderlich B. and Arakawa T., J. Polym. Sci., A2, 3707 (1964).

Gibbs J.H. and DiMarzio E.A., J. Chem. Phys., 28 ,373 (1958).

Gogolewski S. and Pennings A.J., Polymer, 18, 654 (1977)-a.

Goldenfeld N., Polym. Comm., 25, 47 (1984).

Goldstein M., J. Chem. Phys., 39, 3369 (1963).

Hearle J.W.S. "Polymers and Their Properties" vol 1, John Wiley and Sons, New York, 1982, p.271.

Hobbs S.Y., J.Macromol. Sci. Rev. Macromol. Chem., C19(2), 221 (1980).

Hoffman J.D. and Weeks J.J., J. Chem. Phys., 37, 1723 (1962).

Hoffman J.D.,Ross G.S., Frolen L. and Lauritzen J.I.,Jr.,J. Res. Nat. Bur. Stand., 79A, 671 (1975).

Hoffman J.D.,Davis G.T. and Lauritzen J.I.,Jr.,in "Treatise on Solid State Chemistry" (N.B. Hannay Ed.),Plenum Press, New York, 1976,vol 3 p.497.

Hoffman J.D., Faraday Discuss. Chem. Soc., 68, 378 (1979).

Hoffman J.D., Polymer, 23, 656 (1982).

Hoffman J.D., Polymer, 24, 3 (1983).

Hoffman J.D., Polymer, 26, 1763 (1985).

Johnson J.F., Cantow M.J.R., Porter R.S., in "Encyclopedia of Polymer Science and Technology" (N.M. Bikales Ed.),John Wiley and Sons, New York,1967, vol 7, p.231.

Kawai T, Hosoi M and Kamid K., Die Makromolekulare Chemie, 146, 55 (1971).

Keith H.D., Padden F.J. and Vadimsky R.G., J. Polym. Sci., A-2, 4, 267 (1966).

Keller A., Phil. Mag. ,2, 1171 (1957).

Kim H.G. and Mandelkern L., J. Polym. Sci., A-2, 10, 1125 (1972).

Klein J. and Ball R.C., Faraday Discuss. Chem. Soc., 68, 198 (1979).

Lauritzen J.I.,Jr. and Passaglia E., J. Res. Nat. Bur. Std., 71A, 261 (1967).

Lauritzen J.I.,Jr., J. Appl. Phys. ,44, 4353 (1973).

Lauritzen J.I.,Jr. and Hoffman J.D., J. Appl. Phys. ,44, 4430 (1973).

Lindenmeyer P.H., J. Poly. Sci., C-1, 5 (1963).

Lovinger A.J., Davis D.D. and Padden F.J., Polymer ,26, 1595 (1985).

Magill J.H., J. Appl. Phys. ,35, 3269 (1964).

Mandelkern L., J. Polym. Sci., C18, 51 (1967).

Mandelkern L., Proc. Sagamore Army Mater. Res. Conf. 20th, Syracuse Univ. Press, Syracuse, New York, 1975, p.369.

O`Reilly J.M., J. Polym. Sci., 57, 429 (1962).

Peachey L.D., Proceedings of 4th International Conference on Electron Microscopy, Springer Verlag(Berlin),1958.

Pelzbauer Z. and Galeski A., J. Polym. Sci., C38, 23 (1972).

Phillips P.J. and Edwards B.C., J. Polym. Sci., Polym. Phys. Ed., 13, 1819 (1975).

Phillips P.J. and Edwards B.C., J. Polym. Sci. ,Polym. Phys. Ed., 14, 377 (1976).

Phillips P.J., Polym. Prep., 20, 438 (1979).

Phillips P.J. and Sorenson D., J. Polym. Sci., Polym. Let. Ed., 19, 585 (1981).

Phillips P.J. and Tseng H.T., Macromolecules, 18, 1565 (1985).

Philpot R. and Phillips P.J., Polymer Commun., in press.

Point J.J. and Kovacs A.J. Faraday Discuss. Chem. Soc., 68, 167 (1979).

Point J.J., Colet M. Ch. and Dosiere M., J. Polym. Sci., Polym. Phys. Ed., 24, 357 (1986).

Price F.P., J. Chem.Phys., 35, 585 (1981).

Rabek J.F.,"Experimental Methods in Polymer Chemistry", John Wiley and Sons, New York, 1980 p.456.

Rees D.V. and Bassett D.C., J. Polym. Sci., A-2, 9, 385 (1971).

Reneker D.H. and Geil P.H., J. Appl. Phys., 31, No 11, 1916 (1960).

Rensch G.J., Phillips P.J. Vatansever N. and Gonzales V.A., J. Polym. Sci., Part B, Polym. Phys., 24, 1943 (1986).

Sadler D.M., Polymer, 24, 1401 (1983).

Sadler D.M. and Gilmer G.H., Polymer, 25, 1446 (1984).

Sadler D.M., J. Polym. Sci., Polym. Phys. Ed., 23, 1533 (1985).

Sadler D.M., Polym. Commun., 27, 140 (1986).

Sanchez I.C. and Eby R.K., Macromolecules, 8, 638 (1975).

Subramaniam A., Preprints ACS Division Rubber Chem. Paper 78 (1971).

Suzuki T. and Kovacs A.J., Polymer J., 1, 82 (1970).

Till P.H. Jr., J. Polym. Sci., 24, 301 (1957).

Tseng H.T., Ph.D. Dissertation, Univ. of Utah, 1984.

Van Anterwerpen F.V. and Van Krevelen D.W., J. Polym. Sci., Polym. Phys. Ed., 10, 2423 (1972).

Williams M.L., Landel R.F. and Ferry J.D., J. Am. Chem. Soc., 77, 3701 (1955).

Wunderlich B., J. Polym. Sci., A-1, 1245 (1963).

Wunderlich B. and Arakawa T, J.Polym. Sci., A-2, 3697 (1964).

Yoon D.Y. and Flory P.J.,Faraday Discuss. Chem. Soc., 68, 288 (1979).

APPENDIX

Growth rates of hevea rubber fractions with indicated molecular weights at atmospheric pressure.

Temperature (°C)	GROWTH RATE ($\mu m h^{-1}$) $\bar{M}v$ 3.13×10^5	$\bar{M}v$ 3.51×10^5	$\bar{M}v$ $5,43 \times 10^5$	$\bar{M}v$ 8.97×10^5	$\bar{M}v$ 1.42×10^6
-40.0	0.143	0.120	0.075	0.1375	0.040
-35.0	0.222	-	0.183	0.186	-
-32.0	0.262	0.240	-	-	-
-30.0	0.290	-	0.250	-	0.170
-26.0	0.526	0.500	0.400	0.375	0.220
-20.0	0.400	0.360	0.350	0.300	0.180
-15.0	0.333	-	0.232	-	-
-14.0	0.310	-	-	-	-
-12.0	0.296	0.261	-	-	-
-10.0	-	-	0.125	-	-
-9.2	0.263	-	-	-	-
-8.0	-	-	-	0.1744	-
-7.3	0.244	-	-	-	-
-5.0	0.200	0.171	0.049	-	0.025
-3.5	0.096	-	-	-	-
-2.2	-	-	0.046	-	-
-1.0	0.033	0.036	-	-	-
-0.6	-	-	0.238	-	-
+0.8	0.015	-	-	-	-
+1.4	-	-	0.019	-	-
+1.8	0.013	-	-	-	-
+3.0	0.011	-	-	-	-

Lamellar thicknesses of the hevea rubber fractions with indicated molecular weights

Temperature (°C)	LAMELLAR THICKNESS (nm)				
	$\bar{M}v$ 3.13×10^5	$\bar{M}v$ 3.51×10^5	$\bar{M}v$ 5.43×10^5	$\bar{M}v$ 8.97×10^5	$\bar{M}v$ 1.42×10^6
-40.0	5.30	5.70	5.55	5.50	-
-35.0	-	-	5.80	6.00	-
-32.0	6.10	5.90	-	-	-
-30.0	-	-	6.00	-	5.60
-26.0	6.67	7.00	-	6.50	6.20
-20.0	6.80	7.35	6.40	7.12	6.40
-15.0	7.25	-	7.63	-	-
-14.0	7.20	-	-	-	-
-12.0	7.15	7.50	-	-	-
-10.0	-	-	8.00	-	-
-9.2	8.50	-	-	-	-
-8.0	-	-	-	8.16	-
-7.3	9.10	-	-	-	-
-5.0	9.00	9.25	8.56	-	8.40
-3.5	9.80	-	-	-	-
-2.2	-	-	8.50	-	-
-1.0	10.70	10.65	-	-	-
-0.6	-	-	9.00	-	-
0.0	-	-	9.50	-	-
+0.8	10.9	-	-	-	-
+1.4	-	-	9.70	-	-
+1.8	11.3	-	-	-	-
+2.2	-	-	10.50	-	-
+3.0	11.50	-	-	-	-

Growth rates of hevea rubber fractions with indicated molecular weights at 0.5 kilobar

Temperature (°C)	GROWTH RATE ($\mu m h^{-1}$) M_v = 351,000	M_v = 543,000
-17	1.440	1.380
-11	0.430	0.360
0	0.110	0.075
-4.8	0.161	0.118
+4.2	0.021	0.012

Lamellar Thicknesses of the hevea rubber fractions with indicated molecular weights at 0.5 kilobar

Temperature (°C)	LAMELLAR THICKNESS (nm) $\bar{M}_v$ = 351,000	$\bar{M}_v$ = 543,000
-17	5.6	6.0
-11	8.8	8.0
-4.8	10.0	9.0
0	14.0	13.0
+4.2	14.5	14.0

Growth rates and lamellar thicknesses of unfractionated guayule rubber

Temperature (°C)	Growth rate (μmh^{-1})	Lamellar thickness (nm)
-40.0	0.140	-
-34.0	0.316	5.7
-30.0	0.375	5.4
-26.0	0.500	6.0
-21.0	0.400	6.4
-15.0	0.240	6.7
-10.0	0.160	8.0
-5.0	0.104	8.7

VITA

Nurhan Vatansever was born in Aydın, Turkey on August 28 1956. She graduated from Ankara Kız High School in June of 1973. The following September she entered Middle East Technical University. Following a year of English preparatory school she received the Bachelor of Science degree in Chemistry in February of 1979. She started Master of Science studies in the same institution and received her M Sc. degree in Polymer Chemistry in January of 1982.

In March 1982, the author entered the University of Utah Salt Lake City and began to study toward a doctorate degree in Materials Science and Engineering. After three years, she transferred to the University of Tennessee Knoxville along with Professor Paul J. Phillips. She received the doctor of Philosophy degree in December 1986.